Characterising CD47 Phosphatase Signalling in the Hypertensive Heart

Zoë Helen Ross Haines

PhD Thesis

St George's, University of London

November 2022

Declaration

I declare that this thesis has been composed solely by myself and that it has not been submitted, in whole or in part, in any previous application for a degree. The work presented is entirely my own, except where stated otherwise by reference or acknowledgment.

Abstract

Prolonged hypertension can cause hypertensive heart disease (HHD), characterised by cardiac hypertrophy and fibrosis, and is a major cause of heart failure (HF). Activation of CD47 by the matricellular protein, thrombospondin 1 (TSP1), can cause cellular stress by controlling NADPH oxidase 1 (NOX1) expression, which inhibits angiogenesis and promotes endothelial cell (EC) senescence; all mechanisms underpinning cardiac remodelling. One of the potential pathways linking CD47 to NOX1 are the mitogen-activated protein kinases (MAPKs), which include; p38-MAPK, JNK, and ERK1/2, each independently linked as effectors of stress processes. Furthermore, by negatively regulating MAPK signalling, dual specificity phosphatases (DUSPs) have recently been demonstrated to influence cardiac remodelling. However, whether the TSP1-CD47-NOX1 axis impairs cardiac endothelial function in HHD, and whether CD47 activation contributes to MAPK activation in the heart is entirely unknown. Moreover, it is not known whether DUSPs are dysregulated in HHD and can be influenced by CD47 signalling. Therefore, the aims of this project were to identify whether CD47 activation occurs in the hypertensive heart, to identify whether CD47 activation in the cardiac endothelium promotes stress signalling and can regulate DUSP expression.

This project identified that cardiac TSP1 expression was increased in patients with non-ischaemic HF and in mice with angiotensin II-induced hypertension. This project established that CD47 activation promoted NOX1 expression in cardiac ECs, which was found to be a novel instigator of impaired endothelial migration. Additionally, the results demonstrated that CD47 activation promoted MAPK activation in cardiac ECs and regulated the expression of DUSPs. Finally, the data indicated that the expression of cardiac DUSPs in non-ischaemic HF and in rodent models of hypertension was altered. From these results, it is proposed that blockade of CD47, inhibition of NOX1 or inhibition of DUSPs, may be novel strategies to ameliorate impaired cardiac endothelial function and thus cardiac remodelling in HHD.

Table of Contents

List of figures

List of tables

Acknowledgments

I would like to thank my supervisors, Dr Daniel Meijles and Professor Guy Whitley, for their support, guidance, patience, and expertise, and for the opportunity to work with them. My thanks also to Dr Susanna Cooper, for her advice, assistance, and friendship throughout our time together in the Meijles Group. My gratitude goes also to other members of the Vascular Biology department and to Sandra Ashton in the Image Resource Facility for their kind support, and to St George's, University of London for their much-appreciated funding. It was a pleasure to work with you all.

I could not have completed this thesis without the support from my family and friends, who I am sure know more about TSP1 and CD47 than they would like to. I am indebted to my parents, Adrian and Janet, for their unceasing encouragement, and sister, Emma, for her moral support. My heartfelt thanks go to Max's parents, Colin and Denise, for putting up with me over lockdown and during my write-up. A huge thank-you goes to Susie, Ella, Georgina, Krysia, Bryony, Maddie, Maddie, and Lucy for the fantastic support and good chats (and wine) at the end of a long week. I would also like to thank my number one study buddy, Trevor the cat.

Finally, Max, I am forever grateful for your unwavering support; you walked along with me on this journey, and I truly could not have done this without you.

Abbreviations

4-HNE	4-Hydroxylnonenal
ACE	Angiotensin II converting enzyme
ACEI	Angiotensin II converting enzyme inhibitors
AngII	Angiotensin II
ARB	Angiotensin II receptor blocker
ASK1	Apoptosis signal-regulating kinase-1
AT1R	Angiotensin II type 1 receptor
AT2R	Angiotensin II type 2 receptor
BCA	Bicinchoninic assay
BH2	Dihydrobiopterin
BH4	Tetrahydrobiopterin
BSA	Bovine serum albumin
CC	Coiled-coil
CCBs	Calcium channel blockers
cDNA	Complementary DNA
CFR	Coronary flow reserve
cGMP	Cyclic guanosine monophosphate
COMP	Cartilage oligomeric matrix protein
CRY	Cardiac risk in the young
CST	Cell signalling technology
Ctrl	Control
d	Days
DAB	3,3'-Diaminobenzidine
DCM	Dilated cardiomyopathy
DDR2	Discoidin domain receptor tyrosine kinase 2
DUSP	Dual specificity phosphatase
dH_2O	Distilled water
ECs	Endothelial cells
ECM	Extracellular matrix

EDTA	Ethylenediaminetetraacetic acid
EF	Ejection fraction
eNOS	Endothelial nitric oxide synthase
ERK	Extracellular signal-regulated kinase
FAD	Flavin adenine dinucleotide
FBS	Foetal bovine serum
FN1	Fibronectin 1
For	Forward
GAPDH	Glyceraldehyde-3-phosphate dehydrogenase
GPCR	G protein-coupled receptor
h	Hours
H_2O_2	Hydrogen peroxide
HBSS	Hanks balanced salt solution
HCF	Human cardiac fibroblast
HF	Heart failure
HFpEF	Heart failure with preserved ejection fraction
HFrEF	Heart failure with reduced ejection fraction
HHD	Hypertensive heart disease
HIF	hypoxia-inducible factor
HPAEC	Human pulmonary artery endothelial cell
HRP	Horseradish peroxidase
HUVEC	Human umbilical vein endothelial cell
ICAM-1	Intercellular adhesion molecule-1
IHC	Immunohistochemistry
IL	Interleukin
JNK	c-Jun N-terminal kinase
KIM	Kinase interaction motif
LAP	Latency-associated peptide
LV	Left ventricular
LVEDD	Left ventricular end-diastolic diameter

LVH	Left ventricular hypertrophy
m/s	Metres/second
MAPK	Mitogen-activated protein kinase
MKK	MAPK kinase
MAP3K	MAPK kinase kinase
MEK	MAPK/ERK kinase
MEKK	MAPK/ERK kinase kinase
MFI	Mean fluorescence intensity
MI	Myocardial infarction
Min	Minutes
MMP	Matrix metalloproteinase
MTA	Materials transfer agreement
mTORC	Mammalian target of rapamycin
MTT	3-(4, 5-dimethylthiazolyl-2)-2, 5-diphenyltetrazolium bromide
NASH	Non-alcoholic steatohepatitis
NI-HF	Non-ischaemic heart failure
NF-κB	Nuclear factor kappa B
NADPH	Nicotinamide adenine dinucleotide phosphate
NO	Nitric oxide
NOX	NADPH oxidase
NOXA1	NADPH oxidase activator 1
NOXO1	NADPH oxidase organiser 1
P-MAPK	Phosphorylated mitogen-activated protein kinase
PAGE	Polyacrylamide gel electrophoresis
PAH	Pulmonary arterial hypertension
PBS	Phosphate buffered saline
PE	Phenylephrine
PEST	Proline, Glutamine, Serine, Threonine
PKC	Protein kinase C
PKG	Protein kinase G

qPCR	Quantitative real time PCR
RAAS	Renin-angiotensin-aldosterone system
Rev	Reverse
RIPA	Radioimmunoprecipitation assay
RNAseq	RNA sequencing
RT	Room temperature
RTK	Receptor tyrosine kinase
ROS	Reactive oxygen species
s	Seconds
SDS	Sodium dodecyl sulphate
SGHEC-7	St George's hospital endothelial cell-7
SGLT2	Sodium-glucose co-transporter-2
SGUL	St George's, University of London
SHR	Spontaneously hypertensive rat
SIRPα	Signal regulatory protein α
SOD	Superoxide dismutase
SVEC4-10	SV40 transformed endothelial cells from axillary lymph node vessels
T-MAPK	Total mitogen-activated protein kinase
TAC	Transverse aortic constriction
TBS	Tris-buffered saline
TBST	Tris-buffered saline with 0.1% (v/v) Tween 20
TEMED	Tetramethylethylenediamine
THBS1	*Human Thrombospondin 1 gene*
Thbs1	*Rodent Thrombospondin 1 gene*
TGF-β	Transforming growth factor-β
TSP	Thrombospondin
UoR	University of Reading
VCAM-1	Vascular cell adhesion modelule-1
VEGF	Vascular endothelial growth factor
VEGFR2	Vascular endothelial growth factor receptor 2

Veh	Vehicle
VSMC	Vascular smooth muscle cell
VWF	von Willebrand factor
WKY	Wistar Kyoto
WP	Well plate
WT	Wild type

Chapter 1: Introduction

1.1. Hypertension and hypertensive heart disease

Cardiovascular disease is the leading cause of mortality worldwide and was responsible for 18.6 million deaths in 2019[1]. Given that the burden of cardiovascular disease has almost doubled since 1990 to 523 million cases[1], it is not surprising that the number of individuals with heart failure (HF) has also doubled to 64.3 million[2]. Hypertension (blood pressure ≥140/90 mmHg) is a major risk factor for HF. 1 in 20 hypertensive individuals will develop HF, almost twice as many as those with normal blood pressure[3]. The global prevalence of hypertension has been between 32-34% over the last 30 years, and hypertension still presents a significant global burden, despite the development of multiple antihypertensive therapeutics[4].

Hypertension is a multifactorial disease influenced by lifestyle (e.g. salt intake, obesity, exercise, and smoking status), age, sex, and genetics. However, the direct causes of elevated arterial blood pressure are increased stroke volume, increased heart rate or increased peripheral arterial resistance[5]. Prolonged hypertension promotes cardiac adaptation, namely an increase in left ventricular (LV) mass, also known as left ventricular hypertrophy (LVH). In hypertension, LVH functions to maintain cardiac output against elevated afterload, i.e. the pressure that the heart must work against to eject blood[6,7]. When LVH occurs in hypertension, and in the absence of any other cause of LVH, this is termed hypertensive heart disease (HHD)[8]. If hypertension is left untreated, HHD can progress to HF. Indeed, 26.2% of HF cases were attributable to HHD in 2017[2].

1.1.1.1. Progression of HHD

The progression of HHD is classically defined by three phases. The first phase is characterised by adaptive LVH which compensates for elevated blood pressure, and is associated with increased cardiac myocyte size (termed cardiac myocyte hypertrophy) and pathological extracellular matrix (ECM) remodelling (termed cardiac fibrosis)[9]. The second phase is the progression from HHD to HF. This occurs when cardiac adaptation can no longer compensate for elevated blood pressure, and cardiac dysfunction ensues. (Figure 1.1). Initially, worsening cardiac function in HF can be compensated for by increasing the heart rate or by increasing the stroke volume to maintain cardiac output. Further hypertrophic remodelling can contribute to increased stroke volume. In this phase, which is termed compensated HF, the symptoms of HF (e.g. fatigue, dyspnoea, and oedema) are stable or absent. However, HF will eventually progress into decompensated HF, which is the final phase of progression, where ventricular dilatation occurs, the process by which the ventricular chambers become enlarged, and cardiac dysfunction becomes more severe and leading to symptomatic presentation[10].

The processes involved in the transition from HHD to HF are poorly defined[6], but both systolic dysfunction (inability to contract) and diastolic dysfunction (inability to relax) can contribute to HF. Around half of all HF are caused by systolic dysfunction, known as HF with reduced ejection fraction (HFrEF), characterised by an ejection fraction (EF, the proportion of the blood ejected from the left ventricle during systole) of ≤40%. The other half of cases are caused predominately by diastolic dysfunction, known as HF with preserved ejection fraction (HFpEF), characterised by an EF of ≥50%[11]. HHD and other non-ischaemic cardiomyopathies primarily progress to HFpEF, whereas HFrEF is associated with ischaemic heart disease[12,13]. Indeed, between 60-90% of HFpEF patients have underlying hypertension[14].

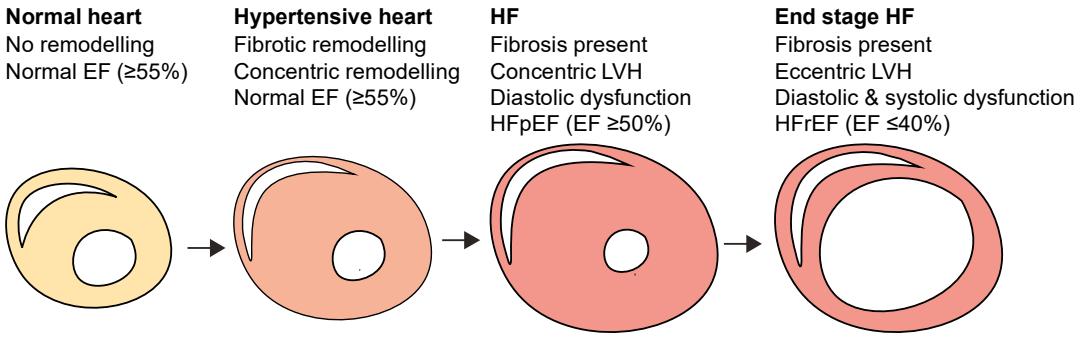

Figure 1.1. Cardiac remodelling during the progression of HHD.
HHD is characterised by fibrotic remodelling and concentric LVH, whilst progression to HF results in eccentric remodelling and vessel dilatation.

1.1.1.2. Therapeutics for HHD and HF

A number of antihypertensive drugs target the renin-angiotensin-aldosterone system (RAAS), which is often activated in human hypertension. Angiotensin II (AngII) is the primary effector of the RAAS. AngII is an 8-residue pro-hypertensive peptide hormone (sequence: DRVYIHPF), which is derived from angiotensinogen by conversion of angiotensinogen to angiotensin I by renin in the kidney, followed by conversion of angiotensin I to AngII by angiotensin-converting enzyme (ACE) in the lungs. AngII promotes hypertension through binding to the AngII type 1 receptor (AT1R), resulting in vasoconstriction, noradrenaline release, stimulation of thirst from the hypothalamus, anti-diuretic hormone release from the posterior pituitary gland, and aldosterone release from the adrenal cortex. Overall, this acts to promote water intake, reduce urinary loss and increases urinary sodium reabsorption, resulting in water retention and raised blood pressure[15]. RAAS-targeting, antihypertensive drugs include AngII-converting enzyme inhibitors (ACEI) (e.g. lisinopril and ramipril), which limit AngII production, and AngII receptor blockers (ARBs) (e.g. losartan and irbesartan) (ACEIs), which prevent AngII from interacting with the AT1R. Other antihypertensive therapeutics

include calcium channel blockers (CCBs) (e.g. amlodipine and felodipine), which act by limiting calcium uptake into arteries to promote vasodilation, and diuretics (e.g. indapamide and chlorthalidone) which reduce blood volume (and therefore pressure) by promoting urine production.

Treatments for HF include: ACEI and ARBs, which promote vasodilation and reduce blood pressure; beta blockers (e.g. atenolol and bisoprolol), which limit heart rate and contractile force; mineralocorticoid receptor antagonists (e.g. spironolactone and eplerenone), which prevent fluid retention by blocking the binding of aldosterone to mineralocorticoid receptors; diuretics, which promote fluid loss; and sodium-glucose co-transporter-2 (SGLT2) inhibitors (e.g. dapagliflozin and empagliflozin). However, these treatments frequently only have disease modifying effects in HFrEF. ACEIs, ARBs, beta blockers, and mineralocorticoid receptor antagonists reduce hospitalisation and mortality rates in HFrEF, but do not influence outcomes in HFpEF patients[16–18]. Although, a recent study found SGLT2 inhibitors reduced hospitalisation rates in both HFrEF and HFpEF[19], and treatment with diuretics is recommended to reduce congestive symptoms in both types of heart failure[16].

Because effective therapies which improve HFpEF prognosis are absent, current guidance involves managing the underlying comorbidities, such as hypertension and diabetes[16]. As such, the only way to prevent hypertension from progressing to HHD and HFpEF is by treating the underlying hypertension[20]. This is problematic, as hypertension is not diagnosed in 41-50% of individuals with high blood pressure, and less than half of all diagnosed hypertension is controlled[4]. This therefore amounts to fewer than 25% of hypertensive individuals having controlled blood pressure. Furthermore, as many as 18% of hypertensive patients have resistant hypertension, defined as hypertension which remains uncontrolled after treatment with three or more antihypertensive drugs[21]. It is in these patients, who either do not know they have hypertension or are unable to control it, where HHD poses the most risk. As such, there is a need for the development of drugs which can directly and effectively limit cardiac remodelling in HHD to halt progression to HFpEF.

1.1.2. Cardiac remodelling in HHD

The lack of therapeutics to attenuate or reverse adverse cardiac remodelling is in part due to its complex nature, involving coordination between different cardiac cell types and multiple signalling pathways. Cardiac remodelling in HHD includes LVH, fibrosis, reduced vascular density and, as HF progresses, myocyte death. These remodelling processes promote diastolic dysfunction, disturbances to cardiac rhythm and perturbed myocardial perfusion, which contribute to cardiac dysfunction[22]. A greater understanding of the cardiac remodelling

process will identify possible therapeutic targets which have the potential to limit the progression of hypertension to HHD and HF.

1.1.2.1. Left ventricular hypertrophy

The long-established paradigm is that hypertension initially promotes adaptive concentric LVH, characterised by enlargement and thickening of the LV wall due to increased cardiac myocyte diameter, which preserves cardiac output by reducing wall stress. Eventually, transition to HF occurs, where LVH becomes eccentric, characterised by enlargement and dilatation of the LV wall due to increasing cardiac myocyte length, causing systolic dysfunction and heart failure[6,23]. However, this paradigm has been challenged; the majority of hypertensive patients do not have LVH[24,25], and one review found that if present, LVH was more likely to be eccentric (~25%) rather than concentric (~18%)[24]. Despite this, a subsequent observational study found concentric LVH (27%) was more common in hypertensive patients than eccentric LVH (9%)[25]. However, neither of these studies were longitudinal, so it cannot be determined whether patients with a normal cardiac geometry subsequently develop LVH, and nor whether patients with concentric LVH progress to eccentric LVH.

As eccentric remodelling is commonly observed following myocardial infarction (MI), the transition of concentric to eccentric hypertrophy may not be part of HHD progression, but instead a product of ischaemia[26,27]. However, hypertension is known to increase the risk of MI, which may be due to its role in atherosclerosis or due to the shared risk factors (e.g. diabetes, obesity, smoking, physical inactivity) for the two diseases[28]. As such, it is not clear whether hypertension is directly involved in the transition of concentric to eccentric remodelling, and the development of HFrEF. Furthermore, eccentric remodelling may not be required for the transition to systolic dysfunction and HFrEF since a small subset of HFrEF patients have concentric remodelling and these patients are more likely to be hypertensive[23,29], indicating eccentric remodelling is not necessary to promote systolic dysfunction.

1.1.2.2. Fibrotic remodelling

Fibrotic remodelling occurs in HHD and can be interstitial (throughout the myocardium) or perivascular (surrounding blood vessels). It is characterised by the following: excessive deposition of ECM proteins such as collagen I and III, and fibronectin; reduced ECM turnover; and altered matricellular protein abundance. Fibrotic remodelling is initiated by the differentiation of fibroblasts into activated fibroblasts, known as myofibroblasts, which are capable of increased collagen synthesis[30].

Several mechanisms promote the differentiation of fibroblasts into active myofibroblasts. Inflammatory cells, recruited into the myocardium following cardiac myocyte damage or by cytokines or chemokines released from endothelial cells (ECs), can secrete pro-fibrotic growth factors such as transforming growth factor-β (TGF-β)[30]. TGF-β is kept in its latent (inactive) form by associating with the latency-associated peptide (LAP), which is displaced for activation. TGF-β can be activated by matricellular proteins (non-structural proteins found in the ECM), including thrombospondin (TSP) 1[31], matrix metalloproteinases (MMPs)[32,33], or by integrins[34,35]. Reactive oxygen species (ROS) can also contribute to TGF-β activation directly through oxidation of the LAP or indirectly by activation of MMPs[36]. Activated TGF-β promotes fibroblast activation and ECM deposition by SMAD-dependent pathways[37].

Other mechanisms may also be involved in fibroblast activation. For instance, mechanical stress can promote myofibroblast differentiation, whilst the deposition of other ECM components can also promote fibroblast activation. This includes the deposition of collagen VI[38], the fibronectin splice variant extradomain-A, alongside matricellular proteins such as TSP1[39], and periostin[40]. Furthermore, for collagen deposition to occur following cardiac injury, polymerised fibronectin is necessary[41], and fibronectin also promotes the assembly of collagen into fibrils, which then cross-link to form mature collagen fibres[42,43].

In addition to the deposition of collagen, ECM turnover can also influence fibrosis. As mentioned above, MMPs can promote fibrosis by activating immunoregulatory molecules, such as TGF-β[44], but MMPs can also degrade the ECM, and as such they can be involved in limiting fibrotic remodelling. However, the removal of established fibrosis destabilises the ECM and can then lead to ventricular dilatation[30]. ROS and the cytokine interleukin (IL)-1 may be implicated in this process by reducing collagen synthesis and increasing MMP activity to promote ECM turnover[45,46].

Interstitial fibrosis negatively impacts the heart by increasing the stiffness of the heart. This contributes to diastolic dysfunction, and disrupts the electrical conductivity of the myocardium, increasing the likelihood of arrhythmias, a cause of sudden cardiac death[47–50]. Perivascular fibrosis also negatively impacts the heart by reducing the maximal coronary blood flow[22,51], and by increasing the oxygen diffusion distance, resulting in impaired oxygen supply to cardiac myocytes[52]. Although the deposition of fibrosis contributes to cardiac dysfunction, collagen degradation in the failing heart is associated with dilatation[47], indicating that the loss of established fibrotic remodelling is also pathogenic. This suggests that as cardiac diseases progress, established fibrosis may be beneficial in preventing ventricular dilatation.

1.1.2.3. Remodelling and the cardiac microvasculature

In the heart, vascular dysfunction can occur within the macrovasculature (i.e. larger vessels such as arteries and arterioles) or in the microvasculature (i.e. capillaries). Macrovascular dysfunction occurs due to vascular stiffening caused by perivascular fibrosis, inflammation, vascular calcification and impaired vasorelaxation[53,54]. In comparison, dysfunction in the microvasculature includes increased capillary permeability, perturbed angiogenesis, and capillary rarefaction (i.e. reduced capillary density). Whilst the macrovasculature influences cardiac function by controlling the blood supply to the heart, the microvasculature influences cardiac function by communicating with the constituent cells of the myocardium, resulting in the alteration of cardiac contractility and changes to cardiac remodelling processes[55].

As the infiltration of inflammatory cells from the circulatory system frequently underpins cardiac fibrosis, the modulation of vascular permeability by the cardiac endothelium can promote fibrotic remodelling. Indeed, increased vascular permeability is associated with cardiac damage in hypertensive patients[56–59], and cytokines released from activated inflammatory cells initiate the activation of myocardial fibroblasts[60]. However, increased capillary wall permeability alone is not sufficient to recruit inflammatory cells, and damaged cardiac myocytes are required to recruit inflammatory cells[61,62].

Capillary rarefaction may result in inadequate perfusion and ischaemia, and has been observed in pathological cardiac hypertrophy[63]. In contrast, adaptive cardiac hypertrophy is associated with a proportional increase in the number of capillaries[63]. Capillary rarefaction may be a product of impaired angiogenesis (the formation of new blood vessels) alongside inflammation, loss of pericytes (cells which wrap around capillaries with several functions including, control of capillary blood flow and vessel development and maintenance[64]), and reduced perfusion (which drives EC death)[65]. Although human hypertension is associated with peripheral capillary rarefaction[66,67], it has not been confirmed whether this also occurs in the heart. Despite this, coronary microvascular rarefaction has been observed in HFpEF patients and individuals with LVH, both of which are associated with hypertension[68].

1.1.3. Pre-clinical models of HHD

Pre-clinical animal models of hypertension recapitulate the disease phenotype to improve understanding of the underlying causes of hypertension and allow the assessment of potential therapeutics which may ameliorate disease progression. In preclinical models of systemic hypertension, multiple organ systems are affected, as in human hypertension, including the heart and the vasculature[69,70]. As such, these models are useful for studying the mechanisms surrounding hypertensive organ damage, including HHD. Rodents are commonly used to

investigate the pathogenesis of hypertension and cardiac remodelling, as they have several advantages over larger animals, namely, they are cost effective, have short gestation periods and lifespans compared with larger mammals, and have tractability for genetic manipulation[71]. An overview of the commonly used pharmacological model of AngII-induced hypertension, and the spontaneously hypertensive rat (SHR), a genetic model of hypertension, are presented below.

1.1.3.1. AngII-induced hypertension

AngII infusion is a common model of hypertension which simulates both pressure overload and neurohormonal involvement. In AngII-induced hypertensive mice, the level of blood pressure elevation is similar to that observed in stage 2 hypertension (blood pressure ≥160/100 mmHg) in patients[71]. Typical AngII doses used for long-term infusion include the slow-pressor dose 400 ng/kg/min, intermediate doses of 490-500 ng/kg/min, and the high dose of 1000 ng/kg/min[71]. Using a dose of 0.8 mg/kg/d, AngII-induced hypertension is established within 24 h of infusion starting, and cardiac output is maintained. Any cardiac changes are reflective of an acute response to hypertension at this phase[72]. At 7 d of continuous infusion of AngII (0.8 mg/kg/d) cardiac and myocyte hypertrophy and fibrosis are observed as the heart adapts to hypertension[72]. At 14 d of continuous AngII (0.8 mg/kg/d) infusion, remodelling becomes more severe and there is a high risk of cardiovascular events occurring, including aortic aneurisms, strokes and cardiac arrythmzias[72].

1.1.3.2. Spontaneously hypertensive rat

The SHR model is the most commonly used genetic model of hypertension[71]. It was developed in 1963 by breeding a hypertensive male rat (blood pressure 150-170 mmHg) and a less hypertensive female rat (blood pressure 130-140 mmHg). Subsequent brother-sister mating established the hypertensive trait, and this model has been useful for identifying genetic loci which confer a predisposition to hypertension[73]. SHRs start to develop increased blood pressure at 6-7 weeks of age, have a stable level of hypertension by 17-19 weeks[73,74]. LVH may begin to develop between 10 and 17 weeks, with compensated LVH apparent at 12 months[75,76]. Generalised fibrosis is observed from 27 weeks, with pronounced fibrosis occurring at 12 months[77]. Transition to HF begins to occur at 20 months, and SHRs in HF display elevated myocardial stiffness and fibrosis compared with non-failing SHRs and WKYs[76,78]. Since SHRs develop hypertension and cardiac remodelling more gradually than other models, they are a good model for essential hypertension, as the onset of hypertension and end organ damage in patients with essential hypertension occurs over a prolonged period.

1.2. The endothelium is dysfunctional in hypertension

1.2.1. Perturbed EC function in the hypertensive heart

Although the most well-studied endothelial function is the control of vascular tone (the degree of constriction of a blood vessel), the endothelium has several other roles, including the regulation of haemostasis following injury, inflammatory cell adhesion and vessel permeability, and angiogenesis[79]. These processes are summarised in Figure 1.2, and are impaired in several diseases states, including hypertension[79–81]. In the hypertensive heart there is also evidence that these functions are dysregulated, with the exception of regulation of haemostasis, which may be dysregulated systemically. The underlying causes of impaired EC function are complex, but oxidative stress and increased ROS production have been implicated.

1.2.1.1. Vascular tone

In large vessels, the endothelium regulates vascular tone through the release of vasoactive compounds which constrict or dilate the surrounding vascular smooth muscle to control blood flow. The vasoactive compounds secreted include vasodilators, such as nitric oxide (NO) and prostacyclin, and vasoconstrictors, such as endothelin-1 and thromboxane[82]. Endothelial dysfunction occurs when there is a deficit in the vasodilatory response to stimuli, primarily caused by impaired bioavailability of endothelium-derived NO. This results in a decreased lumen diameter, restricted blood flow and can contribute to raised blood pressure[79]. The heart is no different despite perfusion occurring during diastole. Endothelial dysfunction in hypertension is well established, and is associated with worse outcomes for hypertensive patients[79,83,84].

1.2.1.2. Inflammatory cell infiltration

Through controlling inflammatory cell adhesion and vessel permeability, ECs regulate tissue inflammation. Following tissue injury or infection, activated ECs secrete pro-inflammatory cytokines and chemokines, attracting and activating leukocytes. Leukocyte adhesion is promoted by P-selectin and E-selectin on activated ECs, whilst immune cell transmigration through the endothelium is promoted by CD31, vascular cell adhesion modelule-1 (VCAM-1) and intercellular adhesion molecule-1 (ICAM-1)[85].

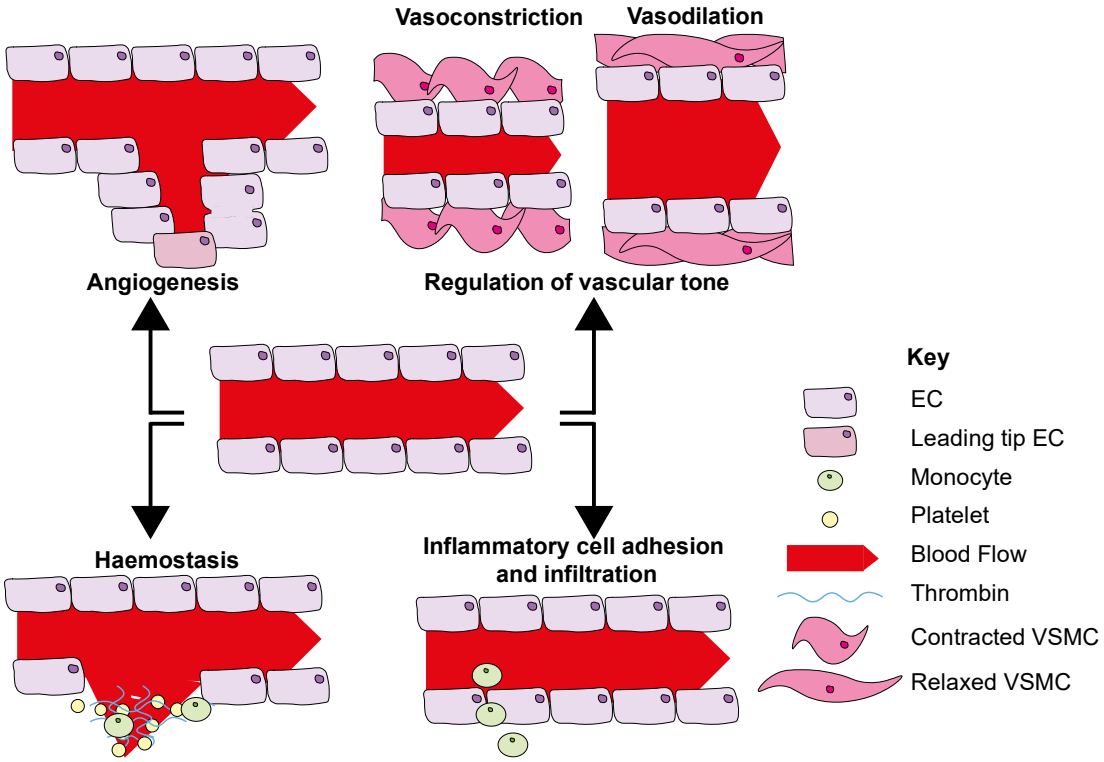

Figure 1.2. Functions of the endothelium.
The endothelium has essential roles in: angiogenesis, where quiescent ECs re-enter the cell cycle to proliferate, migrate and differentiate to form new blood vessels; the regulation of vascular tone, by the release of vasoactive substances; haemostasis, where activated ECs produce procoagulant factors to initiate clotting; and in inflammation, where ECs facilitate monocyte adhesion and infiltration into tissues.

Cardiac inflammation has been observed in both HFpEF, HHD, and in hypertensive pre-clinical models. Endomyocardial biopsy samples from HFpEF patients exhibited elevated CD3+, CD11+ and CD45+ cells alongside increased VCAM-1 expression[86], whilst cardiac tissue from human HHD cases and a mouse model of AngII-induced hypertension had a greater number of CD45+ cells[72]. Despite this, the involvement of cardiac microvascular ECs in cardiac inflammation in hypertension has not been fully characterised. However, inflammation in the vessel wall may be a key step in the pathogenesis of hypertension; blood pressure could be reduced in hypertensive mice by the attenuation of inflammatory cell influx into vessels. Deoxycorticosterone acetate/salt-induced hypertension and AngII-induced hypertension have both been attenuated by limiting the infiltration of macrophages into the aortic wall[87,88]. These studies indicate vessel inflammation contributes to hypertension; however, the direct endothelial involvement is unclear.

1.2.1.3. Angiogenesis and capillary rarefaction

Small arteries (150-300 μm) and arterioles (10-150 μm) are key determinants of peripheral resistance. By constricting or dilating they alter the vascular resistance present in the circulatory system, which influences blood pressure. However, microvascular capillaries also

affect resistance; capillary rarefaction (i.e. the loss of capillary density, due to vessel constriction and lack of perfusion) can increase blood pressure through increased peripheral resistance[89]. In the healthy microvasculature, capillary density is maintained by a balance between rarefaction and de novo angiogenesis. However, in hypertension this balance is perturbed. One study found hypertensive patients had decreased serum levels of the pro-angiogenic factors, angiogenin and basic fibroblast growth factor, whilst the concentration of anti-angiogenic endostatin was elevated[90]. Furthermore, patients with essential hypertension exhibited capillary rarefaction[66], and myocardial capillary density was reduced by 18% in AngII-treated rats, and was also significantly reduced in the SHR model[91,92].

Rodent models have indicated that capillary density may influence the balance between adaptive and pathological cardiac remodelling. Transgenic mice expressing activated AKT, exhibited initial adaptive cardiac hypertrophy, whilst progression to dilatation was associated with reduced capillary density[93]. In this model, inhibition of angiogenesis during the adaptive phase resulted in not only reduced capillary density, but also in impaired cardiac hypertrophy and promoted contractile dysfunction[93]. Another study found the initial hypertrophic response to transverse aortic constriction (TAC) (a common surgical model of pressure overload where aortic ligation limits left ventricular outflow creating pressure overload in the LV, with LVH and fibrotic remodelling observable at 7 d[94]), was associated with increased capillary density which was dependent on hypoxia-inducible factor (HIF)-1-dependent induction of angiogenic factors. Sustained pressure overload inhibited HIF-1, resulting in impaired cardiac angiogenesis, whilst treatment with angiogenic factors increased the number of cardiac vessels, promoted hypertrophy and improved cardiac function[95]. Furthermore, TAC-treated mice, administered with a decoy vascular endothelial growth factor (VEGF) receptor, exhibited reduced capillary density, reduced cardiac hypertrophy and contractile function, whilst ventricle dilatation and fibrotic remodelling were promoted[96]. Thus, angiogenesis can promote adaptive cardiac remodelling to preserve cardiac function in response to pathological stimuli.

1.2.1.4. Cardiac EC-myocyte communication

ECs sense and respond to changes in their environment. This has been most well studied in arteries and large arterioles, where shear stress promotes NO production and release from the endothelium, causing vasodilation of the surrounding vascular smooth muscle cells (VSMCs)[82]. In contrast, cardiac microvascular ECs are not affected by shear stress as flow rates are much lower in the microcirculation, but are subjected to other mechanical stressors including cyclical stretch, compression and load-dependent strain[55]. These stressors may also promote NO production in ECs, which may promote the relaxation of cardiac myocytes during diastole[97]. Mechanistically, NO activates cardiac myocyte guanyl cyclase, catalysing cyclic guanosine monophosphate (cGMP) production and activation of protein kinase G (PKG)[98].

PKG phosphorylates the “massive” sarcomeric protein, titin, which improves the compliance of the protein, thus contributing to the relaxation of cardiac myocytes[99].

In response to the activation of receptors for metabolites, neurohormonal factors, cytokines and growth factor, cardiac ECs can communicate with cardiac myocytes through the secretion of peptides and proteins which act in a paracrine fashion[55]. Of the EC secretome, the most well studied constituents are neuregulin and endothelin-1. Neuregulin is expressed by cardiac ECs in response to hypoxia-reoxygenation and binds to Erb-b2 receptor tyrosine kinases on cardiac myocytes, where it promotes myocyte survival[100], whilst endothelin-1 is known to modulate cardiac myocyte contractility and hypertrophy[101]. However, other proteins secreted by ECs which can influence cardiac function include thrombospondins (TSPs), apelin, periostin, and adrenomedullin[55,102–104]. Despite this, the full extent of the cardiac EC secretome is incompletely defined: there may be additional peptides which influence cardiac myocyte function; the mechanism of peptide synthesis and secretion from the initial stimuli is not well understood; and EC-derived proteins may target not only cardiac myocytes, but also cardiac fibroblasts. Furthermore there is likely to be crosstalk between EC-secreted proteins which may oppose or enhance one another[55]. Consequently, to better understand how cardiac remodelling processes are regulated, the communication between ECs, cardiac myocytes and fibroblasts must be taken into consideration.

1.2.2. ROS promote endothelial dysfunction

Endothelial dysfunction is associated with cardiovascular diseases including hypertension, coronary artery disease, peripheral vascular disease, and HF. It is widely accepted that an imbalance between ROS and antioxidant defence mechanisms are the primary cause of this phenomena[105]. ROS, such as superoxide and hydrogen peroxide (H_2O_2), are unstable oxygen-containing molecules produced either during cellular metabolism or by ROS producing enzymes. Endogenous antioxidants, such as glutathione peroxidase, superoxide dismutase (SOD), and catalase, catalyse ROS breakdown.

When there is equilibrium between ROS and antioxidants, ROS contribute to localised signalling by modification of protein function by oxidation of redox-sensitive thiol groups such as cysteine residues, and iron-sulphur clusters. This is termed redox signalling[106]. Only cysteines with favourable kinetics, such as those ionised into the thiolate form, will react, and signalling tends to occur at the source of ROS production, due to rapid break down of ROS by enzymatic antioxidants (e.g. SOD, catalase and glutathione peroxidase)[107]. Oxidation of cysteines promotes disulphide bond formation, which can alter protein function. For example, the activity of the redox-sensitive protein apoptosis signal-regulating kinase-1 (ASK1) is promoted by oxidation. This can occur by two mechanisms. Firstly, H_2O_2 can promote

oxidation of cysteine residues and disulphide bond formation within thioredoxin, an inhibitory cofactor of ASK1. Thioredoxin is then released and ASK1 is activated. Secondly, oxidation of cysteine residues within ASK1 and subsequent disulphide bond formation can promote dimerization and activation of ASK1 monomers[108]. In contrast, in other proteins, such as phosphatase and tensin homolog, oxidation of cysteine residues and disulphide bond formation is inhibitory, although it can be reversed through reduction by thioredoxin[109].

When the balance between ROS and endogenous antioxidants is tilted in favour of ROS, oxidative stress occurs. Oxidative stress is observed in pathological settings and is associated with DNA, protein and lipid damage, and upregulation of stress responsive pathways, such as the stress-regulated mitogen-activated protein kinase (MAPK) pathways; c-Jun N-terminal kinase (JNK) and p38-MAPK. Following oxidative stress, these pathways regulate cell survival by promoting cellular adaptation, or they control cell death[110].

Hypertension is associated with increased vascular ROS, which may promote endothelial dysfunction through the disruption of NO synthesis[111]. NO production is catalysed by eNOS, a dimeric protein which synthesises NO from L-arginine. The active site of eNOS contains two molecules of the co-factor tetrahydrobiopterin (BH4), which stabilise the eNOS monomers and contribute to L-arginine oxidation during the initial step of NO production. Oxidation of BH4 to dihydrobiopterin (BH2) results in eNOS uncoupling; eNOS dimers are destabilised and electron transfer becomes uncoupled from L-arginine oxidation, and instead of NO production, molecular oxygen is reduced to superoxide[112]. The cessation of NO production and initiation of superoxide production has the dual effect of limiting NO-dependent vasodilation and increasing the oxidative burden, promoting further eNOS-uncoupling.

1.3. TSP1–CD47 signalling in the hypertensive heart

The development of hypertension may be promoted by impaired endothelial function, including a constricted, pro-inflammatory vascular phenotype, and perturbed angiogenesis. In the heart, dysregulated EC function contributes to impaired EC-myocyte communication, which can perturb cardiac myocyte compliance, contractility, survival, and hypertrophy. The matricellular protein thrombospondin 1 (TSP1), influences EC functions including haemostasis and inflammatory cell adhesion and infiltration. By activating the CD47 receptor, TSP1 predisposes the vasculature to a constricted tone and inhibits angiogenesis. Furthermore, TSP1 can influence cardiac remodelling independently of its effects on the endothelium; TSP1 can promote cardiac fibrosis, by activating TGFβ[113], and TSP1-CD47 signalling has been

implicated in cardiac myocyte hypertrophy[114]. The impact of TSP1 and CD47 on endothelial function and cardiac remodelling are discussed below.

1.3.1. TSP1 and CD47: Expression, structure, and binding partners

1.3.1.1. TSP1

The thrombospondin (TSP) family consists of TSP1, TSP2, TSP3, TSP4 and cartilage oligomeric matrix protein (COMP)/TSP5, which are conserved matricellular proteins (a non-structural component of the ECM which modulates cell function and behaviour). TSP1 is a potent anti-angiogenic protein which also has functions in fibrotic remodelling, inflammation resolution and platelet aggregation, and is the most well studied in the context of the cardiovascular system. TSP2 also has anti-angiogenic properties, whilst TSP4 is pro-angiogenic, reduces fibrosis and may have some structural functions in the ECM, whereas COMP is primarily expressed in cartilage[115,116]. Many nucleated cell types express TSP1, including ECs, VSMCs, fibroblasts, and macrophages, and TSP1 is also found in platelets. TSP1 expression is promoted by AngII, hypoxia and glucose[117–121], alongside the transcription factor, c-Jun, the growth factor, fibroblast growth factor 2, and the cytokine, TGF-β[122,123]. Repression of TSP1 expression can occur from hepatocyte growth factor via activating transcription factor 1[124].

TSP1 is a multidomain protein, and each domain binds to multiple ligands and receptors[125,126]. These domains and their binding partners are displayed in Figure 1.3A. Following transcription from the *THBS1* gene, and translation, mature TSP1 is secreted in trimeric form, which is stabilised by inter-subunit cystines in the coiled-coil (CC) oligomerisation domain adjacent to the N-terminal domain (Figure 1.3A-B)[125]. Of the TSP1 binding partners, CD47 and CD36 are the most well described and participate in haemostasis, angiogenesis, and inflammation[127].

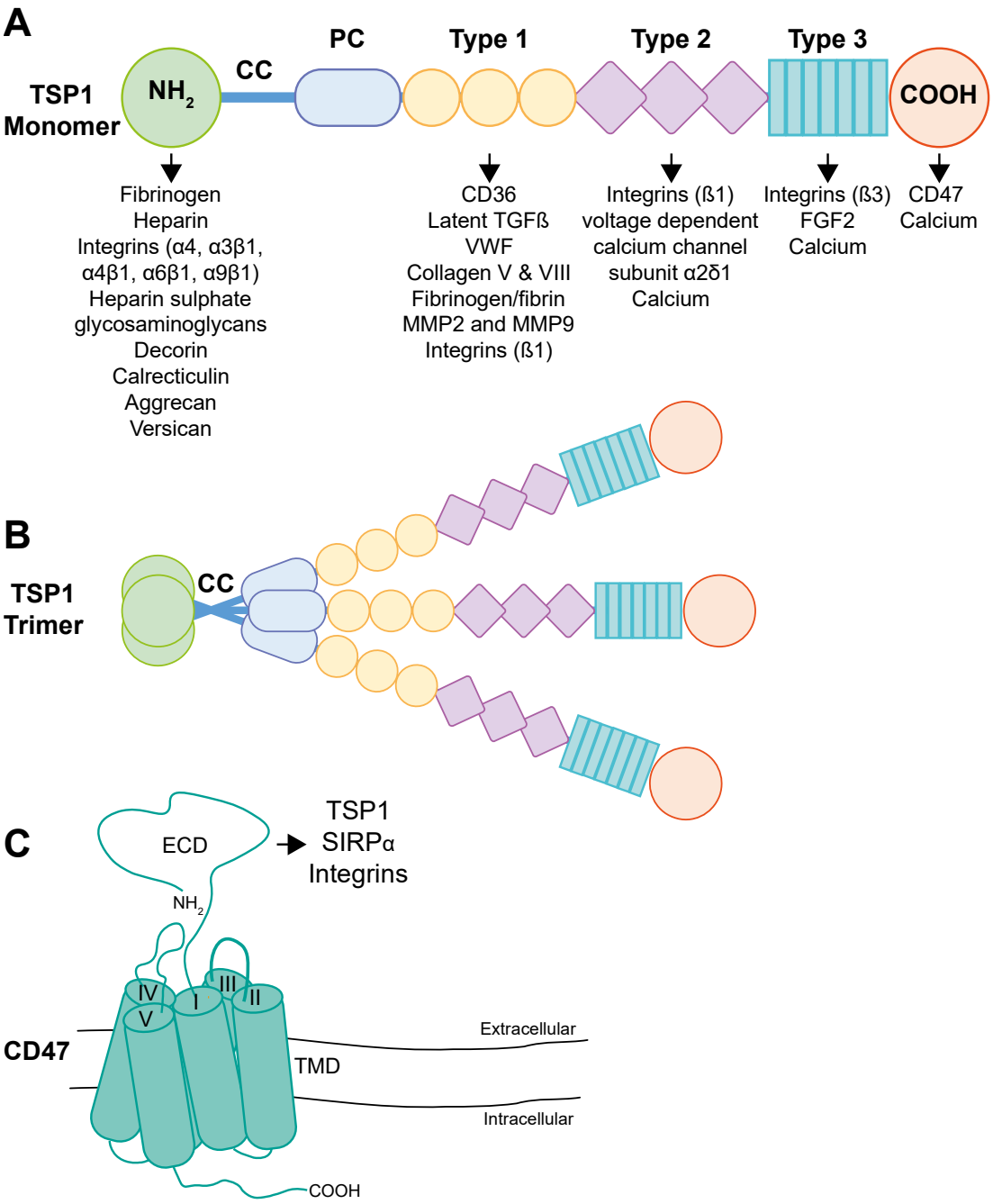

Figure 1.3. Structure and binding partners of TSP1 and CD47.
(**A**) Monomeric TSP1 contains multiple domains; the N terminal domain, a coiled-coil (CC) domain, a procollagen homology domain (PC), three TSP type 1 domains, three TSP type 2 domains (also known as epidermal growth factor-like domains), seven TSP type 3 repeats, and the C-terminal domain[125]. The multi domain structure of TSP1 allows interactions with multiple binding partners, which are listed beneath their binding domain. Image adapted from[126]. (**B**) TSP1 monomers oligomerise into an active trimer via the CC domain. Image adapted from[128]. (**C**) CD47 is a transmembrane receptor, with five alpha helices (I-V) forming the transmembrane domain (TMD), and an N-terminal IgV-like extracellular domain (ECD). The most well described CD47 ligands are TSP1, SIRPα, and integrins. Image adapted from[129].

1.3.1.2. CD47

CD47, also known as integrin associated protein, is an ubiquitous membrane protein, which has been studied in the context of cancer, cardiovascular disease, immune regulation, ageing, and cellular stress. Structurally, CD47 consists of a heavily-glycosylated N-terminal IgV-like extracellular domain, a transmembrane domain consisting of five alpha helices and a small C-terminal domain (Figure 1.3C)[129]. CD47 is known to interact with TSP1, SIRPα and integrins. Intracellular signalling following the interaction and binding of TSP1 to CD47, hereafter referred to as CD47 activation, may be mediated by direct cytoplasmic signalling or by indirect signalling through lateral associations with integrins, VEGFR2, CD36 and FAS[130]. In cancer, CD47 overexpression promotes evasion of the immune system to enhance tumour survival[131]. This occurs through the interaction between CD47 and signal regulatory protein α (SIRPα) which regulates self-recognition, preventing cellular clearance by macrophages[132]. However, in the vasculature, the TSP1-CD47 interaction has been better studied, due to its role in limiting NO production[133,134].

1.3.2. Functions of TSP1-CD47 signalling in the vasculature

1.3.2.1. Regulation of vascular tone

Activation of CD47 by TSP1 predisposes vessels to a constrictive tone, by preventing the phosphorylation of the activating residue of eNOS, Ser^{1177}, thus inhibiting eNOS activation. In VSMCs, reduced NO levels limits the activation of NO-stimulated soluble guanylate cyclase and subsequent cGMP production, preventing vasorelaxation, and predisposing vessels to a constrictive vascular tone[135]. Indeed, TSP1-null vessels exhibited greater endothelial-dependent vasorelaxation, and reduced vasoconstriction following acetylcholine treatment[135]. Furthermore, TSP1-null and CD47-null mice exhibited a greater decrease in mean arterial blood pressure than wild-type mice following treatment with an exogenous NO donor molecule[136]. These studies highlight the pro-vasoconstrictive nature of TSP1-CD47 signalling *in vitro* and *in vivo*.

1.3.2.2. Angiogenesis

The anti-angiogenic properties of TSP1 can be mediated by CD47 and/or CD36. However, although CD36 is sufficient for inhibition of NO-induced angiogenesis, it is not necessary, whilst CD47 is both necessary and sufficient[134]. Primarily, TSP1 inhibits angiogenesis by attenuating VEGF signalling. VEGF promotes angiogenesis by phosphorylation of vascular endothelial growth factor receptor 2 (VEGFR2), and subsequent activation of phosphatidylinositol-3-kinase and AKT, which phosphorylates eNOS at the activating site Ser^{1177} [137,138]. Activated VEGFR2 can also recruit Src to induce Ca^{2+} signalling, further activating eNOS[139]. Ligation of CD47 with TSP1 disrupts the constitutive association between

CD47 and VEGFR2, inhibiting VEGFR2 signalling and preventing enhanced activation of eNOS[140–142]. Additionally, TSP1 can inhibit angiogenesis by directly binding to VEGF and by displacing VEGF from EC heparin sulphate[143]. By limiting NO production, soluble guanylyl cyclase is not activated, which limits cGMP production, preventing PKG activation and inhibiting angiogenesis[144,145]. Indeed, TSP1-null mice exhibited greater cardiac capillary density and were associated with greater levels of VEGF[146], and, following ischaemia, they exhibited enhanced angiogenesis and tissue survival[147]. However, blockade of TSP1-CD47 signalling is more likely to modulate immediate tissue survival by promoting vasodilation and therefore perfusion[148,149].

1.3.2.3. Inflammation

Inflammation occurs following tissue injury and protects damaged tissues by initiating an immune response. However, if prolonged, inflammation becomes chronic and is characterised by pathophysiological processes such as persistent macrophage infiltration, fibroblast proliferation and fibrotic remodelling, which results in further tissue damage[150]. As such, it is essential that inflammation is resolved effectively. TSP1 modulates the inflammatory response by promoting physiological inflammation and its attenuation.

TSP1 mediates physiological inflammation by promoting the adhesion and migration of monocytic cells to the endothelium, and allows macrophage infiltration into tissues, which are essential for the repair of damaged tissue[151]. The interaction of TSP1 with endothelial CD47 upregulates VCAM-1 and ICAM-1 expression thus enhancing monocyte attachment[152], whilst inhibition of endothelial NO synthesis by TSP1 promotes phosphorylation of ICAM-1 by Src, rapidly increasing leukocyte adhesion[153,154]. Furthermore, CD47 promotes neutrophil transmigration across cell monolayers[155]. In addition to promoting physiological inflammation, TSP1-CD47 signalling limits chronic inflammation by increasing the tolerance (i.e. the state of the unresponsiveness of immune cells to antigens) of dendritic cells[156], and by promoting the activation of regulatory T-cells, dampening the immune response[157].

TSP1 and CD47 also participate in inflammation resolution by promoting the clearance of apoptotic immune cells by macrophages. TSP1-CD47 signalling induces T-cell apoptosis independently of caspase activation and cytochrome C release[158,159]. Indeed, in the absence of TSP1-CD47-induced T-cell apoptosis, inflammation is prolonged[160]. However, TSP1 and CD47 can also act independently of one another to promote cell clearance. TSP1 promotes macrophage activation via its interaction with CD36, inducing the expression and activation of toll-like receptor 4, and subsequent nuclear factor kappa B (NF-κB) activation, which is a hallmark of macrophage activation[161]. In contrast, reduced CD47 expression on the surface apoptotic neutrophils promotes their uptake by macrophages, which is likely to be SIRPα

dependent[162]. This is attributable to the role of CD47 in promoting self-recognition. CD47 functions as a potent 'don't-eat-me' signal, preventing phagocytosis by SIRPα expressing macrophages[163,164]. Mechanistically, the CD47-SIRPα interaction initiates a dephosphorylation cascade, directed at phospho-tyrosine in myosin, resulting in myosin inhibition and prevention of contractile engulfment[165]. As such, dying cells with reduced CD47 expression cannot prevent their engulfment and are cleared by macrophages[166].

1.3.2.4. Fibrosis

Physiological fibrosis occurs during the process of wound healing. Pro-inflammatory cytokines such as TGF-β, platelet-derived growth factor, IL-4, IL-1β, and tumour necrosis factor-α stimulate the differentiation of myofibroblasts from fibroblasts[167]. Myofibroblast activation is essential for wound healing by restoring the damaged ECM and initiating wound contraction. However, during chronic inflammation, prolonged myofibroblast activation results in excessive ECM deposition and adverse fibrotic remodelling[167]. TSP1 has a dual function, promoting myofibroblast differentiation by activating TGF-β, and contributing to the attenuation of fibrotic remodelling by inducing fibroblast apoptosis.

TGF-β is kept in its latent form by associating with the LAP. However, upon TSP1 binding to the LAP, TGF-β becomes active and can interact with its receptors to mediate wound healing, ECM formation, cell proliferation, and the immune response[31,168]. As such, TSP1-null mice exhibited reduced TGF-β activation during wound healing, with a delay to macrophage recruitment and capillary angiogenesis and prolonged inflammation[169].

An *in vitro* study indicated that TSP1 secreted by apoptotic fibroblasts induces their clearance during the resolution of wound healing. The secreted TSP1 interacts with CD36 to promote macrophage recruitment and their engulfment[170]. However, *in vivo* studies of chronic diseases characterised by fibrosis did not support this, as the role of TSP1 in promoting fibrosis appears more important. TSP1 expression was found to be elevated in alcoholic cirrhosis and non-alcoholic steatohepatitis (NASH) cirrhosis, and in a mouse model of liver fibrosis[171] Furthermore, in a mouse model of NASH, TSP1 deficiency limited liver fibrosis, confirming the pro-fibrotic role of TSP1[172].

1.3.2.5. Oxidative stress

Although TSP1 can inhibit eNOS activation by preventing VEGF signalling, TSP1 can also inhibit eNOS by interacting with CD47 or CD36 which stimulates ROS production, leading to oxidation of the BH4 cofactors and uncoupling of eNOS dimers, preventing NO production and further promoting superoxide production[112]. TSP1-CD47 signalling activates phospholipase C

catalysed biosynthesis of diacyl glycerol, which stimulates protein kinase C (PKC) activation. PKC can then phosphorylate the nicotinamide adenine dinucleotide phosphate (NADPH) oxidase (NOX) core subunit $p47^{phox}$, resulting in overactivation and enhanced ROS production[173]. In human pulmonary artery endothelial cells (HPAECs), TSP1 promoted the production of superoxide and hydrogen peroxide[174], and TSP1-CD47 signalling promoted NOX1 activation and ROS production, causing endothelial senescence[175]. Another study found TSP1-CD47 promoted ROS production from NOX1 in VSMCs, which impaired the *ex vivo* vasodilation of mouse arteries[173]. However, another study demonstrated that activation of SIRPα by TSP1 in VSMCs also promoted phosphorylation of $p47^{phox}$, NOX1 activation and subsequent superoxide production, which also impaired vasodilation ex-vivo[176]. Mechanistically, activation of SIRPα by TSP1 caused phosphatidylinositol-3-kinase-dependent Rac1 recruitment to Nox1 resulting in its activation[177]. Interestingly, CD47 is likely to participate in TSP1-SIRPα-induced ROS production, hypothesised to be either via parallel activation of CD47 and SIRPα resulting in crosstalk between the two pathways, or via activation of CD47 with downstream activation of SIRPα[176].

1.3.3. TSP1-CD47 signalling in the heart

Cardiac TSP1 is elevated in conditions associated with cardiac remodelling, including in rodent models of; pressure overload[114,178], MI[123,179] and diabetic cardiomyopathy[113,180]. In contrast, TSP1 levels are decreased in the serum of patients with chronic HF and in LV biopsies from patients with end-stage HF[114,181,182], which may indicate TSP1 influences cardiac remodelling early in the pathogenesis of cardiac diseases. Indeed, rats with AngII-induced hypertension exhibited elevated LV TSP1 mRNA levels at 6 h and at 2 weeks of continuous infusion[183]. In the heart, the induction of TSP1 expression has been linked to the induction of fibrosis and of cardiac myocyte hypertrophy. However, whether this is a physiological response to aid cardiac adaptation to an adverse situation, or whether this is a pathophysiological mechanism which leads to further maladaptive remodelling, lending the heart to decompensation, appears to be context dependent and is elaborated below.

1.3.3.1. Regulation of pathophysiological fibrosis by TSP1-CD47 signalling

TSP1 and CD47 have been implicated in cardiac fibrosis; CD47-null mice exhibited diminished cardiac fibrosis alongside improved contractility[114], and several studies have described the pro-fibrotic role of TSP1 in cardiac fibrosis. Streptozotocin-induced diabetic rats with abdominal aortic banding exhibited elevated blood glucose and blood pressure. In these rats, elevated TSP1 expression contributed to increased TGF-β activity and collagen deposition, alongside reduced cardiac function. Blockade of TGF-β activation using the LSKL peptide (a mimetic of the LAP, which binds TSP1, preventing TSP1 from activating TFGβ) limited interstitial and perivascular fibrosis, and promoted cardiac myocyte hypertrophy, which may

have contributed to improved cardiac function[113]. Furthermore, in a model of kidney failure, downregulation of TSP1 by miR-221 reduced cardiac fibrosis and preserved cardiac function[184]. However, loss of TSP1 in obese diabetic mice promoted systolic dysfunction and LV dilatation[180]. As chamber dilatation was associated with accentuated MMP activity and decreased myocardial collagen content, TSP1 may limit MMP activity, preserving collagen and preventing dilatation[180]. Chamber dilatation and increased MMP activity was also observed in TSP1-null mice at 28 d following TAC[178]. Overall, although TSP1 promotes pathological fibrotic remodelling, following chronic stress, fibrotic remodelling may be essential to preserve ECM integrity and prevent chamber dilatation.

1.3.3.2. Hypertrophy

TSP1 and CD47 may also contribute to the hypertrophic response. As above, in a hypertensive diabetic rat model, blockade of TSP1-TGF-β signalling using the LSKL peptide promoted cardiac myocyte hypertrophy[113]. Whilst, following TAC, CD47-null mice and mice treated with a CD47 antagonist antibody were resistant to cardiac and cardiac myocyte hypertrophy[114]. Interestingly, the two mechanisms of limiting CD47 had different functional effects; CD47-null mice had improved cardiac contractility, whilst blockade of CD47 reduced cardiac stiffness and was associated with reduced cardiac cell apoptosis[114]. The cardiac myocyte hypertrophy exhibited is likely to have been modulated by TSP1-CD47 signalling, because in neonatal rat cardiac myocytes 7N3 (a TSP1-derived, CD47-activating peptide) promoted hypertrophy, which was attenuated by blockade of the CD47 receptor[114].

1.3.3.3. Cardiac angiogenesis

Several studies are in support of TSP1 as an inhibitor of cardiac angiogenesis. Elevated cardiac capillary density was observed in TSP1-null mice[146], diabetes-associated vascular rarefaction was attenuated in obese diabetic TSP1-null mice[180], and in biopsy samples from human cardiac allografts, elevated TSP1 mRNA expression was associated with the development with cardiac allograft vasculopathy, which is characterised by a lack of new vessel formation[185]. However, in both sham-treated and TAC-treated mice, TSP1 deficiency did not alter vascular density[178]. As the pressure overload created by TAC occurs rapidly, there may not be time for angiogenesis to occur in this model as the heart adapts. Therefore, the anti-angiogenic properties of TSP1 may be more apparent in diseases which manifest over a prolonged period.

1.3.3.4. Regulation of TSP1 expression and adverse cardiac remodelling in HF

Cardiac biopsies, taken at the time of transplant from patients with end-stage HF, exhibited lower TSP1 mRNA expression levels than controls, and within the failed hearts, severe

dilatation (left ventricular end-diastolic diameter (LVEDD) >70 mm) was associated with lower TSP1 expression than in hearts with LVEDD <70 mm)[182]. This indicates either TSP1 has a role in protective remodelling, or reduced TSP1 expression promotes cardiac dilatation. Indeed, TSP1-null animals exhibited early hypertrophy and enhanced dilatation following TAC[178]. Interestingly, biopsies from idiopathic cardiomyopathy patients with severely impaired cardiac function exhibited elevated cardiac TSP1 expression compared with young patients with preserved cardiac function[186]. Furthermore, TSP1 expression was increased in aged HF-prone mice, compared with young HF-prone mice, whilst in HF-resistant mice, TSP1 expression decreased as they aged[186]. The conflicting results from these studies may be indicative of the underlying aetiology within the cohorts, as the end-stage HF cohort did not distinguish between ischaemic HF and NI-HF, or may be due to a difference between impaired cardiac function and end-stage HF.

1.4. Adaptive *vs* stress signalling in the hypertensive heart

Cardiac remodelling, such as hypertrophy and fibrosis, are governed by upstream signalling cascades, which can be activated by chronic disease, including hypertension[22], diabetes[187], and chronic kidney disease[188], or after acute injury, such as MI[189]. Cardiac remodelling can be adaptive, promoting survival, or maladaptive, promoting cardiac decompensation and failure[190]. For an adaptive response to occur, the cardiac response must be appropriate for the stimuli/damage. Where perturbed cardiac remodelling occurs, the remodelling processes either are not a beneficial response or occur when adaptive remodelling cannot be maintained and maladaptive remodelling ensues, leading to cardiac failure[190]. The mitogen-active protein kinases (MAPKs) are known mediators of cardiac remodelling, influencing cardiac hypertrophy, fibrosis, angiogenesis, and cell death, by regulating gene transcription or by regulating the function of their cytosolic target proteins[191]. Whether MAPK activation promotes an adaptive or a stress response is determined by the particular kinases activated and the specific transcription factors promoted[191]. Furthermore, ROS also influence cardiac remodelling and can act upstream of the MAPKs[192,193]. Consequently, activation of the MAPKs by ROS may influence adaptive and maladaptive cardiac remodelling processes, which ultimately determine whether the heart is able to adapt to adverse conditions, or whether maladaptation occurs and failure is promoted.

1.4.1. MAPKs and remodelling in the hypertensive heart

The MAPKs are a group of signalling proteins which, when activated, control cell physiology in response to growth and stress stimuli. MAPK activation occurs following activation of G protein-coupled receptors and receptor tyrosine kinases, as well as in response to

environmental stress and ROS[191]. The most prominent members of the MAPK family are extracellular signal regulated kinase (ERK) 1/2, p38-MAPK and JNK. ERK1/2 are pro-growth kinases, which are activated in response to growth factors, cytokines, and serum[194]. They regulate various proliferative functions, including cell cycle progression and proliferation, differentiation, senescence, migration, and cell adhesion[194]. In contrast, p38-MAPK and JNK are stress-regulated kinases, both activated in response to UV radiation, oxidative stress, DNA damage, endoplasmic reticulum stress, cytokines, and pathogens. p38-MAPK can also be activated by growth factors, and can modulate the immune response by regulating cytokine production, cell adhesion, and immune cell function[195–197]. It also regulates cell cycle progression, differentiation, migration, and the balance between survival, apoptosis and senescence[198–200]. JNK can also regulate cytokine production, proliferation, differentiation, apoptosis and cell survival, in addition to actin reorganisation, cell mobility and metabolism[191,201].

MAPKs are activated by a phosphorylation cascade, where receptor activation results in phosphorylation and activation of upstream MAPK kinase kinases ((MAP3Ks), also known as MAPK/ERK kinase kinases (MEKKs)) (e.g. c-Raf, MEKK1-4, ASK1). MAP3Ks then phosphorylate and activate MAPK kinases ((MKKs), also known as MAPK/ERK kinases (MEKs)) (e.g. MEK1/2, MKK3/6, MKK4/7). MKKs then phosphorylate the MAPKs (Figure 1.4). The MAPKs are activated by dual phosphorylation of a Thr-X-Tyr motif in the regulatory loop, where X is Gly, Pro, or Glu[191]. Activation of ERK1 occurs by phosphorylation at Thr202 and Tyr204, whilst for ERK2 the residues are Thr185 and Tyr187. p38-MAPK is activated when phosphorylated at Thr180 and Tyr182, whilst JNK is activated by phosphorylation of Thr183 and Tyr185.

Activated MAPKs alter cell function by phosphorylating effector cytosolic proteins, and by phosphorylating transcription factors, altering gene expression. As regulators of cellular physiology, ERK1/2, p38-MAPK and JNK have been studied in the context of cardiac remodelling, where their activation determines whether adaptive or pathological maladaptive remodelling occurs following encounters with stressors such as TAC and AngII infusion[191,202].

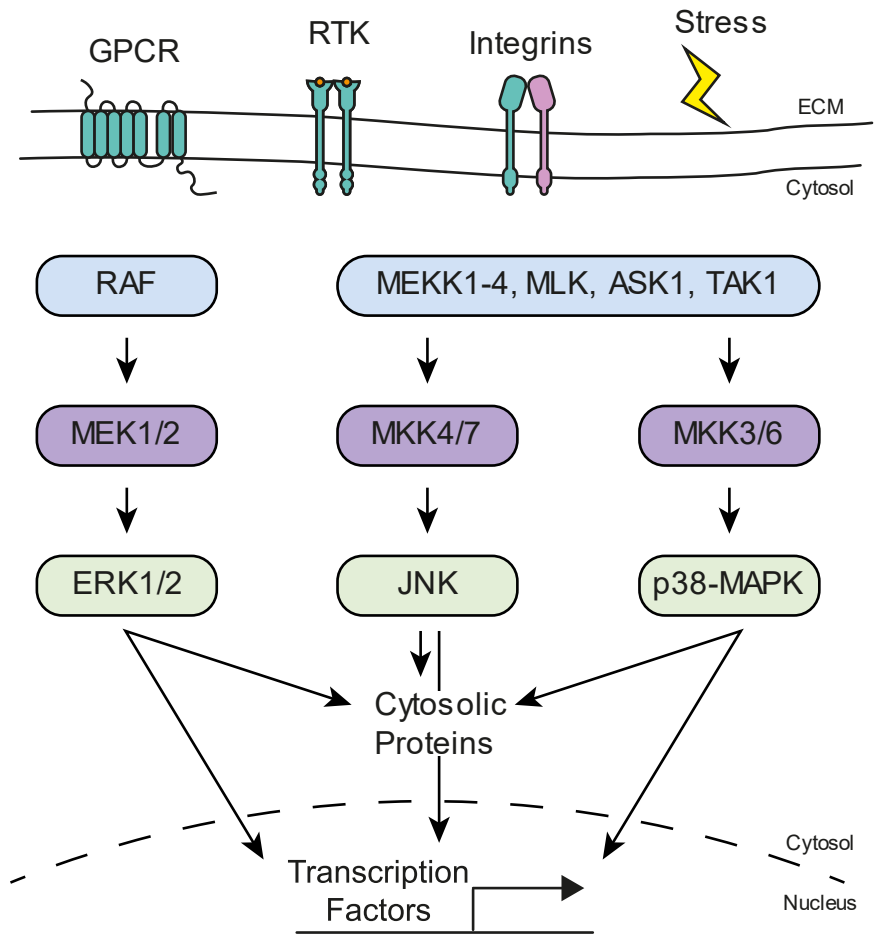

Figure 1.4. MAPK signalling pathways.
MAPKs can be activated by G protein-coupled receptors (GPCRs), receptor tyrosine kinases (RTKs), integrins or stressors such as oxidative stress, osmotic stress, and UV radiation. MAPKKKs (RAF, MEKK1-4, MLK, ASK1, TAK1) are initially activated by phosphorylation, which then phosphorylate MAPKKs (MEK1/2, MKK4/7, MKK3/6), which in turn phosphorylate the MAPKs (ERK1/2, p38-MAPK and JNK). Activated MAPKs phosphorylate cytosolic proteins to alter cell function, or they translocate to the nucleus where they phosphorylate transcription factors, altering gene expression. Image adapted from[191].

1.4.1.1. ERK1/2 and cardiac remodelling

ERK1/2 regulates adaptive hypertrophy in response to pathological stress. Adaptive early concentric remodelling following TAC was associated with elevated ERK1/2 phosphorylation, whilst the transition to late eccentric hypertrophy was associated with reduced ERK1/2 phosphorylation[203]. Other studies have demonstrated that ERK1/2 activation is required for concentric hypertrophy. Cardiac specific expression of dominant-negative c-Raf, a MAP3K which activates MEK1/2 to activate ERK1/2, resulted in attenuation of ERK1/2 activity, impaired the hypertrophic response to TAC, and reduced survival[204]. Furthermore, cardiac myocyte-specific c-Raf knockout mice have displayed eccentric cardiac hypertrophy alongside reduced cardiac function, although cardiac myocyte hypertrophy was not observed[205].

In contrast, transgenic mice expressing constitutively-active ERK1 in cardiac myocytes exhibited cardiac hypertrophy at baseline. Following TAC, although cardiac hypertrophy in these mice was comparable, the transgenic mice exhibited reduced dilatation and fibrosis, and cardiac function was improved[206]. This was also observed in mice overexpressing cardiac Mek1; ERK1/2 activation was greater and mice subsequently developed concentric LVH without interstitial fibrosis, and cardiac function was improved, indicating that cardiac hypertrophy was compensatory[207].

Other studies have used cardiac-specific overexpression of an ERK1/2-selective phosphatase, dual specificity phosphatase (DUSP) 6, to abolish ERK1/2 activation in the heart. This is necessary as ERK2$^{-/-}$ is embryonic lethal and ERK1$^{-/-}$ ERK2$^{+/-}$ is mostly lethal, making studying complete attenuation of ERK1/2 activity difficult. DUSP6 transgenic mice did not exhibit ERK1/2 phosphorylation in response to initial TAC (6 h). However, after prolonged TAC (14 weeks), these transgenic mice exhibited greater cardiac hypertrophy than wild-type mice, although the degree of cardiac myocyte hypertrophy was similar[208]. Despite this, the cardiac function in the DUSP6 transgenic mice was reduced, and hearts from these mice exhibited elevated fibrosis and increased apoptosis following prolonged TAC[208]. It is noteworthy that an ERK1/2 gene deleted model, ERK1$^{-/-}$ ERK2$^{fl/fl\text{-}Nkx\text{-}Cre}$, found ERK1/2-null mice exhibited elevated cardiac hypertrophy in response to co-treatment with AngII and phenylephrine (PE) treatment, with an increased LVEDD which is indicative of dilatation, and reduced cardiac function[209]. PE is an α_1 adrenergic agonist which activates the sympathetic nervous system, and is associated with increased vascular tone and increased cardiac output[210]. Conducting TAC in these ERK1/2-null mice proved lethal, due to their compromised state at baseline[209]. These studies indicate that ERK1/2 contributes to concentric remodelling promoting cardiac adaptation following pressure overload. However, the loss of ERK1/2 does not prevent hypertrophy, but the hypertrophy which develops is associated with cardiac dysfunction. Indeed, activation of ERK1/2 promoted concentric cardiac myocyte hypertrophy, whilst loss of ERK1/2 signalling promoted eccentric hypertrophy[209].

ERK1/2 activation prevents apoptosis in the pressure-overloaded myocardium. Following transition to eccentric hypertrophy and LV dysfunction in response to TAC, ERK1/2 was reduced whilst myocyte apoptosis was elevated[203]. Indeed, cardiac-specific expression of dominant-negative c-Raf, resulted in attenuation of ERK1/2 activity and elevated cardiac myocyte apoptosis was observed in hearts from these transgenic animals[204]. MEK1 transgenic mice, which exhibit elevated ERK1/2 were also partially resistant to apoptosis following ischaemia/reperfusion injury[207], an effect which was lost in ERK2$^{+/-}$ mice[211]. Furthermore, cardiac myocyte-specific c-Raf knockout mice exhibit elevated apoptosis[205].

1.4.1.2. Stress-regulated MAPKs and cardiac remodelling

As previously discussed, maladaptive cardiac remodelling includes eccentric cardiac hypertrophy and dilatation of the cardiac chambers, and interstitial fibrosis. Activation of p38-MAPK and JNK influence these processes, and transgenic and knockout studies have indicated that modulation of these kinases influences the cardiac outcome by modulating hypertrophic, apoptotic, and pro-inflammatory signalling.

Cardiac specific overexpression of activated MKK3 (a MKK which activates p38-MAPK) promoted p38-MAPK activity, which was associated with cardiac fibrosis and biatrial enlargement without LVH or cardiac myocyte hypertrophy. Between 5-7 weeks, mice exhibited signs of congestive HF, with reduced systolic function, reduced LV wall thickness and increased diastolic chamber stiffness. Due to the increase in pathological remodelling, the increased p38-MAPK activation was fatal by 7 weeks[212]. Furthermore, the expression of cardiac-specific dominant negative p38-MAPK or dominant negative MKK3, promoted enhanced cardiac and cardiac myocyte hypertrophy both at baseline and following TAC. In transgenic mice up to 2 months of age, concentric remodelling was promoted, whilst by 4 months, these mice exhibited reduced cardiac function with evidence of dilatation[213]. Despite this, another study found p38-MAPK cardiac-specific knockout mice did not have altered cardiac remodelling at baseline, but following TAC, they exhibited eccentric hypertrophy with interstitial fibrosis, resulting in reduced cardiac function. Interestingly, this was associated with increased cardiac myocyte apoptosis in the p38-MAPK-null mice, with increased JNK activation and activation of MKK3/6[214]. The difference observed between studies may be that a low level of p38-MAPK activation may have anti-apoptotic effects, promoting survival, whilst elevated p38-MAPK activation is pro-apoptotic, promoting cell death[191].

Prolonged inflammation promotes fibrotic remodelling through the differentiation of fibroblasts into myofibroblasts and subsequent ECM deposition. In part, the differentiation of fibroblasts is promoted by TGF-β signalling, which occurs canonically through the SMAD family of transcription factors, and non-canonically by p38-MAPK activation[215]. Indeed, specific deletion of p38-MAPK in cardiac fibroblasts prevented fibroblast to myofibroblast differentiation and reduced cardiac fibrosis following AngII/PE treatment, whilst fibroblast-specific activation of MKK6 promoted p38-MAPK activation and enhanced differentiation into myofibroblasts[216]. At baseline, this was associated with increased interstitial and perivascular fibrosis in multiple organs, including the heart, and following AngII/PE treatment cardiac fibrosis was enhanced[216].

Several studies have indicated JNK activity is upregulated acutely (within 30 min) following pressure overload[217,218219]; however, by 24 h this effect was lost, and JNK activity was

decreased[220]. *In vitro*, activation of JNK promoted cardiac myocyte hypertrophy, whilst attenuation of JNK activity prevented hypertrophy[221,222]. However, cardiac myocyte-specific activation of JNK indicated cardiac hypertrophy is pathological, characterised by induction of foetal genes and contractile dysfunction, and, within 7 weeks following birth, these transgenic mice exhibited congestive HF, resulting in death[223]. However, loss of JNK1 was associated with increased myocyte death and an acute reduction in fractional shortening at 3 d following TAC, indicating loss of cardiac function[224]. Another study found, following TAC, cardiac myocyte-specific loss of JNK activation promoted apoptosis, fibrosis, hypertrophy which resulted in reduced cardiac function[225].

1.4.2. ROS in HHD

1.4.2.1. ROS in cellular physiology

ROS include superoxide, H_2O_2 and peroxynitrites, which can reversibly or irreversibly oxidise proteins, lipids, and DNA. Oxidative stress is a state of elevated intracellular ROS accumulation which is associated with irreversible oxidative damage to cellular molecules. Irreversible oxidation products include; malondialdehyde, a product of lipid peroxidation; 3-nitrotyrosine, an oxidation product formed by peroxynitrite reacting with tyrosine residues; and sulphonic acid which occurs to sulphur containing residues following multiple oxidation steps[226]. In contrast, redox signalling occurs via low levels of localised ROS production and modulates signalling pathways by the reversible oxidation of sulphur containing groups.

ROS production in the cell can occur as a by-product of mitochondrial function or by the professional ROS-producing NOX family of proteins. ROS-induced ROS release can also promote ROS production from enzymes which typically do not produce ROS. As previously described, oxidation of the BH4 dimers of eNOS results in the production of superoxide rather than NO. Furthermore, the reversible oxidation of xanthine oxidoreductase, which converts xanthine into uric acid, causes the enzyme to transition to xanthine oxidase, which still catalases uric acid production but also produces ROS[227]. ROS-induced ROS release also affects the mitochondria. Mitochondrial ROS production occurs as a result of electron leakage from the electron transport chain, which interacts with molecular oxygen to form superoxide. However, under physiological conditions only 0.2-2% of electrons are estimated to leak out[228]. In pathological conditions, ROS can trigger the opening of the mitochondria permeability transition pore, which initiates further production and release of ROS, amplifying the initial signal[229].

As mentioned above, the primary role of the NOX family of proteins is to facilitate ROS production. Of the seven family members, NOX1, 2 and 4 have been most well studied in the cardiovascular system, and are present in multiple cell types, including the endothelium,

VSMCs, cardiac myocytes and fibroblasts[230]. In contrast, NOX3 is primarily expressed in the inner ear, and is not found within the cardiovascular system, and NOX5, although found in the human endothelium and VSMCs, is absent from the rodent genome, making its functions difficult to study *in vivo*[231]. Finally, dual oxidase 1 and 2 are predominantly found in the thyroid and besides their expression in airway epithelia, they have limited expression in other cardiovascular cell types[232,233].

Of the relevant NOXs in the cardiovascular system, NOX1 and 2 produce superoxide and NOX4 produces H_2O_2. NOX2 was the first NOX discovered and was initially described as part of the phagocytic burst in neutrophils and macrophages. Subsequently, its activity has been demonstrated in cardiovascular cell types, including ECs, fibroblasts, cardiac myocytes, and VSMCs[232]. Within the cell, NOX2 has been demonstrated to be found at the lamellipodia leading edge and in redoxisomes (endosomes responsible for early receptor mediated signalling in non-phagocytic cells)[233]. Following the identification of NOX2, NOX1 was subsequently described. NOX1 is most highly expressed in colon epithelium, but is also expressed in VSMCs and ECs alongside other cell types[232]. NOX1 has been reported to be localised to the nucleus, cytoplasm, plasma membrane, endosomes and the endoplasmic reticulum[233–235]. NOX4 was first identified in the kidney and is also found in ECs, fibroblasts and VSMCs. NOX4 is localised to focal adhesions, the endoplasmic reticulum, and the nucleus[232].

Structurally, NOXs contain several conserved regions which are the NADPH binding domain at the C-terminus, a flavin adenine dinucleotide (FAD) binding domain, six conserved transmembrane domains and four highly conserved haem binding histidines[232]. For functionality, NOX2 requires the adaptor proteins, $p47^{phox}$ (the organiser subunit) and $p67^{phox}$ (the activator subunit), alongside $p40^{phox}$ and Rac1. Rac1 is a member of the Rho family of GTPases and can regulate multiple signalling pathways. $p47^{phox}$ contains an auto-inhibitory region, which must be phosphorylated for $p47^{phox}$ activity. When active, $p47^{phox}$ interacts with the conserved membrane adaptor protein, $p22^{phox}$. This interaction promotes the localisation of the activator subunits $p67^{phox}$ which promotes $p40^{phox}$ binding. Finally, Rac1 associates with NOX2 and the complex becomes active[232]. Mechanistically, electron transfer occurs from bound NADPH to FAD, which is regulated by $p67^{phox}$, then to the haem groups where the electron is finally transferred to oxygen to form superoxide[232]. NOX1 also requires the adaptor proteins; NADPH oxidase organiser 1 (NOXO1) (homologous to $p47^{phox}$), NADPH oxidase activator 1 (NOXA1) (homologous to $p67^{phox}$) and Rac1; but once associated, NOX1 is thought to be constitutively active since NOXO1 lacks an autoinhibitory region. However, NOX1 may also act via a non-canonical, hybrid system, where NOX1 associates with $p47^{phox}$ rather than NOXO1[236,237]. As such, this non-canonical pathway has an extra regulatory level, where activity is inducible via $p47^{phox}$ activation. In contrast, NOX4 does not require adaptor proteins,

and is constitutively active. NOX4 produces H_2O_2 rather than superoxide, due to the presence of a histidine residue in the third extracytosolic loop which accelerates spontaneous superoxide dismutation[238]. Figure 1.5 contains a summary of NOX subunit structure and activation.

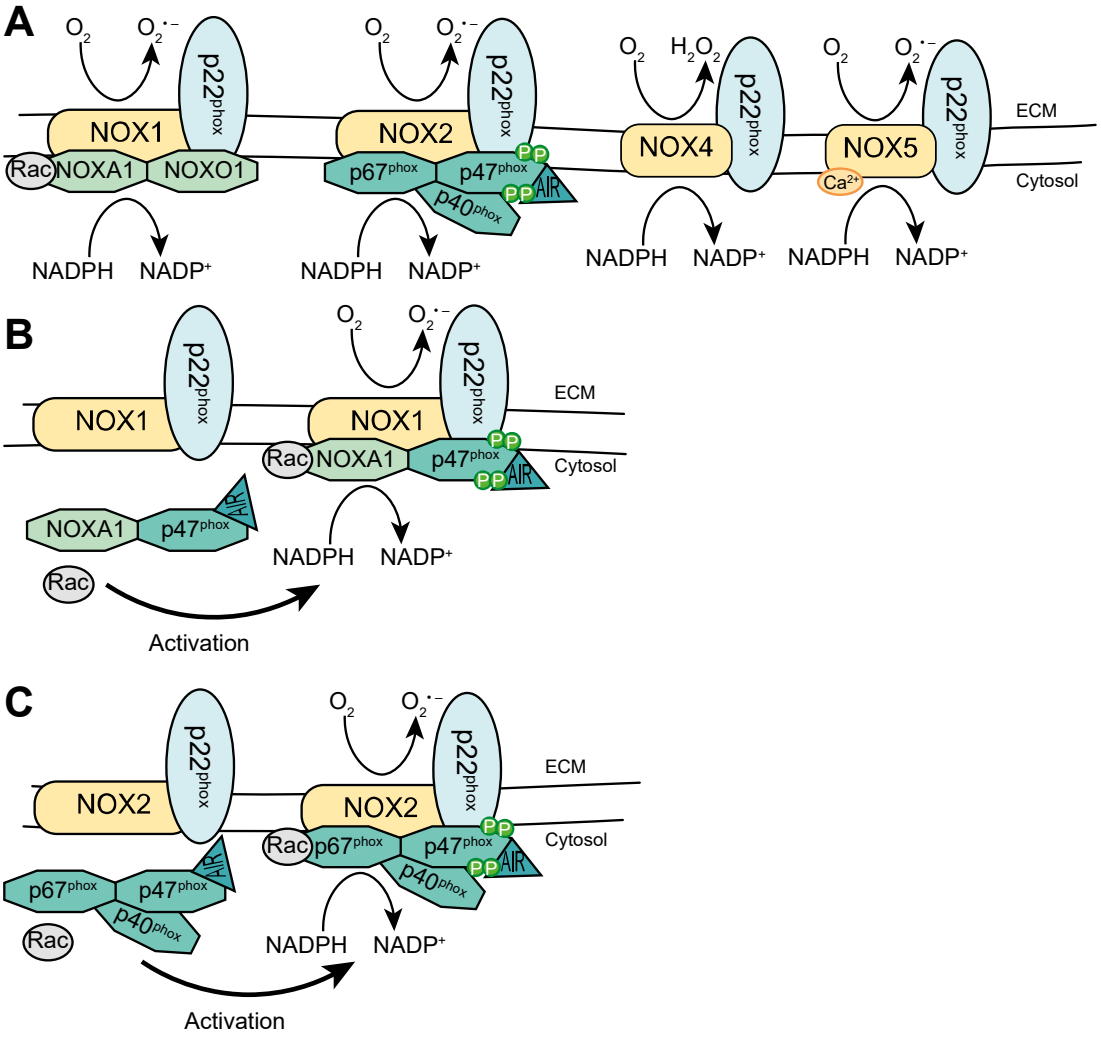

Figure 1.5. NOX subunit structure and activation.
(**A**) Structure of NOXs expressed in cardiovascular system. All NOXs are associated with the transmembrane protein $p22^{phox}$, which is required for activity. NOX1 is also associated with the activator subunit (NOXA1), the organiser subunit (NOXO1) and Rac is canonically active and is associated with NOXA1. NOX2 is associated with $p67^{phox}$ (homologous to NOXA1), $p47^{phox}$ (homologous to NOXO1), $p40^{phox}$ and Rac. $p47^{phox}$ contains an auto-inhibitory region (AIR) and must be phosphorylated to alleviate inhibition by the AIR. NOX4 does not require subunits for activation but produces H_2O_2 rather than superoxide ($O_2^{\bullet -}$). NOX5 does not associate with subunits but is calcium dependent. (**B**) Activation of the non-canonical, hybrid NOX1 system is inducible, as $p47^{phox}$ associates with NOX1 rather than NOXO1. (**C**) For NOX2 activation $p47^{phox}$ must by phosphorylated to relieve inhibition of the AIR, allowing assembly of $p67^{phox}$, $p47^{phox}$ and $p40^{phox}$, which promotes Rac recruitment. Figure adapted from[239,240].

Also contributing to the intracellular redox state are the endogenous antioxidants, SOD, catalase, glutathione peroxidase and peroxiredoxin which rapidly break down ROS into

non-reactive molecules[107]. There are three SOD isoforms: SOD1, which is found throughout the cell; SOD2, which is localised to the mitochondria; and SOD3, which is found in the ECM. All three SOD isoforms catalyse the breakdown of superoxide into H_2O_2 and oxygen, whilst catalase converts H_2O_2 into water[241]. In contrast, glutathione peroxidase and peroxiredoxin reduce oxidised residues by becoming oxidised themselves, and are recycled by the oxidation of glutathione and thioredoxin respectively[107].

1.4.2.2. ROS in hypertension and HF

Several studies have indicated that hypertensive patients exhibit plasma markers of oxidative stress[242,243], and the mechanisms behind oxidative stress in hypertension have been recently reviewed, with NOX, uncoupled eNOS, mitochondrial dysfunction and impaired antioxidant activities all contributing to vascular dysfunction in hypertensive models[53].

Heart failure is also associated with an increased oxidative state. Congestive HF is associated with increased plasma lipid peroxides, a hallmark of systemic oxidative stress[244], and an increased oxidative burden was positively correlated with functional severity of HF in patients[245]. Furthermore, the cardiac expression of the NOX subunits $p22^{phox}$, $p47^{phox}$, $p67^{phox}$ and NOX2 were elevated in human HF and were associated with membrane translocation of $p47^{phox}$, and enhanced malondialdehyde levels[246,247]. In models of experimental MI-induced HF, elevated myocardial 3-nitrotyrosine levels were observed[248], whilst another study found increased lipid peroxidation which was associated with a depressed redox state in cardiac tissue, characterised by reduced/oxidised glutathione ratio and reduced endogenous antioxidant activity[249]. Both hypertension and HF are associated with elevated ROS and oxidative stress, and subsequent studies have implicated ROS as a pathogenic mediator in vascular and cardiac remodelling.

1.4.2.3. ROS production in the cardiovascular system

Several stimuli are known to promote ROS production within the cardiovascular system, including AngII, tumour necrosis factor-α, thrombin, platelet-derived growth factor and IL-1β[250]. ROS production influences cellular signalling by oxidising thiol redox switches in proteins including protein kinase A, PKG, and ASK1, promoting their activation[251–253]. At low levels, ROS regulate physiological signalling, promoting cellular survival; however, high levels of ROS promote oxidative stress which activates cell death pathways, leading to apoptosis and necrosis[254].

In the cardiovascular system, ROS production is associated with expression and/or activation of the NOXs. In VSMCs, platelet-derived growth factor, prostaglandin $F_{2\alpha}$ and AngII promote

ROS production via NOX1[232]. Prostaglandin $F_{2\alpha}$ induces NOX1 expression by transactivation of the epidermal growth factor receptor and activation of downstream ERK1/2 and phosphatidylinositol-3-kinase pathways, which culminate in the activation of activating transcription factor 1 and induction of NOX1 expression[234]. However, AngII can also induce NOX2, and the ROS produced have been shown to promote activation of p38-MAPK and activating transcription factor 2, causing VSMC hypertrophy[255].

In ECs, NOX1 expression can be induced in response to shear stress, via bone morphogenic protein 4 signalling. The induction of NOX1-ROS by the non-canonical system (using $p47^{phox}$ in lieu of NOXO1) promoted ICAM-1 expression and monocyte adhesion[256]. More recently, TSP1-CD47 signalling and hypoxia has been demonstrated to promote endothelial NOX1 expression[175,257]. However, hypoxia-driven NOX1 expression promoted EC proliferation, whilst TSP1-CD47-induced NOX1 expression promoted endothelial senescence[175,257]. AngII can also promote ROS production in ECs; however, this was found to be due to increased mitochondrial ROS production, which could be inhibited by $p22^{phox}$ deletion[258]. This indicated a member of the NOX family was required for mitochondrial ROS-induced ROS release following AngII treatment[258], which subsequently was demonstrated to be NOX2 in human aortic ECs[259].

1.4.2.4. NOX-induced ROS in cardiac remodelling

AngII-induced cardiac hypertrophy has been demonstrated to be mediated by NOX2-induced ROS production[260], with Rac1 and $p47^{phox}$ critical for this function[261,262]. AngII-induced cardiac hypertrophy was reduced in mice null for Nox2, Rac1 or $p47^{phox}$, demonstrating the essential role of these proteins in the NOX2 complex[260–262]. However, the role of NOX2 is disputed in pressure overload models. Several studies have demonstrated that NOX2 promotes cardiac hypertrophy and dysfunction following TAC; Nox2-null mice were protected against contractile dysfunction[260,263] and Rac1-deficient mice had reduced NOX2 activation and hypertrophy[261]. However, two studies found Nox2-null mice were not protected against cardiac hypertrophy and loss of cardiac function following TAC, and did not exhibit reduced ROS[264,265]. Both studies found upregulation of other NOX subunits; $p22^{phox}$ and $p47^{phox}$[264], and NOX4[265]; indicating another NOX may be compensating for the loss of NOX2.

NOX-induced ROS production can also promote fibrotic remodelling. NOX4 has been implicated in the deposition of fibrosis in response to AngII. Following AngII treatment, NOX4 activated NF-κB and activator protein 1 in cardiac fibroblasts, which induced IL-18 expression and MMP9 activation[266]. In turn, this mediated the proliferation and migration of cardiac fibroblasts[266]. Furthermore, the differentiation of fibroblasts to activated myofibroblasts by TGF-β is mediated by NOX4[267]. Despite the pro-fibrotic effects of NOX4, *in vivo*, NOX2

deficiency was sufficient to reduce interstitial fibrosis following TAC[263] and AngII infusion[260]. As previous studies have indicated NOX2 expression is negligible in cardiac fibroblasts, this effect may be mediated by paracrine effects of neighbouring cells[267].

1.4.2.5. NOX4-induced ROS and the cardiac endothelium

NOX4 appears to be cardio-protective via the preservation of myocardial capillary density. NOX4-null mice exhibited reduced capillary density, greater cardiac hypertrophy and contractile dysfunction, whilst cardiac myocyte-specific NOX4 transgenic mice were protected against pressure-overload induce hypertrophy and failure and had greater capillary density[268]. A recent study confirmed the protective role of NOX4; transgenic mice overexpressing endothelial-restricted Nox4 were protected from AngII-induced fibrosis, which was associated with reduced VCAM1 expression and decreased inflammatory cell infiltration[269]. Interestingly, following AngII treatment, hypertrophy and contractile function was comparable between NOX4 transgenic and wild-type mice[269]. Taken together, the induction of cardiac myocyte NOX4 is protective against hypertrophy and contractile dysfunction, and may modulate EC function. In contrast, induction of endothelial NOX4 limits immune cell infiltration, preventing fibrotic remodelling, but does not impact cardiac myocyte function. Finally, although NOX1 modulates EC and VSMC function, in the heart, the role of NOX1 in modulating the function of the cardiac endothelium has not yet been investigated.

1.4.3. Association between ROS and MAPK activation in cardiac remodelling

Whilst cardiac myocyte hypertrophy can be governed by the induction MAPK signalling by ROS *in vitro*; *in vivo*, cardiac remodelling is associated with both ROS induction and MAPK activation[193,270–273]. Failed human hearts exhibited both elevated ROS production and elevated ERK1/2 and p38-MAPK activation[247]. Pressure overload-induced hypertrophy was associated with a progressive increase in ROS production, expression of the NOX subunits, NOX2, $p22^{phox}$, $p47^{phox}$, $p67^{phox}$, and activation of the MAPKs, ERK1/2, p38-MAPK and JNK[274]. In comparison, AngII-induced superoxide production promoted cardiac hypertrophy, fibrosis and apoptosis alongside activation of p38-MAPK and JNK[275]. ASK1-null mice attenuated cardiac remodelling and MAPK activation, indicating the redox activation of ASK1 is implicated in the pathogenesis of AngII-induced cardiac dysfunction[275]. Furthermore, although activation of p38-MAPK is induced by ROS via redox activation of ASK1, in HF models activation of p38-MAPK may promote further ROS production in the myocardium[276,277]. This effect was also observed in AngII-induced hypertension, where p38-MAPK inhibition reduced superoxide production and supressed NOX2 mRNA expression, which resulted in reduced cardiac hypertrophy and fibrosis[278].

These studies indicate that human HF and pre-clinical models of cardiac remodelling, including AngII-induced hypertension, are associated with ROS activation and MAPK signalling. However, ROS may function both upstream to promote MAPK activation, and as a downstream effector of MAPK signalling. Furthermore, inhibition of ROS whether upstream or downstream of MAPKs activation, appears to limit cardiac hypertrophic and fibrotic cardiac remodelling.

1.5. Negative regulation of MAPK signalling

MAPK activation can be regulated in several ways, including by activation from upstream kinases, scaffold proteins, negative feedback from downstream regulators or other pathways, and removal of phosphate groups by protein phosphatases. Phosphatases which attenuate MAPK signalling include protein phosphatase 2A, protein phosphatase 2C, tyrosine phosphatases and the MAPK selective phosphatases, the typical dual specificity phosphatases (DUSPs)[279–281]. The attenuation of MAPK signalling by phosphatases is essential for the physiological downstream signalling. For instance, constitutive ERK1/2 activation promotes cancer progression and is associated with overactivation of upstream signals and decreased DUSP expression[282,283]. By attenuating MAPK signalling, DUSPs influence cellular proliferation, differentiation and migration, and in the heart DUSPs influence hypertrophy, fibrosis and contractility[284,285]. Cardiac DUSP function has been studied in models of cardiac dysfunction induced by TAC, isoprenaline (a non-selective β adrenergic agonist, of which acute treatment mimics stress-induced cardiomyopathy, whilst chronic treatment recapitulates advanced heart failure where there is chronic adrenergic stimulation[286]), and experimental MI. However, the expression and function of cardiac DUSPs has not been investigated in hypertensive models, including the AngII-induced hypertensive mice and the SHR model.

1.5.1. The typical DUSPs

The typical DUSPs are prominent MAPK regulators, which dephosphorylate Ser/Thr and Tyr residues. Within the phosphatase classification system, they are members of subclass II, dual-specificity/VH1-like PTPs, of the class 1 cysteine-based phosphotyrosine phosphatases (PTPs). Within subclass II, there are six subfamilies, which include the typical DUSPs and the atypical DUSPs[284]. The typical DUSP subfamily (previously known as the MAPK phosphatase subfamily) negatively regulates MAPK signalling, and consists of DUSP1, 2, 4, 5, 6, 7, 8, 9, 10 and 16[287]. These typical DUSPs contain a kinase interaction motif (KIM) which facilitates interactions with MAPKs. In contrast, the atypical DUSPs do not contain a KIM, and have a wider range of less well-characterised targets. Furthermore, of the atypical DUSPs, DUSP24

and DUSP27 do not contain the conserved cysteine residue required for catalytic function, and as such lack phosphatase activity[279].

1.5.1.1. Structure, specificity, and localisation

The structure, specificity and localisation of the typical DUSPs (hereinafter referred to simply as DUSPs) has been reviewed previously[279,284,288,289]. Briefly, DUSPs contain several binding domains. The N-terminal MAPK binding domain consists of the KIM, which contains essential arginine residues required for MAPK binding, and the catalytic site[288]. The C-terminal domain is important for regulating protein stability as it contains residues which can be phosphorylated to promote ubiquitination and proteasomal degradation or to improve stability by preventing ubiquitination[288,289]. DUSPs also contain nuclear export signals and/or nuclear localisation signals which determine their subcellular compartmentalisation.

The subcellular localisation and MAPK selectivity varies between the DUSPs and is summarised in Figure 1.6A. DUSP1, DUSP2, DUSP4 and DUSP5 are rapidly inducible and are localised to the nucleus. DUSP1 preferentially binds to p38-MAPK and JNK, but can also interact with ERK1/2, DUSP2 interacts with ERK1/2, p38-MAPK and JNK, DUSP4 preferentially binds to ERK1/2 and JNK, but may also bind to p38-MAPK, whilst DUSP5 is selective for ERK1/2[288,289]. DUSP6, DUSP7 and DUSP9 regulate cytosolic ERK1/2 whilst DUSP8, DUSP10 and DUSP16 are present in the nucleus and cytosol where they regulate p38-MAPK and JNK. However, DUSP8 also targets ERK1/2 in the heart, and DUSP16 preferentially regulates JNK, but can also regulate p38-MAPK[288,290,291]. It is noteworthy that a more recent study, using data generated from The Human Protein Atlas, indicated that the localisation of several DUSPs was not as previously described. DUSP1, classified as a nuclear DUSP, was present in the nucleus and the cytoplasm. DUSP6, thought to be primarily cytosolic, was also present in the nucleus and the cytoplasm. Of the nuclear and cytosolic DUSPs which regulate p38-MAPK and JNK, DUSP8 was predominantly cytosolic, whilst DUSP16 was predominantly localised to the nucleus with some localisation in the cytoplasm[292–294]. The difference observed here compared with the established paradigm in the literature may be due to a difference in cell type or may be dependent on whether DUSP localisation was determined at baseline or following stimulation.

1.5.1.2. Regulation of DUSPs: Transcription and activation

DUSPs are regulated in several ways; primarily by transcriptional activation (Figure 1.6B & C), stabilisation (Figure 1.6D), and ubiquitination and degradation (Figure 1.6E), although a small subset of DUSPs do exhibit elevated catalytic activity following partner binding (Figure 1.6F)[284,289]. DUSP1, DUSP2, DUSP4 and DUSP5 are found in the nucleus and are transcribed at a low basal rate which becomes upregulated in response to stimuli/stressors.

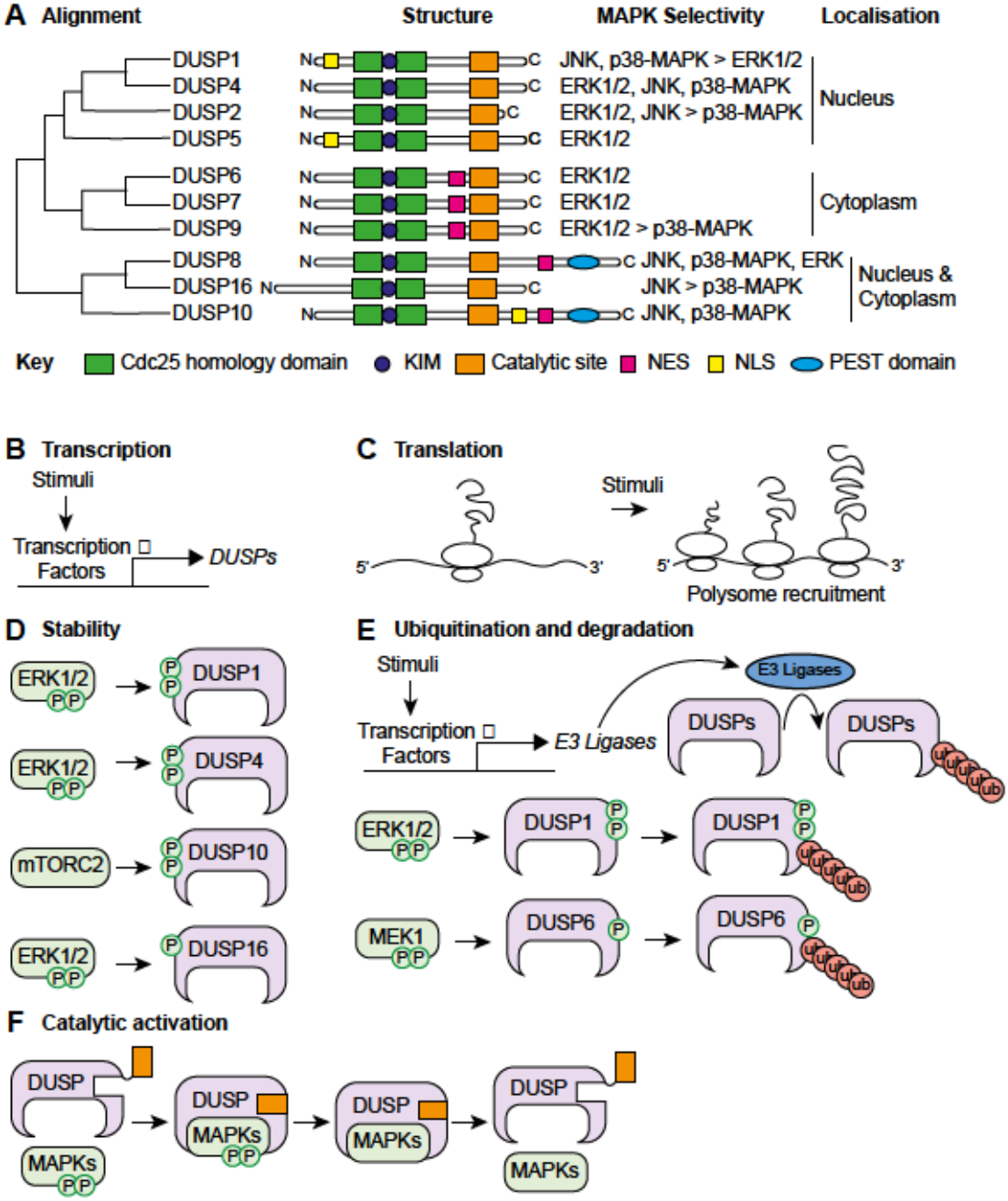

Figure 1.6. DUSP structure and regulation.
(**A**) Phylogenetic tree of mouse DUSPs determined by sequence alignment, with DUSP structure, MAPK selectivity of the DUSPs and subcellular localisation DUSPs. DUSPs contain several domains, motifs, and conserved sequences. The cdc25 homology domain, the kinase interaction motif (KIM) and catalytic site are found in all DUSPs. Several DUSPs contain a nuclear localisation sequence (NLS) and/or a nuclear export sequence (NES), which control subcellular localisation. DUSP8 and DUSP10 also contain a PEST motif, rich in Pro, Glu, Ser and Thr that mediates rapid degradation. Image adapted from[279,288]. DUSPs are primarily regulated by transcription (**B**), translation (**C**), stability (**D**), and ubiquitination and degradation (**E**). (**D**) Phosphorylation of DUSPs by ERK1/2 or by mammalian target of rapamycin (mTORC) 2 improve DUSP stability by ubiquitin-dependent and ubiquitin-independent mechanisms. (**E**) Stimuli which promote the expression of E3 ligases promote the ubiquitination of DUSPs and target for proteasomal degradation. Phosphorylation of DUSPs can also promote ubiquitination and proteasomal degradation. (**F**) DUSP1, 2, 4 and 6 become catalytically active upon substrate binding.

Transcriptional activation of these DUSPs occurs rapidly, and they are induced as immediate early or delayed early genes[288]. The induction of these DUSPs can be mediated by serum, growth factors, lipopolysaccharides (bacterial toxins) and also by environmental stressors including heat shock and UV light, and the transcription factors, activator protein 1, NF-κB and p53 can induce their expression[279,284,289]. Furthermore, the rapid induction of their expression following stimulation may be due to de-repression of their translation. Following lipopolysaccharide treatment, there was an increase to the amount of DUSP1 mRNA associated with polysomes in activated macrophages, indicating translational repression was attenuated[295]. Other DUSPs, such DUSP6, DUSP7, DUSP9 and DUSP10, can be constitutively expressed, although this may be dependent on the cell type or organ investigated[279,284]. Furthermore, the expression of constitutively-expressed DUSPs may be upregulated; for example, prolonged ERK1/2 activation induces further DUSP6 transcription[296]. As such, constitutively active DUSPs negatively regulate MAPK activation at baseline and following any stimuli, whilst inducible DUSPs can only regulate sustained signals, allowing the cell a temporary memory to modulate the effects of subsequent signals[288].

A small subset of DUSPs undergo a conformational change in their catalytic site, following binding of their MAPK partners, which enhances their activity; these are DUSP1, DUSP2, DUSP4 and DUSP6, whereas DUSP5, DUSP8, DUSP10 and DUSP16 do not undergo catalytic activation[279,288].

1.5.1.3. Regulation of DUSPs: Stability and degradation

DUSP stability can be influenced by MAPK binding, phosphorylation and oxidative modifications and has recently been reviewed[289]. The stabilisation of DUSP5 is promoted by ERK2 binding, which prevents its ubiquitination and proteasomal degradation and occurs independently of phosphorylation[297]. Although phosphorylation does not confer activity for the DUSPs, phosphorylation can either promote or inhibit their degradation by ubiquitination and proteasomal degradation. DUSP1 and DUSP4 are phosphorylated by activated ERK1/2, improving their stability by preventing degradation by a mechanism independent of ubiquitination. On DUSP1 these residues are Ser359 and Ser364, and on DUSP4 these residues are Ser386 and Ser391[298,299]. Phosphorylation of DUSP10 by mammalian target of rapamycin complex (mTORC) 2 on Ser224 and Ser230 promotes stability[300]. Additionally, phosphorylation at Ser446 by ERK1/2 increases the stability of DUSP16 by preventing ubiquitination[301,302]. Despite this, phosphorylation can also promote DUSP ubiquitination and degradation. Phosphorylation of DUSP1 at Ser296 and Ser323 and of DUSP6 at Ser159 and Ser197 by ERK1/2 promotes ubiquitination and proteasomal degradation[303–305], as does phosphorylation of DUSP6 at Ser174 by MEK1[296]. In addition to phosphorylation, DUSP8 and DUSP10 contain a PEST (Pro, Glu, Ser and Thr) rich motif which promotes rapid degradation by proteolysis[306].

ROS can modulate DUSP function and abundance; oxidation of DUSP6's catalytic centre attenuated its function[307], whilst ROS promoted proteasomal degradation of DUSP1 and DUSP4. For DUSP1 this was either mediated directly by the oxidative S-glutathionylation modification or indirectly by PKC[308–311]. The regulation of DUSP6 abundance by ROS may be cell type specific; H_2O_2 promoted DUSP6 accumulation in a murine corneal epithelial progenitor cell line, whilst in mature murine corneal epithelial cells, H_2O_2 treatment was associated with reduced DUSP6 abundance[312].

Furthermore, stimuli which promote the expression of ligases, also promote DUSP degradation. ERK1/2 can induce DUSP1 proteasomal degradation by promoting the expression of the transcription factor forkhead box M1, which induces the ubiquitin E3 ligase S-phase kinase-associated protein/cyclin-dependent kinase regulatory subunit 1[289]. Additionally, PKCδ depletion results in increased levels of the E3 ligase, neuronal precursor cell-expressed developmentally down-regulated 4 protein, which targets DUSP6 for degredation[289]. Finally, the E3 ligase speckle-type pox virus and zinc f protein, which accumulates in the cytoplasm following hypoxia, targets DUSP7 for degradation[313].

1.5.1.4. Functions of DUSPs: Anchoring, crosstalk, and redundancy

Although DUSPs are phosphatases, they can also regulate MAPK function by anchoring them to a particular compartment. For example, DUSP5 anchored ERK2 to the nucleus following dephosphorylation, which occurred independently of its phosphatase activity[314]. Additionally, although DUSP16 exerts its phosphatase activity on p38-MAPK and JNK, it has been demonstrated to act as a scaffold for ERK1/2. By sequestering ERK1/2 in the cytoplasm, DUSP16, prolonged cytosolic ERK1/2 activation and prevented ERK1/2-induced transcription[315]. DUSPs can also influence feedback mechanisms within their pathways; for instance, DUSP5 paradoxically increased and prolonged cytosolic ERK1/2 activation, which was partially mediated by inhibition of negative feedback from activated ERK1/2 to the upstream Raf kinases[316].

DUSPs can mediate crosstalk within the MAPK pathways. For example, the attenuation of ERK1/2 activation by DUSP4 promoted destabilisation of DUSP1, as DUSP1 is stabilised by ERK1/2[317]. This may have downstream implications on the activity of ERK1/2, p38-MAPK and JNK, all regulated by DUSP1. This is also the case for DUSP16, a regulator of JNK and p38-MAPK, which can be stabilised by ERK1/2[301]. In addition, by attenuating JNK signalling, DUSP2 promoted the activation of ERK1/2[318], whilst DUSP10 and DUSP16 promoted ERK1/2 phosphorylation by supressing p38-MAPK activation[319].

Genetic redundancy occurs where multiple genes can perform the same function. As there is overlap between the MAPKs regulated by the DUSPs, the DUSPs may compensate for one another following inhibition or knockdown. Indeed, deficiency of DUSP2 (selective for ERK1/2 and p38-MAPK), did not result in enhanced ERK phosphorylation[318], whilst DUSP10 (selective for p38-MAPK and JNK) deficiency did not induce p38-MAPK hyperphosphorylation, although JNK phosphorylation was elevated[320]. Furthermore, cardiac p38-MAPK activity was elevated in DUSP1/4-double-null mice, whilst p38-MAPK phosphorylation was unchanged in mice null for DUSP1 or DUSP4, indicating DUSP1 and 4 can compensate for the loss of one another[321].

1.5.2. DUSPs influence cardiac remodelling

Cardiac DUSPs expression is altered in HF and in models of cardiac remodelling. The majority of data to support this are from pre-clinical models, as data compromising DUSP expression in human cardiac diseases is sparce, although cardiac DUSP4 was found to be upregulated in patients with end-stage HF[322]. In response to TAC-induced pressure overload, the expression of DUSP1, DUSP4, DUSP8 and DUSP10 were elevated[290,321,323]. Following TAC and treatment with isoprenaline DUSP5 expression was reduced[324,325]. Furthermore, the expression of DUSP6 and DUSP8 were elevated in MI models[290,326].

In vivo, genetic manipulation of cardiac DUSPs have indicated the proper regulation of DUSP expression is critical for cardiac function. Overexpression of Dusp1, Dusp4 and Dusp6 promote cardiac dysfunction and decompensation[208,327,328]; however, Dusp1/4-null mice also exhibit cardiomyopathy and ventricular dilatation[321]. In contrast, the overexpression of Dusp6 was protective[329], as was Dusp10 deficiency[323]. These findings will be discussed below.

1.5.2.1. The physiological regulation of DUSP1 prevents maladaptive cardiac remodelling

Although DUSP1 can regulate ERK1/2, p38-MAPK and JNK in cultured cardiac myocytes[365], *in vivo*, DUSP1 preferentially regulates p38-MAPK; Dusp1 overexpression attenuated cardiac p38-MAPK phosphorylation at baseline[365], whilst Dusp1/4-null mice exhibited elevated p38-MAPK phosphorylation, with unchanged ERK1/2 and JNK phosphorylation[321]. However, following treatment with PE, mice overexpressing Dusp1 at a low level exhibited reduced cardiac p38-MAPK and JNK phosphorylation, whilst mice with a high level of Dusp1 overexpression exhibited reduced cardiac phosphorylation of ERK1/2, p38-MAPK and JNK[365].

Transgenic mice expressing high levels of Dusp1 exhibited dilatation during postnatal development, which was fatal by 15 d postnatally, whereas mice expressing low levels of

Dusp1 were overtly normal, although echocardiography indicated mild dilatation with evidence of cardiac dysfunction[365]. Following TAC and isoprenaline infusion, these mice exhibited reduced cardiac hypertrophy, with reduced induction of foetal gene expression following isoprenaline infusion[365]. However, the effect on cardiac function is unknown. In contrast with Dusp1 transgenic mice, Dusp1-null mice were healthy and fertile, without any cardiac pathology or altered MAPK expression, which may have been due to compensation by another DUSP[321]. Indeed, Dusp1/4-null mice exhibited elevated baseline p38-MAPK phosphorylation and age-induced cardiomyopathy (hypertrophy, dilatation and reduced contractile function), which could be attenuated by the p38-MAPK inhibitor SB731445[321]. Furthermore, survival post-TAC was limited in Dusp1/4-null mice[321]. Overall, in the heart, DUSP1 predominantly regulates p38-MAPK activity. Elevated expression of DUSP1 can promote cardiac dysfunction; however, deficiency of Dusp1 had no effect on cardiac function, as the loss of DUSP1 is compensated by DUSP4. This notwithstanding, the loss of both Dusp1 and Dusp4 promoted cardiac dilatation and was associated with worse outcomes following TAC. Thus, dysregulation of p38-MAPK activation causes cardiac dysfunction in post-natal development and following TAC.

1.5.2.2. DUSP4 overexpression promotes pathological remodelling

Although Dusp4-null mice exhibited reduced cardiac contractility at 8 weeks of age, this was not associated with hypertrophy, nor reduced survival[321]. This may have been due to functional compensation by DUSP1, as severe cardiac dysfunction was observed in only Dusp1/4-null mice, and was associated with p38-MAPK activation, as above[321]. Dusp4-overexpression in mice resulted in cardiomyopathy seen at 16 weeks of age, characterised by cardiac hypertrophy, induction of foetal genes, dilatation and cardiac dysfunction[328]. Dusp4-transgenic mice exhibited reduced ERK1/2 phosphorylation, and p38-MAPK and JNK were not investigated[328].

1.5.2.3. Loss of DUSP6 is cardioprotective

Through reducing ERK1/2 phosphorylation, DUSP6 promotes cardiac decompensation and transition to HF, whilst decreased DUSP6 expression is cardioprotective. Dusp6 overexpression attenuated ERK1/2 phosphorylation, without affecting p38-MAPK and JNK phosphorylation, in response to TAC. Following TAC, DUSP6 transgenic mice exhibited greater cardiac hypertrophy with elevated fibrosis and apoptosis, which was associated with reduced cardiac function[208]. In contrast, DUSP6-null mice, which had elevated baseline ERK1/2 phosphorylation in the heart, were protected from decompensation and HF following TAC, although, following TAC cardiac ERK1/2 phosphorylation was similar to that seen in wild-type mice[329]. This may be due to compensation by other DUSPs, or because DUSP6 predominantly regulates baseline, and not inducible ERK1/2 phosphorylation. Indeed, ERK1/2

phosphorylation was unchanged between DUSP6-null and wild-type cardiac myocytes in response to PE, which can induce ERK1/2 activation and promote cardiac myocyte hypertrophy[329–331]. Subsequently, the protection conferred in DUSP6-null mice was attributed to greater cardiac myocyte proliferation in utero[329]. Zebrafish null for Dusp6 were also protected from cardiac injury, due to greater cardiac myocyte proliferation in adult hearts, although cardiac angiogenesis was promoted and fibrosis was reduced[326]. These studies indicate DUSP6 overexpression promotes pathological remodelling, through inhibiting ERK1/2, whereas loss of DUSP6 is protective. However, as DUSP6 deficiency appears to confer protection by altering cardiac myocyte proliferation, the efficacy of DUSP6 inhibition in the human heart is unclear, due to the terminally differentiated nature of mammalian cardiac myocytes[332]. However, as Dusp6-null zebrafish exhibited improved cardiac angiogenesis and reduced fibrosis, DUSP6 inhibition may still improve cardiac function where angiogenesis is impaired and fibrosis occurs.

1.5.2.4. DUSP7 overexpression promotes pathological remodelling

Mice with cardiac-specific Dusp7 overexpression exhibited reduced ERK1/2 phosphorylation and were predisposed to HF. Cardiac hypertrophy was evident with dilatation and induction of foetal genes, and cardiac dysfunction was observed. Furthermore, these mice which were overexpressing Dusp7 died prematurely between 6-10 months of age[333]. In contrast, hearts from Dusp7-null mice were overtly normal and mice were partially protected from cardiac dysfunction induced by isoprenaline, although ERK1/2 activation was unchanged[333]. Loss of DUSP7 may have had a limited effect on ERK1/2 activation as another DUSP may have compensated for the loss DUSP7 and, additionally, other pathways may also be involved in the pathogenesis of isoprenaline-induced cardiac dysfunction.

1.5.2.5. DUSP8 overexpression promotes maladaptive remodelling

Transgenic mice overexpressing cardiac-specific Dusp8 exhibited cardiomyopathy 6 weeks following gene induction. This was characterised by impaired cardiac function, fibrosis and cardiac hypertrophy with eccentric cardiac myocyte hypertrophy[290]. These mice exhibited reduced ERK1/2, p38-MAPK and JNK phosphorylation[290], indicating that proper regulation of MAPKs are essential to prevent maladaptive remodelling. Consistent with this, Dusp8-null mice were protected from cardiac dysfunction following TAC, which was associated with elevated ERK1/2 phosphorylation[290]. However, at baseline these mice had elevated cardiac ERK1/2 phosphorylation and exhibited concentric hypertrophy[290]. As such, it is unclear whether the protective effect of DUSP8 deficiency is due to elevated baseline ERK1/2 or due to the promotion of ERK1/2 phosphorylation following TAC. Furthermore the differences observed to MAPK phosphorylation between DUSP8 overexpressing and DUSP8-null mice may be due to either a loss of specificity of DUSP8 in the transgenic mice, or other DUSPs

may compensate for the loss of DUSP8 to regulate p38-MAPK and JNK in the DUSP8-null mice.

1.5.2.6. The induction of DUSP9 expression is cardioprotective

Although previous reports have indicated DUSP9 is not expressed in the heart[292,334], one study found DUSP9 protein and *Dusp9* mRNA expression was inducible following TAC[335]. As DUSP9 is essential for embryonic development, cardiac-specific loss of DUSP9 was induced in mice at 6 weeks of age using the cre/lox system[335,336]. DUSP9-null mice were similar to controls at baseline, but following TAC these mice exhibited: greater hypertrophy and dilatation; increased induction of foetal genes; elevated interstitial and perivascular fibrosis; and had reduced cardiac function[335]. In contrast, mice overexpressing cardiac-specific DUSP9 exhibited reduced hypertrophy, reduced foetal gene induction, decreased fibrosis and improved cardiac function following TAC, compared with non-transgenic littermates[335]. However, although DUSP9 is regarded as ERK1/2 selective, the protective effect of DUSP9 was mediated by attenuating ASK1, p38-MAPK and JNK phosphorylation[335]. Overall, the induction of DUSP9 following pressure overload is cardioprotective, acting by attenuating the activity of stress-regulated MAPKs.

1.5.2.7. Loss of DUSP10 limits cardiac fibrosis

A recent study indicated that DUSP10 deficiency was protective against TAC-induced cardiac fibrosis. Following TAC, DUSP10-null mice exhibited elevated p38-MAPK and JNK phosphorylation, whilst ERK1/2 was unchanged[323]. This corresponded with improved cardiac function, reduced cardiac hypertrophy, reduced expression of foetal genes, and reduced fibrosis. The reduction in fibrosis was attributed to modulation of MAPK signalling in cardiac macrophages, which promoted collagen turnover through MMP9, limiting fibrotic remodelling[323]. This is particularly interesting, as the reduced fibrotic response may not have been observed in models using cardiac myocyte-specific genetic manipulation of DUSPs. This highlights the relevance of investigating the role and dysregulation of DUSPs in other cardiac cell types, which also influence remodelling processes and thus can modulate cardiac function.

1.5.2.8. DUSP2, DUSP5, and DUSP16

The effect of DUSP2, DUSP5, and DUSP16 on cardiac function has not been investigated *in vivo*. However, *in vitro* studies have been conducted. DUSP2 has been implicated in attenuating ERK1/2 phosphorylation in cardiac myocytes following isoprenaline treatment, although DUSP1 and/or 6 may also be involved[337]. DUSP5 overexpression attenuated cardiac myocyte ERK1/2 phosphorylation in response to PE, and prevented PE-induced cardiac myocyte hypertrophy[325]. DUSP5 was also shown to negatively regulate cardiac fibroblast

proliferation[324]. Interestingly, the loss of DUSP5 promoted postnatal cardiac growth in adolescent mice; however, whether this was retained into adulthood or influences pathological remodelling is unknown[338]. DUSP16-null mice have been generated, but they died perinatally of unknown cause[339], however, consistent with DUSP16 as a regulator of stress-regulated MAPKs, embryonic fibroblasts from DUSP16-null mouse embryos exhibited elevated p38-MAPK and JNK activation in response to H_2O_2[339].

1.6. Hypothesis

Hypertension can be treated by anti-hypertensive medications, including angiotensin converting enzyme inhibitors (ACEI), angiotensin receptor blockers (ARBs), calcium channel blockers (CCBs), and diuretics. However, prolonged and poorly controlled hypertension can lead to cardiac remodelling, namely cardiac hypertrophy and fibrosis. These processes result in the establishment of hypertensive heart disease (HHD), where the only current treatment is blood pressure control by using anti-hypertensive agents. HHD can progress to HF with preserved ejection fraction (HFpEF), where diastolic dysfunction is observed. There are currently no disease modifying treatments for HFpEF, and as such only the symptoms can be managed (i.e. use of diuretics to treat pulmonary congestion and peripheral oedema). This is summarised in Figure 1.7A. By identifying novel targets for inhibition, which can modify the cardiac remodelling processes, improved treatments for HHD may be developed.

This project investigated the role of the Thrombospondin 1 (TSP1)-CD47-NAPDH oxidase 1 (NOX1) axis (i.e. activation of CD47 by TSP1 promotes NOX1 expression/activity) as a mediator of impaired cardiac endothelial function in HHD with a view to targeting this axis for therapeutic benefit. Activation of CD47 by TSP1 has previously been reported to impair endothelial function[112,134–136,140–142,152,175,257] and has been linked with the upregulation of NOX1 and subsequent ROS production and altered endothelial cell (EC) function[175,257]. Altered EC function can lead to inflammation[85], known to promote fibrotic remodelling[30], and can also influence cardiac myocyte compliance, a determinant of diastolic function[99]. In addition, altered EC function can affect angiogenesis, which has previously been shown to influence hypertrophic remodelling in the heart[93,95,96]. As these processes contribute to HHD, impaired EC function caused by the TSP1-CD47-NOX1 axis may underpin cardiac remodelling in HHD, and therefore may be a suitable therapeutic strategy for the treatment of HHD. However, this signalling axis has not previously been investigated in cardiac ECs, nor in the context of HHD. Furthermore, mitogen activation protein kinase (MAPK) activation has been linked with both cardiac remodelling processes[191] and the regulation of endothelial function[340]. The expression of the dual specificity phosphatases (DUSPS), negative regulators of MAPK activation, has also been linked with a range of adverse cardiac remodelling processes[285]. However it is not

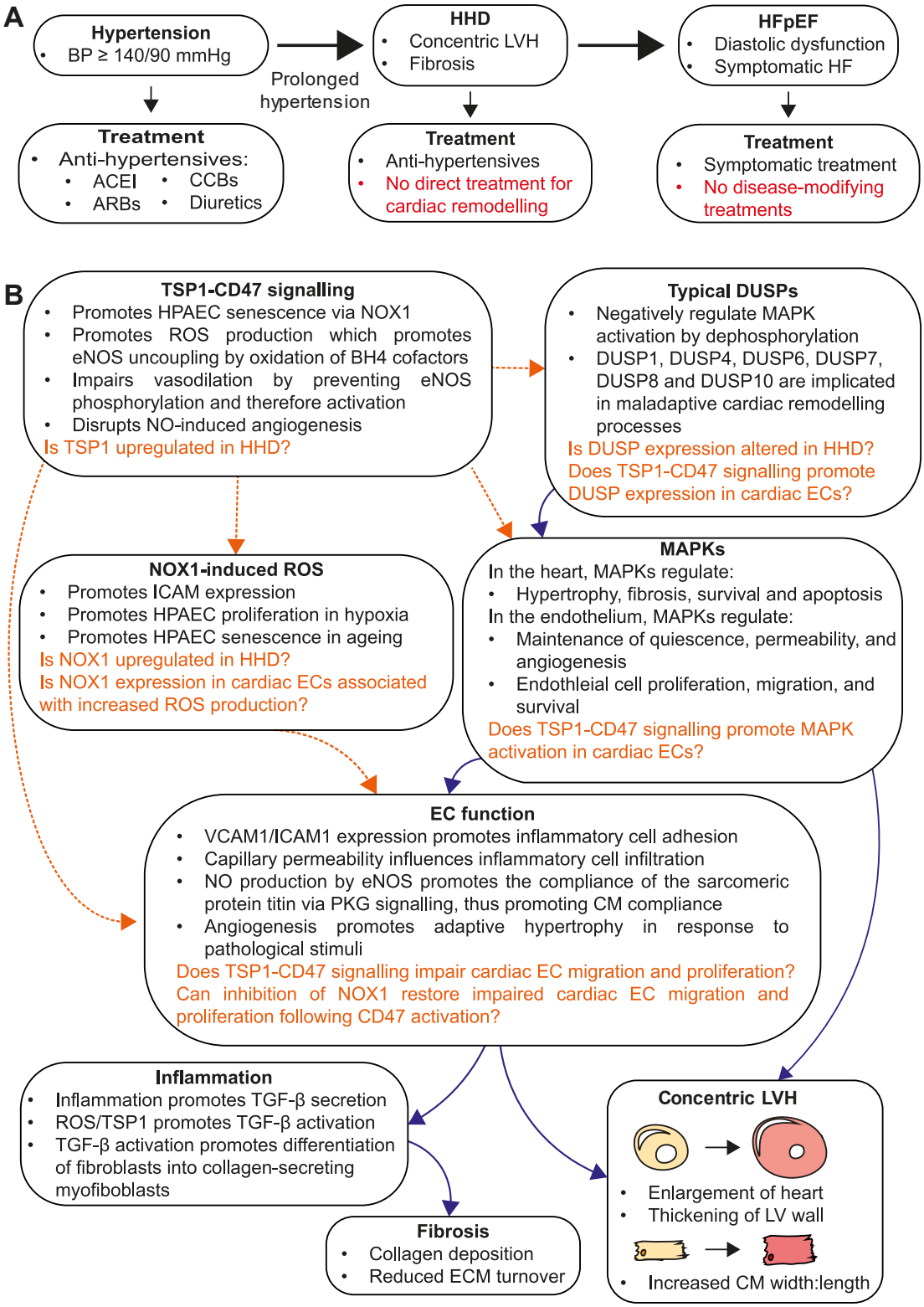

Figure 1.7. Rationale behind characterising CD47 phosphatase signalling in the hypertensive heart

(**A**) Summary of the progression of hypertensive heart disease to HHD and to HFpEF, and their treatments. (**B**) Summary of the mechanisms underpinning cardiac remodelling in HHD relevant to this project, with key knowledge gaps denoted by orange text, and the links this project aims to make in orange dashed arrows, with links known from the literature in blue solid arrows.

known whether activation of CD47 by TSP1 can promote MAPK activation or DUSP expression, and it is not known whether DUSP expression is altered in HHD. This is summarised in Figure 1.7B.

Therefore the hypothesis for this project was that the TSP1-CD47-NOX1 axis promotes cardiac endothelial dysfunction in hypertensive heart disease via stress-MAPK signalling that is attenuated by dephosphorylation by DUSPs.

Aims and Objectives

Aim 1: To investigate whether HF and hypertension are associated with increased cardiac expression of the CD47 interacting protein TSP1, increased cardiac ROS production and elevated cardiac NOX1 expression.

Objective 1: The mRNA and protein expression of TSP1, CD47 and NOX1 will be identified in cardiac tissue from human non-ischaemic heart failure (NI-HF) cases, from AngII-induced hypertensive mice, and from SHRs, by RT-qPCR and by western blot.

Objective 2: ROS production will be determined in cardiac tissue from NI-HF cases, and from AngII-induced hypertensive mice and from SHRs, using cytochrome c reduction to determine superoxide production, and Amplex Red to determine hydrogen peroxide production.

Objective 3: The expression and localisation of TSP1, CD47 and NOX1 will be determined by immunohistochemistry (IHC) in cardiac tissue from HHD cases.

Aim 2: To investigate whether CD47 activation can promote MAPK activation in cardiac cell types and whether NOX1 is the primary mediator of endothelial dysfunction caused by AngII or TSP1-CD47 interactions.

Objective 1: To identify whether 7N3 treatment leads to the phosphorylation of the MAPKS ERK1/2, p38-MAPK and JNK in endothelial cell lines, in primary mouse cardiac ECs, primary cardiac fibroblasts and primary cardiac myocytes, and to compare this with the phosphorylation of these MAPKs in response to AngII, a known hypertensive stimuli.

Objective 2: The mRNA and protein expression of NOX1 will be determined following AngII treatment and following CD47 activation in the SVEC4-10 and SGHEC-7 endothelial cell lines, and in primary mouse cardiac ECs. CD47 activation will be achieved by using the 7N3 peptide, which is derived from the CD47-binding, c-terminal domain of TSP1.

Objective 3: ROS production will be measured following treatment with 7N3 and AngII, and the effects of NOX1 inhibition on ROS production will be determined using a small molecule inhibitor of NOX1/4 (setanaxib) and a peptidic inhibitor of NOX1 (NOXA1ds).

Objective 4: The staining of 4-HNE, a marker of oxidative stress, will be determined by immunofluorescence microscopy in endothelial cell lines treated with 7N3 and AngII, the effects of NOX1 inhibition on 4-HNE staining will be investigated by using setanaxib.

Objective 5: To assess whether EC function is impaired following 7N3 and AngII treatment, the migration of EC will be determined using a wound healing assay, and EC motility, proliferation and cell death will be determined by timelapse microscopy. The NOX1 inhibitors, setanaxib and NOXA1ds will be used to identify whether NOX1 inhibition can restore EC function.

Aim 3: To investigate whether altered cardiac DUSP expression occurs in HF and hypertension, as MAPK phosphorylation is negatively regulated by the typical DUSPs, and to identify whether DUSP expression is influenced by TSP1-CD47 signalling in cardiac ECs.

Objective 1: ERK1/2 and p38-MAPK phosphorylation will be determined in cardiac tissue from the NI-HF cohort, from AngII-induced hypertensive mice, and from SHRs, by western blot.

Objective 2: The mRNA and protein expression of the typical DUSPs will be investigated in cardiac tissue from the NI-HF cohort, from AngII-induced hypertensive mice, and from SHRs, by RT-qPCR and western blot.

Objective 3: Following treatment with 7N3 or AngII the mRNA and protein expression of the typical DUSPs will be investigated in endothelial cell lines and cardiac ECs by RT-qPCR and western blot.

Chapter 2: Materials and methods

2.1. Human heart samples

2.1.1. Non-ischaemic left ventricular (LV) HF samples (Pittsburgh cohort).

Acellular cardiac tissue of human mid-LV origin from control and non-ischaemic HF (NI-HF) patients were kindly provided by Dr C. McTiernan and Prof. M. Rojas (University of Pittsburgh Medical Center) under governance of a University of Pittsburgh Institutional Review Board (IRB) protocol. Failing heart tissue collections were obtained from patients consented to a protocol reviewed and approved by the University of Pittsburgh Institutional Review Board. Control (non-failing) heart samples were collected under University of Pittsburgh Committee for Oversight of Research and Clinical Training Involving Decedents #451. Consent was obtained by the local Organ Procurement Organization, Centre for Organ Recovery and Education.

At the time of cardiac transplantation, transmural tissue at the level of the anterior papillary muscle from the left ventricle of end-stage NI-HF patients was collected. Samples were flash frozen within 20 minutes (min) of excision and were stored at 80°C until use. Control LV tissue was collected from hearts rejected for transplant, with between 20-45 min of time elapsing between cross-clamp and freezing at 80°C. See Appendix Table 1 for further demographics.

Samples were void of all personal and identifiable information. Use of all human tissue samples was governed by an MTA, with strict adherence to local St George's, University of London (SGUL) rules in accordance with the Human Tissue Act, 2009.

2.1.2. Human HHD samples (CRY/SGUL cohort)

Paraffin wax embedded LV sections (10 µm), on 3-aminopropyltriethoxysilane coated slides, from cases where the cause of death was attributed to sudden arrhythmic death syndrome (SADS), and where HHD was a clinical feature, were kindly provided by Professor Mary Sheppard (Cardiac Risk in the Young (CRY) Cardiovascular Pathology Unit, SGUL). For HHD to be an attributable feature, cases had to have an established diagnosis of hypertension pre-mortem, alongside left ventricular hypertrophy (LVH) identified at post-mortem, in the absence of significant coronary disease or extra cardiac pathology. Cases with a clinical history of cardiac failure (LV EF <40%), positive toxicology or with another cause of death were excluded[8]. Cases were age and sex matched to controls with morphologically normal hearts where sudden adult death syndrome (SADS) was a cause of death.

2.2. Rodent models of hypertension

2.2.1. Ethics statement for animal experiments

Animals were housed in the Biological Research Facility at SGUL or the Bioresource Unit at University of Reading (UoR) (both UK registered with a Home Office certificate of designation). All procedures were performed in accordance with UK regulation and the European Community Directive 86/609/EEC for animal experiments. Work was undertaken in accordance with institutional animal care committee procedures (St. George's, University of London and University of Reading) and the U.K. Animals (Scientific Procedures) Act 1986.

2.2.2. Animal housing, husbandry, and welfare

Both mice and rat models of hypertension were used in this PhD thesis. Mice were housed in open top cages (SGUL) and Tecniplast individually ventilated cages (UoR) (total area 512 cm^2, maximum of 5 mice per cage. Mice were provided with water and food (Rm3 pelleted food, Special diet services) *ad libitum*, with a 12 h:12 h light: dark cycle and room temperature (RT) (set point of 21°C). Rats were housed in NKP cages (maximum of 5 rats per cage). Rats were provided with water and food (Rm1 pelleted food, Special diet services) *ad libitum*, with a 12 h: 12 h light: dark cycle and RT set point of 21°C.

Once a day, all animals were checked by a trained competent person and licence holders informed of any welfare issues, with consultation with a Named Veterinary Surgeon when necessary. Mice undergoing procedures were monitored using a score sheet and routinely culled if they reached a predefined endpoint agreed with the Named Veterinary Surgeon. Weights were taken before and at the end of the procedures (see Appendix Table 2 for details).

2.2.3. *In vivo* mouse AngII-induced model of hypertension

The number of mice used in each group was pre-determined using G*Power 3.1 software[341] and was based on similar studies conducted within the research group. The following assumptions were made to calculate the total sample size: Effect size:1; α error: 0.05; Power: 0.95; Number of groups:5.

Male C57Bl/6J wild type (WT) mice (Charles River (UK)) were treated with the pro-hypertensive hormone AngII (Merck) for 24 h, 7 d or 14 d using Alzet osmotic pumps (model 1004; supplied by Charles River) filled according to the manufacturer's instructions in a laminar flow hood using aseptic technique and implanted subcutaneously. Mice were treated with 0.8 mg/kg/d AngII dissolved in acidified phosphate buffered saline (PBS), PBS containing 10 mM acetic acid or with acidified PBS alone. Prior to implantation, the minipumps were incubated overnight in sterile PBS (37°C) to equilibrate. Implantation was performed under

continuous inhalation anaesthesia (induction using 5% isoflurane, maintenance with 2-2.5% isoflurane mixed with 2 L/minute O_2). Prior to surgery, mice were given 0.05 mg/kg (subcutaneous) buprenorphine (Vetergesic, Ceva Animal Health Ltd.) to subdue any post-surgical discomfort and a 1 cm incision was made in the mid scapular region. Minipumps were implanted portal first in a pocket created in the left flank region of the mouse. Wound closure used a simple interrupted suture with polypropylene 4-0 thread (Prolene, Ethicon). Mice were recovered individually and returned to their home cage once completely recovered. Mouse studies were conducted at SGUL, unless otherwise stated.

At the end of the study protocol, mice were culled by schedule 1 (CO_2 followed by cervical dislocation). Hearts were excised quickly, washed in PBS (S8537, Sigma-Aldrich) and snap-frozen in liquid N_2 or fixed in 10% (v/v) buffered formalin for histology. The surgeries and tissue harvesting were conducted by members of the wider research team (Dr Daniel Meijles and Dr Susanna Cooper).

2.2.4. The SHR model

These samples were a kind gift from Professor Iain Greenwood (St Georges, University of London), generated in association with his PhD student's (Sam Baldwin) project. Male and female spontaneously hypertensive rats (SHR) (SHR/NHsd) and Wistar Kyoto (WKY) (WKY/NHsd) normotensive controls were purchased from Envigo. Envigo performed blood pressure measurements prior to shipping and provided written confirmation that the animals were hypertensive. Animals were shipped at 175-200 g and were acclimatised in the Biological Research Facility at SGUL until reaching 250-350 g (11-13 weeks) prior to sacrifice. Rats were culled by cervical dislocation with secondary confirmation by severance of the femoral artery with hearts excised, atria removed, washed in PBS, diced and frozen at -80˚C prior to processing.

2.3. Immunohistochemistry for NOX1, CD47 and TSP1 in the HHD (CRY/SGUL cohort)

Immunohistochemistry was performed by Sandra Ashton (Image Resource Facility, St Georges, University of London). Sections were de-waxed by immersion in xylene 100% (v/v) followed by rehydration in a series of alcohols (ethanol, 95% (v/v) ethanol, 90% (v/v) ethanol, 80% (v/v) ethanol, 70% (v/v) ethanol) following immersion in distilled H_2O, antigen retrieval was completed through addition of 10 mM TRIS-HCl buffer pH 10 to sections and were boiled for 10 min, washed in tris-buffered saline (TBS) and blocked with 10% (v/v) goat serum/1% (w/v) bovine serum albumin (BSA) for 1 h at RT, and were washed in TBS. Sections were then incubated overnight in a humidified chamber with either primary antibodies or IgG control antibodies in 1% (w/v) BSA with 0.025% (v/v) Triton X-100 in TBS. The primary

antibodies used were: monoclonal mouse anti-CD47 (14-479-82, Invitrogen); polyclonal rabbit anti-NOX1 (NBP1-31546, Novus Biologicals); and polyclonal rabbit anti-TSP1 (18304-1-AP, Proteintech). The IgG control antibodies used were: murine myeloma IgG1 isotype control (M5284, Sigma-Aldrich) or the rabbit Ig fraction control (X0903, Agilent).

Following antibody incubation, slides were washed in TBS and endogenous peroxidase activity was blocked with 0.3% (v/v) H_2O_2 in TBS for 15 min and were then washed in TBS. Following washing, sections were incubated with biotinylated secondary antibodies: affinity purified goat anti-mouse (BP-9200, Vector Laboratories) or goat anti-rabbit: (BP-9100, Vector Laboratories).

Sections were then incubated with avidin-D conjugated HRP (A2704, Vector Laboratories) before treatment with 3,3'-diaminobenzidine (DAB) substrate (17718096001, Roche) per manufacturer's instructions. To counter stain, sections were incubated with Harris haematoxylin (HHS16, Sigma-Aldrich), differentiated in 1% (v/v) HCL in 70% (v/v) ethanol, and blued in saturated lithium carbonate, and sequentially dehydrated in 95% (v/v) ethanol, followed by 100% (v/v) ethanol and then xylene. Following this, sections were mounted under a cover slip with DPX. Slides were digitised using the Nanozoomer 2.0RS slide scanner (Hamamatsu). Semi-quantification of sections was performed using Fiji software[342], according to an established protocol[343].

2.4. Cardiac tissue processing for biochemical characterisation

Cardiac tissue from human, mouse or rat samples was homogenised using two independent methods (by pestle and mortar, or by the MP Lysis System) according to the subsequent assays. The buffer used for tissue homogenisation was dependent on the technique used. For the particular buffer and homogenization method used for each tissue type, see the relevant chapter method sections.

2.4.1. Tissue homogenisation by pestle and mortar

Tissues homogenised by pestle and mortar for western blotting were homogenised in ice cold buffer (see Section 2.4.3) until the homogenate was uniform and fibrous tissue had been broken down.

2.4.2. Tissue homogenisation using the MP Lysis System

Tissue was homogenised in ice cold buffer (see Section 2.4.3) using lysing matrix SS tubes (MP biomedicals) with the FastPrep®-24 Classic bead beating grinder and Lysis System (MP Biomedicals).

2.4.3. Buffers used for tissue homogenisation

Tissues were homogenised for western blotting in either:

- Pierce™ radioimmunoprecipitation assay (RIPA) buffer (89900, Thermo Fisher Scientific) buffer with protease inhibitors (A32963, Thermo Fisher Scientific) and PhosSTOP (04 906 837 001, Roche).
- RBD buffer (20 mM Tris (pH 7.6) 1 mM ethylenediaminetetraacetic acid (EDTA), 10% (v/v) glycerol, 1% (v/v) Triton X-100, 100 mM KCL, 5 mM NaF, 0.2 mM NaVO4, 5 mM $MgCl_2$, 0.05% (v/v) 2 mercaptoethanol) with protease inhibitors and PhosSTOP.
- Hanks balanced salt solution (HBSS) (BE10-547F, Lonza) with protease inhibitors.

For RNA isolation, tissues were homogenised in 1 mL of TRIzol™ (15596018, Thermo Fisher Scientific) and were vortexed prior to RNA isolation. For ROS assays, tissues were homogenised in HBSS with protease inhibitors.

2.4.4. Homogenate centrifugation

Prior to centrifugation, homogenates for western blotting prepared in RIPA buffer or RBD buffer were left on ice for 30 min, whilst homogenates intended for ROS assays underwent a freeze-thaw cycle. To remove debris, homogenates were centrifuged at 4°C. For speed and time, see specific chapter method sections. The supernatant was removed and protein concentration was assessed.

2.5. Assessment of protein concentration

To assess protein concentration from HBSS homogenates, the Bradford assay was used. To assess protein concentration from homogenates prepared in RIPA or RBD buffer, the bicinchoninic acid (BCA) assay was used. 0 to 2 mg/mL BSA (A30075, Melford Laboratories Ltd) standards were prepared by serial dilution.

2.5.1. Bradford assay

1 µL of sample was used with 150 µL of 1 x Bradford reagent (39222.02, SERVA) in HBSS per well of a 96-well plate (WP). The absorbance was measured at 595 nm using a Synergy LX multimode reader (BioTek) with Gen5 software. From the absorbance measured, a BSA standard curve was plotted and protein concentration was determined based upon this.

2.5.2. BCA assay

1 µL of sample was used with 200 µL BCA A+B reagent from the Pierce™ BCA Protein Assay Kit (23225, Thermo Fisher Scientific), per well of a 96-WP. This was incubated at 37˚C for 30 min. The absorbance was then measured at 562 nm using a Synergy LX multimode reader (BioTek) with Gen5 software. From the absorbance measured, a BSA standard curve was plotted and protein concentration was determined based upon this.

2.6. Assessment of protein expression by western blotting

2.6.1. Homogenous polyacrylamide gels

Homogenous polyacrylamide gels were hand cast (8%, 10% or 12% (v/v) acrylamide resolving gel with 6% (v/v) acrylamide stacking gel), and were made from 40% acrylamide (A11265, Melford Laboratories Ltd.), 2% bis-acrylamide (A11275, Melford Laboratories), 0.5% (v/v) of 20% (w/v) sodium dodecyl sulphate (SDS) (S/5200/53, Thermo Fisher Scientific), 0.375 M of Tris-HCL (pH 6.8) for the resolving gel or 0.125 M of Tris-HCL (pH 6.8) for the stacking gel, 0.1% (v/v) tetramethylethylenediamine (TEMED) (T/P1904/04, Fischer Chemical), and 0.75% (v/v) of 20% ammonium persulphate (201531000, Acros Organics).

2.6.2. Gradient polyacrylamide gels

Alternatively, gradient polyacrylamide gels were used (Mini-PROTEAN TGX Precast 4-20% Gels, (456-1096, Biorad)). For the gel type used, see the methods section of the relevant Chapter.

2.6.3. Homogenate preparation

Following determination of protein concentration, homogenates were prepared in 4 x SDS-PAGE sample buffer (0.33 M Tris-HCl pH 6.8, 10% (w/v) SDS, 13% (v/v) glycerol, 133 mM dithiothreitol, 0.2 mg/mL bromophenol blue). Samples were then boiled and were loaded directly from the heat block. For tissues samples, approximately 100 or 200 µg of protein was loaded per lane. For cell culture samples, between 20 and 100 µg was loaded per lane (for further details see corresponding chapter methods sections).

2.6.4. Electrophoresis

SDS-polyacrylamide gel electrophoresis (PAGE) was performed using Mini-PROTEAN Tetra Cell (Bio-Rad) gel electrophoresis apparatus operated at 200 V (constant) for 60 min). The running buffer used consisted of 25 mM tris base (SC-715, Santa Cruz), 129 mM glycine (SC-29096, Santa Cruz) and 10 g/L SDS. Precision Plus Protein™ Kaleidoscope™ Prestained Protein Standards (160375, Bio-Rad) were used to determine molecular weight.

2.6.5. Protein transfer

The separated proteins were subsequently transferred from the polyacrylamide gels to 0.45 µm nitrocellulose membranes (1620115, Bio-Rad) using a Trans-Blot® SD Semi-Dry Transfer Cell (Bio-Rad) for 60 min at 10 or 12 V. The buffer used for protein transfer consisted of 10 mM tris base, 77 mM glycine and 20% (v/v) methanol (20847.307, VWR), except for polyacrylamide gels where the proteins separated were intended for TSP1 detection. Transfer of proteins from these gels used a buffer suitable for the transfer of high molecular weight proteins, which consisted of 48 mM tris base, 39 mM glycine, 1.3 mM SDS and was at pH 9.2).

2.6.6. Total protein staining

For total protein staining, nitrocellulose membranes were stained using the REVERT total protein stain and wash kit (926-11015, LI-COR Biosciences) according to manufacturers instructions. Imaging was performed using an Odyssey® CLx Imaging System (LI-COR Biosciences) in the 700 nM channel.

2.6.7. Antibody incubation

To block non-specific antibody binding, 2% (w/v) non-fat skimmed milk (A0830, Panreac Applichem) was used as a non-specific blocking agent. Primary antibodies were diluted in 1% (w/v) BSA (A30075, Melford)/ TBS with 0.1% (v/v) Tween 20 (TBST) and were applied overnight at +4˚C with gentle agitation (see Table 2.1 for antibody information and dilution). Following this, the membranes were washed for 3 x 5 min in TBST at RT with agitation. Horseradish peroxidase (HRP)-conjugated secondary antibodies (see Table 2.1 for antibody information and dilution) were diluted in 1% (w/v) non-fat skimmed milk/TBST and were incubated for 60 min at RT with gentle agitation. Membranes were then washed for 3 x 5 min in TBST at RT with agitation.

2.6.8. Imaging

Secondary antibody staining was visualised using enhanced chemiluminescence using the Amersham ECL Prime Western Blotting System (RPN2232, GE Healthcare) with an ImageQuant LAS4000 camera system (GE Healthcare). Bands were exposed until either the maximum limit of intensity detection was reached or until there was no longer a change in intensity. Band intensity was determined using Fiji software[342].

Table 2.1. Antibody information and concentration for antibodies used for western blotting

Target	Type	Catalogue #	Manufacture	Dilution
GAPDH	Mouse monoclonal	60004-1-Ig	Proteintech	1/1000 or 1/5000
TSP1	Mouse monoclonal	37879	Cell signalling technology (CST)	1/750
CD47	Rabbit monoclonal	SC-12730	Santa Cruz	1/500
	Rabbit polyclonal	63000	CST	1/1000
NOX1	Rabbit monoclonal	ARP46818_P050	Aviva Systems Biology	1/750 or 1/1000
T-ERK1/2	Rabbit monoclonal	4695	CST	1/1000
P-ERK1/2	Rabbit monoclonal	4370	CST	1/1000
T-p38-MAPK	Rabbit monoclonal	8690	CST	1/1000
P-p38-MAPK	Rabbit monoclonal	4511	CST	1/1000
T-JNK	Purified rabbit polyclonal	9252	CST	1/1000
P-JNK	Rabbit monoclonal	4668	CST	1/1000
Dusp1	Rabbit monoclonal	35217	CST	1/750
Dusp2	Affinity purified rabbit polyclonal	SAB4300841	Sigma-Aldrich	1/750
Dusp4	Purified rabbit polyclonal	Ab72593	Abcam	1/750 or 1/1000
Dusp5	Rabbit monoclonal	Ab200708	Abcam	1/750 or 1/1000
Dusp6	Rabbit monoclonal	Ab76310	Abcam	1/750
Dusp7	Rabbit polyclonal	26910-1-AP	Proteintech	1/750 or 1/1000
Dusp8	Rabbit polyclonal	NBP2-92392	Novus Biologicals	1/750
Dusp10	Purified rabbit polyclonal	3483	CST	1/750
Dusp16	Rabbit monoclonal	5523	CST	1/750
Anti-mouse	HRP-conjugated affinity purified goat polyclonal	P0447	DAKO	1/10000
Anti-rabbit	HRP-conjugated affinity purified goat polyclonal	P0448	DAKO	1/10000

2.7. Assessment of gene expression

2.7.1. mRNA isolation

RNA was extracted from samples using TRIzol™. To separate protein, DNA and RNA, 200 µL of chloroform (J67241, Alfa Aesar) was added per mL of TRIzol™ and was incubated for 10 min. Samples were centrifuged at 12000 x *g* for 15 min at 4˚C. The upper RNA containing aqueous phase was transferred to a new tube and 500 µL isopropanol (BP2618, Thermo Fisher Scientific) was added per mL of TRIzol™ and was incubated overnight at -20˚C. After overnight incubation, samples were centrifuged at 12000 x *g* for 10 min at 4˚C. Supernatant was removed and the RNA containing pellets were resuspended in 75% ethanol (ethanol absolute (E/0650PF/17, Thermo Fisher Scientific). Following a quick (1 s) vortex, pellets were centrifuged at 7,500 x *g* for 5 min. Supernatant was removed and the addition of 75% ethanol and centrifugation was repeated. Any remaining ethanol was allowed to evaporate from the RNA at 30°C. The RNA was diluted with UltraPure™ diethyl pyrocarbonate-treated water (750023, Invitrogen) and resolubilised at 55°C. RNA concentration was determined at 280 nm using a DS-11 Spectrophotometer/Fluorometer (Denovix). Purity was assessed by measuring the using the. A260/280 ratio, and only preparations with an A260/280 >1.4 were used.

2.7.2. cDNA synthesis

Complementary DNA (cDNA) was prepared from 0.5 µg RNA derived from primary cardiac ECs cells and the St George's hospital endothelial cell-7 (SGHEC-7) cell line, whilst cDNAs from the SVEC4-10 cell line and tissue samples were prepared from 1 µg RNA. cDNA was synthesised using the High-Capacity cDNA Reverse Transcription Kit (4368814, Thermo Fisher Scientific), used according to manufacturer's instructions, using a Mastercycler Pro S (Eppendorf). The thermocycler was programmed as follows: 25˚C (10 min), 37˚C (120 min), 85 ˚C (5 min), and cooled to 4˚C.

2.7.3. Quantitative real time PCR (qPCR)

Primers were obtained from Invitrogen (for primer details, see Appendix Table 3 (human), Appendix Table 4 (mouse) and Appendix Table 5 (rat). Luna Universal qPCR Master Mix (M3003, New England Biolabs) was used as specified by the manufacturer with 5 µM dual primer solution. qPCR was performed on a CFX96 or a CFX connect Real Time qPCR Detection System (Bio-Rad). The qPCR systems were programmed as follows; heat to 95˚C (1 min); followed by 40 cycles of heating to 95˚C (15 s); followed by cooling to 60˚C (30 s). Melt curves were used to assess primer specificity. Results were analysed using the $2^{-\Delta\Delta CT}$ method[344].

2.8. Assessment of ROS generation

Cardiac ROS production was measured either by either Amplex red for H_2O_2 production (see Section 2.8.1) or by cytochrome c reduction for superoxide production (see Section 2.8.2). These assays are independent and complimentary. Cardiac tissue was homogenised in HBSS and made up to 1 µg/µL in 20 µL for the ROS assays prior to addition to each well. The average emission was taken from technical duplicates or triplicates.

2.8.1. Amplex Red assessment of H_2O_2 production

H_2O_2 production from whole cells and homogenised cells and tissues was measured using the Amplex Red (Invitrogen Inc.) assay. Black 96-WPs were used. From homogenates, 20 µL of sample (see relevant Chapter methods for concentration) was added to each well, containing 80 µL of assay mix in PBS. The assay mix consisted of; 0.1 mM Amplex Red (A12222, Thermo Fisher Scientific), 0.32 U/mL HRP (P8375, Sigma-Aldrich). A standard curve was generated using 0 to 10 µM H_2O_2 standards, prepared by serial dilution of H_2O_2 (H/1750/15, Thermo Fisher Scientific) in PBS. The reaction was initiated by the addition of 20 µL of 0.7 mg/mL NAPDH (N20140, Melford Laboratories Ltd), prepared in HBSS, into each well. For cell culture samples, the NADPH was supplemented with 1.8 mM $CaCl_2$ and 0.8 mM $MgCl_2$. Fluorescence (excitation: 544 nm, emission; 590 nm) was detected continuously using a Flurostar Omega (BMG Labtech) plate reader over 60 min at 30°C for cellular and tissue homogenates and over 75 min at 37°C for whole cells.

Analysis of the Amplex red assay was performed in Excel. The cumulative fluorescence intensity was measured over time following NAPDH addition. The average increase in H_2O_2 generation (mean fluorescence intensity (MFI)) was calculated from the linear rate of H_2O_2 production from technical duplicates or triplicates. Using the MFI and the standard curve generated from the H_2O_2 standards, the rate of H_2O_2 production was determined.

2.8.2. Assessment of superoxide production by Cytochrome C reduction

Superoxide production from tissue homogenates was measured using Cytochrome C reduction. 20 µL of homogenate made up to 1 µg/µL protein was added to each well of a 96-well plate (WP) containing 80 µL of assay mix. The assay mix was prepared in HBSS and contained 2.5 mg/mL cytochrome C (30398, Sigma-Aldrich) and 300 U/mL catalase. The reaction was initiated by the addition of 20 µL of 0.7 mg/mL NAPDH prepared in HBSS, and the absorbance at 550 nm was measured using Synergy LX multimode reader (BioTek) with Gen5 software. The reaction was monitored continuously for 60 min at RT.

Analysis of the Cytochrome C reduction was performed in Excel. The rate of superoxide produced was calculated from the linear rate of cytochrome c reduction over time following NAPDH addition, using the following equation[345]:

$$\text{Superoxide production (nmol/min)} = \frac{\Delta\text{Abs (at 550 nm)/min} \times 0.047619 \times \text{reaction volume (mL)}}{\text{Path length (cm)}}$$

2.9. Isolation of primary mouse cardiac cells

Primary cardiac myocytes and ECs were isolated from male and female adult C57Bl/6J mouse hearts. Protocol was adapted from[346].

2.9.1. Preparation of hearts

Mice were sacrificed, hearts were excised and transported from the Biological Research Facility in ice cold PBS. Hearts were washed in DMEM (4.5 g/L glucose) (LZBE12-614F, Lonza) with 10 mM butanedione monoxime and minced until 1-2 mm pieces remained.

2.9.2. Isolation of mouse myocytes

Myocytes were isolated from minced heart preparations with digest buffer (DMEM (4.5 g/L glucose) supplemented with 10 mM butanedione monoxime and 2.1 mg/mL type 2 collagenase) at 37°C with gentle agitation. The initial digest was for 5 min, and following digests were for 10 min. Following each digest, the digest buffer containing cardiac cells was transferred into a separate tube, where it was neutralised in foetal bovine serum (FBS) (F9665, Sigma-Aldrich). Digest buffer was then added again to the minced hearts, and isolation was repeated. This occurred four times, until tissue appeared white. Myocytes were collected in a cell pellet by centrifuging at 30 x *g* for 5 min and were resuspended in in DMEM (4.5 g/L glucose) with 10 mM butanedione monoxime. Myocytes were used immediately after isolation for experimentation

2.9.3. Isolation of mouse cardiac ECs

After the isolation of myocytes, cardiac ECs were extracted by incubating the remaining minced heart tissue in 0.05% (v/v) trypsin (T4049, Sigma-Aldrich; diluted in PBS) for 5 min at 37°C followed by neutralisation in FBS. This was repeated several times. The resulting suspensions were centrifuged at 30 x *g* for 5 min to clear large debris, and the supernatant was centrifuged at 300 x *g* for 5 min. The EC containing cell pellet was resuspended in DMEM (4.5 g/L glucose) supplemented with 10% (v/v) FBS, 50 U/mL penicillin and 50 µg/mL streptomycin. ECs were plated into gelatine coated 10 cm^2 dishes (for method of gelatine coating see Chapter 2.10.1). After 4 h and after approximately 16 h the medium was replaced, leaving only cells which had adhered to the dish.

2.9.4. Confirmation of EC cell type

To confirm the cell type of the isolated cardiac ECs, the mRNA expression of: the endothelial markers,*Vegfr2* and *Cd31*, and the fibroblast markers, *Discoidin domain receptor tyrosine kinase 2 (Ddr2)* and *fibronectin 1* (*Fn1)*, were determined in mouse cardiac ECs and in the SVEC4-10 cell line (Appendix Figure 1).

2.10. Cell culture

All cell culture practices were performed in a Class 2 biological safety cabinet using aseptic technique. Cells were grown in a humidified incubator set to 37°C, in an atmosphere of 5% CO_2 in air.

2.10.1. Gelatine coating of plasticware for primary cardiac ECs.

Gelatine coated plasticware was prepared in a Class 2 biological safety cabinet. A 1% (v/v) gelatine solution was diluted from 2% bovine skin gelatine (G1393, Sigma-Aldrich) with sterile cell-culture grade PBS. The 1% gelatine solution was pre-warmed at 37°C for at least 20 min before coating cell culture treated plasticware with 5-10 µL of gelatine solution per cm^2. The gelatine was polymerised at 37°C for 30 min, excess gelatine was removed, and the plasticware was dried for 2 h at RT before use.

2.10.2. Primary mouse cardiac ECs

Cardiac ECs isolated as above were cultured in DMEM (4.5 g/L glucose) supplemented with 10% (v/v) FBS and 50 U/mL penicillin and 50 µg/mL streptomycin. Cells were grown to 90% confluency (assessed by light microscopy) in gelatine coasted plasticware prior to subculture (see Section 2.10.6). Cells were used at passage 2 for experiments.

2.10.3. Primary human cardiac fibroblasts

Human cardiac fibroblasts (HCFs) (HCF-c, C-12375; Lot #: 450Z014.1 and 437Z012.4, PromoCell) were grown in Fibroblast Growth Medium 3 (C-23025, PromoCell) with SupplementMix (C-39345). Cells were seeded into 6-WPs and were grown until confluency before subculture (see Section 2.10.6). Cells were used between passage 7 and 8 for experiments.

2.10.4. SGHEC-7 cell line

The St George's hospital endothelial cell-7 (SGHEC-7) cell line, generated from SV40 transfected human umbilical vein endothelial cells (HUVECs)[347], was kindly provided by Professor Guy Whitley (SGUL). SGHEC-7s were grown in 50% (v/v) Medium 199 (12-702F, Lonza) and 50% (v/v) RPMI-1640 (BE12-199F, Lonza), supplemented to a final concentration with 2 mM L-glutamine (25030-024, Gibco), 50 U/mL penicillin and 50 µg/mL streptomycin (P4458, Sigma-Aldrich), 2.5 µg/mL endothelial cell growth supplement from bovine neural

tissue (E2759, Sigma-Aldrich), 16.17 U/mL Heparin (H3149, Sigma-Aldrich), and 5% (v/v) foetal bovine serum (FBS). Cells were grown to confluency (assessed by light microscopy) prior to subculture (see Section 2.10.6). Passages 16-25 were used for experiments.

2.10.5. SVEC4-10 cell line

SVEC4-10 (SV40 transformed ECs from axillary lymph node vessels, ATCC) cells were cultured in DMEM (1 g/L glucose) (LZBE12-707F, Lonza) supplemented with 10% (v/v) FBS, 50 U/mL penicillin and 50 µg/mL streptomycin, unless otherwise stated. Cells were grown to 90% confluency (assessed by light microscopy) prior to subculture (see Section 2.10.6). Passages 22-35 were used for experimentation.

2.10.6. Subculture

Cells were detached by trypsinisation using 0.05% (v/v) trypsin. The cultures were centrifuged at 300 x *g* for 5 min (mouse cardiac EC, HCF, and SVEC4-10), or 300 x *g* for 10 min (SGHEC-7), prior to resuspension of cell pellet.

2.11. *In vitro* cell culture studies

2.11.1. Stimuli and inhibitors

Cells were seeded and synchronised by addition of serum reduced media (see Chapter methods for information), prior to challenge with: 100 nM AngII (4095850, Bachem); 10 µM 7N3 (sequence: FIRVVMYEFGKK, Peptide Protein Research Ltd.), a TSP1 derived, CD47 activating peptide; 1 µM setanaxib (GKT-137831, MedChemExpress), a small molecule inhibitor of NOX1/4; 10 µM NOXA1ds (sequence: EPVDALGKAKV, Peptide Protein Research Ltd), a peptidic inhibitor of NOX1 which prevents NOXA1 binding; or 10 µM of the scrambled NOXA1ds sequence, SCRAM (sequence: LVKGPDAEKVA, Peptide Protein Research Ltd). These concentrations were used throughout. These concentrations were chosen based upon those used for previous studies[134,175,237].

2.11.2. Assessment of protein expression

For western blotting, cells were lysed with either RIPA buffer or G buffer (20 mM β-glycerophosphate (pH 7.5), 50 mM NaF, 2 mM EDTA, 0.004 mM microcystin LR, 1% (v/v) Triton X-100, 5 mM dithiothreitol, 10 mM benzamidine, 0.2 mM leupeptin, 0.01 mM trans-epoxy succinyl-l-leucylamido-(4-guanidino)butane, 0.3 mM phenylmethylsulfonyl fluoride, kindly provided by Professor. Angela. Clerk, University of Reading), a buffer optimised for maintaining protein phosphorylation. Both buffers contained PhosSTOP and protease inhibitors. Homogenate was then passed through a 25 gauge needle (9186158, Braun) and centrifuged for 5 min at 200, 1000 or 1500 x *g* at 4°C and protein concentration was assessed by the BCA assay (Chapter 2.5) and samples were made up to an appropriate concentration with 4 x SDS-PAGE sample buffer. Alternatively, cells were processed for western blotting by

the addition of 1 x SDS-PAGE sample buffer directly to cells. For these samples, protein concentration was not determined. Western blotting was conducted as Chapter 2.6.

2.11.3. Assessment of gene expression

RNA was extracted 0.5 mL TRIzol™ per well of a 6-WP or 6 cm^2 dish. Gene expression was determined as Chapter 2.7.

2.12. Statistical analysis

Statistical analysis was performed using GraphPad Prism 8. Data were assessed for normality, outliers were identified and removed using either the ROUT (Q=1%) or Grubbs test (Alpha = 0.05) and an unpaired T-test or one way ANOVA was performed as appropriate.

Chapter 3: TSP1 expression is upregulated in the hypertensive heart

3.1. Introduction

Cardiac hypertrophy and fibrosis underpin the pathology of hypertensive heart disease (HHD), although, in hypertension, reduced capillary density has also been observed in the heart and in the periphery[66,91,92]. Furthermore, impaired cardiac angiogenesis has been associated with pathological cardiac remodelling, including fibrosis and dilatation, and is associated with reduced cardiac function in rodent models of cardiac hypertrophy[93,95,96].

TSP1 is both a proposed mediator of fibrotic remodelling in diseases including diabetic cardiomyopathy and chronic kidney disease[113,348], and is an ascribed anti-angiogenic protein[134]. The anti-angiogenic properties of TSP1 have been attributed to its interaction with CD47[134,140–142], and the activation of CD47 by TSP1 has also been demonstrated to promote senescence in human pulmonary aortic ECs (HPAECs) by promoting the expression of NOX1 and the subsequent production of ROS[175]. Although TSP1 is upregulated in several diseases where fibrotic remodelling occurs, in the hypertensive heart, which is known to be associated with fibrotic remodelling, it is not known if elevated TSP1 expression occurs.

For this part of the project, the hypothesis was that TSP1-CD47 signalling promotes cardiac ROS production through NOX1 in the hypertensive heart. As such, it was hypothesised that cardiac TSP1 and NOX1 expression, and ROS production would all be elevated in the hypertensive heart, whilst the expression of CD47 would remain unchanged. Therefore, this project investigated the cardiac mRNA and protein expression of TSP1 and CD47 in human non-ischaemic HF (NI-HF), in AngII-induced hypertensive mice, and in spontaneously hypertensive rats (SHRs). Additionally, the localisation of TSP1, CD47 and NOX1 was identified in human HHD, and finally, in NI-HF and in hypertensive rodents, cardiac ROS production and the mRNA and protein expression of cardiac NOX1 were determined.

3.2. Methods

3.2.1. NI-HF and HHD cohorts

Within the Pittsburgh NI-HF cohort, the following aetiologies were included; non-ischaemic, hypertrophic, and dilated cardiomyopathy (DCM), and both male and female hearts were used (details in Appendix Table 1). For TSP1 and CD47 protein expression, cardiac tissue from an additional 7 NI-HF patients and 7 controls was used. This tissue was also part of the Pittsburgh cohort (see Section 2.1.1) and was a kind gift from Associate Professor Natasha Rogers, (The University of Sydney). Group numbers (NI-HF and HHD) were determined based on previous studies, the availability of samples, and the power required for differences to be observed. For further information see Chapter 2.1.

3.2.2. *In vivo* mouse AngII hypertensive model

Mice were treated as detailed in Chapter 2.2.3. For RNA sequencing (RNAseq), mice were treated with either AngII (0.8 mg/kg/d) or acidified PBS (veh) for 7 d. Following cardiac RNA isolation, RNAseq and statistical analysis was conducted by collaborators at the Francis Crick Institute. For qPCR and western blotting, mice were treated with AngII for either 24 h, 7 d or 14 d, or with acidified PBS (veh). To enrich the veh and 7 d AngII data in NOX1 protein expression studies, an additional 4 mice per group, treated at UoR, were used. A summary diagram is presented in Figure 3.1A.

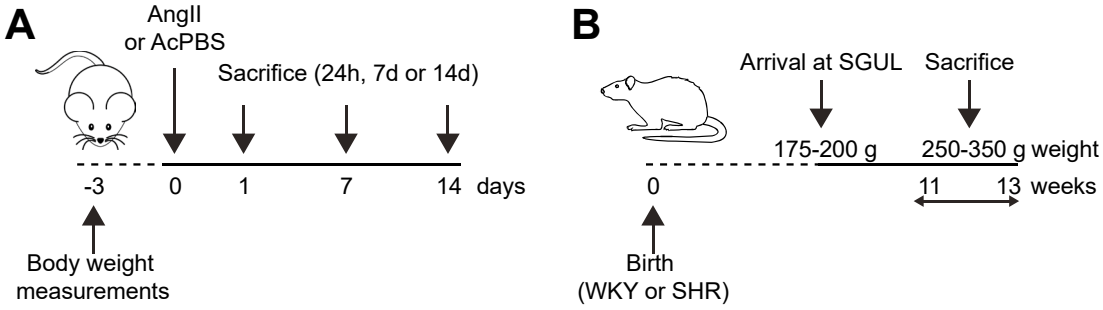

Figure 3.1. Schematic for rodent studies.
(**A**) 3 d prior to minipump implantation, mice were weighed to determine the amount of AngII required for a dose of 0.8 mg/kg/d. Mice were sacrificed 24 h, 7 d or 14 d after minipump implantation. (**B**) Rats weighing 175-200 g were imported from Envigo to SGUL and were acclimatised until reaching 250-350 g (11-13 weeks of age), at which point rats were sacrificed. Following rodent sacrifice, the tissues were harvested for subsequent characterisation.

3.2.3. SHR model

SHRs (11-13 weeks) with confirmed hypertension were used, as detailed in Chapter 2.2.4. The SHR group was comprised of male (n=6) and female (n=6) SHRs, whilst the age-matched

normotensive control group compromised male (n=6) and female (n=6) Wistar Kyotos (WKYs). A summary diagram is presented in Figure 3.1B.

3.2.4. Assessment of tissue mRNA expression

As detailed in Chapters 2.4 and 2.7, mRNA was isolated from human tissue using the MP Lysis System at 5 meters/second (m/s) for 10 seconds (s) and mRNA was isolated from rodents by pestle and mortar homogenisation.

3.2.5. Assessment of tissue protein expression

Tissues were homogenised as detailed in Chapter 2.4 and protein concentration was assessed as per Chapter 2.5, with specific details in Table 3.1. Protein expression was assessed by western blotting as described in Chapter 2.6, with specific details in Table 3.2.

3.2.6. ROS assays

Cardiac tissue was prepared for ROS assays as detailed in Chapter 2.4, ROS assays were performed as per Chapter 2.8. For the homogenisation technique used and amount of protein loaded per well, see Table 3.3.

Table 3.1. Methods used for cardiac tissue homogenisation and assessment of protein concentration

Tissue	Homogenisation buffer†	Homogenisation technique	Centrifugation force (*g*)	Centrifugation time (min)	Assay for determination of protein concentration
Human LV cardiac tissue	RIPA	Pestle and mortar	1500	3	BCA
Mouse cardiac tissue	HBSS	Pestle and mortar (SGUL cohort) MP Lysis System (4 m/s / 5 s) (UoR cohort)	1500	5	Bradford Assay
Rat ventricular tissue	RBD buffer	Pestle and mortar	1500	5	BCA
† All buffers contained protease inhibitors. RIPA and RBD buffers also contained PhosSTOP.					

Table 3.2. Antibody and gel loading information used to determine protein expression in cardiac tissue

Tissue	Antibody	Antibody details	Antibody concentration	Gel %	Protein loaded per lane (µg)
Human LV cardiac tissue	TSP1	37879, CST	1/750	Gradient gel	75
	CD47	SC-12730, Santa Cruz	1/500	10	75
		63000, CST	1/1000		
	NOX1	ARP46818_P050, Aviva Systems Biology	1/750	12	100
Mouse cardiac tissue	TSP1	37879, CST	1/750	8	100
	CD47	SC-12730, Santa Cruz	1/500	8	100
	NOX1	ARP46818_P050, Aviva Systems Biology	1/750	10	100
Rat ventricular tissue	TSP1	37879, CST	1/750	8	200
	CD47	SC-12730, Santa Cruz	1/500	10	200
		63000 CST	1/1000		
	NOX1	ARP46818_P050, Aviva Systems Biology	1/750	10	200

Table 3.3. Homogenisation and protein loading for ROS assessment in cardiac tissue

Tissue	Assay	Homogenisation technique	MP Lysis System speed (m/s)	MP Lysis System time (s)	Centrifugation force (*g*)	Centrifugation time (mins)	Protein loaded per well (µg)
Human LV cardiac tissue	Amplex Red	Pestle and mortar	N/A	N/A	1500	3	25
	Cytochrome C						35
Mouse cardiac tissue	Amplex Red	MP Lysis System	5	5	300	5	100
	Cytochrome C	Pestle and mortar	N/A	N/A	1500	5	100
Rat ventricular tissue	Amplex Red	Pestle and mortar	N/A	N/A	200	5	100
	Cytochrome C				1500	5	100

3.3. Results

3.3.1. TSP1 is elevated in human NI-HF

TSP1 is upregulated in several diseases where fibrotic remodelling occurs; however, it is not known whether this occurs in the hypertensive heart, which is also characterised by fibrosis. Therefore, this project investigated the mRNA and protein expression of TSP1 in NI-HF and in the hypertensive heart.

The results showed that, although there was no change to the number of cardiac *THBS1* transcripts in the NI-HF cohort (Figure 3.2A), TSP1 protein expression was elevated (4.44-fold, $p<0.0001$) (Figure 3.2B). Of the various aetiologies encompassing NI-HF, those clinically characterised by dilated cardiomyopathy and hypertrophic aetiologies tended to have lower TSP1 protein expression compared with the non-ischaemic aetiology. As the key receptor for the anti-angiogenic properties of TSP1 is CD47, CD47 mRNA and protein expression were also investigated; however, both were unchanged in the NI-HF cohort and controls (Figure 3.2A-B). Next, cardiac TSP1 and CD47 protein expression and localisation were investigated by IHC in the HHD cohort. The expression of CD47 (Figure 3.3A), and TSP1 (Figure 3.3B), expression was unchanged, and both CD47 and TSP1 were localised to cardiac myocytes and cardiac vessels, albeit TSP1 staining was greater around vessels (Figure 3.3B). Overall, TSP1 protein expression was elevated in NI-HF but not HHD, where it may localise to cardiac vessels, and there was no change to CD47 in either pathology.

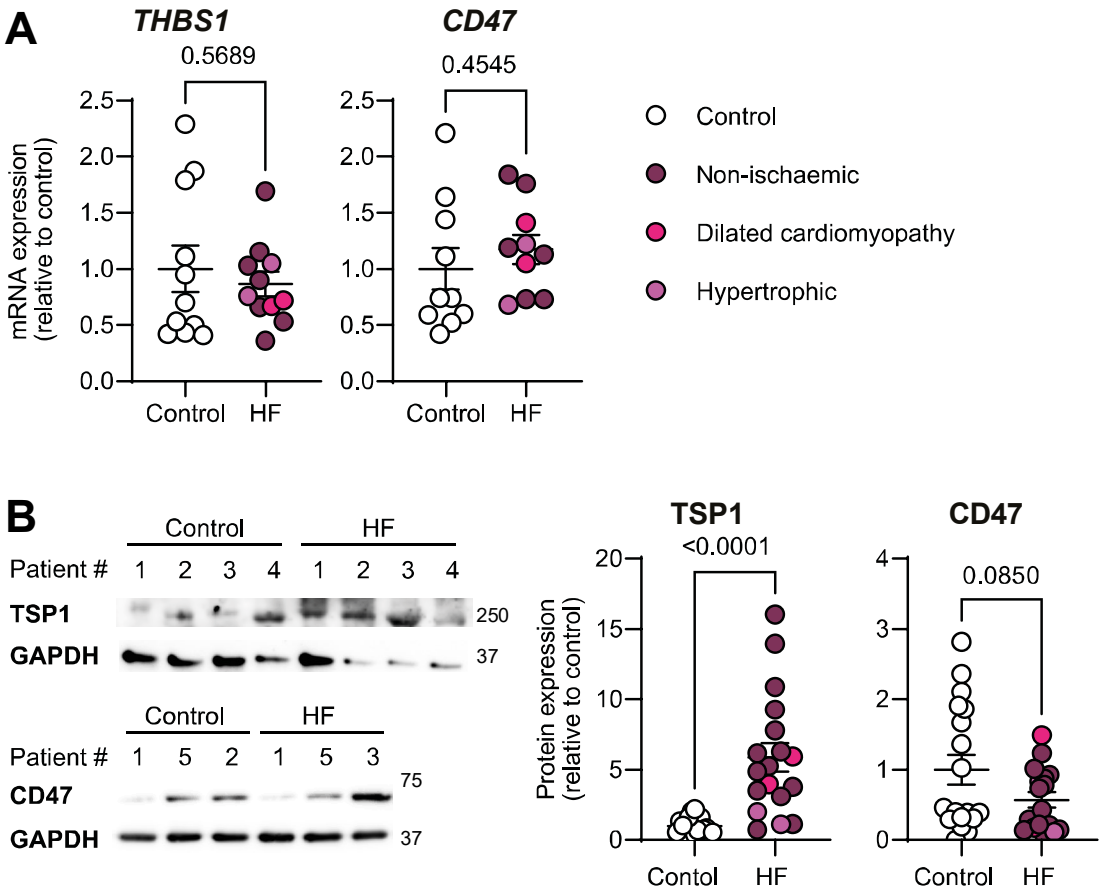

Figure 3.2. The expression of TSP1 is elevated in NI-HF.
Left-ventricular cardiac tissue from the NI-HF cohort was assessed for (**A**) *THBS1* and *CD47* mRNA expression (control: n=12; NI-HF: n=12) and (**B**) TSP1 and CD47 protein expression (control: n=19; NI-HF: n=19). mRNA expression was determined by qPCR, normalised to GAPDH. Protein expression was determined by western blot, with representative blots shown with quantification, normalised to GAPDH. Data are means ± SEM, showing individual values. Statistical test: t-test, reporting p-values.

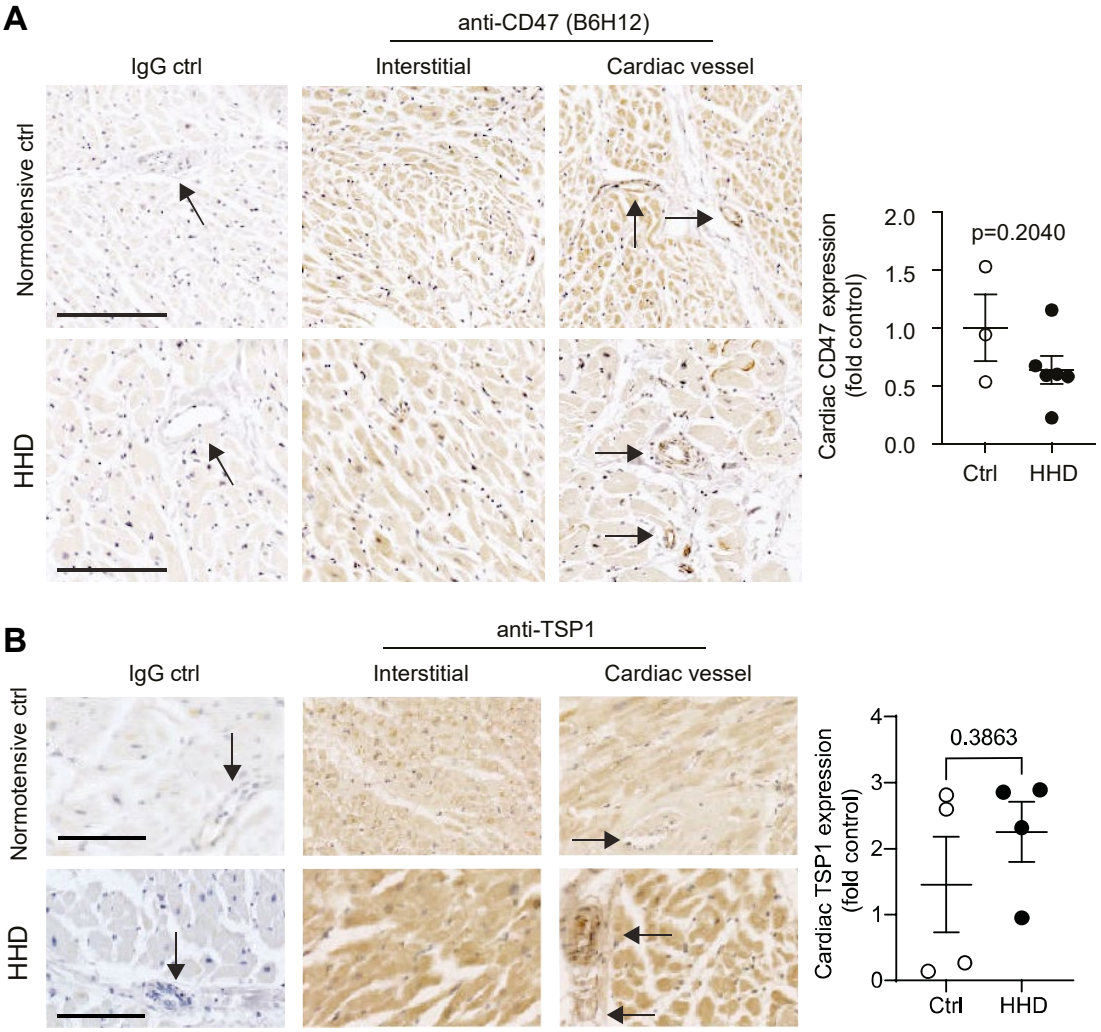

Figure 3.3. No change in cardiac CD47 or TSP1 expression in HHD, which localise to both cardiac muscle and cardiac vessels.

Cardiac sections of human LV posterior walls were labelled by IHC for (**A**) anti-CD47 (control: n=3; HHD: n=6) or (**B**) anti-TSP1 (control: n=4; HHD: n=4) and were compared to IgG controls for each case. Left panels: representative images of normotensive controls *vs*. HHD, assessing both cardiac muscle (interstitial) and intra-cardiac vessel regions. Scale bar: 100 µm. Images taken at 5 x magnification. Arrows highlight vessels. Right panels: Quantification of CD47 or TSP1 expression, normalised to IgG controls (CD47 only), assessed by staining intensity. Data are means ± SEM, showing individual values. Statistical test: t-test, reporting p-values.

3.3.2. Cardiac TSP1 expression levels are elevated in AngII-induced hypertension

As elevated cardiac TSP1 expression had been observed in end stage NI-HF, but not in HHD, it was investigated whether cardiac TSP1 expression was increased throughout the progression of HHD. Initially, the transcriptome of mice treated with AngII for 7 d, reflecting the adaptive phase of hypertension, was assessed by RNAseq. The results indicated that *Thbs1* was one of the most highly elevated genes in this model of AngII-induced hypertension, compared with controls (3.02-fold, adjusted $p=3.76x10^{-14}$) (Figure 3.4A-B). Other TSPs, *Thbs3* (1.75-fold, adjusted p=0.0002) and *Thbs4* (1.83-fold, adjusted $p=4.34x10^{-5}$) were elevated, albeit to a lesser extent than *Thbs1,* whilst *Thbs2* gene expression was unchanged (Figure 3.4B). See Appendix Figure 2 for the individual data points of *Thbs* gene expression. In addition, the gene expression of the TSP1 receptors, *Cd47* and *Cd36*, were unchanged (Figure 3.4B). However, there was a slight elevation in *Sirpα* gene expression (1.34-fold, adjusted p=0.0017), a CD47 ligand (Figure 3.4B).

To confirm elevated TSP1 and unchanged CD47 expression levels in AngII-induced hypertension, and to identify whether increased cardiac TSP1 expression occurred throughout HHD progression in this model, cardiac tissue from AngII-induced hypertensive mice were assessed at 24 h, 7 d and 14 d of continuous AngII infusion for *Thbs1* and *Cd47* mRNA expression levels by RT-qPCR, and TSP1 and CD47 protein expression levels were assessed by western blot. The duration of AngII infusion reflects the acute (24 h), adaptive (7 d) and chronic (14 d) responses of the hearts to AngII. The results showed that *Thbs1* was highly elevated at 24 h following AngII infusion (8.11-fold, p<0.0001) and this change was reflected in the protein by 7 d (7.70-fold, p=0.0065), whilst CD47 expression was unchanged (Figure 3.5A-B).

Furthermore, the SHR model of essential hypertension was used to corroborate the change in expression in these pathways. However, *Cd47* and *Thbs1* mRNA expression levels were unchanged (Figure 3.5C), and the TSP1 protein expression level was also unchanged, whereas the CD47 protein expression level was highly elevated (18.66-fold, p=0.0001) (Figure 3.5D). Overall, in AngII-induced hypertensive mice, the protein expression of TSP1 was elevated, whilst the protein expression of CD47 was unchanged, similar to human NI-HF. In the SHR model, however, the converse was true.

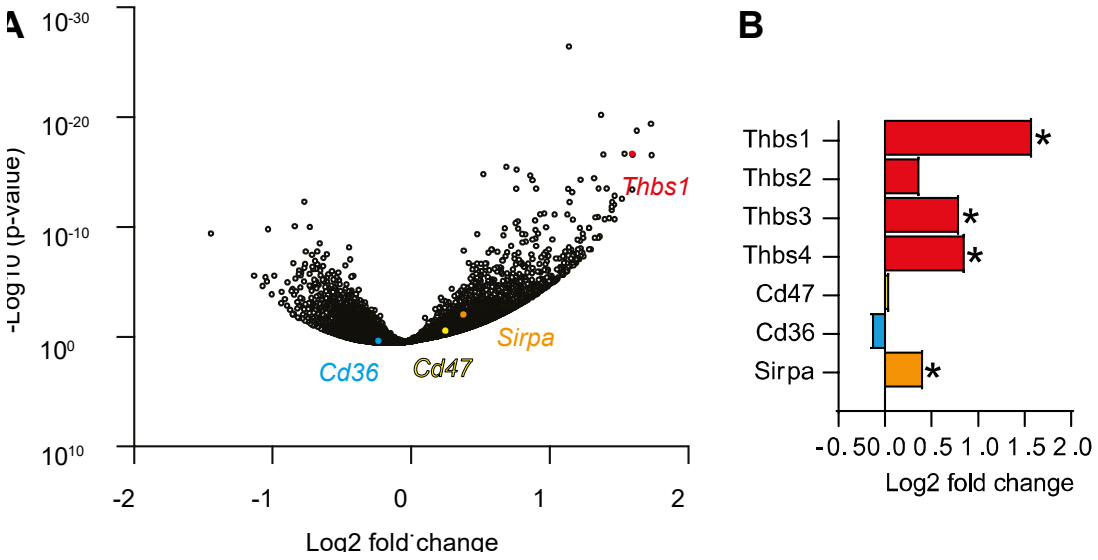

Figure 3.4. Thbs1 is a highly elevated gene in AngII-induced hypertension.
(**A**) Volcano plot summarising RNAseq data for changes in cardiac genes in mice treated with AngII *vs.* veh at 7 d (veh: n=5; AngII: n=5). RNAseq analysis identified a list of 2070 genes that were differentially expressed, with those central to this project highlighted. Data are representative of 5 independent animals per treatment. (**B**) Plots of the log 2-fold change of RNAseq data from 7 d-treated mice. The log2 fold change values and adjusted p-values were calculated using DESeq2. Adjusted p-values of <0.05 are denoted by *.

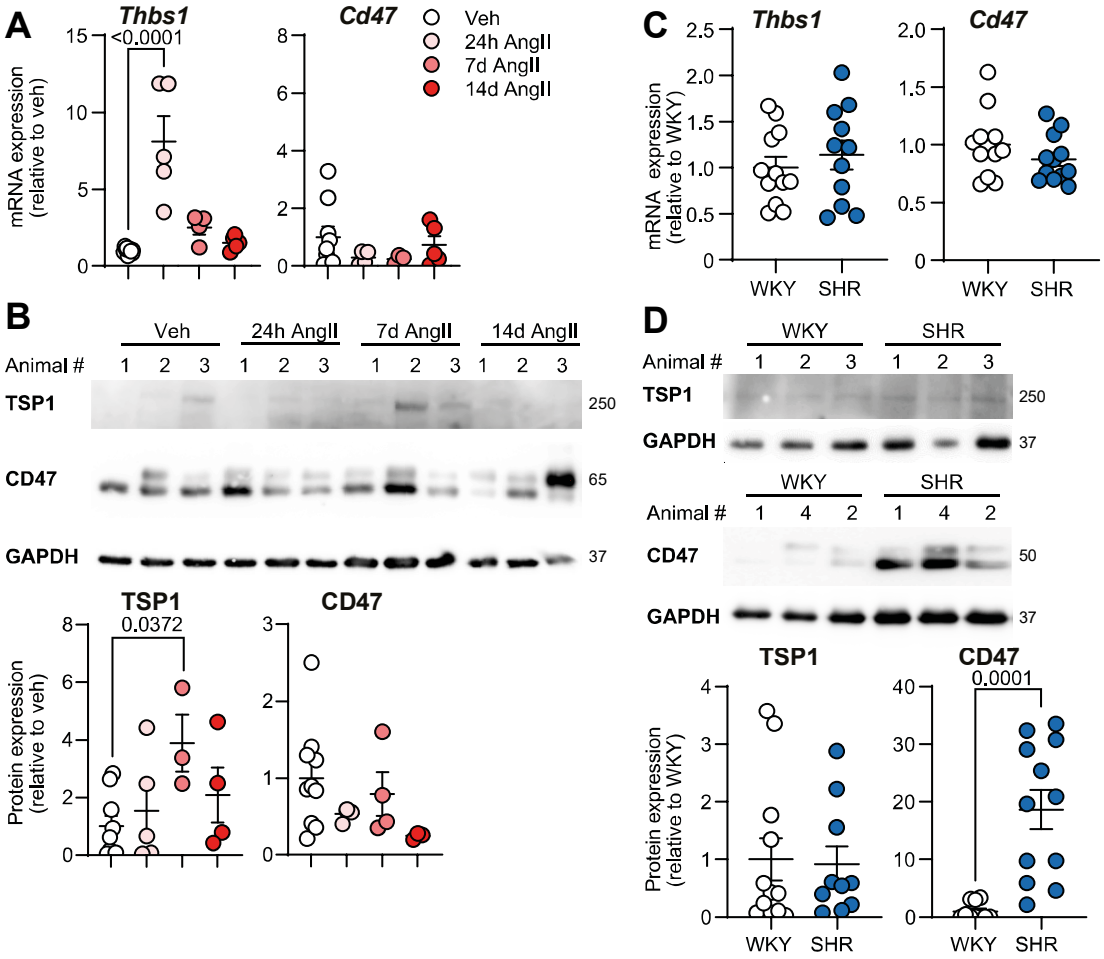

Figure 3.5. TSP1 and CD47 expression are altered in hypertensive rodents.
(**A**) *Thsb1* and *Cd47* mRNA expression levels and (**B**) TSP1 and CD47 protein expression levels were assessed in cardiac tissue from mice treated with AngII for 24 h, 7 d and 14 d (n=5 per group) or veh (n=10). (**C**) *Thsb1* and *Cd47* mRNA expression levels and (**D**) TSP1 and CD47 protein expression levels were assessed in cardiac tissue from SHRs (n=12) and was compared to WKY normotensive controls (n=12). The mRNA expression levels were determined by RT-qPCR, normalised to *Gapdh*, relative to control. Protein expression levels were determined by western blot with quantitative imaging. Representative images are displayed in the upper panels of **B** and **D** with quantification normalised to GAPDH, relative to control displayed below. Data are means ± SEM, showing individual values. Statistical tests: one-way ANOVA with Holm-Sidak post hoc test (mice) or t-test (rats), reporting p-values <0.05.

3.3.3. ROS production is elevated in human NI-HF and hypertensive rodents

As remodelling processes are associated with oxidative stress, it was investigated if elevated cardiac ROS (superoxide and H_2O_2) occurred in NI-HF and in hypertensive rodents. The results showed that cardiac superoxide production was unchanged in NH-HF and in hypertensive rodents (Figure 3.6), but cardiac H_2O_2 production was elevated in NI-HF (1.70 µmol/mg increase, p=0.0012) (Figure 3.6A), and also in the chronic phase (14 d) of AngII-induced hypertension in mice (0.44 µmol/mg increase, p=0.0200) (Figure 3.6B), and was elevated in the SHR model (1.76 µmol/mg increase, p=0.0324) (Figure 3.6C).

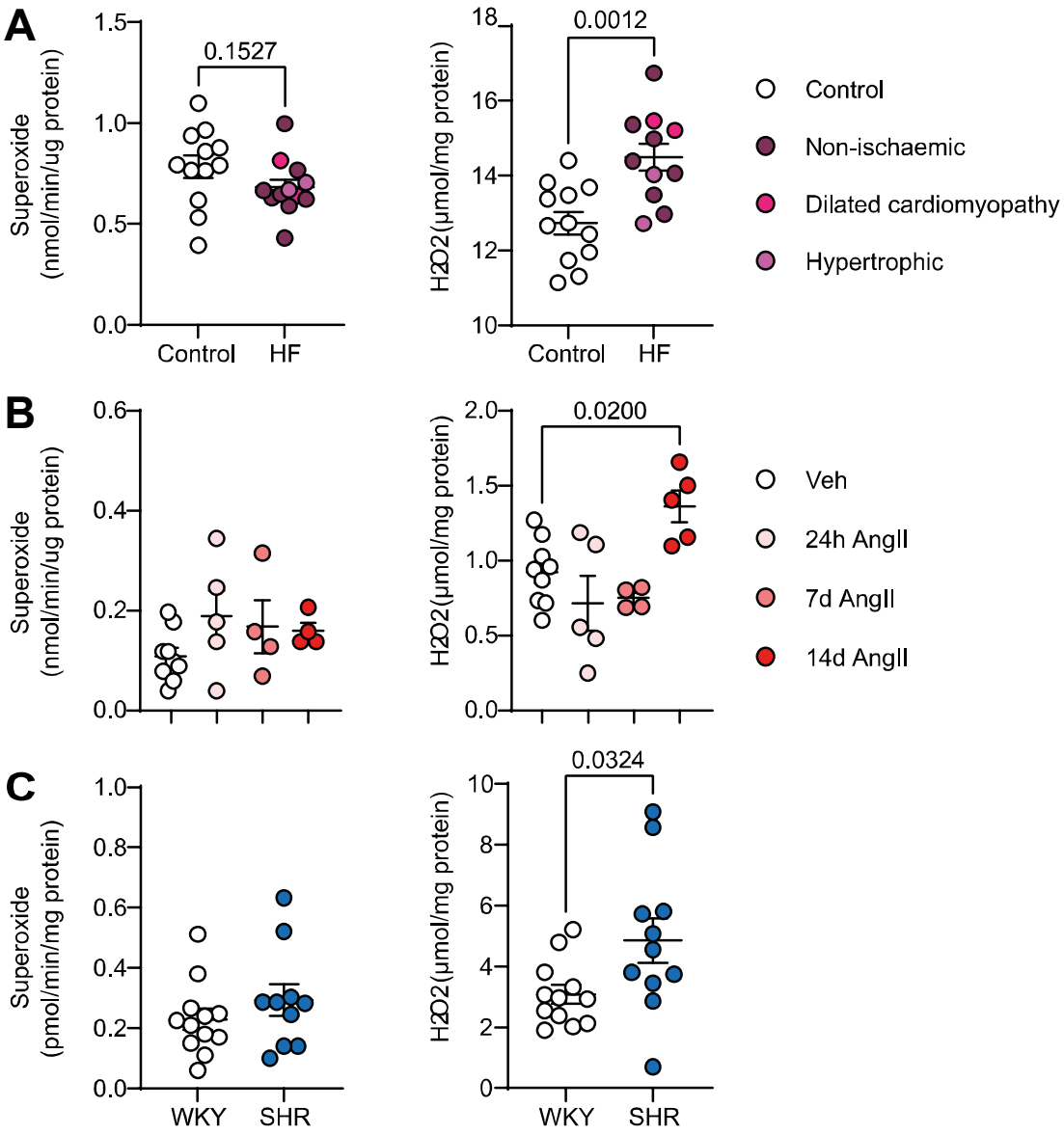

Figure 3.6. ROS production is elevated in human HF and hypertensive rodent hearts. ROS production was assessed in cardiac tissue from (**A**) NI-HF cases (n=12) or controls (n=12), (**B**) mice treated with AngII for 24 h, 7 d and 14 d (n=5 per group) or veh (n=10) and (**C**) SHRs (n=12) or WKY normotensive controls (n=12). Left panels: superoxide production assessed by cytochrome c reduction. Right panels: catalase-inhibitable H_2O_2 production determined using the Amplex red assay. Data are means ± SEM, showing individual values. Statistical tests: t-test (human and rat), one-way ANOVA with Holm-Sidak post hoc test (mice). Reporting p-values (humans) and p values <0.05 (rodents).

3.3.4. Cardiac NOX1 is elevated in end-stage HF, but not in hypertension

TSP1-CD47 has previously been demonstrated promote ROS production through modulation of NOX1 expression. Therefore, as cardiac TSP1 expression levels were elevated in NI-HF (Figure 3.2B) and in AngII-induced hypertension (Figure 3.4B & Figure 3.5A-B), and as cardiac ROS production was also elevated in in NI-HF and in hypertensive rodents (Figure 3.6A-C), cardiac NOX1 expression was investigated in NI-HF and hypertensive rodents. In addition NOX1 localisation was investigated in the HHD cohort.

The results showed that the human NI-HF cohort exhibited elevated NOX1 gene (*NOX1*; 2.59-fold, $p=0.0471$) and protein expression (NOX1; 4.15-fold, $p<0.0001$) (Figure 3.7A-B). However, in human HHD, although NOX1 appeared to be localised with cardiac vessels, NOX1 expression was unchanged throughout the myocardium (Figure 3.7C). Rodent hypertensive models did not exhibit elevated NOX1 gene nor protein expression (Figure 3.8A-D), and furthermore, in the SHR model, NOX1 mRNA expression was decreased (0.77-fold, $p=0.0474$) (Figure 3.8C). In NI-HF, as elevated NOX1 was correlated with increased ROS production, NOX1 may underpin the increase in ROS production observed. However, in the rodent models of HHD, increased ROS production was not correlated with increased ROS production, although an increase in endothelial NOX1 expression may contribute to some ROS production localised to the cardiac vessels, as observed in the HHD cohort.

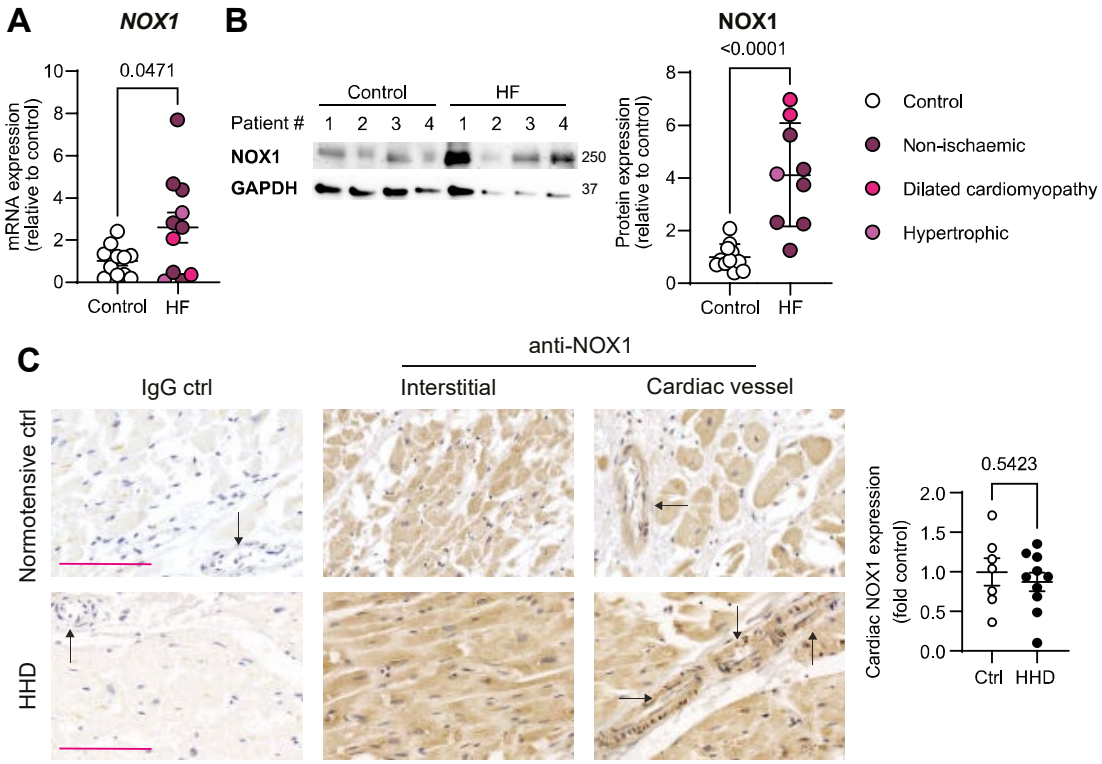

Figure 3.7. NOX1 is elevated in NI-HF and is localised to cardiac muscle and vessels in HHD.

Left-ventricular cardiac tissue from human NI-HF cases (n=12) and controls (n=12) was assessed for (**A**) *NOX1* gene expression by qPCR, normalised to *GAPDH* and (**B**) NOX1 protein expression by western blotting, normalised to GAPDH with representative blots shown and quantification. (**C**) Cardiac sections of human LV posterior walls were labelled by IHC for IgG controls or anti-NOX1 (HHD: n=10, controls: n=7) and probed by DAB. Left panels: 5X representative images of normotensive controls *vs*. HHD, assessing both cardiac muscle (interstitial) and intra-cardiac vessel regions. Scale bar: 100 µm. Arrows highlight vessels. Right panel: NOX1 expression quantified by DAB intensity, normalised to IgG control intensity, and expressed as a fold of normotensive controls. Data are means ± SEM, showing individual values. Statistical test: t-test, reporting p-values.

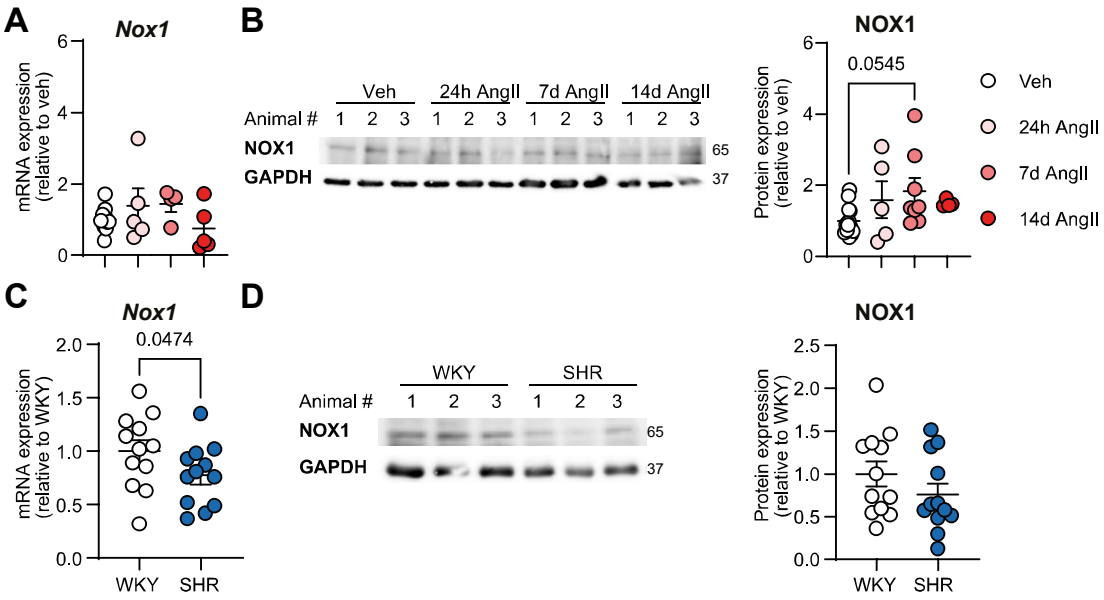

Figure 3.8. NOX1 is not elevated in hypertensive rodent hearts.
Mice treated with AngII for 24 h, 7 d and 14 d were assessed for (**A**) cardiac *Nox1* mRNA expression and (**B**) representative western blots with quantification of NOX1 protein expression, normalised to GAPDH. Cardiac tissue from SHRs was compared with WKY normotensive controls for the assessment of (**C**) *Nox1* mRNA expression (**D**) and representative western blots with quantification of NOX1 protein expression, normalised to GAPDH. mRNA expression was determined by qPCR, normalised to *Gapdh*. Data are means ± SEM, showing individual values. Statistical tests: one-way ANOVA with Holm-Sidak post hoc test (mice) or t-test (rats), reporting p-values <0.05.

3.4. Discussion

TSP1 is known to contribute to remodelling processes by modifying the ECM, interacting with growth factors and cytokines, and can influence influencing intracellular and paracrine signalling[127]. In cardiovascular diseases, TSP1-CD47 signalling is an established mediator of vessel remodelling in atherosclerosis and pulmonary hypertrophy, and influences cellular functions including angiogenesis, wound healing and cell adhesion[127,349]. In tissues, TSP1-CD47 signalling has been implicated in renal fibrosis in the pathogenesis of chronic kidney disease[350], and in hypertrophic remodelling in a pressure overload model of LV HF[114]. HHD is associated with cardiac hypertrophy, fibrosis, and impaired vascular functions, including angiogenesis. However, it is not known whether TSP1-CD47 signalling is implicated in pathogenic remodelling in the hypertensive heart. Here, this project characterised TSP1 and CD47 expression in NI-HF, HHD, and rodent models of the hypertensive heart at varying phases of disease progression.

3.4.1. Remodelling

The results indicate that TSP1 expression levels were elevated in NI-HF (Figure 3.2B), whilst RNAseq data indicated that in AngII-induced hypertension, the adaptive phase (7 d) was associated with increased cardiac *Thsb1*, *Thsb3* and *Thsb4* transcripts; with, *Thsb1* being the most highly elevated gene, indicating it may have a more predominant role (Figure 3.4B). Further investigation indicated *Thbs1* transcripts were dramatically elevated in the acute (24 h) response to AngII, which was reflected in the TSP1 protein expression in the adaptive (7 d) response (Figure 3.5A-B). Although some studies have also found *Thbs1* transcripts were elevated in models of hypertensive HF and pressure overload[351,352], it has also been demonstrated that *THSB1* mRNA expression levels were reduced in NI-HF[114]. However, these studies did not confirm the protein expression level of TSP1, and as such the abundance of TSP1 protein within the myocardium in these settings is not known for certain. With this in mind and based on this project's findings, elevated TSP1 may be associated with cardiac remodelling in both the hypertensive heart and in NI-HF.

3.4.2. Inflammation

The expression of CD47 was unchanged in NI-HF (Figure 3.2A-B), HHD (Figure 3.3A), and AngII-induced hypertension (Figure 3.5A-B). However, in the SHR model, it was found that CD47 protein expression levels were highly elevated (Figure 3.5D). Elevated cardiac CD47 expression has not previously been identified in hypertensive models, although increased CD47 and TSP1 expression has been reported in pulmonary tissue from individuals with pulmonary arterial hypertension (PAH)[353]. Elevated CD47 has also been reported in the core of atherosclerotic plaques and on dying cardiac myocytes following MI[354,355]. Inflammation is

a hallmark of both atherosclerosis and MI, and in these settings, the upregulation of CD47 prevents clearance of dying cells and cellular debris, as CD47 is an established “don’t eat me” signal, which prevents cell engulfment and clearance by binding to macrophage SIRPα[163]. It has previously been reported that cardiac inflammation occurs in the acute (24 h) phase of experimental AngII-hypertension[72], and that renal inflammation occurs by 12-13 weeks in the SHR model, indicative of a heightened inflammatory state[356]. Thus, elevated CD47 protein expression in the SHR model may be a response to cardiac inflammation. The results also showed further evidence of cardiac inflammation in the adaptive response to AngII-hypertension; the data generated by RNAseq indicated that *Sirpα*, a membrane protein which is expressed on macrophages, was slightly, but significantly, upregulated (Figure 3.4B).

3.4.3. Disease progression

Cardiac tissue from several disease states and models was used which reflected the phases of disease progression. Within the NI-HF cohort, cases had a similar severity of disease (i.e. decompensated end-stage HF) and had a pathology which was not characterised by ischaemia. As such, this cohort included several aetiologies; hypertrophic and dilated cardiomyopathies, alongside the non-ischaemic phenotype. In contrast, cases from the HHD cohort were not in decompensated HF, indicating that the phase of disease progression was less severe than the NI-HF cohort. The HHD cohort were also all characterised by the same aetiology: HHD. The distinct phases of disease progression are associated with different remodelling processes. HHD is characterised by LVH, fibrosis, ECM remodelling, whilst transition to HFpEF, usually involves further fibrotic remodelling and stiffening of the ventricle, whilst decompensated HF is typically characterised by LV dilatation and an enlarged chamber size[357]. As increased TSP1 and NOX1 expression was observed in NI-HF (Figures 3.2B and 3.7A-B) but not in HHD (Figures 3.3B & 3.7C), TSP1 and NOX1 upregulation may be associated with the final stage of the disease. Indeed, elevated NOX1 expression has been demonstrated in human non-ischaemic DCM hearts, whilst TSP1 is upregulated in HF prone mice with dilated cardiomyopathy[186,358]. However, TSP1 upregulation may be specific to NI-HF, as a previous study using LV biopsies from human ischaemic and non-ischaemic end-stage HF found fewer cardiac *THBS1* transcripts[182].

Furthermore, TSP1 upregulation is also dependent on the phase of disease progression, as TSP1 protein expression was only elevated in the adaptive phase of AngII-induced hypertension (Figure 3.5C) and was not observed in the SHR model (Figure 3.5D). Hypertension develops slowly in the SHR model and is first established at 6-7 weeks, and as such, cardiac end-organ damage also occurs over a prolonged period of time; HF is typically observed at 20 months[73,74,76,78]. In contrast, hypertension develops rapidly (within 24 h) in mice with hypertension induced by 0.8 mg/kg/day AngII, and, depending on dose cardiac

dysfunction and failure occurs between 21 and 28 d[359–362]. Thus, increased TSP1 protein expression may not have been observed in the SHR model as this model may represent an earlier phase of HHD, prior to the adaptive phase of AngII-induced hypertension. Increased cardiac NOX1 expression was not observed in hypertensive rodents (Figure 3.8A-D), likely due to the earlier phases of HHD these studies represent. The increase in CD47 protein expression observed in the SHR model (Figure 3.5D) may be due to chronic inflammation, which may not occur in mice with AngII-induced hypertension, where inflammation is more likely to be acute as disease progression occurs more rapidly.

3.4.4. Oxidative stress

This project found that cardiac H_2O_2, but not superoxide, was elevated in NI-HF, chronic (14 d) AngII-hypertension, and in the SHR model (Figure 3.6A-C). Although NOX1 produces superoxide, within the cell superoxide is rapidly converted to H_2O_2 by SOD, a reaction which can also occur spontaneously[241]. As H_2O_2 is more stable than superoxide, this which may account for why only increased H_2O_2 was observed.

ROS can promote cardiac remodelling, including fibrosis, hypertrophy and cardiac myocyte cell death[363]. Several studies have found attenuation of ROS production abolishes fibrotic remodelling; knockout of NOX1 and NOX2 abrogates ROS generation and fibrogenesis in models of hepatic fibrosis[364], whilst in models of lung injury, both genetic and pharmacologic targeting of NOX4 attenuate fibrotic remodelling[365]. Thus, by identifying and inhibiting the mechanism underlying ROS production, it may be possible to reduce pathological remodelling in the hypertensive heart. As it was identified that elevated TSP1 protein expression occurred in NI-HF and in AngII-induced hypertension (Figures 3.2B & 3.5C), and since TSP1-CD47 signalling promotes NOX1-induced ROS in HPAECs[175], NOX1 expression was investigated in these settings. In NI-HF, cardiac NOX1 expression was elevated (Figure 3.7A-B), implicating it as a potential source of ROS in this cohort. However, there was no change to cardiac NOX1 in hypertensive rodents (Figure 3.8A-D). Instead, the elevated ROS observed may have another source, such as a different NOX or the mitochondria of EC-resident cells, or may occur as a result of immune cell infiltration[366]. It is noteworthy that in HHD, NOX1 was localised to cardiac vessels, as was TSP1 (Figures 3.3B & 3.7C). Therefore, in the hypertensive heart, the TSP1-CD47-NOX1-ROS axis may be limited to the cardiac endothelium, which may account for why elevated NOX1 was not observed in AngII-induced hypertension.

3.4.5. Conclusion

In summary, this project found cardiac TSP1 expression was elevated in human NI-HF and experimental AngII-hypertension, whilst CD47 expression was unchanged. Thus, in these settings, elevated TSP1 may promote TSP1-CD47 signalling. In HF, elevated cardiac NOX1

may underscore the increased ROS production observed. However, in hypertensive rodents, the increased ROS is unlikely to be caused by NOX1, instead it may the result of cardiac inflammation. Despite this, in non-failing human HHD hearts, activation of the TSP1-CD47-NOX1 axis may occur in the endothelium, as TSP1 and NOX1 staining were localised to cardiac vessels. Therefore, whilst the TSP1-CD47-NOX1-ROS axis is active throughout the myocardium in failing hearts, in the hypertensive heart, this may only occur within the endothelium. This may contribute to perturbed cardiac endothelial function, influencing cardiac remodelling through altered paracrine signalling to cardiac myocytes and cardiac fibroblasts.

Chapter 4: The TSP1-CD47-NOX1 axis impairs EC migration

4.1. Introduction

This project found elevated cardiac thrombospondin 1 (TSP1) in human non-ischaemic HF (NI-HF) (Figure 3.2B) and in the adaptive phase of AngII-induced hypertension in mice (Figure 3.5B). As TSP1 abundance was elevated around cardiac vessels in hypertensive heart disease (HHD) (Figure 3.3B) and since TSP1-CD47 signalling promotes endothelial dysfunction in aged cells[175], CD47 activation may modulate the cardiac EC stress response, resulting in impaired EC function.

Key modulators of the cellular stress response in the heart include the MAPKs: p38-MAPK and JNK[191]. JNK signalling is dynamic and activation is stimuli dependent; *in vivo*, JNK activation promotes pathological cardiac remodelling without hypertrophy, whilst *in vitro*, activation promotes cardiac myocyte hypertrophy[191]. In contrast, p38-MAPK stimulates pathological remodelling; *in vivo*, activation increases interstitial fibrosis, promotes ventricular wall thinning and cardiac failure, whilst deletion results in increased apoptosis, fibrosis and chamber dilatation and decreased left ventricle (LV) function[191]. Cardiac remodelling can also be influenced by pro-growth extracellular signal-regulated kinase (ERK1/2), which promotes hypertrophy and ECM remodelling[191]. As p38-MAPK and JNK can orchestrate the cardiac stress response, it was hypothesised that the cellular stress caused by CD47 activation in cardiac ECs is regulated by the stress-responsive MAPKs, p38-MAPK and JNK. As such, it was established whether intracellular signal transduction following CD47 activation in cardiac ECs occurs via MAPK activation.

Furthermore, as this project had identified that NOX1 was localised to cardiac vessels in HHD (Figure 3.7C) and as a previous study had identified that the activation of CD47 by TSP1 promoted cellular stress by inducing NOX1 expression and subsequent ROS production in the lung vasculature[175], it was hypothesised that CD47 activation promotes the expression of NOX1 in cardiac ECs. Therefore, NOX1 expression was investigated in cardiac ECs treated with the 7N3 peptide, to achieve CD47 activation, and was compared to cardiac ECs treated with AngII, a known hypertensive stimulus. The 7N3 peptide was identified from a CD47-binding sequence in the c-terminal domain of TSP1, and was found to inhibit NO-stimulated EC adhesion, a response indicative of CD47 activation. This response was maximal at 10 μM 7N3[134], and 7N3 has also been demonstrated to bind to CD47 at the lower concentration of 1 μM[367].

Activation of the cellular stress response can alter cellular function. For instance p38-MAPK activation is a key regulator of the oxidative stress response in ECs where it can increase EC permeability, which has been associated with pro-inflammatory processes[340]. Furthermore, p38-MAPK activation can also promote endothelial senescence, and has also been associated with promoting EC migration in response to hypoxia[340]. As inflammation underpins cardiac fibrosis, and both endothelial migration and senescence influence angiogenesis, which has been previously demonstrated to affect cardiac hypertrophy[93,95,96], perturbed endothelial function may promote pathological cardiac remodelling in hypertensive heart disease. As TSP1 is a known anti-angiogenic protein[144], which was upregulated in NI-HF (Figure 3.2B) and in AngII induced hypertension (Figure 3.5B), and as activation of CD47 by TSP1 has previously been demonstrated to contribute to HPAEC senescence , by promoting NOX1 expression[175], it was hypothesised that activation of CD47 impairs cardiac EC function by promoting NOX1 expression and subsequently increasing ROS production; and that NOX1 inhibition will ameliorate endothelial function following CD47 activation. Therefore, the capacity of TSP1-CD47 signalling to alter EC functions (cell migration, defined as directional cell movement; cell motility, defined as random cell movement; proliferation; and survival) essential for angiogenesis was investigated.

Additionally, the suitability of NOX1 as a target to restore EC function, following CD47 activation, was investigated using NOX1 inhibitors. The small molecule NOX1/4 inhibitor, setanaxib, was used alongside NOXA1ds, a peptidic inhibitor of NOX1. Setanaxib has an inhibitory constant (Ki) for NOX1 of 140 nM and for NOX4 of 110 nM[368], and is currently in clinical trials for the treatment of primary biliary cholangitis and liver stiffness[369] and idiopathic pulmonary fibrosis[370]. NOXA1ds is a peptide which mimics the activation domain of the NOXA1 subunit, which is required for canonical NOX1 activation. By preventing NOXA1 binding, NOXA1ds inhibits NOX1 activation and therefore superoxide production. In cell free systems, NOXA1ds has been shown to selectively inhibit NOX1 derived superoxide production, with no effect on NOX2, NOX4 or NOX5 derived ROS, and was shown to cross the plasma membrane and inhibit NOX1 in the HT-29 human colon cancer cell line expressing NOX1[371]. The effect of these NOX1 inhibitors on endothelial migration, motility, proliferation and survival was determined following CD47 activation, achieved by using the 7N3 peptide, and after AngII treatment.

4.2. Methods

4.2.1. Cell culture

Isolation of mouse cardiac cells was performed as per Chapter 2.9, cell culture was carried out as per Chapter 2.10, and cultured cells were synchronised by serum starvation when cells reached confluency.

4.2.2. Identification of MAPK phosphorylation

MAPK phosphorylation was assessed by western blot in the SGHEC-7 and SVEC4-10 cell lines, isolated mouse cardiac ECs, human cardiac fibroblasts, and isolated mouse cardiac myocytes. Experimentation and sample processing were as per Chapter 2.11. Cardiac myocytes were used immediately after harvest; experimentation was conducted in DMEM (4.5 g/L glucose) with 10 mM butanedione monoxime and cells were lysed with RIPA with protease inhibitors, PhosSTOP and microcystin LR. Western blotting was conducted as per Chapter 2.6, using 10% polyacrylamide gels. For cardiac myocytes, western blotting was conducted using 20 µg, 30 µg or 40 µg of protein. For further details of experimentation in non-myocytes, see Table 4.1. Antibody information and concentration is listed in Table 2.1.

4.2.3. Identification of NOX1 protein expression

NOX1 protein expression was assessed by western blot in the SGHEC-7 and SVEC4-10 cell lines following treatment as detailed in Chapter 2.11. Western blotting was conducted as per Chapter 2.6, using either 12% (SGHEC-7) or 10% (SVEC4-10) polyacrylamide gels. For further details of experimentation, see Table 4.2. Antibody information and concentration is listed in Table 2.1.

Table 4.1 Experiment parameters for assessment of MAPK phosphorylation in non-myocytes

Cell type	Cell culture		Serum starve		Harvest Buffer‡	Amount loaded
	Vessel	Seeding density	Medium†	Duration (h)		
SGHEC-7	6-WP	0.3/0.7 x 10^6 cells/well	Medium 199 with 0.5% (v/v) FBS	4	1 x SDS-PAGE sample buffer	5 µL of sample
					G Buffer	25 µg of protein
SVEC4-10	6-WP	0.2/0.7 x 10^6 cells/well	Medium 199 with 0.5% (v/v) FBS	4	RIPA	20 µg of protein
					G Buffer	20 µg of protein
Cardiac EC	6 cm^2 dish	0.1 x 10^6 cells/dish	DMEM with 0.1% (v/v) FBS	17-18	G Buffer	40 µg of protein
HCF	6-WP	0.4/0.7 x 10^6 cells/well	Medium 199 with 0.5% (v/v) FBS	4	RIPA	20 µg of protein

†All media was supplemented with 50 U/mL penicillin and 50 µg/mL streptomycin. DMEM contained 1g/L glucose.
‡RIPA and G buffer were supplemented with protease inhibitors, PhosSTOP and microcystin LR.

Table 4.2. Experiment parameters for assessment of NOX1 protein expression in ECs

Cell type	Cell culture		Serum starve		Harvest Buffer‡	Amount loaded
	Vessel	Seeding density	Medium†	Duration (h)		
SGHEC-7	6-WP	0.4 x 10^6 cells/well	Medium 199 with 0.5% (v/v) FBS	24	1 x SDS-PAGE sample buffer	10 µL of sample
SVEC4-10	6 cm^2 dish	0.8 x 10^6 cells/dish	DMEM with 0.1% (v/v) FBS	24	RIPA	100 µg of protein

†All media was supplemented with 50 U/mL penicillin and 50 µg/mL streptomycin. DMEM contained 1g/L glucose.
‡RIPA was supplemented with protease inhibitors, PhosSTOP and microcystin LR.

4.2.4. NOX1 gene expression

The expression of *NOX1* mRNA was determined in the SGHEC-7 and SVEC4-10 cell lines and in isolated cardiac ECs. Experimentation and sample processing were as per Chapter 2.11, with confluent cells used for experimentation, which were synchronised by serum starvation. RNA isolation, cDNA synthesis and RT-qPCR was conducted as per Chapter 2.7. The human primers for *NOX1* mRNA were: (Forward (For)) 5'-GTTTTACCGCTCCCAGCAGAA-3' and (Reverse (Rev)) 5'-GGATGCCATTCCAGGAGAGAG-3'. The mouse primers for *Nox1* mRNA were: (For) 5'-GTTTTACCGCTCCCAGCAGAA-3' and (Rev) 5'-GGATGCCACTCCAGGAAGGAA-3'. For cell culture seeding density and vessel used, and for serum starvation medium and duration, see Table 4.3.

Table 4.3. Experiment parameters for assessment of *NOX1* mRNA expression in ECs

Cell type	Cell culture		Serum starve	
	Vessel	**Seeding density**	**Medium†**	**Duration (prior to harvest)**
SGHEC-7	6-WP	0.3 or 0.7 x 10^6 cells/well	Medium 199 with 0.5% (v/v) FBS	7N3: 28 h (n1-n5)
				AngII: 28h (n1-n4) or 44h (n5-n6)
SVEC4-10	6-WP	7N3: 0.3 x 10^6 cells/well	Medium 199 with 0.5% (v/v) FBS	7N3: 28 h
		AngII: 0.3 or 0.4 x 10^6 cells/well		AngII: 10 h
Cardiac EC	6 cm^2 dish	0.1 x 10^6 cells/dish	DMEM (1g/L glucose) with 0.1% (v/v) FBS	20 h
† Medium was supplemented with 50 U/mL penicillin and 50 µg/mL streptomycin				

4.2.5. Immunofluorescence for 4-HNE staining

Staining for 4-hydroxynonenal (4-HNE) was conducted in the SGHEC-7 and SVEC4-10 cell lines. Studies were conducted in 8-well chamber slides, seeded with either 5000 cells per well (SGHEC-7) or with 100000 or 10000 cells per well (SVEC4-10). The following day, cells were synchronised in either DMEM (1g/L glucose) supplemented with 0.1% (v/v) FBS (SVEC4-10), or in Medium 199 supplemented with 0.5% (v/v) FBS (SGHEC-7), for 17-18 h prior to experiment start. Both media contained 50 U/mL penicillin and 50 µg/mL streptomycin. Cells were pre-treated with 1 µM setanaxib or veh (media only) for 15 min before a 1 h incubation period with 100 nM AngII, the 10 µM 7N3 peptide, or veh. Cells were fixed in 4% (w/v) paraformaldehyde, rinsed in PBS, permeabilised with 0.5% (v/v) Triton X-100 at RT for 15 min, washed and blocked (2% (w/v) BSA/0.1% (v/v) Tween 20 in PBS) for 30 min at RT. The 4-HNE antibody (bs-6313R, Bioss Antibodies) was used at a 1:200 dilution, prepared in 1% (w/v) BSA/0.05% (v/v) Tween 20 in PBS and was incubated overnight at 4°C in a humidified chamber. The secondary antibody (Alexa Fluor™ 594 anti-rabbit (R37114, Invitrogen, used as per manufacturer's instructions) was incubated in a humidified chamber at RT for 1 h, protected from light. Chambers were removed and slides were mounted under a coverslip using Vectashield mounting medium containing DAPI (H1200, Vector). 5 images from each well were taken with the A1R Confocal microscope (Nikon). Quantification of MFI from each image was performed with Fiji software[342].

4.2.6. Measurement of H_2O_2 production

4.2.6.1. H_2O_2 production from cell lysate

H_2O_2 production was assessed in the SVEC4-10 cell line and in isolated cardiac ECs, treated as per Chapter 2.11. Cardiac ECs were isolated as per Chapter 2.9 and cell culture was conducted as per Chapter 2.10, with cells seeded at 0.8 x 10^6 cells/6 cm^2 dish (SVEC4-10) or at 0.1 x 10^6 cells/6 cm^2 dish (cardiac ECs). Cells were synchronised by serum starvation, using DMEM (1g/L glucose) supplemented 0.1% (v/v) FBS with 50 U/mL penicillin and 50 µg/mL streptomycin, for either 24 h (SVEC4-10s) or for 22-23 h (cardiac ECs). Confluent cells were used for experimentation. At the end of experiment, cells were washed twice with PBS to remove residual media and were harvested into HBSS containing protease inhibitors. Lysate was then passed through a 25-gauge needle (9186158, Braun) and centrifuged at 1000 x *g* (SVEC4-10 or cardiac ECs) for 5 min at 4°C. The lysate underwent a freeze-thaw cycle, followed by assessment of protein concentration using the Bradford assay (see Chapter 2.5). H_2O_2 production was determined using the Amplex red assay (see Chapter 2.8.1.), either with 25 µg of protein (SVEC4-10, cardiac EC; n=2, n=3), or with 50 µg (cardiac EC; n=1).

4.2.6.2. H_2O_2 production from whole cells

Whole cell H_2O_2 production from SVEC4-10s was determined using the Amplex red assay, as per Chapter 2.8.1, with modifications. 1000 cells/well were seeded directly into a black 96-WP with DMEM (1g/L glucose) supplemented with 1% (v/v) FBS, 50 U/mL penicillin and 50 µg/mL streptomycin. After 24 h, the medium was exchanged for phenol-red free RPMI medium (R7509, Sigma-Aldrich), without additives. The assay mix, stimuli (100 nM AngII, 10 µM 7N3 peptide), inhibitors (1 µM setanaxib, 10 µM NOXA1ds), and controls (veh, media only; 10 µM SCRAM) were prepared as per Chapter 2.8.1 in phenol-red free RPMI, rather than PBS. Inhibitors were pre-incubated for 15 min, whilst stimuli were added after the addition of Amplex red to the well, immediately before the plate was read. NADPH was not used.

4.2.7. Assessment of cellular migration by wound healing

The migratory response of SVEC4-10s was determined using a wound healing assay by Dr Daniel Meijles. Cells were cultured in 24-WP (see Chapter 2.10.5) until confluent. Using a 200 µL pipette tip, a single scratch was made in the centre of each well. Media was removed and either 1 µM setanaxib, 10 µM NOXA1ds, 10 µM SCRAM or veh (media only) controls were incubated for 15 min prior to addition of 100 nM AngII or 10 µM 7N3 peptide. Images were taken 24 h after stimuli addition using Olympus IX70 microscope (Olympus Life-Science). The area of the wound was quantified using Fiji software[342].

4.2.8. Assessment of cellular proliferation by the MTT assay

SVEC4-10 cells were seeded into a 96-WP with DMEM (1 g/L glucose) supplemented with 0.1% (v/v) FBS. The following day cells were treated with inhibitors (1 µM; setanaxib or 10 µM NOXA1ds) or veh (media only or 10 µM SCRAM) for 15 min prior to stimuli addition (100 nM AngII or 10 µM 7N3,) or veh (media only). Then 24 h after stimuli addition, the 3-(4,5-dimethylthiazol-2-yl)-2, 5-diphenyltetrazolium bromine (MTT) assay was performed as per manufacturer's instructions. 10 µL of MTT reagent (5mg/mL) (158990010, Acros organics) was added to each well, and was incubated for 2-4 h. Stimuli media was removed, and cells permeabilised by the addition of 100 µL of DMSO. The plate was then read at 570 nm using Synergy LX multimode reader (BioTek) with Gen5 software. This was performed in collaboration with Dr Daniel Meijles.

4.2.9. Assessment of cellular motility, proliferation, and death by time-lapse imaging

Time-lapse migration studies were conducted in 12-WPs, using SGHEC-7s seeded at approximately 50000 cells per well into Medium 199 supplemented with 0.5% (v/v) FBS and

50 U/mL penicillin and 50 µg/mL streptomycin. After 20 h, inhibitors (setanaxib, 1 µM; NOX1A1ds, 10 µM) or veh were incubated for ~15 min prior to stimuli addition (AngII, 100 nM; 7N3, 10 µM) or veh (media only). Cellular behaviour was monitored by time-lapse digital microscopy Olympus IX71 microscope (Olympus Life-Science) equipped with a Hamamatsu C4742-95 digital camera. An image (frame) of 1 set point in each well was taken every 15 min. Cells were maintained in a humidified chamber with 4% CO_2 at 37°C for the duration of the study.

4.2.9.1. Analysis

At the beginning of each sequence of frames, 30 cells were randomly selected from the field of view. 25 cells which did not leave the field of view over 22 h were assessed for migration, cell division and cell death. Cell motility, defined as the non-directional distance moved by each cell, was assessed using the MTrakJ[372] plugin in Fiji. Any movement following cell death was not included in analysis. Cell division was recorded and scored according to the frame where cells had clearly divided. Following division, one daughter cell was tracked subsequently. Cell death was recorded when cells demonstrated either an obvious apoptotic appearance (transition to a phase-bright appearance, decrease in cytoplasmic and nuclear size, and formation of a membrane bleb or blister) or at the point when the cell had transitioned to a phase-bright appearance for many frames and did not divide[373].

4.3. Results

4.3.1. Differential regulation of MAPK activation in cardiac ECs, cardiac fibroblasts, and cardiac myocytes.

This project demonstrated that hypertensive cardiac vasculature is associated with increased TSP1 (Figure 3.3B). TSP1 is a known cellular stressor and TSP1-CD47 signalling can perturb EC function[175]; however, the intracellular signalling pathway is not well understood. Due to their established role in cardiac remodelling processes[191], MAPK phosphorylation following CD47 activation was investigated, and was compared to treatment with AngII, a known hypertensive instigator.

In EC cell lines, CD47 activation, induced by the TSP1-derived peptide, 7N3, activated ERK1/2 (maximal at 5 min, maintained until 30 min) (Figure 4.1A-B). In terms of stress-regulated MAPKs, activation of p38-MAPK was delayed (maximal at 15 min) and only occurred in SVEC4-10s, whilst there was no effect on JNK signalling (Figure 4.1A-B). AngII promoted ERK1/2 activation in both EC cell lines (Figure 4.2A-B); however, the activation of stress-regulated kinases was not concordant; AngII promoted activation of p38-MAPK but not of JNK in SGHEC-7s (Figure 4.2A), whilst AngII promoted JNK activation with limited p38-MAPK activation in SVEC4-10s (Figure 4.2B). Both CD47 activation (Figure 4.1C) and AngII treatment (Figure 4.2C) promoted activation of all MAPKs in cardiac ECs; p38-MAPK was significantly activated at 5 min (7N3: 3.23-fold, $p=0.0002$; AngII: 4.38-fold, $p=0.0022$), JNK activation occurred later at 15 min (7N3: 4.69-fold, $p=0.0245$; AngII: 4.69-fold, $p=0.0238$), whilst ERK1/2 activation may have been significant at 5 min were an additional experiment to have been run. However, this was not possible due to the closure of the Biological Resource Facility. The trends of MAPK activation observed in cardiac ECs are presented in Figure 4.5A.

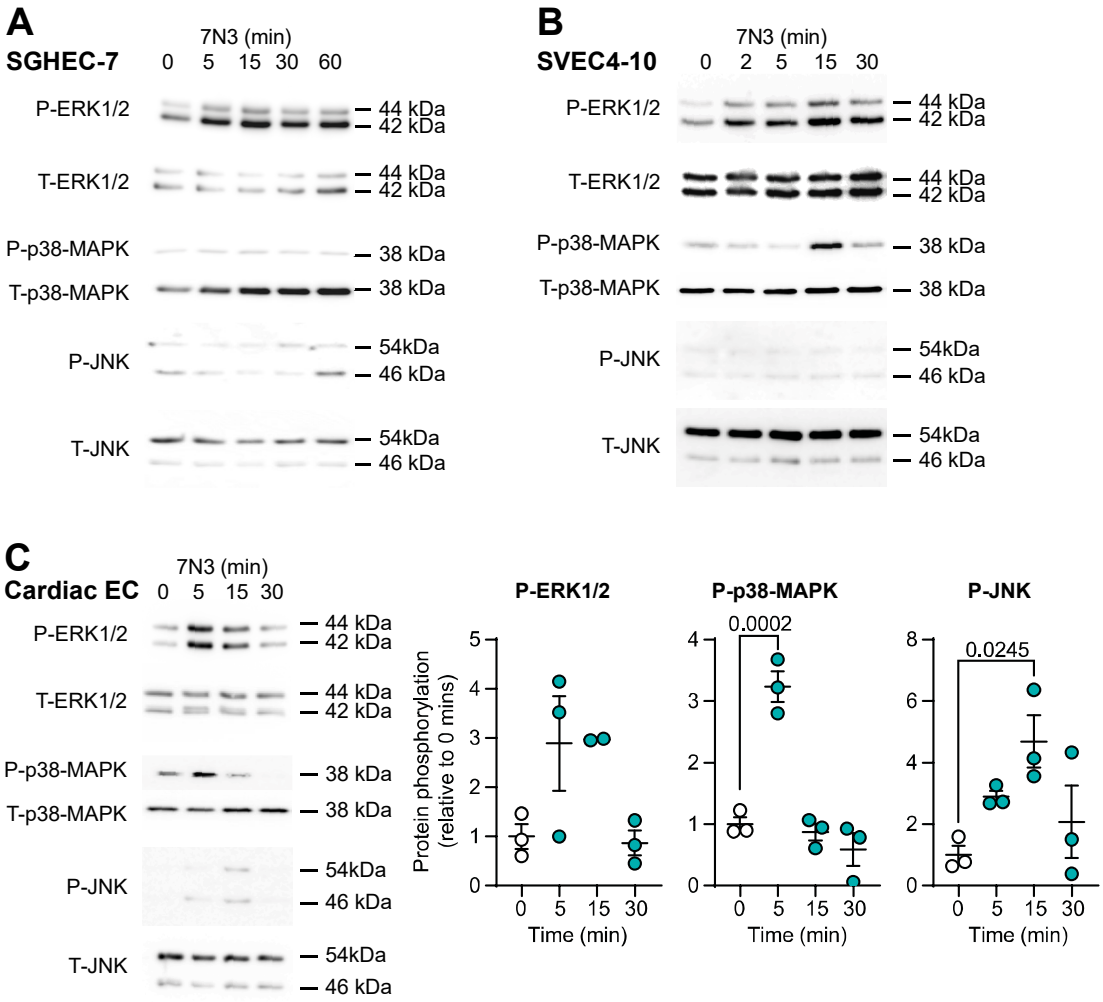

Figure 4.1. CD47 activation influences MAPK signalling in cardiac ECs.
Western blots of MAPK phosphorylation following 7N3 treatment in (**A**) SGHEC-7s (representative blot from n=7), (**B**) SVEC4-10s (representative blot from n=6) and (**C**) mouse cardiac ECs (n=3), with representative western blots (left panel) and quantification of phosphorylated (P)-MAPKs) normalised to Total (T)-MAPKs (right panel). Data are means ± SEM, showing individual values. Statistical test: one-way ANOVA with Holm-Sidak post hoc test, reporting p-values <0.05.

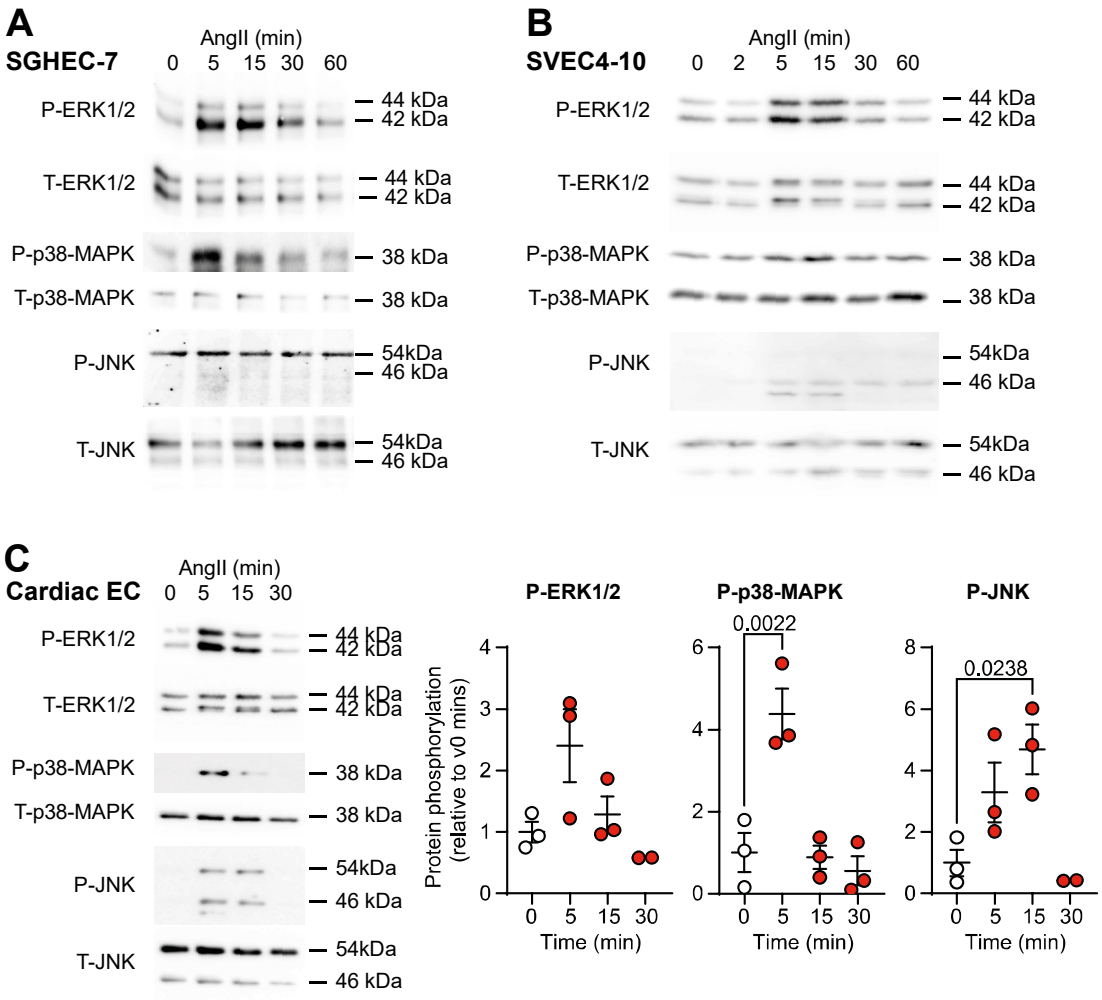

Figure 4.2. AngII treatment influences MAPK signalling in cardiac ECs.
Western blots of MAPK phosphorylation following AngII treatment in (**A**) SGHEC-7s (representative blot from n=7), (**B**) SVEC4-10s (representative blot from n=3) and (**C**) mouse cardiac ECs (n=3), with representative western blots (left panel) and quantification of P-MAPKs normalised to T-MAPKs (right panel). Data are means ± SEM or range (**C**, P-JNK and P-ERK1/2, 30 min), showing individual values. Statistical test: one-way ANOVA with Holm-Sidak post hoc test, reporting p-values <0.05.

In the heart, cardiac fibroblasts and myocytes are in direct association with cardiac capillaries[374]. Therefore, as TSP1 is a matricellular protein, and was found to be localised to cardiac vessels (Figure 3.3B), TSP1-CD47 signalling may also activate MAPK signalling in cardiac fibroblasts and myocytes. Hence, MAPK phosphorylation in response to CD47 activation in cardiac fibroblasts and myocytes was next characterised and was compared to the AngII response. In cardiac fibroblasts, CD47 activation promoted phosphorylation of p38-MAPK (5 min: 2.00-fold, p=0.0329; 15 min: 2.10-fold, p=0.0226) and JNK (10 min: 3.54-fold, p=0.0352) (Figure 4.3A). Although ERK1/2 was not significantly activated, phosphorylation was observed in several experiments. Cardiac myocytes exhibited phosphorylation of ERK1/2 (15 min: 2.45-fold, p=0.0204) together with diminished JNK activation (5-30 min) (Figure 4.3B). In cardiac fibroblasts, AngII treatment promoted ERK1/2 phosphorylation (10 min: 2.14-fold, p=0.0372) whilst p38-MAPK and JNK phosphorylation was unchanged (Figure 4.4A). However, AngII did not promote cardiac myocyte MAPK phosphorylation (Figure 4.4B). The trends of MAPK activation observed in cardiac fibroblasts and cardiac myocytes are presented in Figure 4.5B-C.

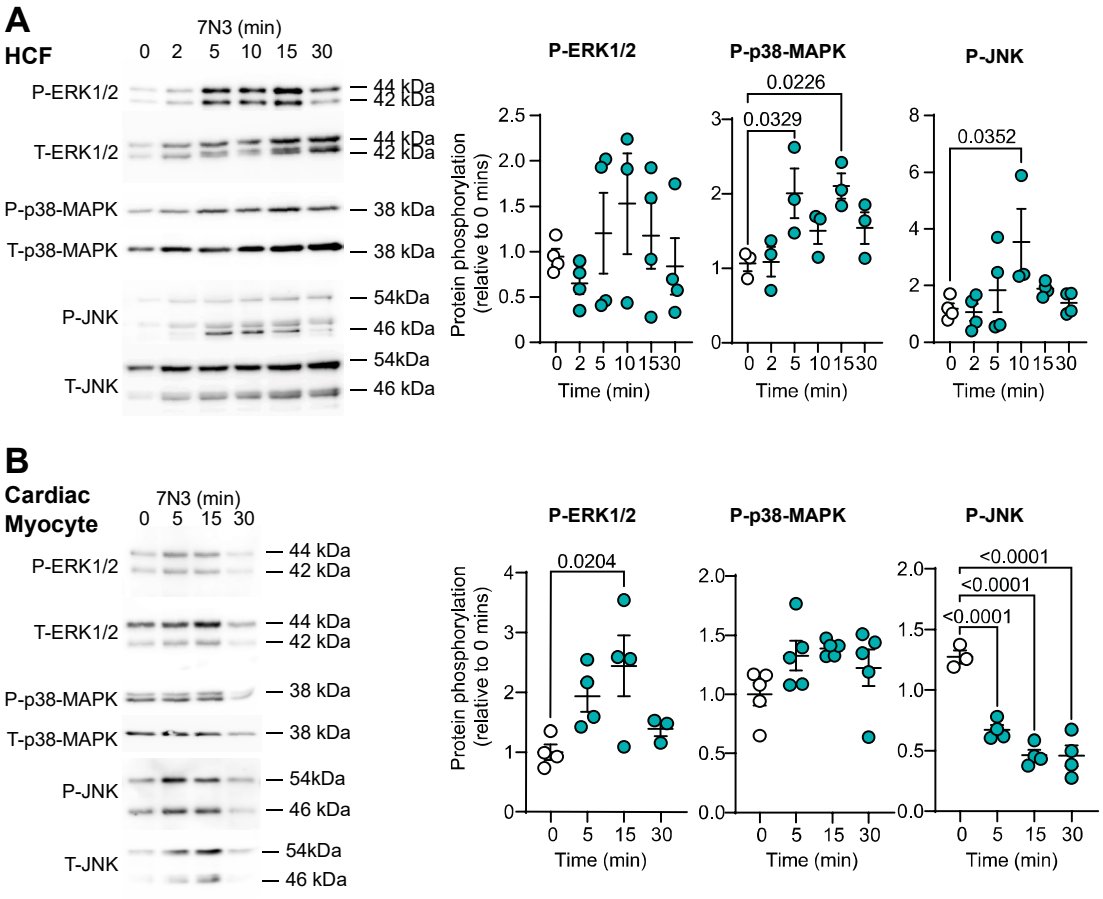

Figure 4.3. Cardiac MAPK activation in response to CD47 activation is cell type specific. Western blots of MAPK phosphorylation following CD47 activation by 7N3 in (**A**) HCFs (n=4) and (**B**) adult mouse cardiac myocytes (n=4). Representative western blots displayed (left panels) with quantification of P-MAPK normalised to T-MAPK (right panels). Data are means ± SEM, showing individual values. Statistical test: one-way ANOVA with Holm-Sidak post hoc test, reporting p-values <0.05.

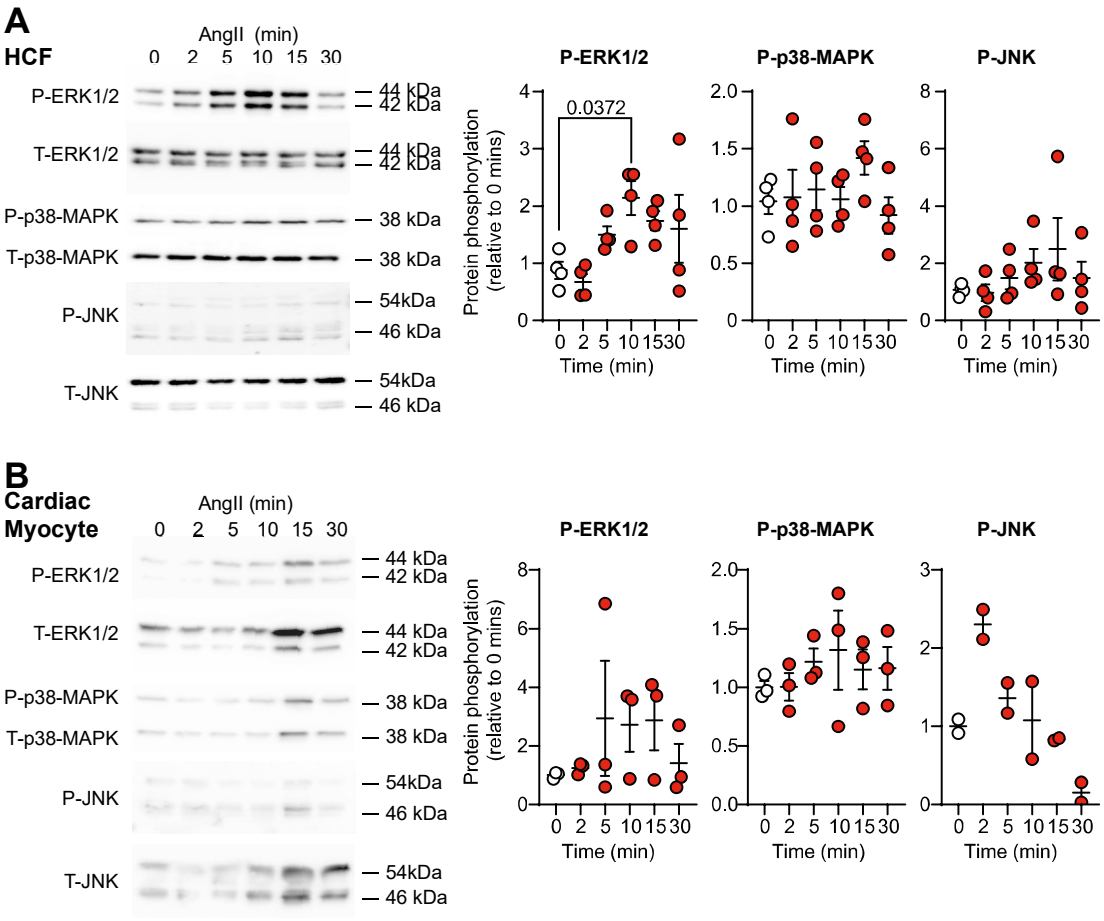

Figure 4.4. Cardiac MAPK activation in response to AngII is cell type specific.
Western blots of MAPK phosphorylation following AngII treatment in (**A**) HCFs (n=4) and (**B**) adult mouse cardiac myocytes (n=3: ERK1/2, p38-MAPK; n=2: JNK). Representative western blots displayed (left panels) with quantification of P MAPK normalised to T MAPK (right panels). Data are means ± SEM or range (**B**, P-JNK), showing individual values. Statistical test: One way ANOVA with Holm-Sidak post hoc test, reporting p values <0.05. Statistical analysis was not performed for **B**, P-JNK.

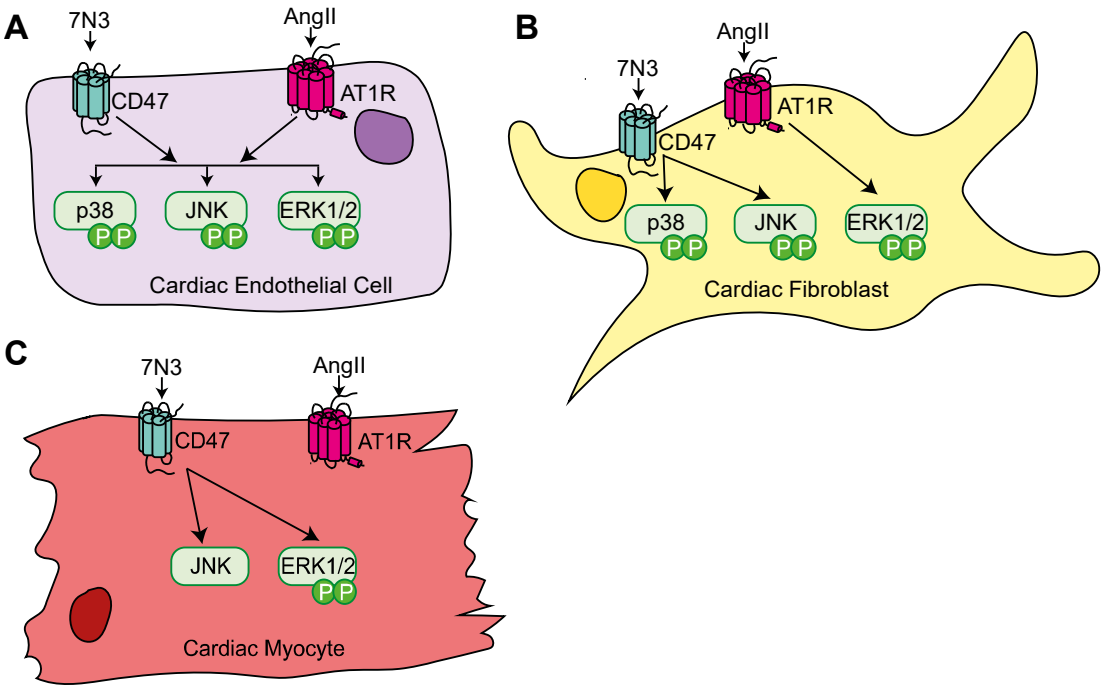

Figure 4.5. Overview of MAPK signalling in cardiac cell types.
(**A**) MAPK activation in cardiac ECs; CD47 and AngII promote phosphorylation of stress-regulated MAPKs; p38-MAPK and JNK, and pro-growth ERK1/2. (**B**) MAPK activation in cardiac fibroblasts; CD47 activation promotes phosphorylation of stress-regulated MAPKs; p38-MAPK and JNK whilst AngII promotes phosphorylation of pro-growth ERK1/2. (**C**) MAPK activation in cardiac myocytes; CD47 promotes ERK1/2 phosphorylation and diminishes JNK phosphorylation. AngII does not affect MAPK phosphorylation.

4.3.2. TSP1-CD47 signalling promotes NOX1 expression in ECs.

As TSP1 and NOX1 were localised to vessels in HHD (Figures 3.3B & 3.7C), and previous work indicated TSP1 promotes NOX1 expression in HPAECs[175], it was investigated whether TSP1-CD47 signalling can promote NOX1 expression in EC cell lines and cardiac ECs. Initial studies in SGHEC-7s indicated that, at 24 h, CD47 activation promoted NOX1 protein (1.98-fold, p=0.0027) but not mRNA expression (Figure 4.6A-B). Subsequent studies in SVEC4-10s, used earlier timepoints for the activation of CD47 activation by the 7N3 peptide; however, *Nox1* mRNA expression was unchanged, whilst NOX1 protein expression was elevated at 2 h (1.84-fold, p=0.0414) (Figure 4.6A & C). This indicated that *Nox1* mRNA expression may be elevated earlier. As such, in cardiac ECs, it was observed elevated *Nox1* mRNA expression at 30 min (2.84-fold, p=0.0327) in response to CD47 activation (Figure 4.6A), unfortunately however, NOX1 protein expression could not be confirmed in isolated cardiac ECs, due to the closure of the Biological Resource Facility, and a lack of any viable alternative primary ECs.

In all ECs tested, AngII did not promote NOX1 mRNA expression (Figure 4.6D), nor did it promote NOX1 expression in SGHEC-7s (Figure 4.6E). Overall, this indicates that CD47 activation promotes NOX1 expression as an acute response, whereas AngII treatment does not.

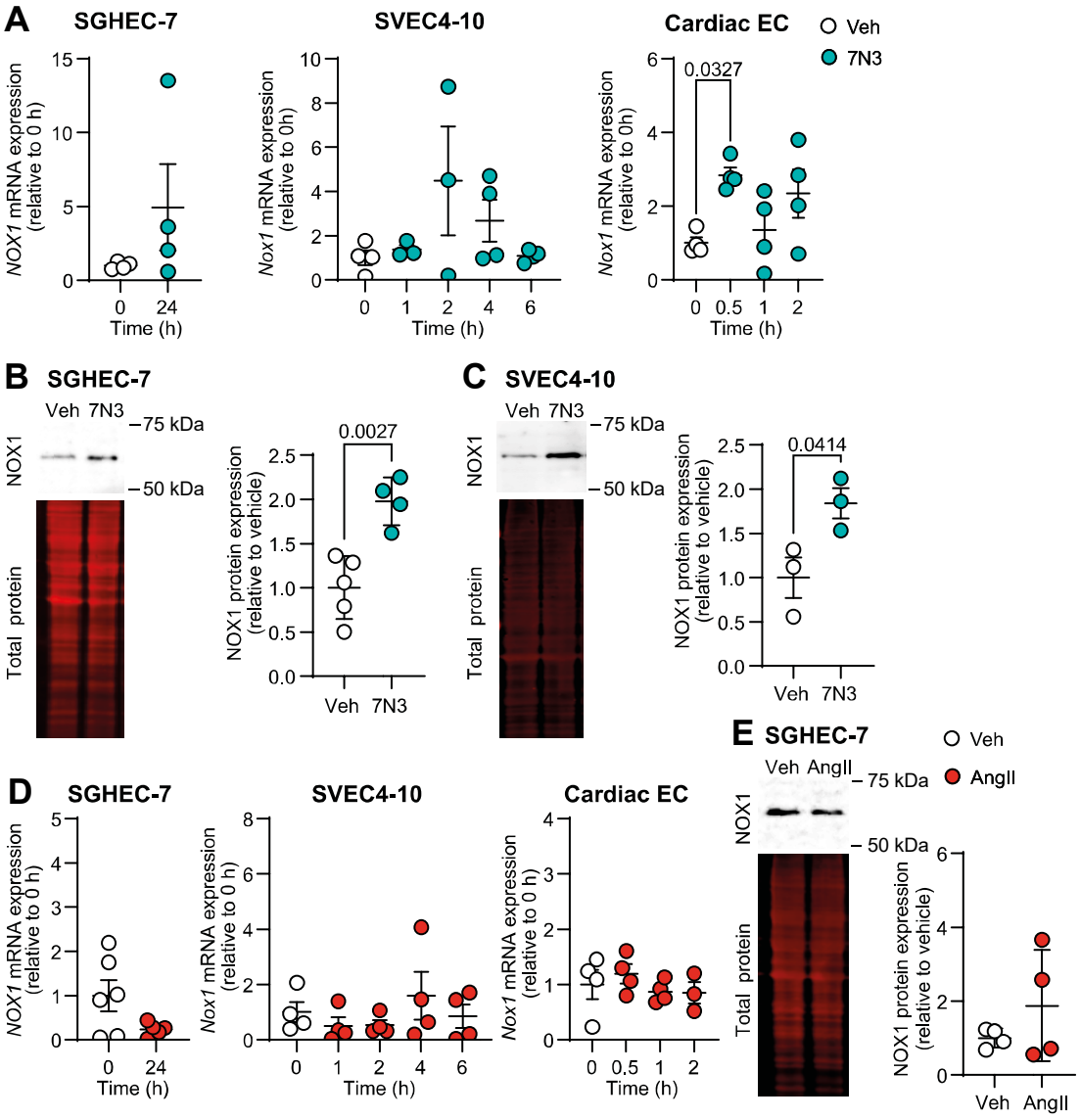

Figure 4.6. TSP1-CD47 signalling promotes NOX1 expression in ECs.
Following CD47 activation by 7N3, (**A**) *NOX1* mRNA expression was determined in ECs (n=4). NOX1 protein expression was assessed in (**B**) SGHEC-7s at 24 h (n=4) and (**C**) SVEC4-10s at 2 h (n=3). Following AngII treatment, (**D**) *NOX1* mRNA expression was determined in ECs (SGHEC-7, n=6; SVEC4-10 and cardiac EC, n=4) and (**E**) NOX1 protein expression was determined in SGHEC-7s at 24 h (n=4). mRNA expression assessed by qPCR, normalised to GAPDH. Protein expression assessed by western blotting normalised to total protein. Data are means ± SEM, showing individual values. Statistical tests: T test or one way ANOVA with Holm-Sidak post hoc test. p values <0.05 reported.

4.3.3. TSP1-CD47 interactions may promote ROS production in ECs

Having demonstrated that CD47 activation promotes NOX1 expression in ECs, it was subsequently investigated whether this was also associated with elevated ROS production. NOX1 is a known ROS producer; in HPAECs it mediates hypoxia-induced ROS[375], whilst TSP1-CD47 signalling promotes increased NOX1 protein expression and subsequent ROS production[175]. H_2O_2 production was unchanged both in cell homogenates from SVEC4-10s and in cardiac ECs treated with 7N3 or AngII (Figure 4.7A-B). However, intact cultured SVEC4-10s treated with 7N3, but not with AngII, did exhibit increased H_2O_2 production (Figure 4.7C-D). This is indicative of elevated extracellular ROS, as Amplex red is cell-impermeable. Interestingly, setanaxib (a dual NOX1/4 inhibitor) attenuated 7N3-induced ROS in intact SVEC4-10s (Figure 4.7C-D), whereas NOXA1ds (a peptidic inhibitor of NOX1) did not.

During oxidative stress, elevated ROS cause cellular damage and dysfunction through the oxidation of proteins, DNA, and lipids. Therefore, lipid oxidation was assessed by 4-HNE staining in SGHEC-7s (Figure 4.8A) and SVEC4-10s (Figure 4.8B), treated with either 7N3 or AngII. Neither CD47 activation, AngII treatment nor NOX1 inhibition affected lipid peroxidation, indicating that, although ROS production may be elevated, this is unlikely to promote oxidative stress.

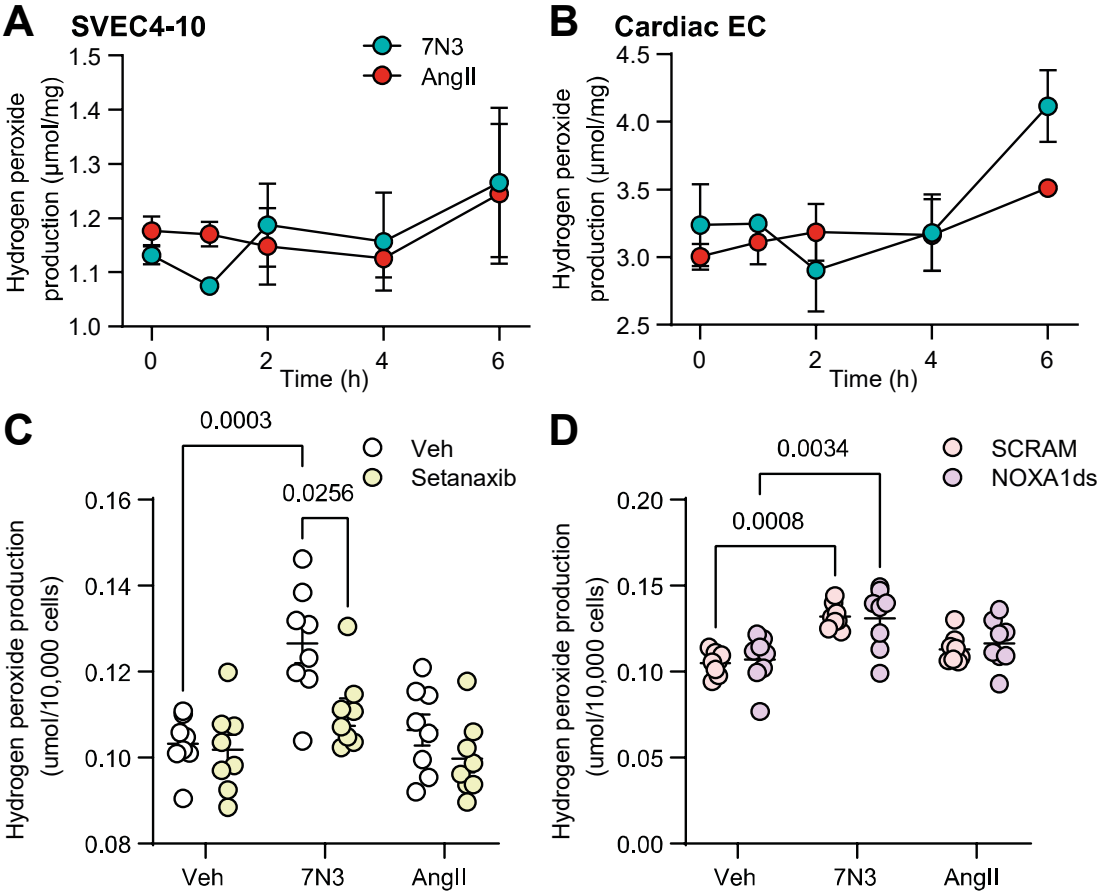

Figure 4.7. TSP1-CD47 signalling promotes ROS production in ECs.
H_2O_2 production from homogenates treated with the 7N3 peptide or AngII in (**A**) SVEC4-10 (n=3) or (**B**) Primary mouse cardiac ECs (n=3, except 6 h, which is n=2). Data is average of replicates ± SEM or range (**B**, 6 h). H_2O_2 production from intact SVEC4-10 cells, after 30 min treatment with 7N3 or AngII with NOX1 inhibitors (**C**) setanaxib or (**D**) NOXA1ds, with SCRAM control. Data are means ± SEM, showing individual values. Statistical tests: **A** and **B**; one-way ANOVA with Holm-Sidak post hoc test (not performed on 6 h timepoint in **B**), **C** and **D**; Two-way ANOVA with Holm-Sidak post-hoc test. p values <0.05 are reported.

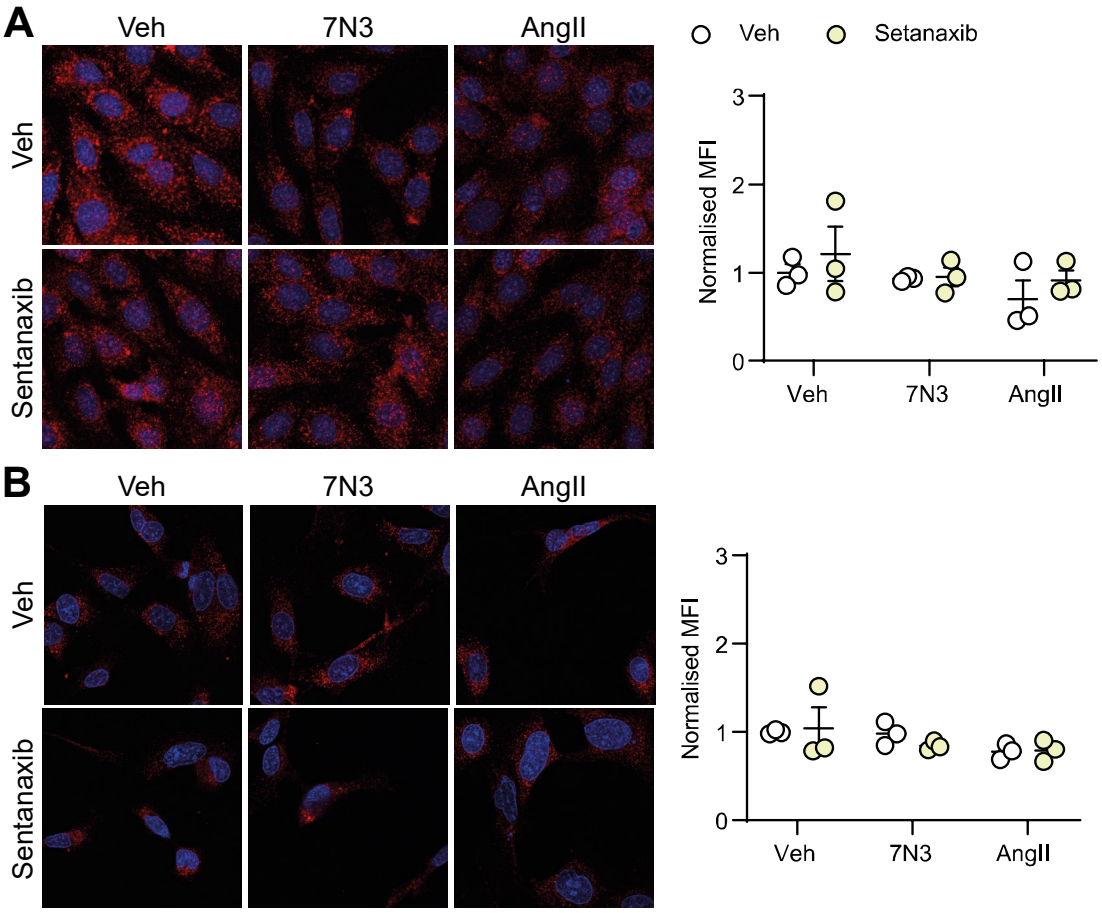

Figure 4.8. CD47 activation does not promote lipid peroxidation in ECs.
4-HNE staining in (**A**) SGHEC-7s (n=3) and (**B**) SVEC4-10s (n=3). Cells were treated with 7N3 or AngII or veh (media only) for 1 h in the presence of the NOX1/4 inhibitor setanaxib or veh. 60 x confocal images were taken with 4-HNE staining in the TRITC channel (red) and DAPI staining in the DAPI channel (blue). The mean fluorescence intensity (MFI) of 4-HNE staining was quantified and normalised to veh-veh. Data are means ± SEM, showing individual values, from an average of 5 images per treatment. Statistical test: Two-way ANOVA with Holm-Sidak post hoc test.

4.3.4. NOX1 is responsible for the diminished migratory response of ECs following CD47 activation.

Although this project found limited evidence that CD47 promotes oxidative stress in ECs via NOX1, NOX1-ROS may participate in redox signalling. By oxidation of redox-sensitive residues, ROS can alter protein structure and function, affecting downstream signalling[106,193]. Therefore, localised ROS production by NOX1 may not be measurable by Amplex red but could still modulate EC function. Indeed, ROS generated by NOX have been demonstrated to affect cell migration[376], whilst ROS produced by NOX2 and NOX4 have been implicated in human umbilical vein endothelial cell (HUVEC) proliferation and migration following VEGF treatment[377]. Furthermore, NOX1 inhibition attenuated TSP1-induced senescence in HPAECs[175]. To determine whether NOX1 has a role in influencing EC behaviour following CD47 activation, cellular migration, proliferation, and death were assessed in EC cell lines, in the presence of the small molecule NOX1/4 inhibitor, setanaxib, and the peptidic NOX1 inhibitor, NOXA1ds.

In SVEC4-10s, both CD47 activation and AngII treatment significantly reduced the rate of wound closure. NOXA1ds restored wound closure following CD47 activation and AngII treatment, whereas setanaxib restored closure following only CD47 activation (Figure 4.9A-B). This data implicates NOX1 as a downstream effector of CD47 activation, promoting impaired EC function. As increased expression of NOX1 was only observed following CD47 activation, whilst the NOX1 inhibitor NOXA1ds restored wound closure after both CD47 and AngII treatment, it may be that the activation of NOX1 by NOXA1 binding and subsequent complex assembly is more important to consider than NOX1 expression in this context. Furthermore, as setanaxib did not restore wound closure following AngII treatment, but did effectively restore wound closure following CD47 activation, whilst NOXA1ds restored wound closure to both AngII and 7N3 treated cells, this may indicate that NOXA1ds is a more effective NOX1 inhibitor that setanaxib, which is known to have a greater binding affinity for NOX4 than NOX1.

In SGHEC-7s, the preliminary data indicated NOXA1ds may have reduced cell motility; whereas CD47 activation and AngII had no effect (Figure 4.10A), however statistical analysis could not be ascertained. EC proliferation was not affected by CD47 activation nor AngII treatment, nor by NOX1 inhibition (Figures 4.9C & 4.10C), and the preliminary data did not indicate a clear trend to cell death following CD47 activation, AngII treatment nor following inhibition of NOX1 (Figure 4.10E). Due to the closure of the Biological Resource Facility and the lack of viable alternative source of primary cardiac ECs, cardiac EC function could not be assessed.

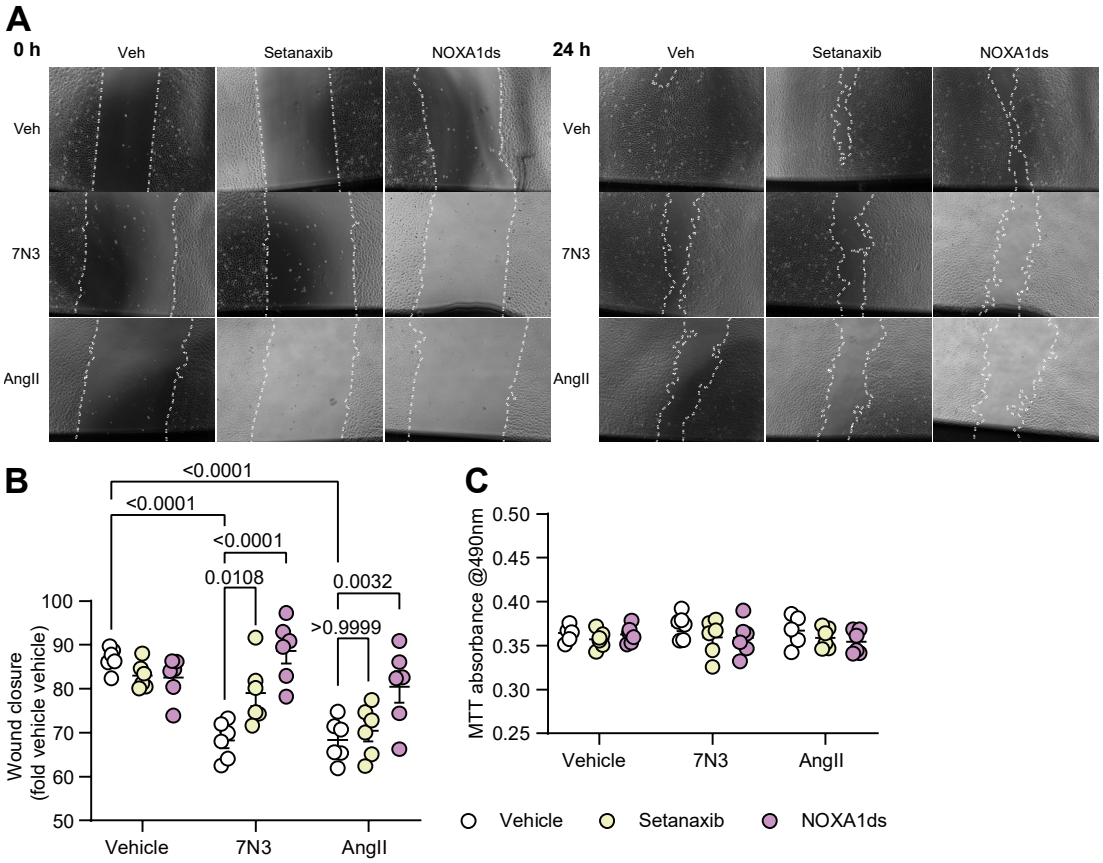

Figure 4.9. NOX1 Inhibition abates the diminished migratory response of ECs following CD47 activation.

SVEC4-10s were assessed for cell migration and proliferation, 24 h following 7N3 or AngII treatment with NOX1 inhibition (setanaxib or NOXA1ds). Cell migration (n=6) was assessed by wound closure with (**A**) representative images at 0 and 24 h displayed with the leading edge highlighted, and (**B**) quantification of the wound area. (**C**) Cell proliferation (n=6) was determined by MTT absorbance. Data are individual values ± SEM. Statistical test (**B** & **C**): Two-way ANOVA with Holm-Sidak post hoc test, p values <0.05 reported.

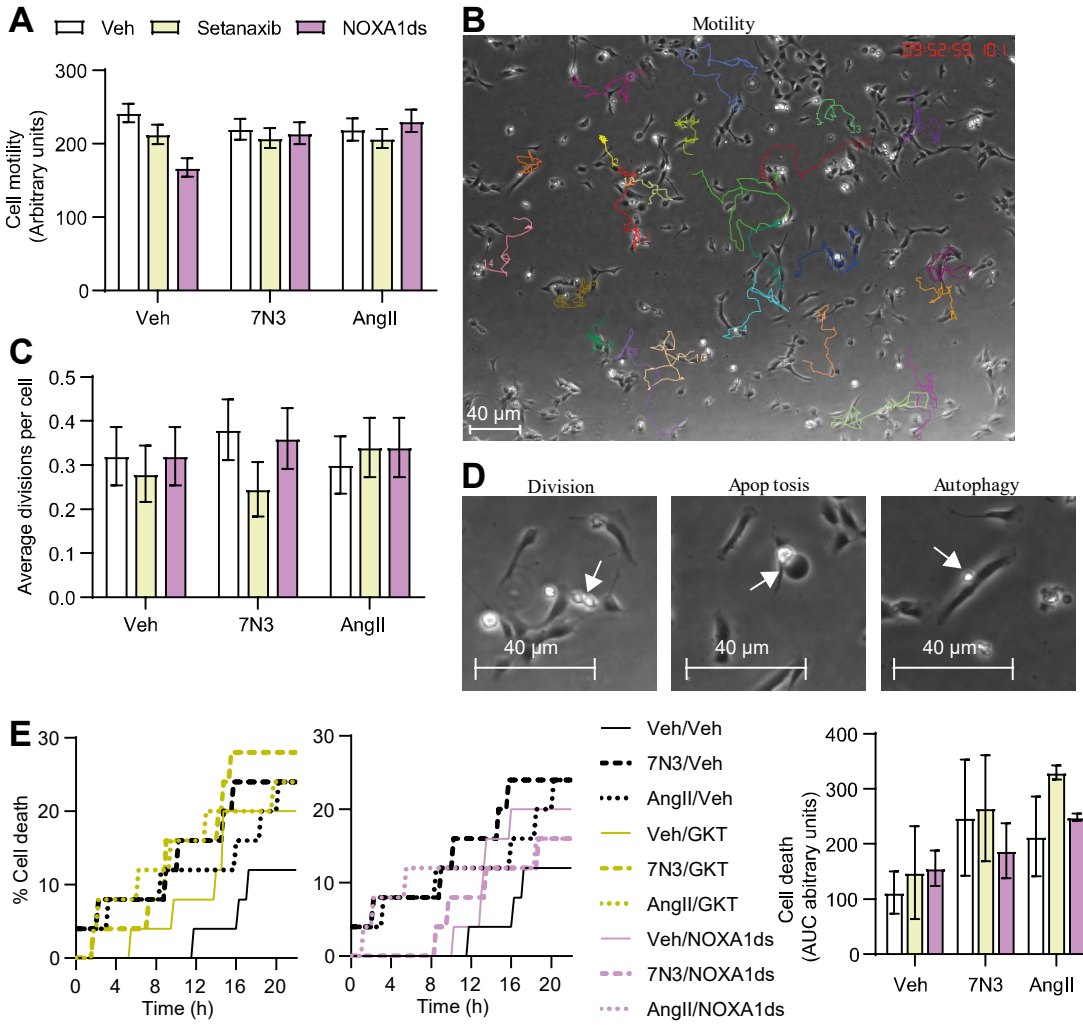

Figure 4.10. NOX1 Inhibition has no effect on EC motility, division or death following CD47 activation.

The responses of SGHEC-7s following CD47 activation (by treatment with the 7N3 peptide) or AngII treatment with NOX1 inhibitors (setanaxib or NOXA1ds) were determined by time-lapse microscopy over 22 h. (**A**) Quantification of cell motility (defined as the length of migratory path) with (**B**) a representative image of tracked cell paths at 72 h. (**C**) Average number of divisions per cell. Cell divisions were counted when a cell entered the bright-phase and proceeded to clearly divide. Examples of cell division, apoptosis and autophagy are denoted in (**D**). (**A** & **C**) Data are the average of 50 cells tracked across 2 independent experiments ± SEM. (**E**) Cell death (apoptosis and autophagy) displayed as representative survival curves (left panels) from one experiment and with quantification of the area under the curve (AUC) (n=2) (right panels), displayed as the average ± range, and statistical analysis was not ascertained.

4.4. Discussion

TSP1 perturbs endothelial responses including proliferation, adhesion and chemotaxis, and attenuates angiogenesis by inhibition of NO signalling[127,144,378]. In both VSMCs and ECs, TSP1-CD47 signalling promotes ROS production, causing vascular dysfunction and endothelial senescence[127]. In ECS, NOX1 has been proposed to be the source of ROS[175]. However, the mechanism of signal propagation from CD47 activation to NOX1 is unknown. As MAPKs are known to regulate cardiac remodelling and the cellular stress response[191,201], they were investigated as potential propagators of intracellular signalling following CD47 activation. Here, it was demonstrated that CD47 activation influences MAPK phosphorylation, and hence activity, in cardiac ECs, fibroblasts and myocytes. ROS production following CD47 activation was subsequently determined in EC cell lines and cardiac ECs following CD47 activation and was compared to cells treated with AngII. Finally, the effect of NOX1 inhibition on EC migration, proliferation, cell death and lipid peroxidation was investigated.

4.4.1. CD47 activation and AngII differentially regulates MAPKs phosphorylation in cardiac resident cells.

4.4.1.1. MAPK signalling following CD47 activation in myocardial cell types

CD47 activation promoted stress-regulated (p38-MAPK and JNK) and pro-growth (ERK1/2) MAPK phosphorylation in cardiac ECs (Figure 4.1C), promoted stress-regulated MAPK phosphorylation in HCFs (Figure 4.3A), and promoted pro-growth MAPK phosphorylation in cardiac myocytes, with reduced JNK activation (Figure 4.3B). This is summarised in Figure 4.5 and is an entirely novel finding, no previous studies have investigated MAPK signalling following CD47 activation in ECs, fibroblasts or myocytes, and studies in other cell types are limited, and have mainly investigated CD47 activation in immune cells. In accord with the results of this project, in the Jurkat T-lymphoma cell line, activation of CD47 by 7N3 promoted ERK1/2 phosphorylation[379]. However, several studies have also indicated TSP1-CD47 signalling diminishes ERK1/2 phosphorylation; in activated Jurkat T cells, TSP1-CD47 signalling reduced ERK1/2 phosphorylation in response to hydrogen sulphide[380], and in aortic VSMCs, activation of CD47 by 4N1K (a peptide derived from the c-terminal domain of TSP1) attenuated ERK1/2 activation[381]. Partially consistent with this projects' findings, ligation of CD47 with B6H12 (a CD47-blocking antibody), which may cause CD47 activation on binding, promoted p38-MAPK and JNK activation whilst diminishing ERK1/2 phosphorylation in Epstein Barr Virus-transformed B cells[382]. Another TSP1-derived peptide (peptide 246, derived from the heparin binding type I repeats of TSP1), has also been demonstrated to promote p38-MAPK and JNK phosphorylation[379]. This project is the first to demonstrate that CD47 activation achieved by using the 7N3 peptide promotes stress-regulated MAPK signalling, similar to that which has been observed with TSP1 and other CD47 binding ligands, and it confirms that CD47 activation can promote ERK1/2 phosphorylation in a cell type-dependent

manner. Furthermore, as CD47 activation by 7N3 regulates MAPK signalling differently in each cardiac-resident cell type (cardiac ECs, HCFs, and cardiac myocytes), this project also highlights that the effect of TSP1-CD47 signalling is likely to be cell type dependent.

4.4.1.2. MAPK signalling following AngII stimulation in myocardial cell types

AngII promoted stress-regulated (p38-MAPK and JNK) and pro-growth (ERK1/2) MAPK phosphorylation in cardiac ECs (Figure 4.2C), promoted ERK1/2 phosphorylation in HCFs (Figure 4.4A), whilst cardiac myocytes did not respond to AngII (Figure 4.4B). A summary is presented in Figure 4.5. Although MAPK activation by AngII is well characterised in ECs, the activation profile presented here for cardiac ECs is novel. This project indicates AngII promotes p38-MAPK and JNK phosphorylation in cardiac ECs, as seen in AngII (10 µM)-treated HUVECs[383,384]. However, in these studies ERK1/2 was not phosphorylated. It is noteworthy that in VSMCs, AngII at a concentration of 10 µM mediates the phosphorylation of ERK1/2, p38-MAPK and JNK[385]. Thus, the ERK1/2 phosphorylation observed may be a function of cardiac ECs or could be a result of the lower concentration of AngII used (100 nM).

In HCFs, AngII promoted phosphorylation of ERK/12, but not of p38-MAPK nor of JNK. However, previous studies found ERK1/2, p38-MAPK and JNK were phosphorylated in neonatal rat cardiac fibroblasts after 15 min following AngII (concentration not stated) treatment[386]. Activation of ERK1/2, p38-MAPK and JNK was also observed in adult mouse atrial fibroblasts AngII (1 M) treatment[387]. However, others found only p38-MAPK and ERK1/2 were activated in adult rat cardiac fibroblasts following 100 nM AngII treatment[388,389]. The difference observed between this project and previous studies, may be due to either the species of the fibroblast, or due to the AngII dose used.

This project indicates that adult cardiac myocytes do not respond to AngII stimulation. This contrasts with results in rat neonatal cardiac myocytes, where activation of ERK1/2, p38-MAPK and JNK occurs following AngII (1 µM) treatment[390,391]. It is worth noting that these studies used cultured cardiac myocytes, where purity, if reported, is ~90-95%. Consequently, the MAPK activation observed in these studies may arise from paracrine signals (such as TGF-β and endothelin-1) from contaminating non-myocyte cell types (particularly fibroblasts) that respond to AngII, causing paracrine pathway stimulation which affects the cardiac myocytes[392].

4.4.1.3. CD47 activation and AngII have opposing effects on MAPKs phosphorylation in cardiac resident cells

Despite the concordance seen between the two stimuli in cardiac ECs, the cellular MAPK responses diverged in cardiac fibroblasts and cardiac myocytes. In cardiac fibroblasts, CD47 signalling resulted in activation of stress-regulated MAPKs (Figure 4.3A), whilst AngII promoted pro-growth ERK1/2 (Figure 4.4A). In contrast, CD47 activation promoted ERK1/2 phosphorylation in cardiac myocytes with a decrease in activation of JNK (Figure 4.3B), whereas AngII had no significant effect on MAPK activation in cardiac myocytes (Figure 4.4B). The discord observed between MAPK activation in cardiac myocytes and fibroblasts suggests that the functional changes exerted on the myocardium by these stimuli are cell type specific and that the response of each cell type is stimuli dependent. In cardiac ECs, the MAPK activation profiles following CD47 activation and following AngII treatment are similar; therefore, any functional differences are likely to be due to interactions within the intracellular signalling network.

4.4.2. CD47 activation promotes NOX1 expression and ROS production.

Having characterised kinase activation following CD47 signalling and AngII treatment, it was next established whether CD47 activation promoted NOX1 expression and ROS production in cardiac ECs. As this project identified that e*x vivo* ROS production was enhanced in cardiac tissue from NI-HF patients, in the SHR model and in the AngII-induced model of hypertension (Figure 3.6A-C), but only NI-HF was associated with increased NOX1 expression (Figures 3.7-3.8), however as NOX1 appeared localised to vessels in HHD (Figure 3.7C), it was hypothesised that NOX1 expression may be localised cardiac vessels in non-failed hearts. Furthermore, NOX1 is a known mediator of ROS production in the vasculature[393]; and previous work indicates that AngII promotes mitochondrial ROS production in a NOX-dependent manner in ECs[258], whilst CD47 signalling promotes ROS production via NOX1 in aged vascular ECs[175]. Therefore, it was hypothesised that endothelial NOX1 may be a key mediator of CD47-dependent ROS production in hypertension. As such, NOX1 expression and ROS production were investigated in cardiac ECs following CD47 activation, to determine whether CD47 activation promotes the expression of NOX1 and subsequent ROS production.

4.4.2.1. CD47 activation promotes NOX1 expression whereas AngII does not

CD47 signalling promoted *NOX1* mRNA expression in EC cell lines and cardiac ECs (Figure 4.6), and increased NOX1 protein expression was confirmed in EC cell lines (Figure 4.6B-C). Due to constraints inflicted by the closure of the Biological Research Facility at SGUL, and a lack of a viable alternative source of primary cardiac ECs, NOX1 protein expression could not be determined in cardiac ECs. AngII did not affect *NOX1* mRNA expression in EC cell lines or cardiac ECs (Figure 4.6D) nor NOX1 protein expression in the SGHEC-7 cell line (Figure 4.6E); this is consistent with another study which found that NOX2 promoted ROS production in AngII-treated HPAECs, whereas NOX1 did not[259]. However, in VSMCs, AngII is known to increase NOX1 expression[394,395], which may account for the elevated *Nox1* mRNA expression observed in AngII-infused aortas[396]. This projects findings confirm that CD47 activation induces NOX1 expression in cardiac ECs, consistent with a previous study[175], and suggests that changes to EC NOX1 expression occur independently of AngII in hypertension. Consequently, CD47-NOX1 signalling may represent a novel pathway regulating endothelial oxidative stress in hypertension, which is summarised in Figure 4.11.

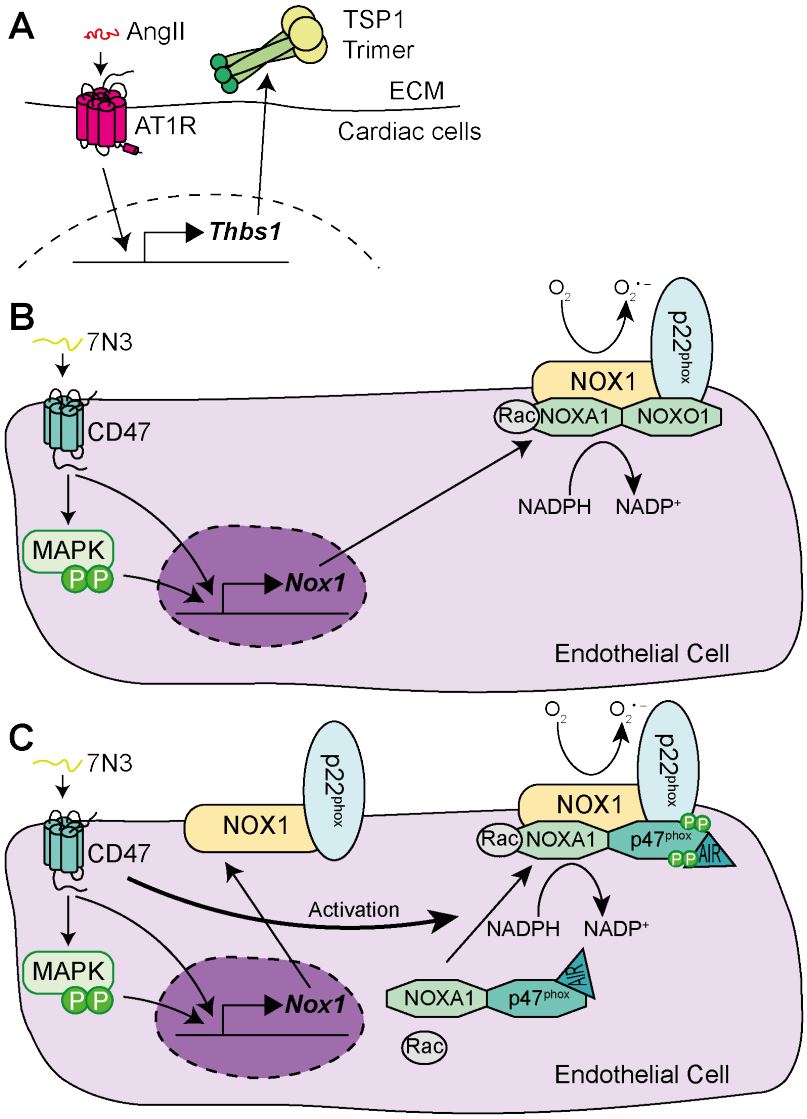

Figure 4.11. Overview of CD47-NOX1 signalling in ECs.
(**A**) AngII promotes *Thbs1* gene expression and TSP1 protein expression in cardiac cells. CD47 activation by 7N3 (a peptide derived from the C-terminus of TSP1) promotes *Nox1* mRNA and NOX1 protein expression in ECs, through both/either MAPK-dependent and/or MAPK-independent pathways, resulting in ROS production by (**B**) the constitutively-active canonical NOX1 system, or (**C**) the inducible, hybrid NOX1 system. CD47 activation may also promote induction of the inducible NOX1 system, by phosphorylation of the autoinhibitory region (AIR) leading to a conformational change of $p47^{phox}$ and association and activation of the NOX1 complex.

4.4.2.2. ROS production following CD47 activation could be extracellular

It was next investigated whether CD47 activation stimulated ROS production, indicative of oxidative stress. However, following CD47 activation, ROS production in cardiac ECs (Figure 4.7B) and the SGHEC-7 cell line was not increased (Figure 4.7A), whilst H_2O_2 production measured in cultured SVEC4-10 was significantly elevated (Figure 4.7C). As Amplex red is cell-impermeable, this finding demonstrates that the ROS produced is extracellular. Indeed, the NOXs are membrane proteins, and have been demonstrated to be localised to the plasma membrane as follows: NOX1 to caveolae; NOX2 to phagosomes and

the lamellipodia leading edge; and NOX4 to focal adhesions[233]. This indicates that NOXs have the capacity to produce extracellular ROS. Alternatively, as H_2O_2 is membrane-permeable, H_2O_2 produced within the cell may diffuse through the plasma membrane, where it then reacts with the Amplex red reagent.

4.4.2.3. NOX1 may promote non-canonical ROS production following CD47 activation

This project found CD47-mediated H_2O_2 production was attenuated by the NOX1/4 inhibitor setanaxib (Figure 4.7C), but not by the specific NOX1 inhibitor, NOXA1ds (Figure 4.7D). This may indicate that CD47 promotes NOX4-mediated ROS production, or that NOX1-ROS is produced by the non-canonical hybrid system. The canonical system requires NOX1 to associate with NOXO1 and NOXA1 for ROS production to occur. NOXA1ds is designed to impede canonical NOX1 complex assembly, by binding to the NOXA1ds docking site, preventing NOXA1 binding and thus inhibiting ROS production[371]. Whilst the non-canonical hybrid NOX1 system is generally thought to use $p47^{phox}$ in lieu of NOXO1[237], the initial studies which identified NOXO1 and NOXA1, also indicated that NOX1 can use both $p47^{phox}$ (in lieu of NOXO1) and $p67^{phox}$ (in lieu of NOXA1) to generate stimuli dependent ROS[236]. As such, if $p67^{phox}$ participated in NOX1 activation, alongside $p47^{phox}$, then NOXA1ds may not inhibit this interaction, and this may account for the lack of inhibition observed with the NOXA1ds peptide.

It is possible that the timepoints used to assess NOX1-induced ROS may not have been sufficient. Although increased *Nox1* transcription was detectable at 30 min in cardiac ECs (Figure 4.6A), changes to NOX1 protein expression occurred between 2 and 24 h (Figure 4.6B-C). Thus, a longer duration of timepoints than those used (0-6 h) may be needed to identify increased ROS production due to elevated NOX1 expression. However, in intact SGHEC-7s, H_2O_2 was significantly elevated at 30 minutes (Figure 4.7C). This further indicates that the NOX1 hybrid system is in play, as $p47^{phox}$ can be rapidly activated following phosphorylation, removing it from its auto-inhibited form, whilst the canonical system is thought to regulate low-level constitutive ROS production[232,397]. A summary of CD47-NOX1 signalling is presented in Figure 4.11.

Alternatively, NOX1-ROS may participate in redox signalling, occurring when ROS act in a rapid and localised manner to regulate cell function by oxidation of protein residues, namely cysteines[107]. As this ROS is produced rapidly and is highly controlled by degradation via cellular antioxidants, it may not be measurable in cellular homogenates. This may also explain the lack of ROS production observed in homogenates (Figure 4.7A-B), coupled with elevated NOX1 expression (Figure 4.6A-C), and the fact that NOX1 inhibition restored wound closure following CD47 activation (Figure 4.9A-B). In summary, the lack of ROS observed following

CD47 activation may in part, be due to: the participation of the hybrid NOX1 system; insufficient timepoints; or a potential role for NOX1 in redox signalling.

4.4.2.4. AngII does not promote ROS production

It is widely accepted that AngII induces ROS production; however, the findings here oppose this. Elevated ROS production following AngII treatment in either EC cell lines or in cardiac ECs was not observed in this project. Previous studies have attributed AngII-induced ROS to NOX1 in VSMCs from large arteries and NOX2 in small resistance arteries[398]. Cardiac microvascular ECs treated with AngII exhibited increased diphenyleneiodonium-inhibitable superoxide production. As diphenyleneiodonium inhibits flavoproteins such as the NOXs, this indicated that the ROS produced may have been attributable to a NOX[399]. In the SVEC4-10 cell line, this was subsequently deduced to be NOX2[400].

4.4.2.5. NOX1 does not contribute to oxidative stress following CD47 activation nor following AngII treatment

As CD47 activation had been demonstrated to promote EC NOX1 expression and ROS production in intact cells, whether this response results in cellular stress was investigated. Given extracellular ROS was elevated, it was hypothesised that membrane peroxidation, determined by 4-HNE staining, would also be increased. However, neither CD47 activation nor AngII treatment promoted lipid peroxidation on either SGHEC-7s (Figure 4.8A) or SVEC4-10s (Figure 4.8B), and setanaxib did not limit lipid peroxidation. This suggests that CD47-induced ROS does not contribute to cellular oxidative stress in this context, despite other published findings demonstrating this. TSP1-CD47 signalling promoted oxidative stress and DNA damage in HPAECs by NOX1[175], and in pulmonary arterial hypertension induced by hypoxia, TSP1-CD47 signalling also promoted oxidative stress, although ROS were produced by uncoupled eNOS[353], although another study indicated that ROS production was elevated in hypoxic HPAECs was due to increased NOX1 expression[257]. Additionally, lung tissue from CD47-null mice exhibited reduced 4-HNE and 3-nitrotyrosine staining than compared with their control counterparts[174]. The lack of concordance of these results arise from the inherent nature of the cell lines used, as these could behave differently compared with ECs from large blood vessels[401]. Overall, it is unlikely that acute activation of CD47 promotes oxidative stress sufficiently to cause elevated lipid peroxidation. Therefore, any acute response instigated by NOX1-ROS, may be due to redox signalling rather than to oxidative stress.

4.4.3. CD47 activation diminishes the migratory response of ECs in a NOX1-dependent manner.

Although this project found that CD47 activation did promote oxidative stress in ECs, elevated NOX1 expression and subsequent micro-domain ROS production could be indicative of redox signalling resulting in functional changes. Redox signalling involves modification of redox-sensitive residues within close proximity to the source of ROS production, as ROS are rapidly broken down by endogenous antioxidants, attenuating signal transduction. Redox signalling via NOX1 may alter protein function, resulting in perturbed EC behaviour following CD47 activation. Here, the effect of CD47 activation and NOX1 inhibition on EC migration, motility, proliferation, and death was investigated, as the hypothesis was that CD47 activation impairs cardiac EC function by promoting NOX1 expression and subsequently increasing ROS production.

4.4.3.1. CD47 activation attenuated EC migration

This project identified that CD47 activation attenuated SVEC4-10 migration, as determined by a wound healing assay (Figure 4.9A-B); however, there was no change to SVEC4-10 proliferation, as determined by MTT (Figure 4.9C). The preliminary data generated by time-lapse microscopy suggested that there was no change to SGHEC-7 motility (Figure 4.10A) or proliferation (Figure 4.10C) following CD47 activation. This is in contrast to previous studies, where both CD47 expression and activation of CD47 by TSP1 has been demonstrated to be anti-angiogenic, preventing *in vivo* angiogenesis, *ex vivo* sprouting, EC proliferation, migration and tube formation and, promoting HPAEC senescence[134,175,378,402–404]. This project found that, in cell lines, CD47 activation only reduced EC migration, with no change to proliferation or motility. Although senescence was not measured directly, reduced proliferation would have been expected to be observed if senescence had been initiated. However, as these experiments were conducted in cell lines, which divide more frequently than primary ECs, proliferative pathways are likely to be upregulated, and as such, the effect of CD47 activation may be minimal compared with primary cells, which are normally quiescent *in vivo*.

CD47 activation did not appear to promote cell death (Figure 4.10E), and induction of cell death by TSP1 is considered to occur via induction of CD36[405,406]. However, the 4N1K peptide (a peptide derived from the c-terminal domain of TSP1, as is the 7N3 peptide) induced apoptosis via ROS production in mouse cortical neurons[407], and, in cerebral ECs, it promoted cytotoxicity and reduced migration and EC tube formation[408]. CD47-mediated cell death has only been observed in HUVECs following turbulent flow conditions, where apoptosis may be induced by TSP1-CD47 with participation from the $\alpha_V\beta_3$ integrin[409]. The preliminary time-lapse study presented, indicated that CD47 activation is unlikely to promote cell death in SGHEC-7s

(Figure 4.10E). Overall, and partially consistent with previous studies, CD47 activation attenuated EC migration, but did not alter cell motility, proliferation nor death.

4.4.3.2. AngII decreased EC migration

Here, AngII treatment decreased the migratory ability of the SVEC4-10 cell line (Figures 4.9A-B) but did not affect motility, proliferation nor cell death (Figure 4.10A-E). However, AngII is regarded to be pro-angiogenic, through stimulation of the AT1R, the most well-studied AngII receptor. Through AT1R signalling, AngII promotes tube formation, cell migration, and can promote proliferation[410–413]. Only one study, using HUVECs, found AngII inhibited migration via the AT1R[414]. However, activation of the AT2R by AngII, although less well characterised, has found to be anti-angiogenic. AngII inhibits VEGF-induced migration and dermal microvascular EC tube formation via the AT2R[415]. However, these studies have used primary cells (HUVECs, human aortic ECs, lymphatic ECs, bovine retinal ECs, and human dermal microvascular ECs) rather than cell lines to investigate angiogenesis. Thus, differences between this project and other studies could be due to the use the SGHEC-7 and SVEC4-10 cell lines, where AngII may preferentially signal through the AT2R. Alternatively, AngII-induced ROS may be required to promote angiogenesis, and as AngII did not promote ROS production in this project, this may explain why AngII was not pro-angiogenic in this context.

4.4.3.3. Inhibition of NOX1 restored EC migration following CD47 activation and AngII treatment.

In the literature, EC migration appears to be promoted by ROS, including NOX1-ROS[416]. For example, thrombin initiated ROS production, which promoted aortic VSMC migration in a NOX1-dependent manner[417]; NOX1 was required for bFGF-induced aortic outgrowth[418]; and NOX1 promoted wound closure and proliferation of HPAECs by modulating cyclic adenosine monophosphate response element-binding protein expression following hypoxia[375]. Furthermore, NOX1-deficient mice exhibit impaired angiogenesis, and *in vitro* data from other studies indicate that NOX1 is required for ROS production, EC migration and sprouting induced by VEGF or bFGF in HUVECs and mouse primary lung ECs[419]. However, age-associated decreases to murine aortic EC migration and aortic sprouting, could be attenuated through NOX1 inhibition using NOXA1ds[420]. Clearly, NOX1 regulates angiogenesis, but whether it is pro-angiogenic or anti-angiogenic is context dependent.

Based upon the majority of previous studies, following inhibition of NOX1, reduced migration would be expected to be observed at baseline. This would exacerbate impaired migration following CD47 activation or AngII treatment. Instead, it was found that wound closure was unaltered with NOX1 inhibition; however, following CD47 activation or AngII treatment, NOX1

inhibition restored SVEC4-10 migration (Figure 4.9A-B). The difference observed may be due to the stimuli used to promote migration in previous studies (e.g. VEGF, bFGF, and hypoxia), which may act in a different manner compared with CD47 activation or AngII. However, preliminary timelapse data indicated NOX1 inhibition may reduce SGHEC-7 motility at baseline (Figure 4.10A), which is more in line with previous studies, and may indicate that the response seen is cell type or species specific; SVEC4-10s are a mouse lymphatic EC cell line, whilst the SGHEC-7 cell line is a HUVEC lineage with an extended lifespan. As such, cardiac ECs may not respond similarly; however, due to the closure of the Biological Resource Facility, and the lack of any viable alternative source of primary cardiac ECs, the work to ascertain this could not be conducted.

The NOX1 inhibitors used behaved differently. NOX1 inhibition by NOXA1ds restored SVEC4-10 migration following CD47 activation and AngII treatment, whilst NOX1 inhibition by setanaxib restored wound closure following CD47 activation, but not after AngII treatment (Figure 4.9A-B). Based on this, following CD47 activation, it is clear that NOX1 is required for perturbed EC migration. However, following AngII treatment, only NOXA1ds restored wound closure; this may indicate that NOXA1ds is a more effective NOX1 inhibitor than setanaxib. Indeed, setanaxib has an inhibitory constant (Ki) for NOX1 of 140 nM, whilst for NOX4 the Ki is 110 nM, indicating it is more selective for NOX4 than NOX1[368]. In addition, as NOXA1ds can effectively inhibit migration, this supports that NOXA1 is participating in the activation of the NOX1 system following CD47 activation and AngII treatment.

4.4.3.4. EC proliferation and death are not affected by CD47 activation, by AngII treatment nor by NOX1 inhibition

Here, neither CD47 activation, AngII treatment nor NOX1 inhibition affected SVEC4-10 proliferation (Figure 4.9C). Furthermore, observations in SGHEC-7s indicated that the stimuli and NOX1 inhibitors were unlikely to affect proliferation or cell death (Figure 4.10C & E). Despite this, TSP1 has been demonstrated to promote HPAEC senescence[175], whilst NOX1 inhibition by NOXA1ds attenuated age-induced senescence in aortic ECs[420]. Based on these studies, it could be expected that activation of CD47 by 7N3 would attenuate proliferation. However, this was not observed, it may be that another TSP1 receptor (such as CD36 or integrins) is responsible for the role of TSP1 in EC senescence. Furthermore, this projects findings demonstrate that CD47 activation is unlikely to promote apoptosis, indeed previous work has indicated that TSP1 induced apoptosis in human brain microvascular ECs occurs in a CD36-dependent manner, rather than by CD47[421]. Previous studies have also indicated that NOX1 is proapoptotic; NOX1-ROS promoted apoptosis in sinusoidal ECs[422] and, NOX1-null mouse lung ECs were protected from hyperoxia-induced apoptosis[423]. However, for NOX1 to influence cell death, a situation where cell death occurs may be needed, and as neither CD47

activation nor AngII treatment caused cell death in SGHEC-7s, this may be why NOX1 inhibition did not improve cell survival.

4.4.4. Conclusion

In the hypertensive heart, cardiac remodelling may be governed by interplay between CD47 activation and AngII signalling. Although CD47 activation and AngII treatment induced MAPK phosphorylation similarly in cardiac ECs; cardiac fibroblasts and myocytes exhibit a markedly different response, with stress-regulated MAPKs activated in fibroblasts following CD47 activation, and pro-growth ERK1/2 activated following AngII treatment. Cardiac myocytes did not respond to AngII, but CD47 activation promoted ERK1/2 phosphorylation. This highlights that underlying cardiac remodelling processes are the individual cell types of the heart and their distinct responses. Understanding the interactions between these cell types, and how their individual intra-cellular signalling networks interact will enhance understanding of the hypertensive myocardium, to identify key signalling proteins involved in the progression of HHD. One such signalling protein is NOX1. Here, CD47 activation increased NOX1 transcription in cardiac ECs, whilst AngII treatment did not. However, the initial EC ROS production following CD47 activation was unlikely to contribute to oxidative stress. Increased NOX1 protein expression may result in localised ROS production, modulating redox signalling to affect cellular function. Indeed, NOX1 inhibited SVEC4-10 migration following CD47 activation and AngII treatment. However, future studies are needed to confirm the role of NOX1 in cardiac ECs. If cardiac ECs respond as cell lines, NOX1 may be a target to promote EC function in the hypertensive heart, attenuating impaired EC function in response to AngII and TSP1.

Chapter 5: Altered DUSP expression may contribute to the pathogenesis of HHD

5.1. Introduction

MAPK activation coordinates cellular responses to external stimuli, such as proliferation, migration, cell survival and death. In the heart, MAPKs are integral for cardiac development, hypertrophic and fibrotic remodelling, and myocardial cell death[191]. Thus, cardiac MAPK signalling is either detrimental, by promoting dilatation and progression to failure, or is adaptive, by promoting concentric remodelling, preventing fibrosis and delaying progression to heart failure (HF)[191]. How these kinases are inactivated by phosphatases is a growing area of research, and by understanding how these "off" switches function in the heart may lead to the identification of new therapeutic targets which, through inhibition, may limit maladaptive processes remodelling processes which regulate the transition to failure/decompensation.

The typical dual specificity family of phosphatases (DUSPs) dephosphorylate Ser/Thr and Tyr residues, and are prominent MAPK regulators, affecting proliferation, differentiation, and migration. In the heart, DUSP expression is altered in cardiac diseases and can influence hypertrophy, fibrosis and contractility[208,284,285,327,328]. Consequently, targeted inhibition of overexpressed DUSPs in cardiac diseases may improve cardiac function, through ameliorating MAPK signalling in the heart. However, previous studies of DUSPs in the heart have used TAC, isoprenaline and AngII/PE models, and cardiac DUSP expression has not been previously investigated in AngII-induced hypertension nor in the SHR model. As such, it is not known whether DUSPs contribute to pathological cardiac remodelling in the hypertensive heart nor whether they influence disease progression in HHD.

As the expression of DUSPs has been demonstrated to be altered in several models of cardiac remodelling, and as cardiac remodelling is known to occur in hypertensive heart disease, it was hypothesised that the mRNA and protein expression of DUSPs would be altered in the hypertensive heart, and that DUSP expression can be regulated by CD47 activation in cardiac ECs. Therefore, MAPK phosphorylation and DUSP expression was identified in NI-HF and hypertensive models, and a novel role for CD47 activation in influencing DUSP expression was found in cardiac ECs.

5.2. Methods

For details of the non-ischaemic HF (NI-HF) cohort, the *in vivo* mouse AngII hypertensive model and the SHR model, see Chapter 3.2. RNAseq and assessment of mRNA expression was conducted as per Chapter 3.2. For DUSP primers see Appendix Tables 3, 4 and 5.

5.2.1. Tissue MAPK and DUSP protein expression

Tissues were homogenised as per Chapter 2.4 and protein concentration was assessed as per Chapter 2.5, with specific details in Table 5.1. Western blotting was conducted as per Chapter 2.6 with 100 µg of protein per lane for DUSPs and 50 µg of protein per lane for ERK1/2 and p38-MAPK. 10% polyacrylamide gels were used. For antibody information, see Table 2.1.

Table 5.1. Methods used for cardiac tissue homogenisation and assessment of protein concentration

Tissue	Homogenisation buffer†	Homogenisation technique	Centrifugation force (*g*)	Centrifugation time (min)	Assay for determination of protein concentration
Human LV cardiac tissue	RIPA	Pestle and mortar	1500	3	BCA
Mouse cardiac tissue	HBSS (DUSP6, 7, 8, 10, 16)	Pestle and mortar	1500	5	Bradford Assay
	HBSS + RBD (MAPKs & DUSP1, 2, 4, 5)‡	MP Lysis System (4 m/s / 5 s)	300	5	BCA
Rat ventricular tissue	RBD buffer	Pestle and mortar	1500	5	BCA

† All buffers contained protease inhibitors. RIPA and RBD buffers also contained PhosSTOP.
‡Tissue was homogenised in HBSS with protease inhibitors using the MP Lysis System. Lysate was centrifuged at 300 x *g* for 5 min. RBD buffer was then added and protein concentration was assessed by BCA.

5.2.2. Cellular DUSP mRNA expression

DUSP mRNA expression was investigated in the SGHEC-7 and SVEC4-10 cell lines, and in cardiac ECs. Experimentation was conducted as per Chapter 4.2.4, with the exception that for SGHEC-7s, the seeding density used was 0.4 x 10^6 cells/well, and cells were synchronised in serum reduced medium for 6 h prior to harvest.

5.2.3. DUSP protein expression in SVEC4-10s

Experimentation was conducted as per Chapter 2.11, with protein expression assessed by western blot as per Chapter 2.6. For DUSP antibody information, see Table 2.1.

5.3. Results

5.3.1. Human NI-HF is associated with ERK1/2 phosphorylation and reduced p38-MAPK phosphorylation

MAPKs can control cardiac remodelling. Activation of ERK1/2 following pathological stress promotes cardiac hypertrophy with concentric remodelling and is cardioprotective, preventing apoptosis following injury[191,209]. Activation of p38-MAPK supports fibrotic remodelling by promoting fibroblast to myofibroblast differentiation[424]. In contrast, JNK has an established role in myocardial ischaemia/reperfusion injury, where rapid transient JNK signalling promotes cardiac myocyte apoptosis[425]. As the hypothesis for this part of the project was that DUSP expression is altered in HF and in the progression of HHD, it was first investigated whether the activation of ERK1/2 and p38-MAPK was altered in NI-HF and in the hypertensive rodent models. As previous studies have indicated that JNK1/2 predominantly regulates cardiac myocyte death in the heart, and as in the hypertensive heart, there is limited evidence of cardiac myocyte death, JNK1/2 activation was not investigated.

It was found that in human NI-HF, ERK1/2 phosphorylation was elevated (2.83-fold, p=0.0113), and therefore activated, whilst p38-MAPK phosphorylation was reduced (0.38-fold, p=0.0006) (Figure 5.1A), indicating reduced activation. However, in rodent models of hypertension, cardiac ERK1/2 and p38-MAPK phosphorylation was unchanged (Figure 5.1B-C).

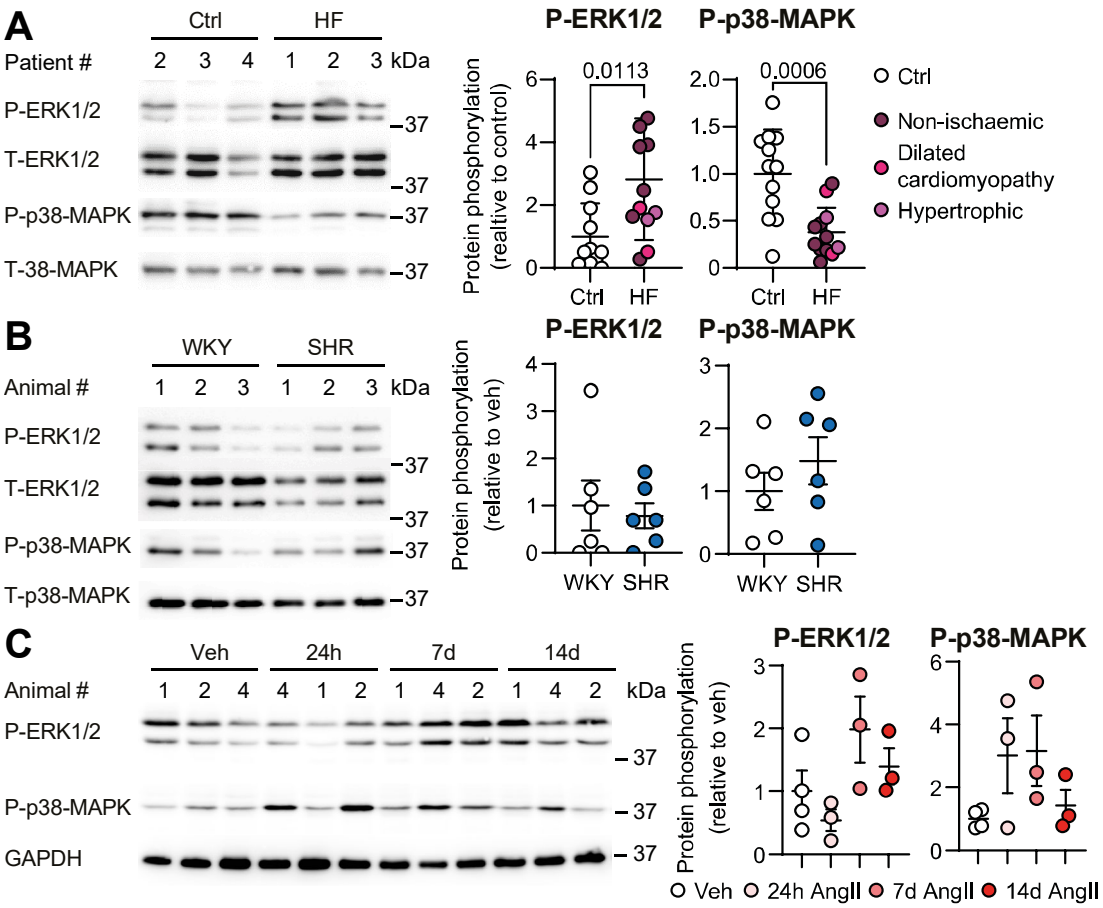

Figure 5.1. Cardiac MAPK phosphorylation in human NI-HF and in hypertensive rodents.

The phosphorylation of ERK1/2 and p38-MAPK was assessed by western blot with quantification in cardiac tissue from (**A**) NI-HF patients (n=12) (**B**) SHRs (n=6) and (**C**) AngII-induced hypertensive mice (veh: n=4; 24 h, 7 d and 14 d: n=3). Representative blots are displayed. P-ERK1/2 and P-p38-MAPK were normalised to T-ERK1/2 and T-p38-MAPK respectively, and are relative to controls. Data are means ± SEM, showing individual values. Statistical tests: (**A**-**B**) unpaired t-test (**C**) one-way ANOVA with Holm-Sidak post hoc test, reporting p-values <0.05.

5.3.2. DUSP expression is perturbed in human NI-HF and hypertensive hearts

Having identified elevated ERK1/2 phosphorylation and reduced p38-MAPK phosphorylation in human HF, and no change to ERK1/2 or p38-MAPK in hypertensive rodents, it was next determined whether DUSP expression was altered in these settings. Here, the mRNA expression of DUSP1, 2, 4, 5, 6, 7, 8, 9, 10 and 16 was characterised, and the protein expression of DUSP1, 2, 4, 5, 6, 7, 8, 10 and 16 was determined in cardiac tissue from NI-HF patients and from hypertensive rodents, as these are the typical DUSPs, which are known to specifically and selectively dephosphorylate the MAPKs[288]. Although DUSP9 is also a typical DUSP, the protein expression of DUSP9 was not investigated as previous studies have indicated DUSP9 protein expression in the heart is limited[292,334].

In end-stage human NI-HF, *DUSP7* mRNA expression, which regulates cytosolic ERK1/2, was decreased (0.53-fold, p=0.0065) (Figure 5.2A). However, the protein expression was unaffected (Figure 5.2B). In contrast, the protein expression of DUSP5 (1.37-fold, p=0.0379) and DUSP8 (1.70-fold, p=0.0462) was significantly elevated in NI-HF (Figure 5.2B), although, the mRNA expression of DUSP5 could not be ascertained and there was no change to DUSP8 mRNA (Figure 5.2A). Interestingly, despite the classification of DUSP8 as p38-MAPK and JNK selective, in the heart it preferentially targets ERK1/2[290], and DUSP5 also selectively dephosphorylates nuclear ERK1/2. Consequently, this indicates that ERK1/2-selective DUSPs are upregulated in HF.

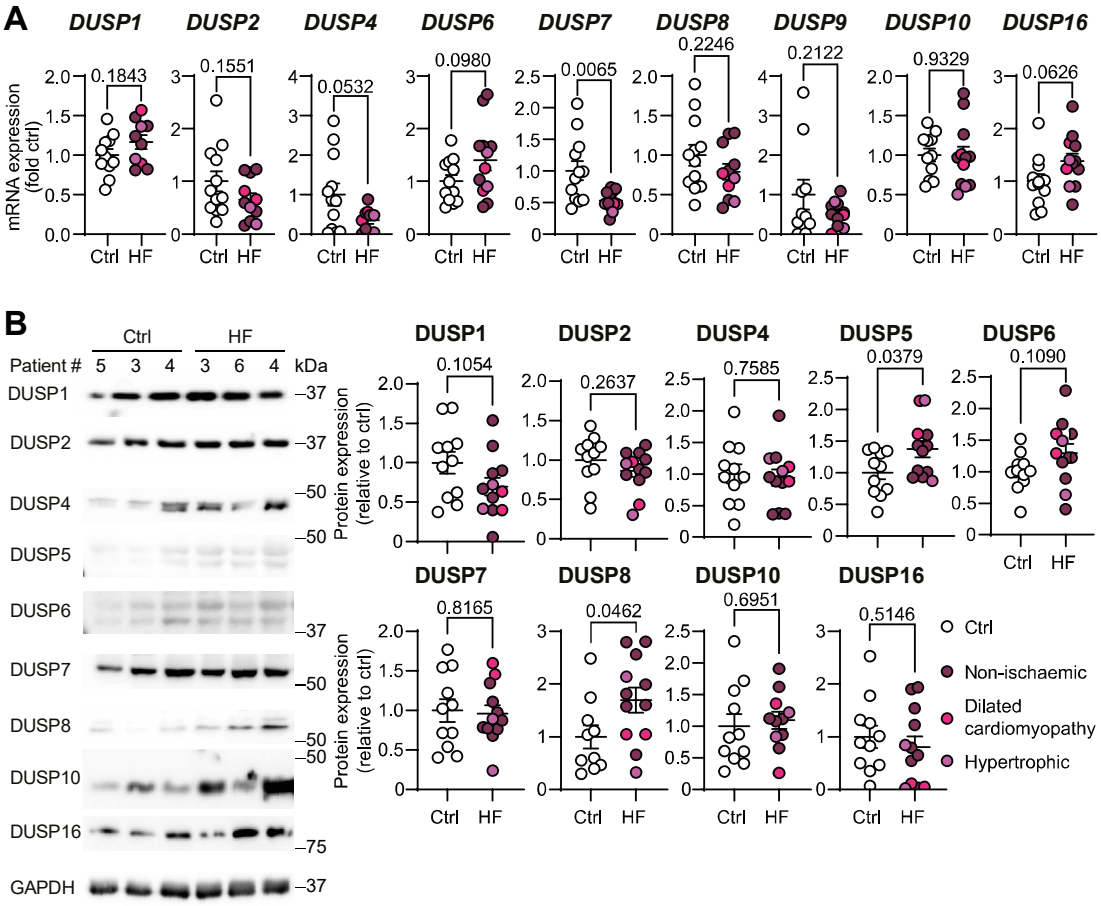

Figure 5.2. DUSPs regulating ERK1/2 phosphorylation are altered in NI-HF.
Left ventricular cardiac tissue from NI-HF patients was assessed (**A**) for *DUSP* mRNA expression by RT-qPCR normalised to *GAPDH*, relative to non-failed controls, and (**B**) for DUSP protein expression by western blot. (**B**) Left panel: representative western blots. Right panel: quantification of protein expression, normalised to GAPDH, relative to controls with underlying aetiologies (non-ischaemic, hypertrophic, and dilated cardiomyopathy) displayed. Data are means ± SEM, showing individual values (n=12). Statistical test: t-test, reporting p-values.

Next, *Dusp* mRNA expression in the SHR model was determined. Of these, *Dusp2* (1.35-fold, p=0.0039) and *Dusp4* (1.66-fold, p=0.0052) mRNAs (both regulating nuclear MAPK targets) were elevated (Figure 5.3A), but this did not relate to the protein, as DUSP2 and DUSP4 expression remained unchanged (Figure 5.3B). Similarly, a mismatch was observed between *Dusp6* and *Dusp7* transcription (Figure 5.3A) and DUSP6 and 7 protein expression (Figure 5.3B). Both regulate cytosolic ERK1/2 and exhibited elevated gene expression (*Dusp6*: 1.58-fold, p=0.0030; *Dusp7*: 1.39-fold, p=0.0310) but reduced protein expression (DUSP6: 0.30-fold, p=0.0205; DUSP7: 0.43-fold, p=0.0153). In contrast, DUSPs typically regulating p38-MAPK and JNK exhibited different profiles: DUSP8 had elevated mRNA expression (2.06-fold, p<0.0001); however, DUSP8 protein expression remained unchanged; DUSP10 exhibited reduced mRNA expression (0.5945-fold, p=0.0410), however the protein expression was not detectable; DUSP16 did not have altered gene expression (Figure 5.3A), but the protein expression was increased (4.87-fold, p=0.0148) (Figure 5.3B). Overall, in SHR hearts, there was no change to the protein expression of DUSPs regulating nuclear MAPKs, whilst the protein expression of DUSP6 and DUSP7, regulators of cytosolic ERK1/2, was reduced, and the protein expression of DUSP16, a regulator of p38-MAPK and JNK, was elevated.

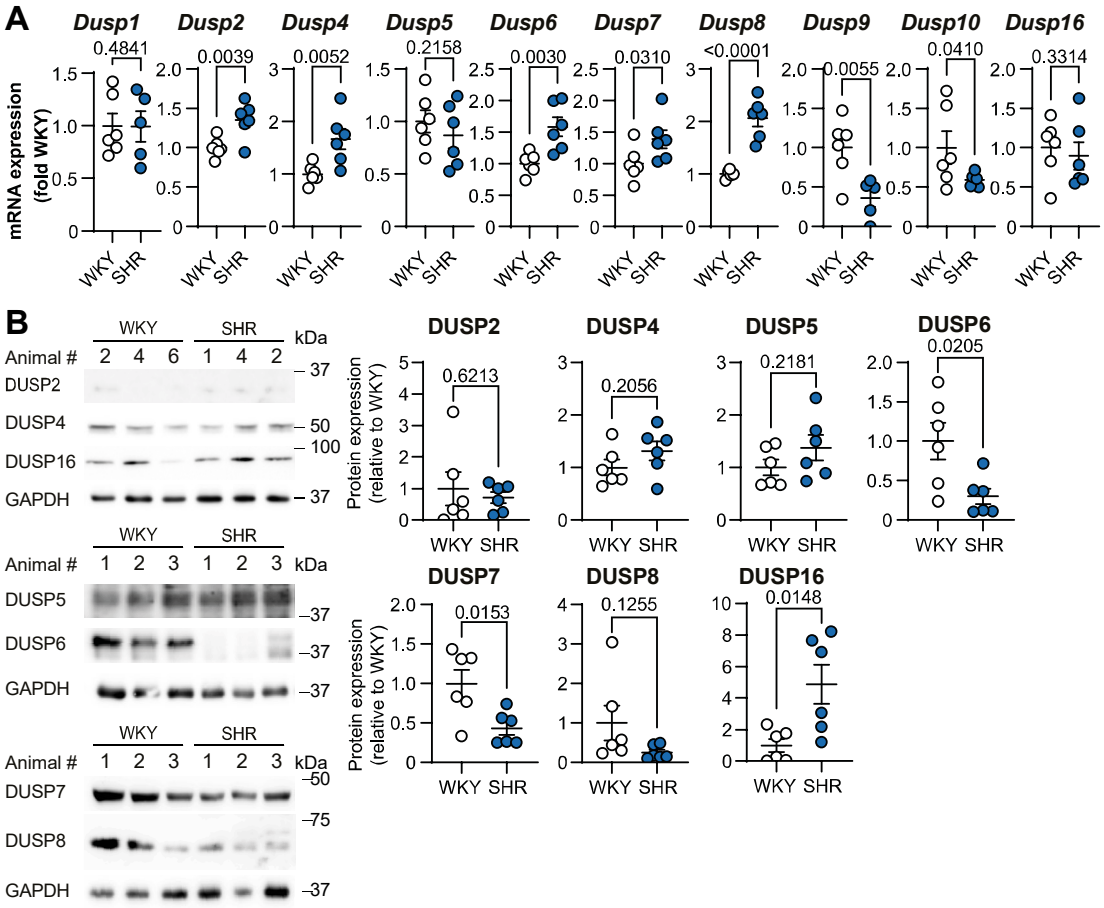

Figure 5.3. DUSPs regulating cytosolic MAPK phosphorylation are altered in the SHR model of essential hypertension.

Cardiac tissue from SHRs was compared to WKY normotensive controls for the assessment of (**A**) *Dusp* mRNA expression, determined by RT-qPCR, normalised to *Gapdh* and (**B**) DUSP protein expression, determined by western blot. (**B**) Left panel: representative western blots, right panel: quantification of protein expression, normalised to GAPDH. Data are means ± SEM, showing individual values (n=6). Statistical tests: t-test, reporting p-values.

Finally, the expression of cardiac DUSPs in the AngII model of hypertension was investigated. RNAseq data from the 7 d AngII-induced hypertensive mice indicated that there was no change to cardiac *Dusp* gene expression (Figure 5.4A). As poor concordance between DUSP mRNA and protein expression was previously observed, this may not be reflected in the protein expression. Furthermore, DUSP mRNA expression may be time-sensitive in the phasing of disease progression. As such, cardiac DUSP mRNA and protein expression in mice treated with AngII for 24 h, 7 d and 14 d were characterised.

With acute (24 h) AngII treatment, the mRNA expression levels of DUSPs regulating nuclear MAPKs were elevated in the heart (*Dusp2*: 2.11-fold, p=0.0004; *Dusp4*: 1.90-fold, p=0.0001; *Dusp5*: 2.23-fold, p=0.0003), except for *Dusp1*, which was decreased (0.64-fold, p=0.0016) (Figure 5.4B). Of the nuclear MAPKs, only the protein expression of DUSP1 was altered, where it was reduced at 24 h (0.55-fold, p=0.0350) and at 7 d (0.33-fold, p=0.0059). The protein expression of DUSP7, a regulator of cytosolic ERK1/2, was also reduced at 7 d (0.38-fold, p=0.0219) (Figure 5.4C). DUSP2 and DUSP5 may have been significantly elevated had a larger cohort size been used; there was variation in the protein expression of DUSP2 in controls and a possible outlier at 24 h and 7 d for DUSP5 (Figure 5.4C). The mRNA expression of *Dusp6* (1.45-fold, p=0.0223) and *Dusp9* (3.30-fold, p=0.0063), regulating cytosolic ERK1/2, was acutely elevated (Figure 5.4B). By 7 d; however, only *Dusp6* mRNA expression remained elevated (1.46-fold, p=0.0223), which corresponded to increased DUSP6 protein expression at 7 d (2.72-fold, p=0.0470) which was maintained at 14 d (2.95-fold, p=0.0213) (Figure 5.4C). With chronic (14 d) AngII treatment, there were no further changes to DUSP mRNA or protein expression (Figure 5.4B-C). Of note, the protein expression of DUSP10 and of DUSP16 was not detectable, despite transcripts being measurable. Overall, it was found that the cardiac expression levels of DUSPs regulating nuclear MAPKs were rapidly altered in the acute response to AngII, and DUSPs regulating ERK1/2 were altered in the adaptive and chronic phase of AngII-induced hypertension.

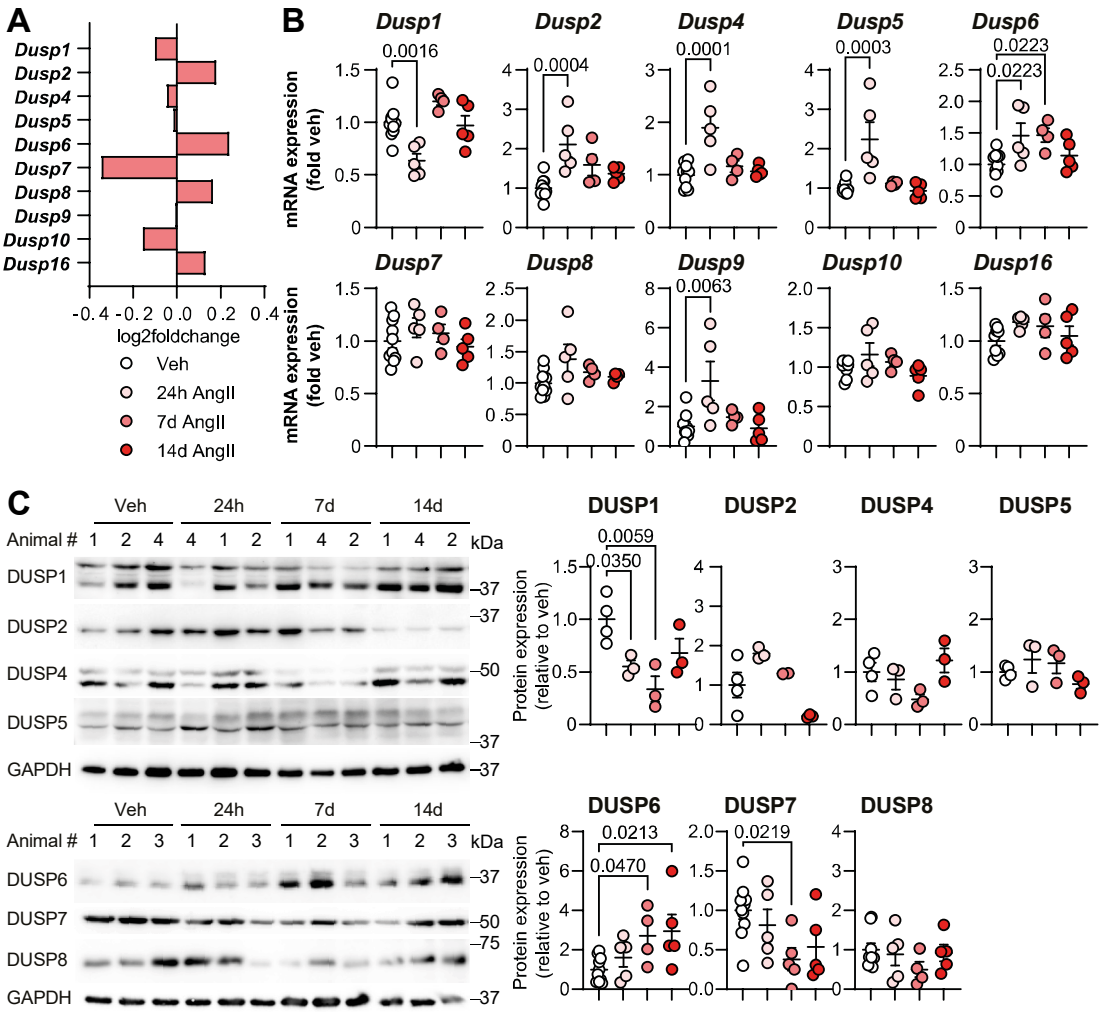

Figure 5.4. The expression of cardiac DUSPs targeting P-ERK1/2 is perturbed in AngII-induced hypertensive mice.

(**A**) Log 2-fold change plots of Dusp RNAseq data from 7 d AngII-induced hypertensive mice. Cardiac tissue from mice treated with 0.8 mg/kg/d AngII for 24 h, 7 d and 14 d (n=5 per group) or veh (n=10) were assessed for (**B**) *Dusp* mRNA expression determined by RT-qPCR, normalised to *Gapdh* or (**C**) protein expression assessed by western blot (DUSP1, 2, 4 and 5; veh, n=4; 24 h, 7 d and 14 d AngII, n=3 per group). (**C**) Left panel; representative western blots, right panel: quantification of protein expression, normalised to GAPDH. Data are means ± SEM, showing individual values. Statistical tests: one-way ANOVA with Holm-Sidak post hoc test, reporting p-values <0.05.

5.3.3. AngII and CD47 promote the expression of DUSPs in cardiac ECs.

This project found that altered DUSP expression occurred in both NI-HF, regardless of MAPK activation, and found that there was rapid MAPK activation in response to AngII and CD47 activation in cardiac ECs (Figures 4.1C & 4.2C). However, attenuation of MAPK signalling by DUSPs has not been widely investigated in ECs and the effect of CD47 on DUSP expression is entirely unknown. Therefore, *DUSP* mRNA expression in EC cell lines (human: SGHEC-7; mouse: SVEC4-10) and in primary cardiac ECs isolated from wild-type mice was characterised in response to AngII and CD47 activation, assessing nuclear *vs* cytosolic *DUSP* mRNA expression patterns.

In terms of DUSPs with nuclear localisation, both 7N3 and AngII rapidly (<2 h) promoted significant increases to the mRNA expression of *Dusp1* and *Dusp2* in SVEC4-10s (Figures 5.5A & 5.6A). In primary cardiac ECs and *Dusp1* mRNA expression was elevated 30 mins following CD47 activation (2.96-fold, p=0.0063) (Figure 5.5C) and in response to AngII (2.39-fold, p=0.0164) (Figure 5.6C). However, whilst AngII had no effect on *DUSP4* and *DUSP5* transcription in ECs (Figure 5.6A-C), CD47 activation resulted in significantly reduced *Dusp4* transcription in SVEC4-10s, whilst *Dusp5* was rapidly (<2 h) and significantly elevated in both SVEC4-10s (Figure 5.5A) and in cardiac ECs at 30 mins (1.83-fold, p=0.0018) (Figure 5.5C). Of note, *DUSP5* mRNA was not detected in SGHEC-7s (Figure 5.5B). In terms of protein expression, it was confirmed that CD47 activation significantly increased DUSP5 protein expression in SVEC4-10s (2.47-fold, p=0.0008) (Figure 5.5D). A summary is presented in Figure 5.7.

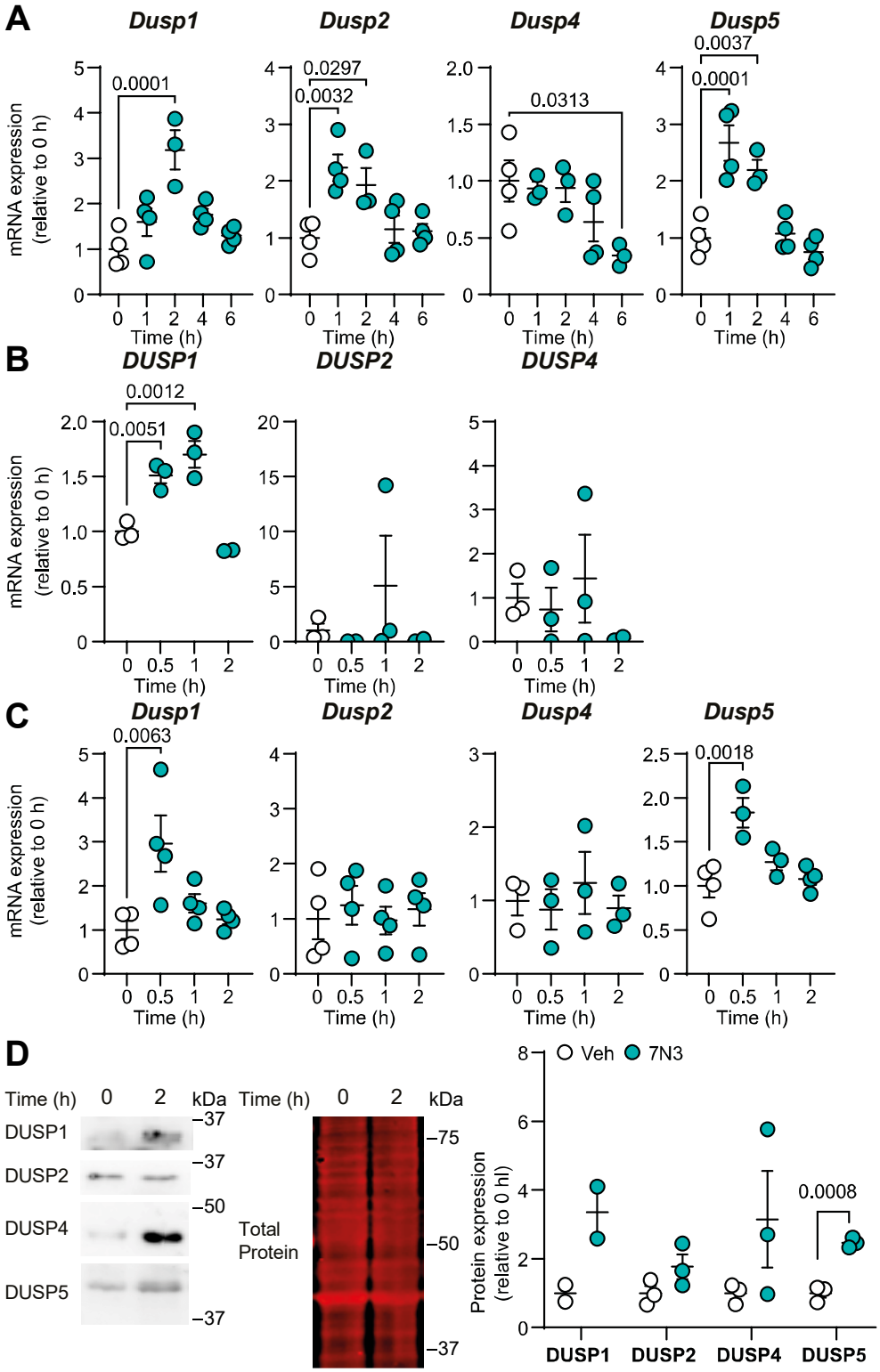

Figure 5.5. CD47 activation promotes expression of nuclear localised DUSPs in ECs. DUSP1, 2 ,4 and 5 mRNA expression following CD47 activation by treatment with the 7N3 peptide in (**A**) SVEC4-10s (n=4), (**B**) SGHEC-7s (n=3) and (**C**) cardiac ECs, assessed by RT-qPCR normalised to GAPDH, relative to untreated (0 h) cells. (**D**) Protein expression of DUSP1, 2, 4 and 5 in SVEC4-10s treated with 7N3 for 2 h (n=3, except DUSP1, which is n=2) assessed by western blotting, normalised to total protein, relative to untreated cells. Representative blots are shown. Data are means ± SEM (except (**D**), where the range is displayed for DUSP1), showing individual values. Statistical tests: (**A**-**C**) one-way ANOVA with Holm-Sidak post hoc test, (**D**) unpaired t-test, reporting p-values <0.05. A statistical test was not performed for DUSP1 protein expression.

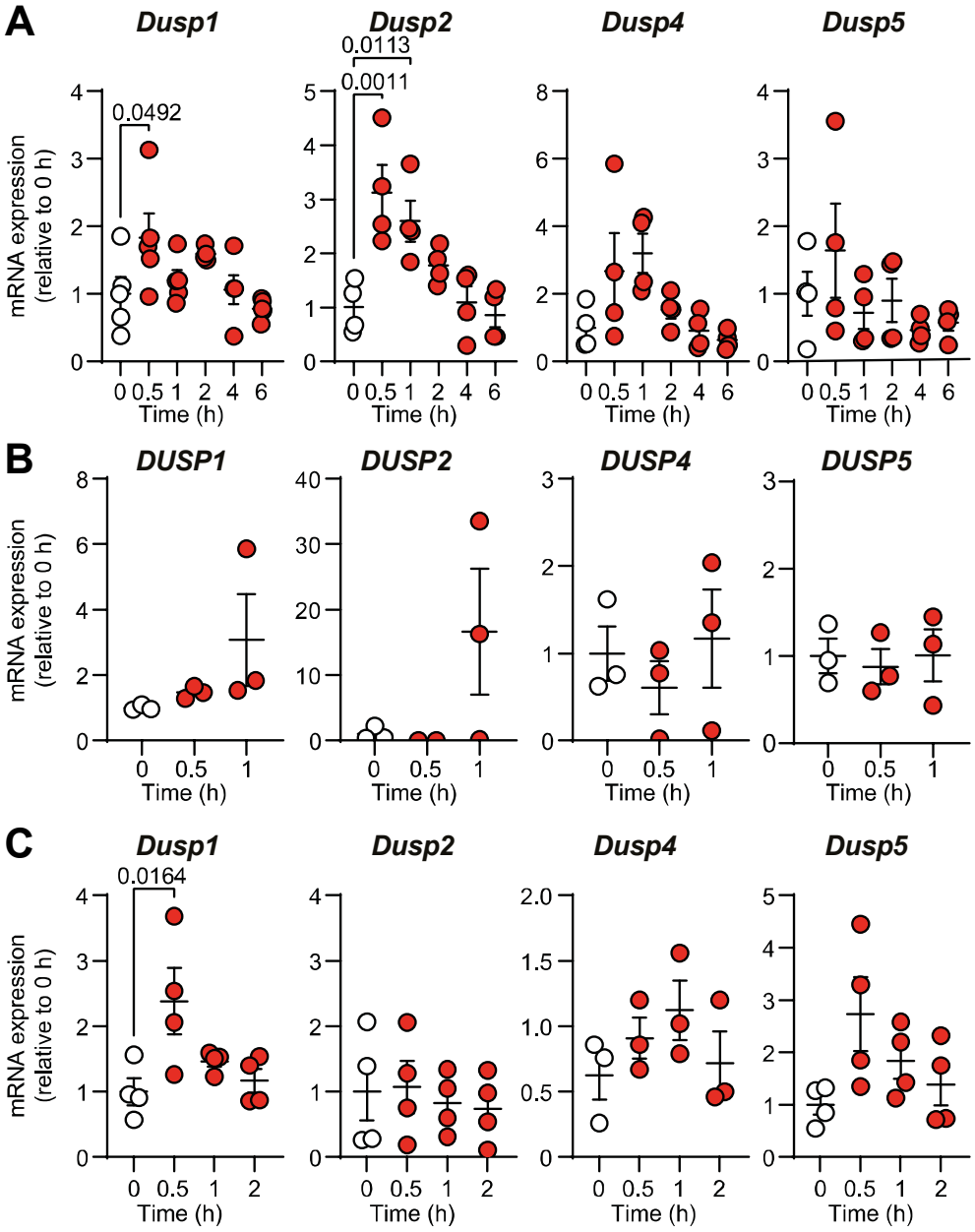

Figure 5.6. Nuclear DUSPs are transcribed in response to AngII in ECs.
DUSP1, *2*, *4* and *5* mRNA expression following AngII treatment in (**A**) SVEC4-10s (n=4), (**B**) SGHEC-7s (n=3) and (**C**) cardiac ECs (n=4). Gene expression was assessed by RT-qPCR normalised to *GAPDH*, relative to untreated (0 h) cells. Data are means ± SEM, showing individual values. Statistical test: one-way ANOVA with Holm-Sidak post hoc test, reporting p-values <0.05.

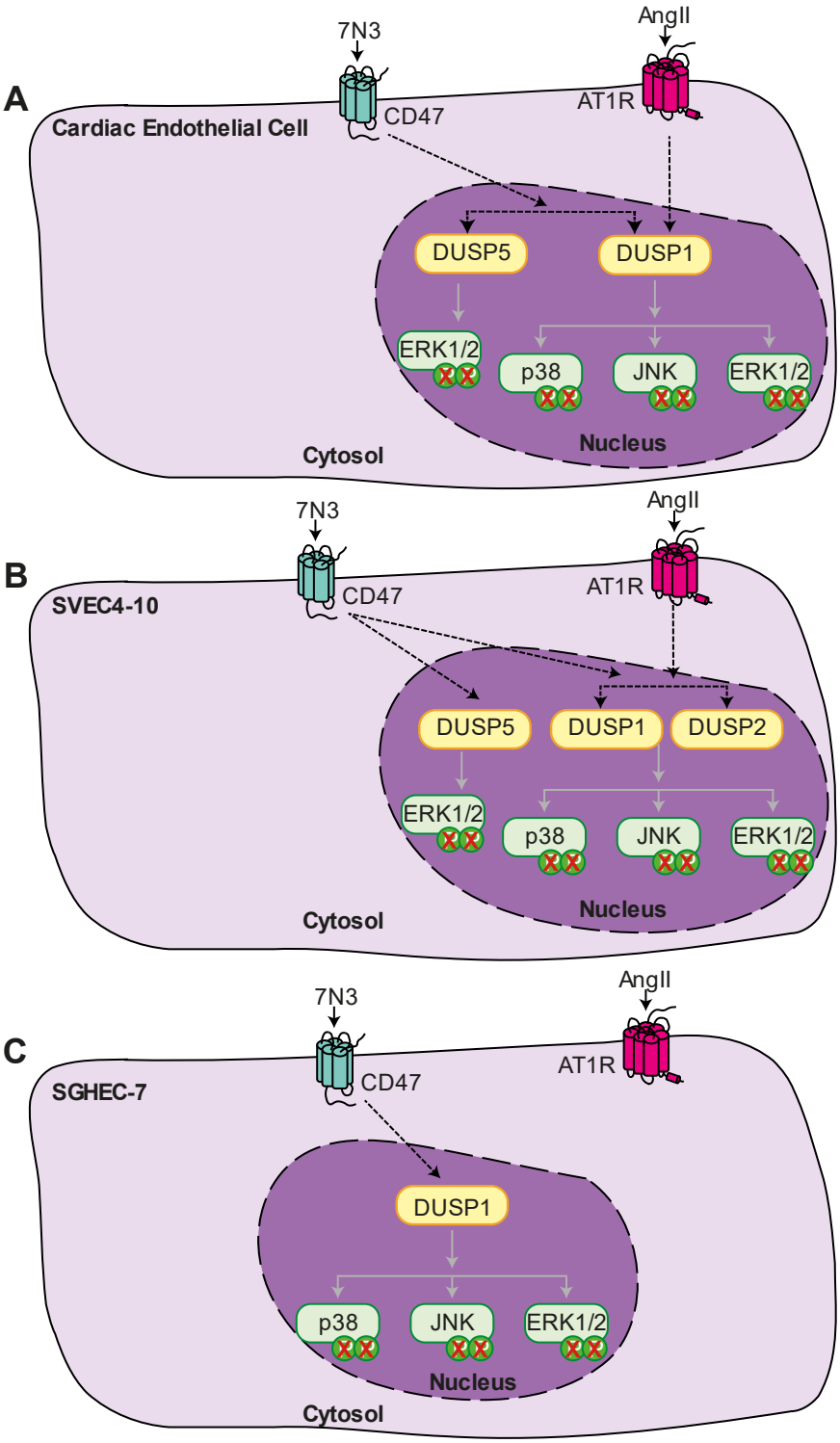

Figure 5.7. Regulation of the mRNA expression of DUSPs selective for nuclear MAPKs
Summary of the mRNA expression (denoted by dashed lines) of *DUSP*s selective for nuclear MAPKs in the acute (≤ 2 h) response to CD47 activation by the 7N3 peptide, and to AngII treatment in (**A**) cardiac ECs, (**B**) the SVEC4-10 cell line and (**C**) the SGHEC-7 cell line. The hypothetical regulation of MAPKs by DUSPs, as has been indicated by the literature[288,289], is denoted by grey lines, with dephosphorylation denoted by X.

Next, the mRNA expression of cytosolic DUSPs regulating ERK1/2 was investigated. CD47 activation significantly promoted *Dusp6* mRNA expression (Figure 5.8A) and DUSP6 protein expression in SVEC4-10s (2.54-fold, $p<0.0001$) (Figure 5.8D). However, CD47 activation did not affect the transcription of DUSPs regulating cytosolic ERK1/2 in SGHEC-7s (Figure 5.8B) nor in cardiac ECs (Figure 5.8C). Similar to CD47 activation, AngII treatment significantly promoted *Dusp6* mRNA expression in SVEC4-10s (Figure 5.9A), but resulted in significantly reduced *DUSP9* expression in SGHEC-7s (Figure 5.9B). In cardiac ECs, AngII did not affect the transcription of DUSPs which regulate ERK1/2 (Figure 5.9C). A summary is presented in Figure 5.10.

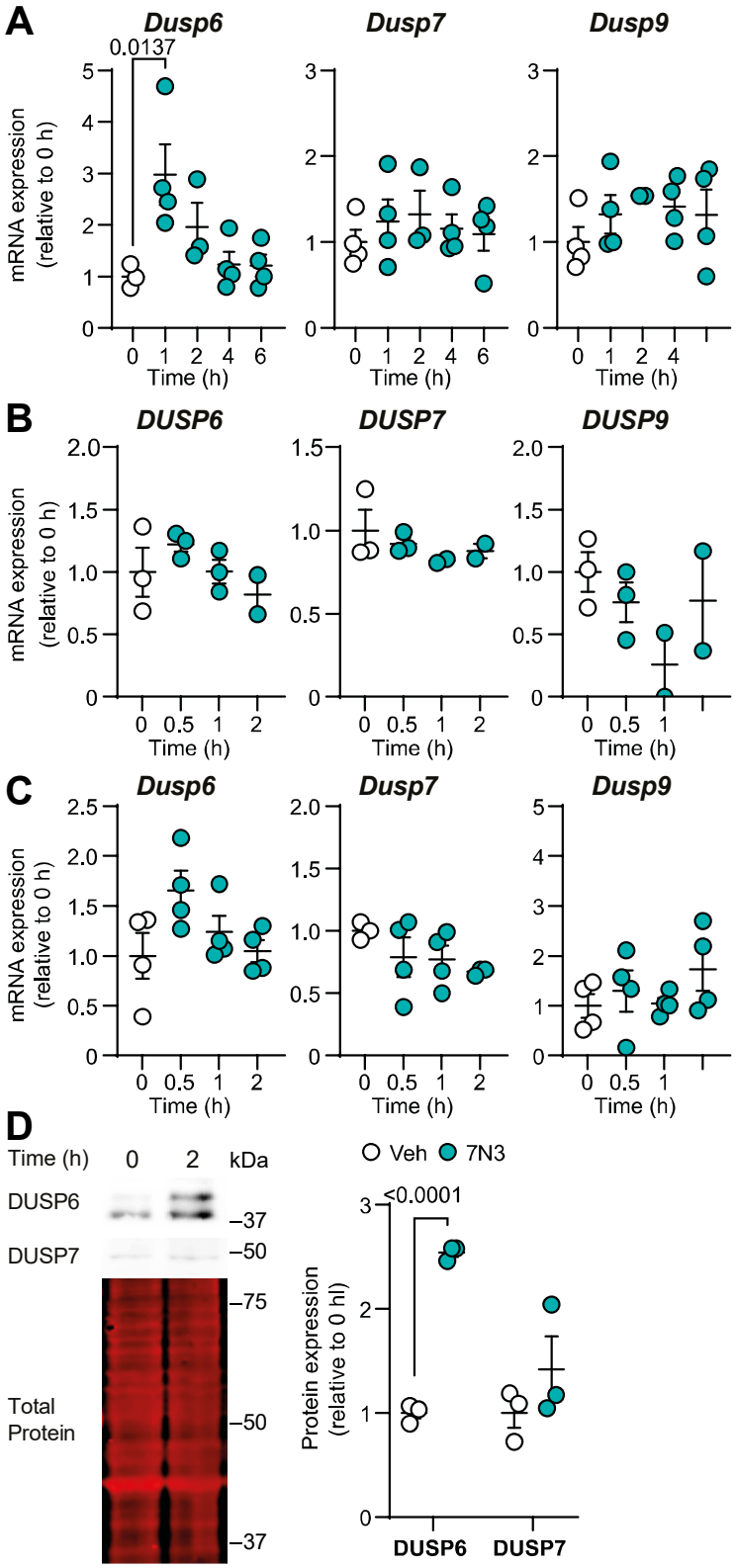

Figure 5.8. CD47 activation promotes expression of ERK1/2-selective DUSP6 in ECs. *DUSP6*, *7* and *9* mRNA expression following 7N3 treatment in (**A**) SVEC4-10s (n=4), (**B**) SGHEC-7s (n=3) and (**C**) cardiac ECs (n=4), assessed by RT-qPCR normalised to *GAPDH*, relative to untreated (0 h) cells. (**D**) Protein expression of DUSP6, 7 and 9 in SVEC4-10s treated with 7N3 for 2 h (n=3), assessed by western blotting, normalised to total protein, relative to untreated cells. Representative blots are shown. Data are means ± SEM, showing individual values. Statistical tests: (**A**-**C**) one-way ANOVA with Holm-Sidak post hoc test, (**D**) unpaired t-test, reporting p-values <0.05.

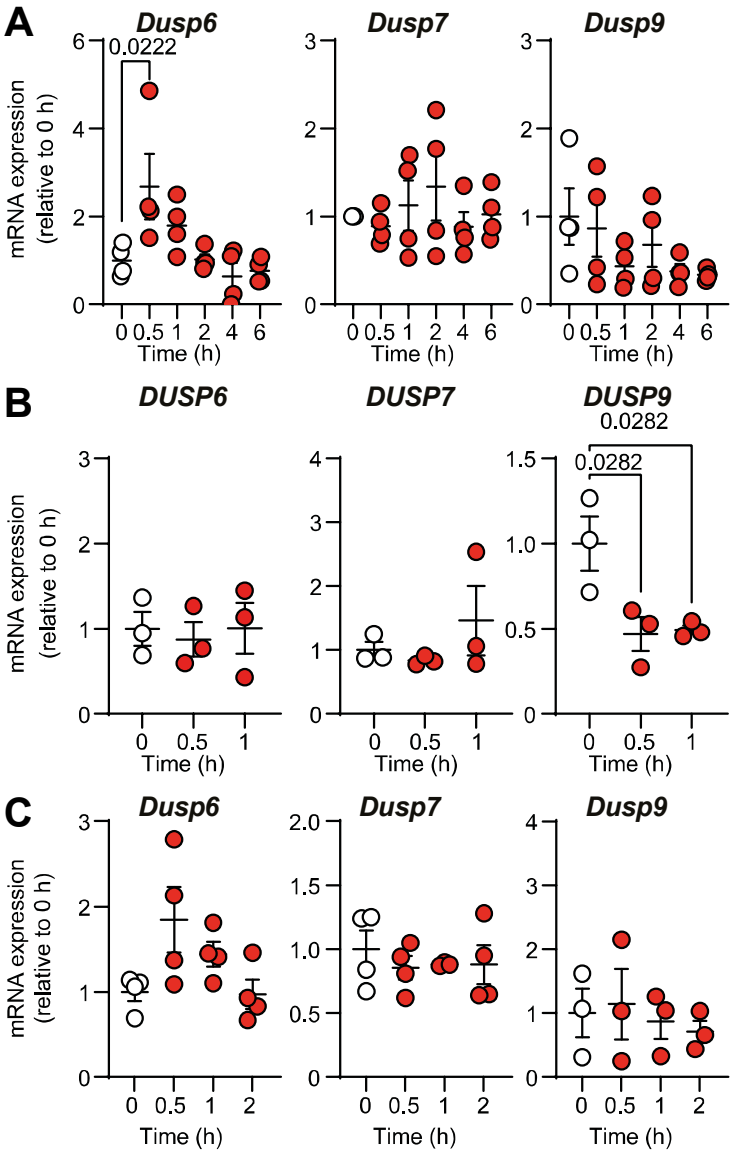

Figure 5.9. Cytosolic DUSPs with ERK1/2 selectivity are transcribed in response AngII in ECs.

DUSP6, 7 and *9* mRNA expression following AngII treatment in (**A**) SVEC4-10s (n=4), (**B**) SGHEC-7s (n=3) and (**C**) cardiac (n=4). Gene expression was assessed by RT-qPCR normalised to *GAPDH*, relative to untreated (0 h) cells. Data are means ± SEM, showing individual values. Statistical test: one-way ANOVA with Holm-Sidak post hoc test, reporting p-values <0.05.

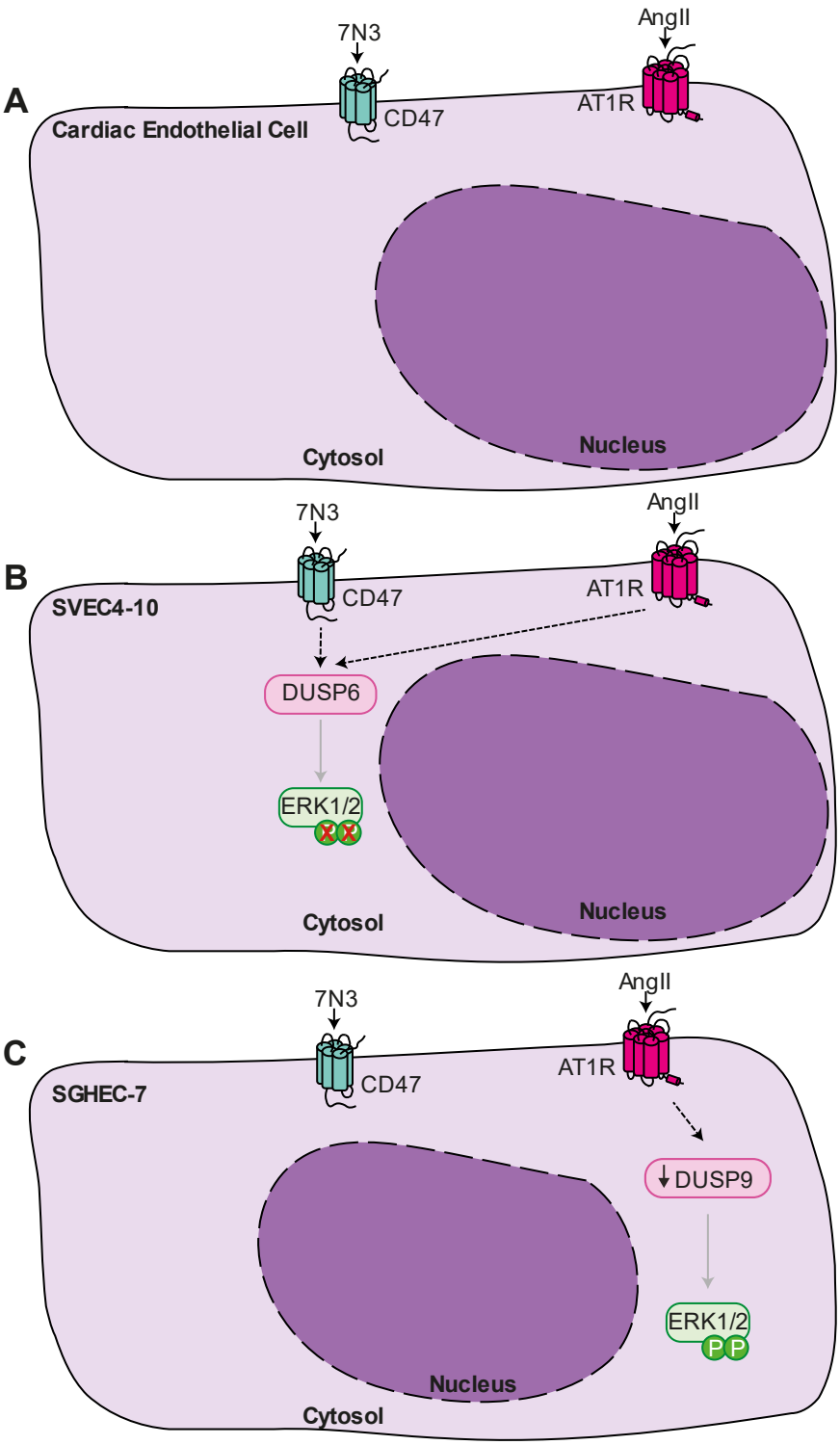

Figure 5.10. Regulation of the mRNA expression of DUSPs selective for cytosolic ERK1/2

Summary of the mRNA expression of *DUSP*s (denoted by dashed lines) selective for cytosolic ERK1/2 in response to CD47 activation by the 7N3 peptide and in response to AngII treatment in (**A**) cardiac ECs, (**B**) the SVEC4-10 cell line and (**C**) the SGHEC-7 cell line. The hypothetical regulation of MAPKs by DUSPs, as has been indicated by the literature[288,289], is denoted by grey lines, with dephosphorylation denoted by X.

Finally, the expression of DUSPs regulating p38-MAPK and JNK in response to CD47 activation and AngII treatment was assessed. The expression levels of DUSPs regulating p38-MAPK and JNK were altered following CD47 activation. *DUSP16* transcription was significantly decreased in SGHEC-7s (Figure 5.11B), although this corresponded with elevated DUSP16 protein expression in SVEC4-10s (2.22-fold, p=0.353) (Figure 5.11D). *Dusp8* mRNA expression was elevated in cardiac ECs 30 mins following CD47 activation (2.41-fold, p=0.0136) (Figure 5.11C), as was DUSP8 protein expression in SVEC4-10s 2 h following CD47 activation (1.79-fold, p=0.0336) (Figure 5.11D). In contrast, AngII treatment did not affect the mRNA expression of DUSPs regulating p38-MAPK and JNK in any of the EC types studied (Figure 5.12). A summary is presented in Figure 5.13.

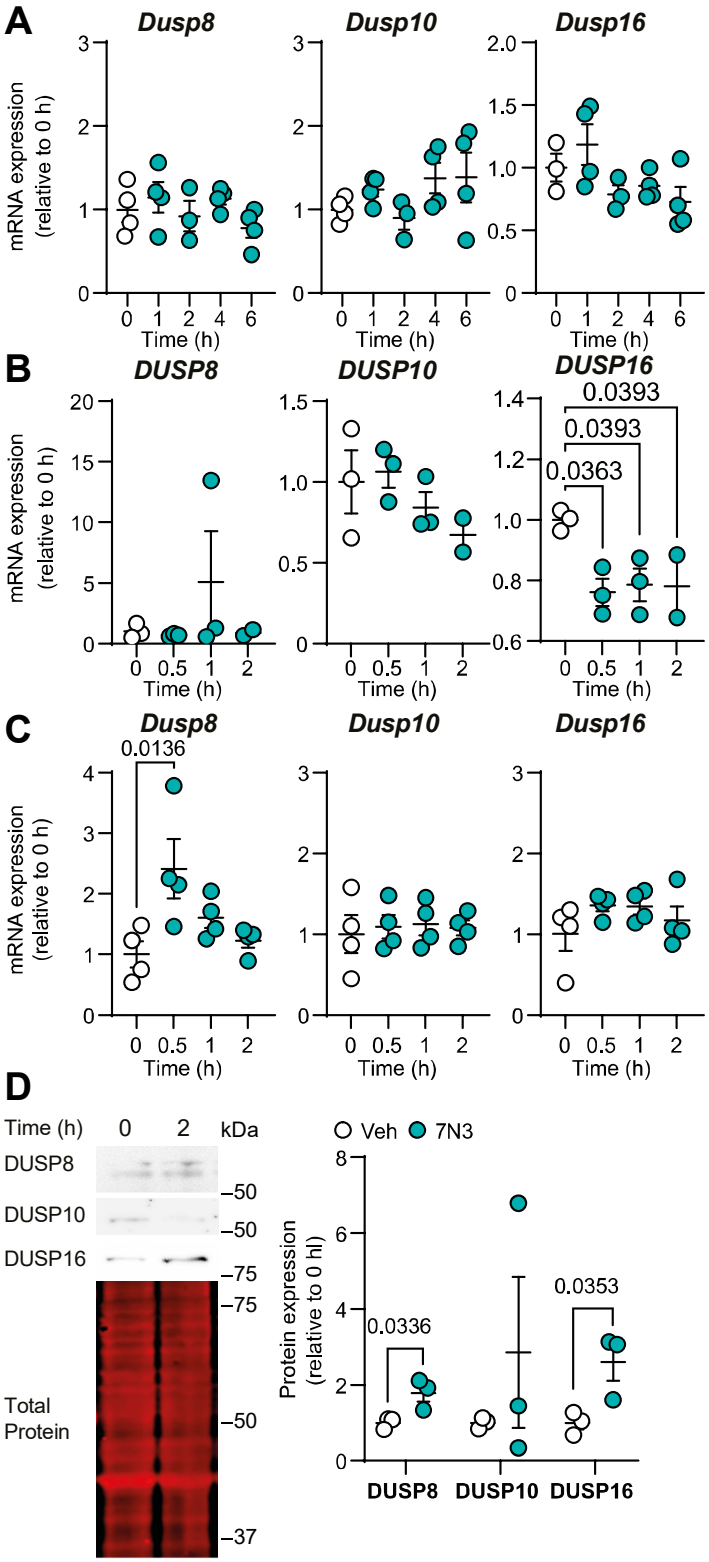

Figure 5.11. CD47 activation promotes expression of DUSP8 and DUSP16, targeting p38-MAPK and JNK.

DUSP8, *10* and *16* mRNA expression following 7N3 treatment in (**A**) SVEC4-10s (n=4), (**B**) SGHEC-7s (n=3) and (**C**) cardiac ECs (n=4), assessed by RT-qPCR normalised to *GAPDH*, relative to untreated (0 h) cells. (**D**) Protein expression of DUSP8, 10 and 16 in SVEC4-10s treated with 7N3 for 2 h (n=3), assessed by western blotting, normalised to total protein, relative to untreated cells. Representative blots are shown. Data are means ± SEM, showing individual values. Statistical tests: (**A**-**C**) one-way ANOVA with Holm-Sidak post hoc test, (**D**) unpaired t-test, reporting p-values <0.05.

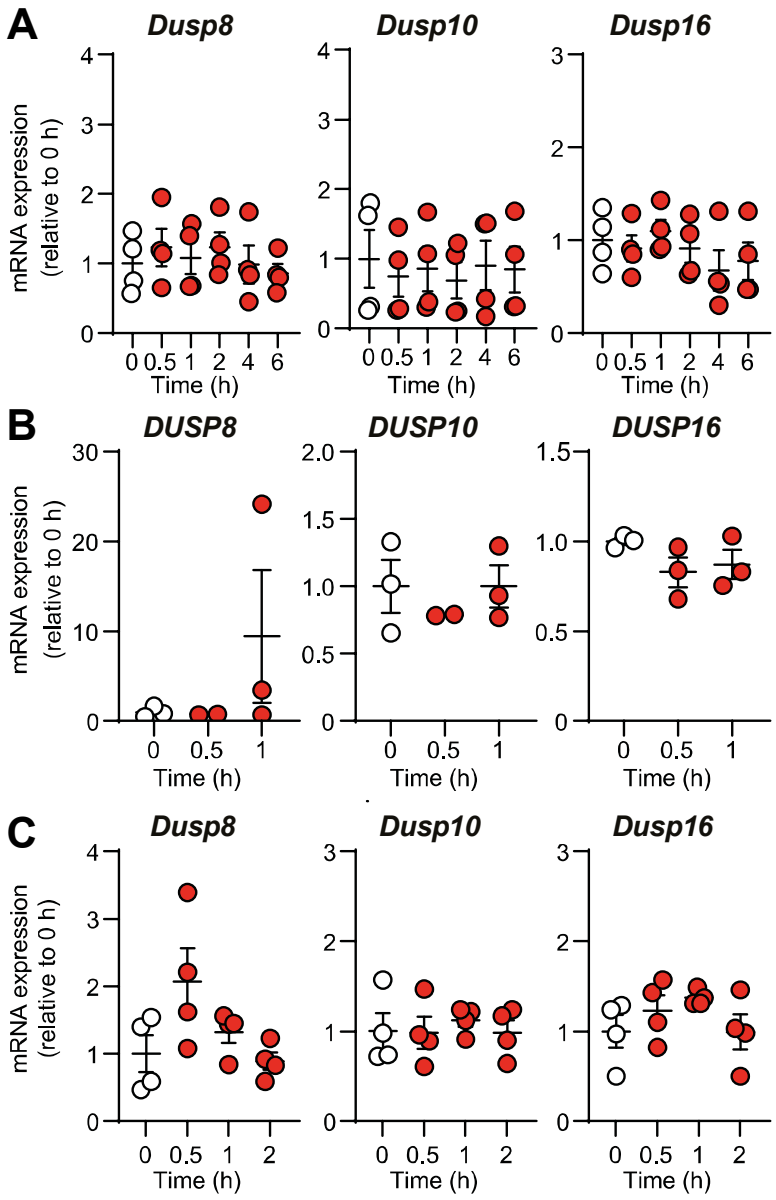

Figure 5.12. DUSPs regulating nuclear and cytosolic p38-MAPK and JNK are unaffected by AngII.

DUSP8, *10* and *16* mRNA expression following AngII treatment in (**A**) SVEC4-10s (n=4), (**B**) SGHEC-7s (n=3) and (**C**) cardiac ECs (n=4). Gene expression was assessed by RT-qPCR normalised to *GAPDH*, relative to untreated (0 h) cells. Data are means ± SEM, showing individual values. Statistical test: one-way ANOVA with Holm-Sidak post hoc test, reporting p-values <0.05.

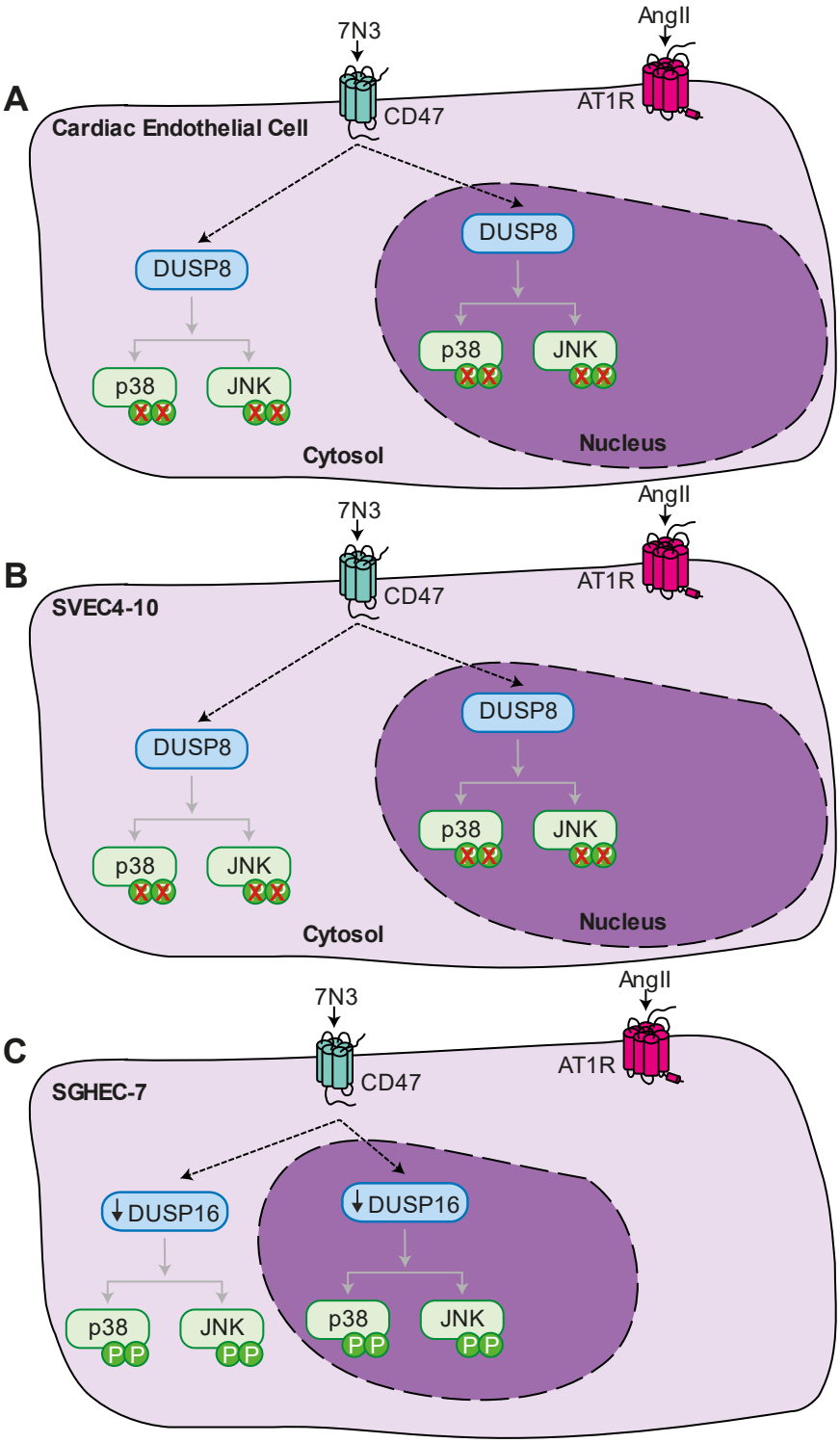

Figure 5.13. Regulation of the mRNA expression of DUSPs selective for p38-MAPK and JNK

Summary of the mRNA expression of *DUSP*s (denoted by dashed lines) selective for nuclear and cytosolic p38-MAPK and JNK in response to CD47 activation by the 7N3 peptide and in response to AngII treatment in (**A**) cardiac ECs, (**B**) the SVEC4-10 cell line and (**C**) the SGHEC-7 cell line. The hypothetical regulation of MAPKs by DUSPs, as has been indicated by the literature[288,289], is denoted by grey lines, with dephosphorylation denoted by X.

5.4. Discussion

Cardiac remodelling is influenced by MAPK activation, for instance the balance between ERK1/2 and p38-MAPK regulates hypertrophy and fibrosis[191]. In end-stage NI-HF, ERK1/2 phosphorylation was elevated whilst p38-MAPK phosphorylation was reduced (Figure 5.1A). However, in the hypertensive models, where fibrotic and hypertrophic remodelling processes occur[78,193,426], MAPK phosphorylation was unchanged (Figure 5.1B & C). As DUSPs influence cardiac remodelling by attenuating MAPK phosphorylation[285], DUSP expression in rodent hypertensive models and in NI-HF was characterised. The results indicated that DUSPs selective for ERK1/2 were upregulated in NI-HF (Figure 5.2B) and were altered in the adaptive and chronic phase of AngII-induced hypertension (Figure 5.4C), whilst in the SHR model, the protein expression of DUSPs regulating cytosolic ERK1/2 were reduced (Figure 5.3B). Furthermore, the protein expression of DUSP1, which regulates nuclear MAPKs, was reduced in the acute response to AngII (Figure 5.4C), whilst the protein expression of DUSP16, which regulates p38-MAPK and JNK, was elevated in the SHR model (Figure 5.3B). Through comparing these findings with the functional effects observed in studies where the expression of cardiac DUSPs has been manipulated, it is considered whether altered DUSP expression in HHD and NI-HF was beneficial in promoting adaptive remodelling, or was maladaptive, promoting pathological remodelling and progression to failure. Finally, the possible implications of altered DUSP expression following CD47 activation on cardiac EC function are discussed. If the perturbations in DUSP expression observed in hypertension and HF are maladaptive, these DUSPs may prove to be suitable therapeutic targets capable of modifying disease progression.

5.4.1. MAPK phosphorylation in the progression of HHD

In end-stage NI-HF, the elevated ERK1/2 phosphorylation and reduced p38-MAPK phosphorylation observed (Figure 5.1A) may prevent further deterioration of cardiac function. Transgenic models have demonstrated that ERK1/2 activation in cardiac myocytes preserves heart function, through promoting adaptive hypertrophy and limiting fibrosis[206,207], whilst the absence of ERK1/2 activation promotes cardiac dilatation, progression to failure and is associated with reduced survival[204,205,209]. Furthermore, 1-8 weeks following TAC, cardiac ERK1/2 activation corresponded with adaptive hypertrophy, but as remodelling progressed, between 12-16 weeks, ERK1/2 phosphorylation was reduced, and dilatation occurred alongside progression to HF[203]. Consequently, in end-stage NI-HF, ERK1/2 may be being reactivated, which may either be a final endeavour to prevent further deterioration, or a potential effect of therapeutics used to manage the patient's HF symptoms. However, other studies have not found ERK1/2 activation in human HF or in chronic AngII-induced HF in rats[322,427]; therefore, it is more likely that the ERK1/2 activation in NI-HF is not part of the disease pathogenesis.

Previous studies have demonstrated that HF is associated with reduced p38-MAPK activation[322,427,428], which is in concordance with this project's findings. Furthermore, in a rat model of hypertension, p38-MAPK inhibition promoted survival by minimising LVH and cardiac dysfunction in the hypertensive heart[429], conversely, p38-MAPK overactivation promoted interstitial fibrosis, dilatation and cardiac failure[212]. This suggests that the increase in ERK1/2 phosphorylation and decrease in p38-MAPK phosphorylation observed in NI-HF both promote survival.

However, in HHD models, cardiac MAPK phosphorylation was unaltered (Figure 5.1B-C). This contrasts with other studies which have found that cardiac ERK1/2, p38-MAPK and JNK are activated in response to pressure overload and AngII treatment, and indicate that a greater increase in model severity corresponds with a greater level of MAPK actviation[430,431]. Therefore, the lack of MAPK activation observed in AngII-induced hypertension may be a result of the mid-level dosage used. However, as a more recent study found activation of p38-MAPK, ERK1/2 and JNK in the hearts of C57BL6/J mice infused with 0.8 mg/kg/day of AngII for 14 d[262], the lack of significant MAPK activation may have been due to reduced power in the small group sizes used in this project.

5.4.2. DUSP expression in the progression of HHD

The typical DUSPs are specific MAPK phosphatases that influence cardiac remodelling by attenuating MAPK signalling, and may constitute potential targets to prevent pathological cardiac remodelling[285]. Due to the lack of viable and selective DUSP inhibitors, the effect of DUSPs on cardiac remodelling and MAPK activation has relied on genetic manipulation studies in mice, with remodelling induced by TAC and/or isoprenaline. Consequently, there is limited knowledge of DUSP expression in HF and in specific models of hypertension. Here, characterisation of cardiac DUSP mRNA and protein expression in human NI-HF and in the SHR/AngII-induced hypertensive models revealed distinct expression profiles relative to disease phase.

5.4.2.1. Expression of DUSPs selective for ERK1/2 in NI-HF

Human NI-HF was associated with elevated protein expression of DUSP5 and DUSP8 (Figure 5.2B). In the heart, DUSP5 regulates ERK1/2 phosphorylation, consistent with other settings[324,325,432], whilst DUSP8 may preferentially regulate ERK1/2 in the heart, rather than p38-MAPK and JNK[290]. DUSP5 has been proposed to negatively regulate hypertrophy and fibrosis. For example, following TAC, an established cause of hypertrophy, DUSP5 expression was reduced, whilst DUSP5 overexpression in neonatal rat ventricular myocytes prevented

PE-induced myocyte hypertrophy[325]. Furthermore, DUSP5 has also been proposed to be a negative regulator of fibroblast proliferation; isoprenaline-induced cardiac fibrosis was associated with reduced cardiac DUSP5 expression, whilst DUSP5 overexpression in cardiac fibroblasts attenuated their proliferative abilities[324]. Thus, in NI-HF, elevated DUSP5 may act to prevent further hypertrophic and fibrotic remodelling by dephosphorylating ERK1/2.

DUSP8 appears to oppose this; DUSP8-null mice exhibited concentric hypertrophy and were protected from cardiac dysfunction following TAC and AngII/PE treatment, whilst DUSP8 overexpression promoted fibrosis, eccentric hypertrophy with evidence of cardiac dysfunction in transgenic mice[290]. Interestingly, DUSP8-null mice exhibited elevated cardiac ERK1/2 phosphorylation, whilst DUSP8 transgenic mice exhibited reduced ERK1/2, p38-MAPK and JNK phosphorylation[290]. Thus, in NI-HF, elevated DUSP8 expression may promote maladaptive remodelling and cardiac dysfunction by attenuating MAPK activation.

Despite the expression of ERK1/2-selective DUSPs in NI-HF, ERK1/2 was phosphorylated (Figure 5.1A). This could in part, be due to the actions of DUSP5. DUSP5 is selective for nuclear ERK1/2, and as such can dephosphorylate and anchor ERK1/2 in the nucleus. This can have the paradoxical effect of promoting cytosolic ERK1/2 phosphorylation, as when anchored in the nucleus, ERK1/2 can no longer negatively regulate its upstream kinases in the cytosol, thus the upstream kinases remain active and so cytosolic ERK1/2 phosphorylation, and therefore activation, is promoted[316].

5.4.2.2. Expression of DUSPs selective for ERK1/2 in the hypertensive heart

The SHR model was associated with reduced protein expression of DUSP6 and of DUSP7 (Figure 5.3B), which regulate cytosolic ERK1/2 phosphorylation. The mouse model of AngII-induced hypertension found that in the adaptive phase (7 d), the protein expression of DUSP6 was elevated, whilst DUSP7 protein expression was reduced, and in the chronic phase (14 d), DUSP6 alone was elevated (Figure 5.4C). Therefore, DUSP6 and DUSP7 are likely to be important regulators of ERK1/2 in the progression of HHD.

Indeed, previous studies have indicated that DUSP6 can promote cardiac decompensation and transition to HF by attenuating ERK1/2 phosphorylation, whilst decreased DUSP6 expression is cardioprotective[208,326,329]. As such, reduced DUSP6 expression in the SHR model may be a protective response to hypertension. However, increased DUSP6 in the adaptive and chronic phases of AngII-induced hypertension may contribute to disease progression. Despite this, as the protection conferred in DUSP6-null models was attributed to greater cardiac myocyte proliferation either *in utero* in mice, or in the adult hearts of zebrafish,

DUSP6 may not be an appropriate target in the adult mammalian heart as cardiac myocytes are terminally differentiated[326,329,332]. However, the DUSP1/6 inhibitor BCI, promoted not only myocyte proliferation in zebrafish, but also promoted angiogenesis and reduced fibrosis following cardiac injury[326], and DUSP6-null mice also exhibited reduced fibrosis[329]. Therefore, inhibition of DUSP6 may improve cardiac function in the hypertensive mammalian heart by promoting angiogenesis and reducing fibrosis, although this remains to be seen.

Reduced protein expression of DUSP7 in the SHR (Figure 5.3B) and AngII (Figure 5.4C) models may promote cardiac adaptation. DUSP7-null mice were somewhat protected from cardiac dysfunction induced by isoprenaline, whilst overexpression of DUSP7 reduced ERK1/2 phosphorylation and hearts were predisposed to failure[333]. Of note, DUSP7-null mice did not exhibit significantly elevated ERK1/2 activation, but were still protected from dysfunction[333]. Therefore, although altered ERK1/2 phosphorylation was not observed in either the SHR (Figure 5.1B) or AngII-induced (Figure 5.1C) hypertensive models, this does not negate the potential for DUSP7 to limit cardiac dysfunction and promote adaptation to hypertension.

Interestingly, there was limited concordance observed between DUSP6 and DUSP7 mRNA and protein expression. In SHRs, *Dusp6* and *Dusp7* mRNA expression was increased (Figure 5.3A), whilst their protein expression was reduced (Figure 5.3B). In AngII-induced hypertension, *Dusp6* mRNA expression was increased in the acute and adaptive phases (Figure 5.4B), whilst DUSP6 protein expression was elevated in the adaptive and chronic phases (Figure 5.4C). Furthermore, *Dusp7* mRNA expression was unchanged (Figure 5.4B), but DUSP7 protein expression was decreased in AngII-induced hypertension (Figure 5.4C). This lack of concordance may be indicative of altered protein stability and turnover, which are known mechanisms of DUSP regulation[289].

5.4.2.3. Expression of DUSPs selective for p38-MAPK and JNK in the hypertensive heart

The mRNA and protein expression of DUSP10 and DUSP16, which dephosphorylate p38-MAPK and JNK, were unaltered in NI-HF (Figure 5.2A-B) and in AngII-induced hypertension (Figure 5.4A-B), whilst only the protein expression of DUSP16 was elevated in SHRs (Figure 5.3B). As the expression of DUSP10 was unchanged in NI-HF, in AngII-induced hypertension and in the SHR model, altered DUSP10 expression is unlikely to contribute to cardiac remodelling in these settings. Despite this, inhibition of DUSP10 may prevent pathological cardiac remodelling, as DUSP10-null mice have improved cardiac function, reduced hypertrophy and reduced fibrosis, following TAC[323]. However, these mice exhibited elevated *Dusp10* mRNA expression following TAC, which was not observed in NI-HF, in

AngII-induced hypertension nor in the SHR model. Therefore, DUSP10 inhibition may not be beneficial in the treatment of hypertensive heart disease.

Despite observing elevated DUSP16 in the SHR model (Figure 5.3B), the role of DUSP16 in the heart has not been studied previously and so the effect of DUSP16 on cardiac function and remodelling cannot be inferred. As such, this project identifies DUSP16 as a novel protein which may alter cardiac function as a negative regulator of p38-MAPK and JNK activation.

5.4.2.4. Expression of DUSPs selective for nuclear MAPKs in the hypertensive heart

Of the DUSPs regulating nuclear MAPKs, only DUSP1 protein expression was altered, where its expression was reduced in the acute (24 h) and in the adaptive (7 d) phases of AngII-induced hypertension (Figure 5.4C). This indicates the expression of nuclear DUSPs may be dependent on the model, and the phase of disease progression. Indeed, others have found decreased DUSP1 protein expression in a rat model of diabetic cardiomyopathy, whilst TAC promoted *Dusp1* mRNA expression in mice[321,433]. Although altered protein expression of DUSP2 and DUSP4 was not observed in NI-HF (Figure 5.2B), in SHRs (Figure 5.3B) and in AngII-induced hypertension (Figure 5.4C), the mRNA expression of *Dusp2* and *Dusp4* was elevated in the SHR model (Figure 5.3A) and in the acute AngII response (1 d) (Figure 5.4B), but was unchanged in human NI-HF (Figure 5.2A). DUSP2 has not previously been investigated in the heart; however, somewhat consistent with this project, previous studies found that elevated cardiac *Dusp4* mRNA expression occurred following TAC, and DUSP4 protein expression was elevated in human HF with idiopathic dilated cardiomyopathy[321,322]. This suggests DUSP4 expression may be promoted during cardiac remodelling. However, the lack of elevated DUSP2 and DUSP4 protein expression observed in the AngII and SHR models in this project, may be due to increased protein turnover[289], and suggests that at these stages of disease progression, in these models, DUSP2 and DUSP4 are unlikely to influence cardiac remodelling. Furthermore, as DUSP4 protein expression was elevated in human HF with idiopathic dilated cardiomyopathy[322], but was not found to be increased in human NI-HF (Figure 5.2B), and as DUSP1 expression was reduced in AngII-induced hypertension (Figure 5.4B-C), but not in the SHR model (Figure 5.3A), this indicates that the expression of DUSPs regulating nuclear MAPKs may reflect the particular pathophysiology of the underlying cause of HF or of the hypertensive model.

It is unclear whether the reduced DUSP1 protein expression in AngII-induced hypertension would influence cardiac remodelling, as although previous studies have indicated that the hearts of DUSP1-null mice appeared normal at baseline, the cardiac response to pro-hypertrophic stimuli in DUSP1 null mice was not investigated[321]. However, at baseline, in DUSP1/DUSP4-null mice ventricular dilatation and reduced survival was observed[321],

indicative of redundancy between DUSP1 and DUSP4. As DUSP4 protein expression was not reduced alongside DUSP1 in AngII-induced hypertension, it is unlikely that reduced DUSP1 expression alone would promote disease progression.

5.4.2.5. Conclusion

The acute response to hypertension is associated with reduced DUSP1 expression, selective for nuclear MAPKs. In the early phases of HHD progression, DUSP16, regulating p38-MAPK and JNK, is elevated, and may be a novel target to modulate cardiac remodelling processes. DUSPs targeting cytosolic ERK1/2 are altered as the disease progresses. Initially DUSP6 and DUSP7 expression is reduced, which previous studies indicate may be protective, promoting cardiac adaptation. As the disease progresses into the chronic phase, elevated DUSP6 expression may encourage cardiac decompensation and transition to HF. In HF, the protein expression of DUSP5 and DUSP8 were elevated. Previous studies indicate DUSP5 and DUSP8 may have opposing functions, with DUSP5 preventing fibrotic and hypertrophic remodelling, whilst DUSP8 may promote cardiac dysfunction by promoting eccentric remodelling and fibrosis. Overall, DUSP1 may support the acute adaptation to hypertension, whilst DUSP6 and 7 modulate the progression of disease. Finally, in HF, DUSP5 and DUSP8 influence the final outcome. A summary of cardiac DUSP protein expression throughout the progression of hypertensive heart disease, as modelled in the SHR and AngII-induced hypertensive models, and in end stage NI-HF patients is presented in Figure 5.14.

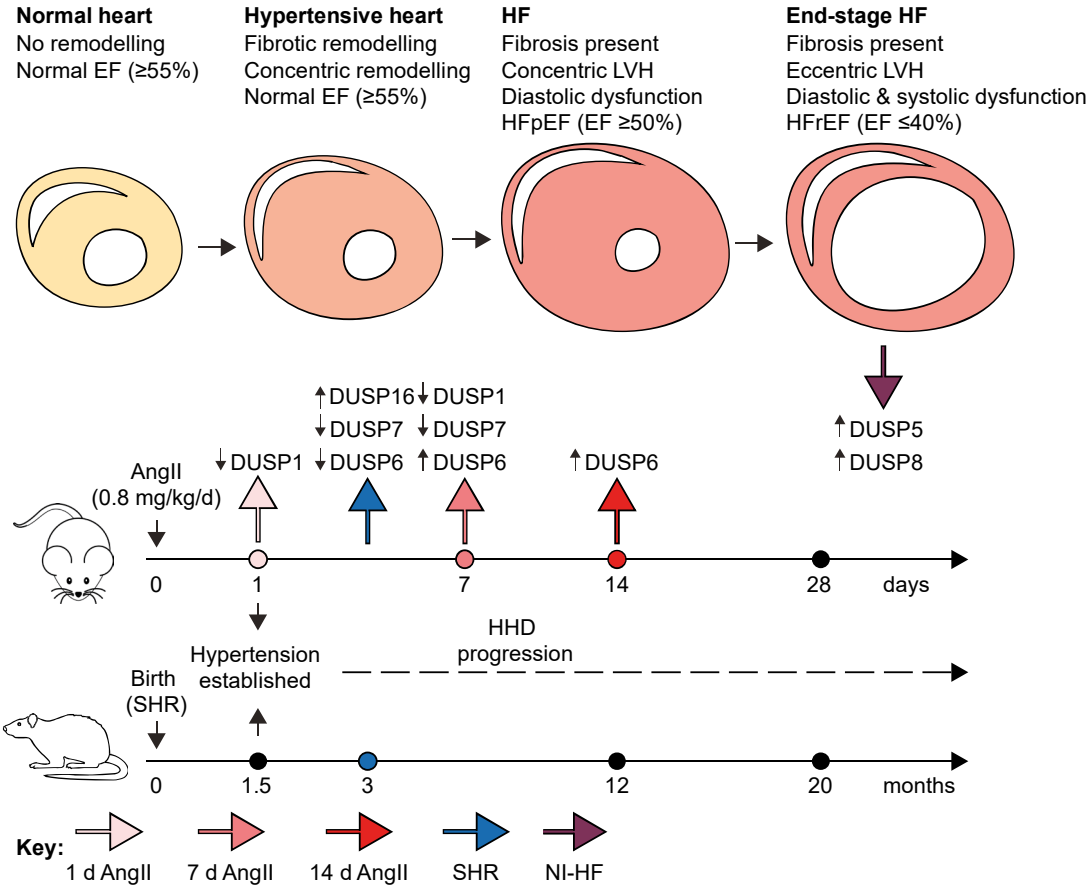

Figure 5.14. Timeline of cardiac remodelling and DUSP expression in HHD progression and NI-HF.

HHD is characterised by fibrotic remodelling and concentric LVH, whilst progression into HF results in eccentric remodelling and vessel dilatation. The corresponding phases of HHD progression in AngII mouse model and SHR rat model are displayed below, with open circles reflecting the timepoints used. The changes to cardiac DUSP expression observed in the hypertensive models and HF are also shown.

5.4.3. Cellular stressors cause cardiac cell-specific DUSP expression profiles

Through regulating MAPK dephosphorylation, DUSPs are key controllers of MAPK signalling. Here, this project demonstrated that DUSPs are rapidly transcribed in response to AngII and CD47 activation, and have identified key DUSPs involved in MAPK signal attenuation in cardiac ECs (DUSP1, DUSP5, DUSP8) and ECs (DUSP1, DUSP5, DUSP6 and DUSP16). In cardiac ECs, CD47 activation promoted the mRNA expression of *Dusp1* and *Dusp5* (Figure 5.5C), and *Dusp8* (Figure 5.11C), whilst AngII promoted the mRNA expression of *Dusp1* (Figure 5.6C). In the SVEC4-10 cell line, both CD47 activation and AngII promoted the mRNA expression of *Dusp1* (Figures 5.5A & 5.6A), and promoted the mRNA expression of *Dusp6* (Figures 5.8A & 5.9B), which was reflected in the protein expression following CD47 activation (Figures 5.8D). The protein expression of DUSP8 and DUSP16 (Figure 5.11D) was also increased following CD47 activation in the SVEC4-10 cell line. Similar to cardiac ECs and

SVEC4-10s, *DUSP1* mRNA expression was increased following CD47 activation in SGHEC-7s (Figure 5.5B), however *DUSP16* mRNA expression was reduced following CD47 activation (Figure 5.11B), and *DUSP9* mRNA expression was reduced in response to AngII (Figure 5.9B).

5.4.3.1. Implications of perturbed DUSP expression on EC function

DUSP1 and *DUSP5*, regulating nuclear MAPKs, were rapidly transcribed in cardiac ECs and EC cell lines. DUSP1 was rapidly transcribed in response to CD47 activation (Figure 5.5A-C) and AngII treatment (Figure 5.6A & C), whilst *DUSP5* mRNA expression was elevated following CD47 activation only (Figure 5.5A & C). In SVEC4-10s, the protein expression of DUSP5 was increased following CD47 activation, and the protein expression of DUSP1 may also have been significantly elevated had an additional replicate been carried out (Figure 5.5D). Others studies have also found that AngII promotes DUSP1 transcription in cardiac microvascular ECs[434], but there have been no studies investigating DUSP expression following CD47 activation.

In HUVECs, DUSP1 regulates p38-MAPK dephosphorylation and is found in both the nucleus and cytoplasm[435,436], whilst DUSP5 regulates nuclear ERK1/2. DUSP5 has been demonstrated to have the dual functions of dephosphorylating ERK1/2, and anchoring ERK1/2 to the nucleus, thus minimising the pool of cytoplasmic ERK1/2 available for activation[435,436]. Functionally, DUSP1 inhibits EC migration, reducing wound healing potential, without affecting proliferation or cell death[435,436]. As both CD47 activation and AngII treatment prevented wound closure in SVEC4-10s (Figure 4.9A-B), this effect may have been influenced by DUSP1 expression. Although DUSP5 has been proposed to inhibit EC proliferation and to promote cell death[435,436], cell proliferation and cell death was not altered following CD47 activation (Figures 4.9C & 4.10C-E), indicating DUSP5 is unlikely to promote these functions in response to CD47 activation.

Expression of DUSP6 in SVEC4-10s in response to CD47 activation (Figure 5.8A & D) and AngII treatment (Figure 5.9A) may be indicative of perturbed EC function. DUSP6 is known to be selective for ERK1/2, although it can inactivate both ERK1/2 and JNK in HUVECs[437], and is known to impair cardiac angiogenesis[326], promote endothelial inflammation[437], and disrupt eNOS transcription[438]. Indeed, impaired wound healing was observed in response to AngII and CD47 activation (Figure 4.9A-B). As this project found, in response to CD47 activation, *DUSP6* mRNA expression was elevated in SVEC4-10s (Figure 5.8A), but not in the SGHEC-7s (Figure 5.8B), a human cell line, this may indicate that increased DUSP6 expression may be a product of the species of the cell type used. Alternatively, the difference

may be due to the origin of the cell line, as the SGHEC-7 cell line is HUVEC in origin, whilst the SVEC4-10 cell line is lymphatic in origin.

Although p38-MAPK and JNK were activated in response to AngII and CD47 activation (Figures 4.1C & 4.2C) in cardiac ECs, it was only after CD47 activation (Figure 5.11A-D) that the expression of DUSPs regulating p38-MAPK and JNK were altered. *Dusp8* transcription was elevated in cardiac ECs (Figure 5.11C), and the protein expression of DUSP8 and DUSP16 were both elevated in SVEC4-10s (Figure 5.11D). There is limited research encompassing the function of DUSP8 and DUSP16 in ECs, although they have been studied in the context of cancers and the immune system. In colorectal carcinoma DUSP8 overexpression suppressed cell migration and proliferation[439], whilst DUSP8 expression in macrophages impaired migration and adhesion[440]. DUSP16 has been proposed to regulate VCAM-1 expression in ECs[441], whilst in cancer, DUSP16 overexpression promotes cell survival[442] and its silencing promotes cellular senescence[443]. Therefore, in SVEC4-10s, elevated DUSP16 expression may promote cell survival following CD47 activation, whilst in cardiac ECs, elevated DUSP8 may inhibit the migratory capacity and supress cardiac EC proliferation. However, these roles are yet to be assessed.

5.4.3.2. *Regulation of DUSPs by AngII and CD47 activation may prevent subsequent MAPK signalling*

This project demonstrated that DUSPs are rapidly expressed in response to CD47 activation or to AngII treatment, with *Dusp* mRNA expression elevated within 30 min in cardiac ECs, and with DUSP protein expression elevated by 2 h in the SVEC4-10 cell line. However, MAPK activation following CD47 activation or AngII treatment occurs within 5-15 min, and MAPK dephosphorylation occurs just as rapidly. As such, the changes to DUSP expression observed is unlikely to contribute to the initial attenuation of MAPK signalling. Rather, changes to DUSP expression may modulate subsequent MAPK signalling. This is of particular relevance to *in vivo* studies and the disease setting, where extracellular stimuli are potentially more stable than in cell culture conditions and are constantly being replenished through the blood supply or through cellular secretions. Therefore, as this project has identified DUSP1, DUSP5 and DUSP8 as key regulators of cardiac EC function, the role of these DUSPs in the vasculature should be investigated in an *in vivo* setting.

5.4.4. Limitations

There were a number of limitations to this project which should be noted. Firstly, in human tissue samples and in cell culture samples from human cells (SGHEC-7), there were issues with amplification when using the human DUSP5 primer, although this primer was obtained

from the literature[444]; primerblast indicated that this primer pair should amplify DUSP5 mRNA; and there are no known variants in region of the DUSP5 transcript the primer was designed from. However, as DUSPs are regulated by protein turnover, the protein expression, which could be successfully detected, is likely to be more relevant than the mRNA expression.

Secondly, DUSP9 protein expression was not investigated, as previously, DUSP9 expression was found to be limited in the heart[292,334]. However, *DUSP9* mRNA expression was detectable in cardiac tissue samples from NI-HF, was acutely increased at 24 h in AngII-induced hypertension and was reduced in the SHR model. In cardiac ECs, *DUSP9* mRNA expression was unchanged following stimuli. Furthermore, a recent study found DUSP9 protein expression was elevated following TAC, and in neonatal rat ventricular myocytes following AngII treatment[335], indicating that DUSP9 can be induced following stress. Based on these findings, DUSP9 would ideally have been investigated in these samples.

Finally, due to the closure of the Biological Research Facility at SGUL, and in the absence of another source of viable primary cardiac ECs, DUSP protein expression in response to AngII and CD47 activation could not be confirmed in cardiac ECs. However, in SVEC4-10s, DUSP protein expression was relatively concordant with the mRNA expression, and similar trends were observed between the DUSPs upregulated in cardiac ECs and in SVEC4-10s. Therefore, in cardiac ECs, the DUSP protein expression may align with the altered mRNA expression observed. However, *DUSP* mRNA expression was altered between EC cell lines from humans (SGHEC-7s) and mice (SVEC4-10). This may have been due to the difference in species, or in EC type, as the SGHEC-7 cell line is derived from HUVECs, whilst SVEC4-10s are lymphoid in origin. Therefore, if the difference is due to the species, the DUSPs identified in murine cardiac ECs may not be applicable to human cardiac ECs. However, due a lack of viable human cardiac microvascular ECs, *DUSP* mRNA expression could not be confirmed in the human setting.

5.4.5. Conclusion

The MAPKs are known modulators of cardiac remodelling and thus cardiac function. In NI-HF, ERK1/2 activation and p38-MAPK deactivation may promote survival by supporting cardiac function and preventing further exacerbations of cardiac function. However, MAPK activation was unchanged in hypertensive models. DUSPs may influence cardiac remodelling and disease progression in the hypertensive heart by modulating MAPK phosphorylation. As such, DUSP expression was investigated as dysregulated DUSPs may be potential targets to promote adaptive remodelling and prevent decompensation. This project found the acute response to hypertension may be governed by DUSP1, whilst DUSPs regulating cytosolic ERK1/2 (DUSP6 and DUSP7) have the potential to modulate disease progression. This project

identified a potential novel role for DUSP16 in the regulation of cardiac remodelling. In HF, the balance between cardio-protection and further adverse remodelling was governed by DUSP5 and DUSP8. The key DUSPs identified in HHD progression and NI-HF, i.e. DUSP1, DUSP5, DUSP6, DUSP8 and DUSP16, were also expressed in response to CD47 activation in ECs, and DUSP1, DUSP5 and DUSP8 were expressed in cardiac ECs. Previous studies indicate these DUSPs can modulate cellular function; however, whether DUSPs can modulate cellular function following CD47 activation is not known. Since this project found activation of MAPKs in ECs, which are established governors of cell function, this warrants further exploration. Through inhibition of DUSPs, CD47-mediated endothelial dysfunction and HHD progression may be ameliorated.

Chapter 6: Discussion and conclusion

This project demonstrated that TSP1, but not CD47, was upregulated in human NI-HF and in AngII-induced hypertension, and that activation of CD47 by TSP1 promoted phosphorylation of ERK1/2, p38-MAPK and JNK, and expression of NOX1 in cardiac ECs. In ECs, NOX1 expression was found to be associated with ROS production and impaired endothelial migration. This suggests that TSP1-CD47 signalling contributes to impaired angiogenesis in HHD by promoting NOX1 expression. Activation of CD47 by TSP1 and NOX1 upregulation have been associated with impaired endothelial function in other diseases, including pulmonary arterial hypertension (PAH), non-alcoholic steatohepatitis (NASH), and diabetic cardiomyopathy. Therefore, the implications of the results from this project focusing on the hypertensive heart and HF will be discussed in the context of the findings from studies using models of these other diseases.

6.1. Consequences of the CD47-TSP1-NOX1 axis on endothelial function

6.1.1. Activation of CD47 by TSP1 impairs endothelial function

This project identified that the activation of CD47 by TSP1 impairs endothelial migration. Consistent with this, previous studies have indicated that TSP1-null mice exhibit greater cardiac capillary density[147], whilst aged-CD47-null mice exhibit improved angiogenesis[378]. However, a previous study indicated that TSP1-CD47 signalling may impair angiogenesis by inducing HPAEC senescence via NOX1[175,402]. Despite this, this project did not find that EC proliferation was altered following TSP1-CD47 signalling, suggesting that impaired angiogenesis may occurs through an alternative mechanism in other cell types. However, as the SVEC4-10 cell line was used to determine endothelial proliferation following CD47 activation was created by transfection with the SV40 large T antigen, an oncoprotein which promotes cellular proliferation, the impact of CD47 activation in attenuating cellular proliferation may not have been observable. As such, in primary cardiac ECs activation of CD47 may well have impaired proliferation, indicating that these cells may have become senescent.

This project focused on the angiogenic functions of ECs (migration, proliferation and survival), as impaired cardiac angiogenesis can promote pathological hypertrophy[93,95,96], and therefore impaired angiogenesis may modulate cardiac hypertrophy in HHD. However, TSP1-CD47 signalling may also promote endothelial activation, and may be implicated in inflammation. Other studies have found that in ECs, activation of CD47 by TSP1 promoted the expression of the adhesion proteins, VCAM-1 and ICAM-1, which enhanced monocyte attachment[152], and inhibition of endothelial NO synthesis by TSP1 promoted phosphorylation of ICAM-1 by Src

which rapidly increased leukocyte adhesion[153,154]. In addition, as previous studies have indicated that VCAM1 expression can be regulated by MAPK activation[445,446], and here it is demonstrated that CD47 activation promotes MAPK activation, CD47 activation may regulate VCAM1 expression via the MAPKs. Furthermore, CD47 was found to promote neutrophil transmigration across cell monolayers[155], and blockade of CD47 with the anti-CD47 antibody, MIAP410, attenuated neutrophil infiltration into the livers of mice with NASH induced by an amylin liver NASH diet[447]. In addition, TSP1 deficiency reduced macrophage infiltration into the kidneys of mice with renal dysfunction induced by a high fat diet[448]. As HHD is associated with inflammatory cell infiltration[72], TSP1 and CD47 may also contribute to endothelial activation and immune cell infiltration in the hypertensive heart.

Furthermore, TSP1-CD47 signalling has been implicated in endothelial dysfunction, although this project did not investigate it. In PAH induced by hypoxia, activation of CD47 by TSP1 promoted the production of eNOS-derived superoxide, a key step in initiating the disease[353]. Furthermore, distal pulmonary arteries from PH patients had improved sensitivity to acetylcholine-induced vasodilation following CD47 inhibition[449], and exposure to TSP1 in normal distal pulmonary arteries impaired sodium nitroprusside-induced vasodilation, whilst blockade of CD47 restored vasodilation in the presence of TSP1[449]. As TSP1-CD47 signalling contributes to endothelial dysfunction in the pulmonary vasculature of PAH, it may also contribute to endothelial dysfunction in the cardiac vasculature in HHD. As endothelial dysfunction is characterised by reduced NO production, endothelial dysfunction may promote cardiac dysfunction, since eNOS-derived NO: enhances myocardial relaxation; enhances LV compliance; mediates the positive inotropic effect in response to increased preload; and limits mitochondrial respiration to improve mechanical efficiency[97]. Overall, TSP1-CD47 signalling may cause endothelial dysfunction in HHD, and the associated reduced NO production may impair cardiac myocyte function.

6.1.2. Upregulation of NOX1 alters endothelial function

Although this project found that the TSP1-CD47-NOX1 axis impaired EC migration, other studies found NOX1 promoted EC proliferation or induced senescence, and could regulate the expression of vascular adhesion molecules. In a model of PAH, NOX1 promoted HPAEC proliferation in response to hypoxia[257], whilst NOX1 promoted HPAEC senescence in response to CD47 activation[175]. Interestingly, PAH patients and mice with PAH induced by hypoxia exhibit increased expression of TSP1 and CD47 in the lung tissue and in the pulmonary arteries[353,449], although TSP1-CD47 signalling has not been identified as a cause of NOX1 upregulation in PAH. NOX1 may also regulate endothelial activation by promoting the expression of vascular adhesion molecules. Mice with diabetes induced by a high fat/high sucrose diet and streptozotocin, exhibited enhanced VCAM-1 and ICAM-1 protein expression in myocardial vessels, which was attenuated in NOX1-null mice[450]. As such, elevated NOX1

expression may promote adhesion protein expression in HHD, which could contribute to cardiac inflammation in HHD.

6.2. DUSP dysregulation in other cardiovascular diseases

This project identified that TSP1-CD47 signalling promoted MAPK activation and DUSP expression in cardiac ECs, whilst cardiac DUSPs were dysregulated in NI-HF and in hypertensive rodent models. Therefore, DUSPs may also be implicated in other diseases where there is evidence of CD47 activation by TSP1 and MAPK activation. However, there have been few studies investigating DUSPs in these diseases. In PAH, pulmonary vessels exhibit activation of ERK1/2 and p38-MAPK[451], and DUSP1 and DUSP5 have both been implicated in PAH. DUSP5 was protective against VSMC proliferation and prevented the development of pulmonary hypertension in AngII-infused mice[452], whilst variants of DUSP1 and DUSP5 are associated with the development of PAH in patients with bronchopulmonary dysplasia[453]. In obese patients with NASH and non-alcoholic fatty liver disease, JNK and p38-MAPK activation has been observed[454–456]. Furthermore, in high fat diet-induced NASH, DUSP9 was identified as a key suppressor of p38-MAPK and JNK activation, acting by preventing ASK1 phosphorylation. By preventing the activation of stress-regulated MAPKs, DUSP9 prevented inflammation and fibrosis and also limited steatosis[457]. Taken together these studies indicate that DUSPs may also be implicated in tissue remodelling in other diseases characterised by TSP1-CD47 signalling.

6.3. Therapeutics to target the TSP1-CD47-NOX1 and TSP1-CD47-MAPK/DUSP axis in HHD

As this project found cardiac TSP1 upregulation in HF and AngII-induced hypertension and demonstrated that TSP1-CD47 signalling limits endothelial migration, it can be concluded that cardiac angiogenesis may be impaired in hypertensive heart disease. Previous studies have indicated that reduced cardiac vessel density has been implicated in pathological cardiac remodelling[93,95,96]; improving the angiogenic function of ECs by inhibiting the TSP1-CD47-NOX1 axis may, therefore, limit pathological cardiac remodelling.

6.3.1. Blockade of CD47

Although this project found that activation of CD47 by TSP1 impairs endothelial migration *in vitro*, it is not known whether TSP1-CD47 signalling impairs angiogenesis *in vivo*, however angiogenesis was improved in aged-CD47-null mice compared with aged wild-type mice[378]. If activation of CD47 by TSP1 does impair angiogenesis in the hypertensive heart in HHD, then blockade of CD47 may improve the angiogenic function of the cardiac endothelium, which may in turn ameliorate pathological cardiac remodelling.

The anti-CD47 antibody, MIAP410, has been used to investigate the role of CD47 in both inflammation and fibrosis in preclinical models of NASH and pulmonary fibrosis, and also in plaque development in models of atherosclerosis[354,447,458,459]. However, antibodies against CD47 block both the CD47-SIRPα interaction and the CD47-TSP1 interaction. Therefore, novel peptides have been identified to selectively block the TSP1-CD47 interaction. The recombinant human CD47 peptide, rh-CD47p, which acts as a decoy receptor protein to bind to TSP1 preventing it from interacting with endogenous CD47, restored TSP1-dependent endothelial dysfunction[460]. In addition, the TAX2 peptide, which is a peptide derived from CD47 and which selectively inhibits the CD47 activation by TSP1, has been recently developed, and was shown to limit arterial thrombosis[461]. These peptides, which selectively inhibit the TSP1-CD47 interaction, may have therapeutic potential in hypertensive pre-clinical models.

Several monoclonal antibodies have been developed against CD47 for the treatment of cancer, where CD47 is frequently upregulated. In cancer, CD47 interacts with macrophage SIRPα to prevent cellular clearance; therefore, antibodies targeting CD47 prevent its interaction with SIRPα which facilitates the clearance of cancer cells by the immune system[131]. This is an effective strategy, and several monoclonal anti-CD47 antibodies are in phase I and II clinical trials for the treatment of multiple cancers[462]. If these trials are successful, and if future studies indicate that knockdown or blockade of CD47 signalling is beneficial in HHD, these antibodies may be a viable option to prevent the progression of HHD into HF. It must, however, be considered that the interactions of TSP1 with both CD47 and SIPRα would be attenuated using these therapeutics.

6.3.2. Inhibition of NOX1

This project demonstrated that the TSP1-CD47-NOX1 axis impaired EC migration, a key function required for angiogenesis, and found localisation of TSP1 and NOX1 to cardiac vessels in HHD, which may be indicative of impaired angiogenesis in the hypertensive heart. Although these results suggest NOX1 inhibition may improve cardiac angiogenesis, no study has directly supported this. One study found that the NOX1/4 inhibitor, setanaxib, reduced the angiogenic potential of mesenteric arteries in a model of portal hypertension[463], and treatment of wild-type lung ECs with GKT13690, a NOX1/4 inhibitor, reduced EC migration and tube formation[419]. However, in these models, NOX1/4 derived ROS promoted cardiac angiogenesis, whilst this project demonstrated that NOX1 induced by TSP1-CD47 signalling impaired EC migration. Therefore, based upon the results of this project, NOX1 inhibition may improve angiogenesis in the hypertensive heart. Furthermore, the TSP1-CD47-NOX1 axis has previously been implicated in promoting endothelial senescence, and it has been suggested that by ameliorating endothelial senescence, NOX1 inhibition may restore the

angiogenic potential of the endothelium[175,420]. Consequently, inhibition of NOX1 may improve cardiac angiogenesis if endothelial senescence occurs in the hypertensive heart.

Although impaired cardiac angiogenesis has been implicated as a cause of adverse cardiac remodelling[93,95,96], NOX1 may also mediate cardiac fibrosis and hypertrophy. NOX1 promoted the expression of pro-fibrotic genes in isolated cardiac fibroblasts[464] and contributed to cardiac hypertrophy in SHRs and in a diabetic mouse model[450,465]. Furthermore, the dual NOX1/4 inhibitor setanaxib has been demonstrated to limit cardiac hypertrophy and cardiac fibrosis in SHRs and in experimental hypertension induced by abdominal artery coarctation[465,466]. However, some studies suggest that the anti-fibrotic effect of setanaxib is mediated through NOX4 inhibition[266,467], whilst others indicate it through NOX1 inhibition[468]. Despite this, the selective NOX1 inhibitor, ML171, attenuated cardiac fibrosis in rats with diabetic cardiomyopathy[464]. Therefore, although it is unclear whether NOX1 inhibition may ameliorate impaired angiogenesis, NOX1 inhibition may limit cardiac fibrosis and hypertrophy in HHD. Finally, as setanaxib is currently in a phase II/III clinical trial for the treatment of primary biliary cholangitis and liver stiffness[369] and is in a phase II clinical trial for the treatment of idiopathic pulmonary fibrosis[370], it may be an ideal candidate drug for the treatment of HHD if proved effective in preclinical studies.

6.3.3. Inhibition of DUSPs

This project identified that the expression of DUSPs was altered in NI-HF, in hypertensive rodents and in cardiac ECs, following CD47 activation. Although the expression of DUSPs targeting p38-MAPK and JNK was altered, these DUSPs are likely to be beneficial in the hypertensive heart by attenuating the activation of stress-regulated kinases. As such, only DUSPs targeting ERK1/2 are candidates for inhibition, since attenuation of ERK1/2 signalling may prevent adaptive hypertrophy, leading to cardiac decompensation. At present, the only selective DUSP inhibitor is BCI, which targets both DUSP1 and DUSP6. Although a previous study found that BCI improved cardiac function following cardiac injury in zebrafish, this protection was due to enhanced cardiac myocyte proliferation in adult zebrafish[326]. As such, the use of BCI in adult mammals may not give the same level of protection as the myocytes are already terminally differentiated, although, some protection may be conferred as in zebrafish treated with BCI, angiogenesis was promoted and fibrosis was reduced following cardiac injury[326]. Furthermore, as DUSP6 protein expression was elevated in the adaptive and chronic phase of AngII-induced hypertension, inhibition of DUSP6 at this point of disease progression may be beneficial.

The lack of available DUSP inhibitors is, in part, because previously the DUSPs were considered un-targetable. This is due to their overlapping substrate specificity, shallow and

feature-poor active sites, redox sensitivity, and difficulties testing the efficacy of small molecules, as *in vitro* assay do not always replicate the activity of these enzymes in their biological context[469]. However, there has been renewed interest in DUSPs, in part due to the recognition that their expression levels are widely altered in cancer. DUSPs have been implicated in tumorigenesis for a wide range of cancers, and in resistance to anti-cancer therapeutics[470]. As such, DUSP inhibitors have begun to be developed and optimised. Sanguinarine and NU-126 were shown to inhibit DUSP1 but have poor cellular permeability and a lack of selectivity. BCI analogs have also been identified, BCI-214[471] and BCI-215[469]. In addition, one group has made progress in identifying DUSP5 inhibitors, although the effects of the potential compounds are yet to be validated *in vitro* or *in vivo*[472], and DUSP16 inhibitors have been identified through *in silico* screens, but may also inhibit DUSP10 and DUSP25[473]. If selective inhibitors are successfully developed for DUSPs targeting ERK1/2, these may be of use for the treatment of HHD, as this project identified altered expression of DUSPs which regulate ERK1/2 throughout the progression of the disease in rodents, and in NI-HF patients.

6.4. Limitations

There are several limitations associated with this project. Firstly, there were some discrepancies between the hypertensive rodent models; TSP1 was upregulated in mice with AngII-induced hypertension, whilst CD47 was upregulated in SHRs, and the expression levels of DUSP1, DUSP6 and DUSP16 were found to be altered between the models. As the SHRs were only investigated at one timepoint, it is unclear whether these differences were due to the stage of disease progression or due to differences between the models themselves. Furthermore, although NOX1 upregulation was identified in cardiac tissue from NI-HF patients, upregulation of NOX1 was not observed in AngII-induced heart failure, nor in the SHR model. It is possible that NOX1 upregulation throughout the myocardium only occurs in HF, and prior to the development of HF, upregulation of endothelial NOX1 may contribute to impaired EC function, but may not be expressed to detectable levels in cardiac tissue. Alternatively, the lack of NOX1 upregulation observed in experimental hypertensive models may have been due to the age of the rodents. Previously, as NOX1 upregulation occurs in aged vasculature[175,420], the process of ageing may be a prerequisite for the induction of NOX1 expression in the cardiac endothelium. Indeed, HFpEF tends to affect older individuals, whilst hypertension onset occurs in middle age, with early onset hypertension starting before 55 years[474]. Furthermore, the NI-HF cohort had a median age of 60.5 years, whereas the rodents were in early adulthood. Therefore, ageing may promote endothelial NOX1-derived ROS in the hearts of hypertensive animals, which may contribute to disease progression in older animals.

In addition, the sex of the animals used and that of the NI-HF cohort was a limitation for this project, as endogenous oestrogens lower the risk of cardiovascular disease in women of reproductive age[475]. As such, the use of male mice in this project may not replicate what occurs

in females, and, although the NI-HF cohort contained both male and female patients, the power was not sufficient to determine whether there was a significant difference in gene/protein expression between male and female individuals. However, female rats were included in the SHR study to give a response typical of both sexes for TSP1, CD47 and NOX1 expression. Despite this, MAPK activation and DUSP expression was not determined in female SHRs, since tissue was taken during different phases of the oestrous cycle, where ERK1/2 activation is known to oscillate[476].

Another limitation was that several findings observed in EC cell lines could not be confirmed in primary cardiac ECs, due to the closure of the Biological Research Facility at SGUL which prevented further cellular isolations from mouse hearts. In addition, the findings of this project generated using mouse cardiac ECs, could not be confirmed in human cardiac cells, due to a lack of lack of viable human cardiac ECs available.

Finally, this work has investigated the TSP1-CD47 axis in isolated cardiac ECs, cardiac myocytes, and cardiac fibroblasts, with functional studies undertaken in cardiac ECs. However, the responses of these cell types *in vivo* and *in vitro* may differ due to loss of paracrine communication between different cardiac cell types *in vitro*, as paracrine communication may contribute to the overall outcome by modulating the intracellular signalling networks.

6.5. Future Work

As this project identified elevated cardiac TSP1 expression in NI-HF and in AngII-induced hypertension, and also found activation of CD47 by TSP1 impaired endothelial migration, cardiac angiogenesis may be impaired in HHD. Indeed, previous studies have found that CD47-TSP1 signalling perturbs angiogenesis[134,402], and furthermore, TSP1-CD47 signalling can promote fibrosis[350], cardiac myocyte hypertrophy[114] and can contribute to endothelial dysfunction[353], and inflammatory cell infiltration[152,155]. Therefore, the role of TSP1-CD47 signalling should be investigated in the hearts of hypertensive rodent models to determine whether targeting the TSP1-CD47 axis is a viable therapeutic strategy for ameliorating cardiac endothelial function and cardiac remodelling in HHD. Strategies to determine the role of TSP1-CD47 signalling in hypertensive rodent models include: infusion with the 7N3 peptide; attenuation of CD47 activation using anti-CD47 antibodies; or the use of the TAX2 or rh-CD47p peptides, which selectively inhibit the CD47-TSP1 interaction. However, in AngII-induced hypertension, TSP1 expression was only upregulated in the adaptive phase, indicating that inhibition of the TSP1-CD47 interaction may only effectively ameliorate cardiac remodelling in certain phases of the disease, potentially once inflammation has occurred in the acute phase, but coinciding with fibrotic deposition in the adaptive phase[72].

Although this project demonstrated that NOX1 was upregulated in cardiac ECs, where it impaired endothelial migration, whether NOX1 impairs angiogenesis in the hypertensive heart should be confirmed. It should also be determined whether NOX1 inhibition is an effective therapeutic strategy for HHD. As such, the effect of NOX1 inhibition on cardiac function and remodelling in hypertensive models should be investigated. To delineate the role of endothelial NOX1 in the hypertensive heart, endothelial specific NOX1-null mice could be used. In addition, as women of a reproductive age have a lower risk of cardiovascular disease, which is in part due to oestrogen limiting oxidative stress[475,477], whether this occurs through a NOX1-mediated mechanism should be investigated, to identify whether NOX1 inhibition has the same effects in females and in males, and in females pre-menopause and post-menopause.

Previous studies which have elucidated the effects of DUSPs on cardiac remodelling processes typically involve genetic manipulation of DUSP expression. However, the use of such genetically modified animals has not been investigated in hypertensive pre-clinical models, and as such, the role of DUSPs in HHD is unclear. As this project identified upregulation of cardiac DUSP6 and DUSP16 in hypertensive rodent models, their role should be studied in the hypertensive heart. Since DUSP16 has not previously been studied in any cardiac model, its role in the hypertensive heart should be ascertained using genetic manipulation. DUSP6 has previously been characterised in cardiac remodelling processes and can be inhibited with the DUSP1/6 inhibitor, BCI. As DUSP6 negatively regulates ERK1/2 activation, inhibition of DUSP6 may lead to prolonged ERK1/2 signalling which may ameliorate cardiac remodelling processes in HHD. As such, the effect of BCI on cardiac remodelling should be investigated in hypertensive models.

6.6. Conclusion

In summary, this project identified TSP1 upregulation in the hearts of NI-HF patients and AngII-induced hypertension. This project identified activation of CD47 by TSP1 as a novel instigator of impaired cardiac endothelial function, which is mediated by NOX1. Furthermore, it was identified, for the first time that activation of CD47 by TSP1 promotes: phosphorylation of ERK1/2, p38-MAPK and JNK in cardiac ECs; phosphorylation of pro-growth ERK1/2 in cardiac myocytes; and phosphorylation of stress-regulated kinases in cardiac fibroblasts. Furthermore, this project identified altered regulation of cardiac DUSPs in NI-HF and in rodent models of hypertension, and CD47-TSP1 signalling was identified as a novel regulator of DUSP expression. From these results, it is proposed that targeting the TSP1-CD47 signalling axis through blockade of CD47, inhibition of NOX1, or inhibition of DUSP6, may be novel

strategies to ameliorate impaired cardiac endothelial function and cardiac remodelling in HHD, which may delay progression to HF.

References

1. Roth, G. A. *et al.* Global Burden of Cardiovascular Diseases and Risk Factors, 1990-2019: Update From the GBD 2019 Study. *J. Am. Coll. Cardiol.* **76**, 2982–3021 (2020).
2. Bragazzi, N. L. *et al.* Burden of heart failure and underlying causes in 195 countries and territories from 1990 to 2017. *Eur. J. Prev. Cardiol.* **28**, 1682–1690 (2021).
3. Rapsomaniki, E. *et al.* Blood pressure and incidence of twelve cardiovascular diseases: Lifetime risks, healthy life-years lost, and age-specific associations in 1·25 million people. *Lancet* **383**, 1899–1911 (2014).
4. Zhou, B. *et al.* Worldwide trends in hypertension prevalence and progress in treatment and control from 1990 to 2019: a pooled analysis of 1201 population-representative studies with 104 million participants. *Lancet* **398**, 957–980 (2021).
5. Mayet, J. & Hughes, A. Cardiac and vascular pathophysiology in hypertension. *Heart* **89**, 1104–1109 (2003).
6. Drazner, M. H. The progression of hypertensive heart disease. *Circulation* **123**, 327–334 (2011).
7. Tsuda, T. Clinical assessment of ventricular wall stress in understanding compensatory hypertrophic response and maladaptive ventricular remodeling. *J. Cardiovasc. Dev. Dis.* **8**, (2021).
8. Westaby, J. D. *et al.* Characterisation of hypertensive heart disease: pathological insights from a sudden cardiac death cohort to inform clinical practice. *J. Hum. Hypertens.* **36**, 246–253 (2022).
9. Berk, B. C., Fujiwara, K. & Lehoux, S. ECM remodeling in hypertensive heart disease. *J. Clin. Invest.* **117**, 568 (2007).
10. Millane, T., Jackson, G., Gibbs, C. R. & Lip, G. Y. H. ABC of heart failure. Acute and chronic management strategies. *Br. Med. J.* **320**, 559–562 (2000).
11. Dunlay, S. M., Roger, V. L. & Redfield, M. M. Epidemiology of heart failure with preserved ejection fraction. *Nat. Rev. Cardiol.* **14**, 591–602 (2017).
12. Vedin, O. *et al.* Significance of Ischemic Heart Disease in Patients with Heart Failure and Preserved, Midrange, and Reduced Ejection Fraction: A Nationwide Cohort Study. *Circ. Hear. Fail.* **10**, 1–9 (2017).
13. Zakeri, R. & Cowie, M. R. Heart failure with preserved ejection fraction: Controversies, challenges and future directions. *Heart* **104**, 377–384 (2018).
14. Kjeldsen, S. E. *et al.* Medical Therapies for Heart Failure With Preserved Ejection Fraction. *Hypertension* **75**, 23–32 (2020).
15. Patel, S., Rauf, A., Khan, H. & Abu-Izneid, T. Renin-angiotensin-aldosterone (RAAS):

The ubiquitous system for homeostasis and pathologies. *Biomed. Pharmacother.* **94**, 317–325 (2017).

16. Taylor, C. J., Moore, J. & O'Flynn, N. Diagnosis and management of chronic heart failure: NICE guideline update 2018. *Br. J. Gen. Pract.* **69**, 265–266 (2019).

17. Andersen, M. J. & Borlaug, B. A. Heart failure with preserved ejection fraction: Current understandings and challenges. *Curr. Cardiol. Rep.* **16**, (2014).

18. Pfeffer, M. A. *et al.* Regional variation in patients and outcomes in the treatment of preserved cardiac function heart failure with an aldosterone antagonist (TOPCAT) trial. *Circulation* **131**, 34–42 (2015).

19. Anker, S. D. *et al.* Empagliflozin in Heart Failure with a Preserved Ejection Fraction. *N. Engl. J. Med.* **385**, 1451–1461 (2021).

20. Tackling, G. & Borhade, M. B. Hypertensive Heart Disease. *StatPearls [Internet]* https://www.ncbi.nlm.nih.gov/books/NBK539800/ (2021).

21. Sheppard, J. P., Martin, U. & McManus, R. J. Diagnosis and management of resistant hypertension. *Heart* **103**, 1295–1302 (2017).

22. González, A. *et al.* Myocardial remodeling in hypertension toward a new view of hypertensive heart disease. *Hypertension* **72**, 549–558 (2018).

23. Nauta, J. F. *et al.* Concentric vs. eccentric remodelling in heart failure with reduced ejection fraction: clinical characteristics, pathophysiology and response to treatment. *Eur. J. Heart Fail.* **22**, 1147–1155 (2020).

24. Cuspidi, C., Sala, C., Negri, F., Mancia, G. & Morganti, A. Prevalence of left-ventricular hypertrophy in hypertension: An updated review of echocardiographic studies. *J. Hum. Hypertens.* **26**, 343–349 (2012).

25. Rodrigues, J. C. L. *et al.* Comprehensive characterisation of hypertensive heart disease left ventricular phenotypes. *Heart* **102**, 1671–1679 (2016).

26. Drazner, M. H. *et al.* Increased left ventricular mass is a risk factor for the development of a depressed left ventricular ejection fraction within five years: The Cardiovascular Health Study. *J. Am. Coll. Cardiol.* **43**, 2207–2215 (2004).

27. Rame, J. E. *et al.* Development of a depressed left ventricular ejection fraction in patients with left ventricular hypertrophy and a normal ejection fraction. *Am. J. Cardiol.* **93**, 234–237 (2004).

28. Picariello, C. *et al.* The impact of hypertension on patients with acute coronary syndromes. *Int. J. Hypertens.* **2011**, 563657 (2011).

29. Shah, A. Ventricular Remodeling in Heart Failure with Preserved Ejection Fraction. *Curr. Heart Fail. Rep.* **10**, 341–349 (2013).

30. Kong, P., Christia, P. & Frangogiannis, N. G. The Pathogenesis of Cardiac Fibrosis. *Cell. Mol. Life Sci.* **71**, 549–574 (2014).

31. Schultz-Cherry, S. *et al.* Regulation of transforming growth factor-β activation by discrete sequences of thrombospondin 1. *J. Biol. Chem.* **270**, 7304–7310 (1995).

32. Yu, Q. & Stamenkovic, I. Cell surface-localized matrix metalloproteinase-9 proteolytically activates TGF-β and promotes tumor invasion and angiogenesis. *Genes Dev.* **14**, 163–176 (2000).

33. Wang, M. *et al.* Matrix metalloproteinase 2 activation of Transforming Growth Factor-β1 (TGF-β1) and TGF-β1-type II receptor signaling within the aged arterial wall. *Arterioscler. Thromb. Vasc. Biol.* **26**, 1503–1509 (2006).

34. Mu, D. *et al.* The integrin αvβ8 mediates epithelial homeostasis through MT1-MMP-dependent activation of TGF-β1. *J. Cell Biol.* **157**, 493–507 (2002).

35. Munger, J. S. *et al.* The integrin αvβ6 binds and activates latent TGFβ1: A mechanism for regulating pulmonary inflammation and fibrosis. *Cell* **96**, 319–328 (1999).

36. Liu, R. M. & Desai, L. P. Reciprocal regulation of TGF-β and reactive oxygen species: A perverse cycle for fibrosis. *Redox Biol.* **6**, 565–577 (2015).

37. Khalil, H. *et al.* Fibroblast-specific TGF-β-Smad2/3 signaling underlies cardiac fibrosis. *J. Clin. Invest.* **127**, 3770–3783 (2017).

38. Naugle, J. E. *et al.* Type VI collagen induces cardiac myofibroblast differentiation: Implications for postinfarction remodeling. *Am. J. Physiol. Hear. Circ. Physiol.* **290**, H323–H330 (2006).

39. Murphy-Ullrich, J. E. & Suto, M. J. Thrombospondin-1 regulation of latent TGF-β activation: A therapeutic target for fibrotic disease. *Matrix Biol.* **68**–**69**, 28–43 (2018).

40. Oka, T. *et al.* Genetic manipulation of periostin expression reveals a role in cardiac hypertrophy and ventricular remodeling. *Circ. Res.* **101**, 313–321 (2007).

41. Valiente-Alandi, I. *et al.* Inhibiting fibronectin attenuates fibrosis and improves cardiac function in a model of heart failure. *Circulation* **138**, 1236–1252 (2018).

42. Paten, J. A. *et al.* Molecular Interactions between Collagen and Fibronectin: A Reciprocal Relationship that Regulates De Novo Fibrillogenesis. *Chem* **5**, 2126–2145 (2019).

43. González, A., Schelbert, E. B., Díez, J. & Butler, J. Myocardial Interstitial Fibrosis in Heart Failure: Biological and Translational Perspectives. *J. Am. Coll. Cardiol.* **71**, 1696–1706 (2018).

44. Giannandrea, M. & Parks, W. C. Diverse functions of matrix metalloproteinases during fibrosis. *Dis. Model. Mech.* **7**, 193–203 (2014).

45. Bujak, M. *et al.* Interleukin-1 receptor type I signaling critically regulates infarct healing and cardiac remodeling. *Am. J. Pathol.* **173**, 57–67 (2008).

46. Siwik, D. A., Pagano, P. J. & Colucci, W. S. Oxidative stress regulates collagen synthesis and matrix metalloproteinase activity in cardiac fibroblasts. *Am. J. Physiol. Cell Physiol.* **280**, 53–60 (2001).

47. Brower, G. L. *et al.* The relationship between myocardial extracellular matrix remodeling and ventricular function. *Eur. J. Cardio-thoracic Surg.* **30**, 604–610 (2006).

48. McLenachan, J. M. & Dargie, H. J. Ventricular arrhythmias in hypertensive left ventricular hypertrophy. *Am. J. Hypertens.* **3**, 735–740 (1990).

49. Harris, P. & Lysitsas, D. Ventricular arrhythmias and sudden cardiac death. *BJA Educ.* **16**, 221–229 (2016).

50. Rockey, D. C., Bell, P. D. & Hill, J. A. Fibrosis — A Common Pathway to Organ Injury and Failure. *N. Engl. J. Med.* **372**, 1138–1149 (2015).

51. Dai, Z., Aoki, T., Fukumoto, Y. & Shimokawa, H. Coronary perivascular fibrosis is associated with impairment of coronary blood flow in patients with non-ischemic heart failure. *J. Cardiol.* **60**, 416–421 (2012).

52. Gkontra, P. *et al.* Deciphering microvascular changes after myocardial infarction through 3D fully automated image analysis. *Sci. Rep.* **8**, 1854 (2018).

53. Griendling, K. K. *et al.* Oxidative Stress and Hypertension. *Circ. Res.* **128**, 993–1020 (2021).

54. Giles, T. D., Sander, G. E., Nossaman, B. D. & Kadowitz, P. J. Impaired Vasodilation in the Pathogenesis of Hypertension: Focus on Nitric Oxide, Endothelial-Derived Hyperpolarizing Factors, and Prostaglandins. *J. Clin. Hypertens.* **14**, 198–205 (2012).

55. Segers, V. F. M., Brutsaert, D. L. & De Keulenaer, G. W. Cardiac remodeling: Endothelial cells have more to say than just NO. *Front. Physiol.* **9**, 382 (2018).

56. Viazzi, F. *et al.* Vascular permeability, blood pressure, and organ damage in primary hypertension. *Hypertens. Res.* **31**, 873–879 (2008).

57. Theuer, J. *et al.* Angiotensin II induced inflammation in the kidney and in the heart of double transgenic rats. **2**, 3 (2002).

58. Yoshida, K. *et al.* Excess Aldosterone under Normal Salt Diet Induces Cardiac Hypertrophy and Infiltration via Oxidative Stress. **28**, 447–455 (2005).

59. Liu, X., Shi, G. P. & Guo, J. Innate Immune Cells in Pressure Overload-Induced Cardiac Hypertrophy and Remodeling. *Front. Cell Dev. Biol.* **9**, 659666 (2021).

60. Shinde, A. V. & Frangogiannis, N. G. Mechanisms of Fibroblast Activation in the

Remodeling Myocardium. *Curr. Pathobiol. Rep.* **5**, 145–152 (2017).

61. Abelanet, A. *et al.* Increased Capillary Permeability in Heart Induces Diastolic Dysfunction Independently of Inflammation, Fibrosis, or Cardiomyocyte Dysfunction. *Arterioscler. Thromb. Vasc. Biol.* **42**, 745–763 (2022).

62. Ghigo, A., Franco, I., Morello, F. & Hirsch, E. Myocyte signalling in leucocyte recruitment to the heart. *Cardiovasc. Res.* **102**, 270–280 (2014).

63. Oldfield, C. J., Duhamel, T. A. & Dhalla, N. S. Mechanisms for the transition from physiological to pathological cardiac hypertrophy. *Can. J. Physiol. Pharmacol.* **98**, 74–84 (2020).

64. Brown, L. S. *et al.* Pericytes and neurovascular function in the healthy and diseased brain. *Front. Cell. Neurosci.* **13**, 282 (2019).

65. Afsar, B. *et al.* Capillary rarefaction from the kidney point of view. *Clin. Kidney J.* **11**, 295–301 (2018).

66. Serné, E. H. *et al.* Impaired skin capillary recruitment in essential hypertension is caused by both functional and structural capillary rarefaction. *Hypertension* **38**, 238–242 (2001).

67. Triantafyllou, A. *et al.* Capillary Rarefaction as an Index for the Microvascular Assessment of Hypertensive Patients. *Curr. Hypertens. Rep.* **17**, (2015).

68. Camici, P. G., Tschöpe, C., Di Carli, M. F., Rimoldi, O. & Van Linthout, S. Coronary microvascular dysfunction in hypertrophy and heart failure. *Cardiovasc. Res.* **116**, 806–816 (2020).

69. Mensah, G. A. Hypertension and target organ damage: Don't believe everything you think. *Ethn. Dis.* **26**, 275–278 (2016).

70. Reaven, G. M., Lithell, H. & Landsberg, L. Hypertension and Associated Metabolic Abnormalities — The Role of Insulin Resistance and the Sympathoadrenal System. *N. Engl. J. Med.* **334**, 374–381 (1996).

71. Lerman, L. O. *et al.* Animal Models of Hypertension: A Scientific Statement From the American Heart Association. *Hypertension* **73**, e87–e120 (2019).

72. Cooper, S. T. E. *et al.* Of Mouse and Man : Cross-Species Characterization of Hypertensive Cardiac Remodeling. *Int. J. Mol. Sci.* **23**, 7709 (2022).

73. Doris, P. A. Genetics of hypertension: an assessment of progress in the spontaneously hypertensive rat. *Physiol. Genomics* **49**, 617 (2017).

74. Reckelhoff, J. F., Yanes Cardozo, L. L. & Fortepiani, M. L. A. *Chapter 52 - Models of Hypertension in Aging*. *Conn's Handbook of Models for Human Aging* (Academic Press, 2018).

75. Soesanto, W. *et al.* Mammalian target of rapamycin is a critical regulator of cardiac hypertrophy in spontaneously hypertensive rats. *Hypertension* **54**, 1321–1327 (2009).

76. Brooks, W. W., Shen, S. S., Conrad, C. H., Goldstein, R. H. & Bing, O. H. L. Transition from compensated hypertrophy to systolic heart failure in the spontaneously hypertensive rat: Structure, function, and transcript analysis. *Genomics* **95**, 84–92 (2010).

77. Herrmann, H. J., Fiedler, U. & Blödner, R. Pathogenesis of myocardial fibrosis in spontaneously hypertensive rats (SHR). *Eur. Heart J.* **16**, 243–252 (1995).

78. Conrad, C. H. *et al.* Myocardial Fibrosis and Stiffness With Hypertrophy and Heart Failure in the Spontaneously Hypertensive Rat. *Circulation* **91**, 161–170 (1995).

79. Rajendran, P. *et al.* The vascular endothelium and human diseases. *Int. J. Biol. Sci.* **9**, 1057–1069 (2013).

80. Kwaifa, I. K., Bahari, H., Yong, Y. K. & Md Noor, S. Endothelial dysfunction in obesity-induced inflammation: Molecular mechanisms and clinical implications. *Biomolecules* **10**, 291 (2020).

81. Murdaca, G. *et al.* Endothelial dysfunction in rheumatic autoimmune diseases. *Atherosclerosis* **224**, 309–317 (2012).

82. Sandoo, A., Veldhuijzen van Zanten, J. J. C. ., Metsios, G. S., Carroll, D. & Kitas, G. D. The Endothelium and Its Role in Regulating Vascular Tone. *Open Cardiovasc. Med. J.* **4**, 302–312 (2010).

83. Panza, J. A., Garcia, C. E., Kilcoyne, C. M., Quyyumi, A. A. & Cannon, R. O. No Impaired Endothelium-Dependent Vasodilation in Patients With Essential Hypertension. *Circulation* **91**, 1732–1738 (1995).

84. Perticone, F. *et al.* Prognostic significance of endothelial dysfunction in hypertensive patients. *Circulation* **104**, 191–196 (2001).

85. Mai, J., Virtue, A., Shen, J., Wang, H. & Yang, X. F. An evolving new paradigm: Endothelial cells - Conditional innate immune cells. *J. Hematol. Oncol.* **6**, 1–13 (2013).

86. Westermann, D. *et al.* Cardiac inflammation contributes to changes in the extracellular matrix in patients with heart failure and normal ejection fraction. *Circ. Heart Fail.* **4**, 44–52 (2011).

87. Chan, C. T. *et al.* Reversal of vascular macrophage accumulation and hypertension by a CCR2 antagonist in deoxycorticosterone/salt-treated mice. *Hypertension* **60**, 1207–1212 (2012).

88. Wenzel, P. *et al.* Lysozyme M-positive monocytes mediate angiotensin ii-induced arterial hypertension and vascular dysfunction. *Circulation* **124**, 1370–1381 (2011).

89. Humar, R., Zimmerli, L. & Battegay, E. Angiogenesis and hypertension: An update. *J. Hum. Hypertens.* **23**, 773–782 (2009).

90. Marek-Trzonkowska, N. *et al.* Arterial hypertension is characterized by imbalance of pro-angiogenic versus anti-angiogenic factors. *PLoS One* **10**, e0126190 (2015).

91. Sabri, A. *et al.* Microvasculature in angiotensin II-dependent cardiac hypertrophy in the rat. *Hypertension* **32**, 371–375 (1998).

92. Pu, Q., Larouche, I. & Schiffrin, E. L. Effect of Dual Angiotensin Converting Enzyme/ Neutral Endopeptidase Inhibition, Angiotensin Converting Enzyme Inhibition, or AT1 Antagonism on Coronary Microvasculature in Spontaneously Hypertensive Rats. *Am. J. Hypertens.* **16**, 931–937 (2003).

93. Shiojima, I. *et al.* Disruption of coordinated cardiac hypertrophy and angiogenesis contributes to the transition to heart failure. *J. Clin. Invest.* **115**, 2108–2118 (2005).

94. Xia, Y. *et al.* Characterization of the inflammatory and fibrotic response in a mouse model of cardiac pressure overload. *Histochem. Cell Biol.* **131**, 471–481 (2009).

95. Sano, M. *et al.* p53-induced inhibition of Hif-1 causes cardiac dysfunction during pressure overload. *Nature* **446**, 444–448 (2007).

96. Izumiya, Y. *et al.* Vascular endothelial growth factor blockade promotes the transition from compensatory cardiac hypertrophy to failure in response to pressure overload. *Hypertension* **47**, 887–893 (2006).

97. Seddon, M., Shah, A. M. & Casadei, B. Cardiomyocytes as effectors of nitric oxide signalling. *Cardiovasc. Res.* **75**, 315–326 (2007).

98. Massion, P. B., Feron, O., Dessy, C. & Balligand, J. L. Nitric oxide and cardiac function: Ten years after, and continuing. *Circ. Res.* **93**, 388–398 (2003).

99. Paulus, W. J. & Tschöpe, C. A novel paradigm for heart failure with preserved ejection fraction: Comorbidities drive myocardial dysfunction and remodeling through coronary microvascular endothelial inflammation. *J. Am. Coll. Cardiol.* **62**, 263–271 (2013).

100. Hedhli, N. *et al.* Endothelium-derived neuregulin protects the heart against ischemic injury. *Circulation* **123**, 2254–2262 (2011).

101. Drawnel, F. M., Archer, C. R. & Roderick, H. L. The role of the paracrine/autocrine mediator endothelin-1 in regulation of cardiac contractility and growth. *Br. J. Pharmacol.* **168**, 296–317 (2013).

102. Brutsaert, D. L. Cardiac Endothelial-Myocardial Signaling: Its Role in Cardiac Growth, Contractile Performance, and Rhythmicity. *Physiol. Rev.* **83**, 59–115 (2003).

103. Kamo, T., Akazawa, H. & Komuro, I. Cardiac Nonmyocytes in the Hub of Cardiac Hypertrophy. *Circ. Res.* **117**, 89–98 (2015).

104. Talman, V. & Kivelä, R. Cardiomyocyte—Endothelial Cell Interactions in Cardiac Remodeling and Regeneration. *Front. Cardiovasc. Med.* **5**, 101 (2018).

105. Incalza, M. A. *et al.* Oxidative stress and reactive oxygen species in endothelial dysfunction associated with cardiovascular and metabolic diseases. *Vascul. Pharmacol.* **100**, 1–19 (2018).

106. D'Autréaux, B. & Toledano, M. B. ROS as signalling molecules: Mechanisms that generate specificity in ROS homeostasis. *Nat. Rev. Mol. Cell Biol.* **8**, 813–824 (2007).

107. Forman, H. J., Ursini, F. & Maiorino, M. An overview of mechanisms of redox signaling. *J. Mol. Cell. Cardiol.* **0**, 2–9 (2014).

108. Nadeau, P. J., Charette, S. J., Toledano, M. B. & Landry, J. Disulfide bond-mediated multimerization of Ask1 and its reduction by thioredoxin-1 regulate H2O2-induced c-Jun NH 2-terminal kinase activation and apoptosis. *Mol. Biol. Cell* **18**, 3903–3913 (2007).

109. Lee, S. R. *et al.* Reversible inactivation of the tumor suppressor PTEN by H2O2. *J. Biol. Chem.* **277**, 20336–20342 (2002).

110. Schieber, M. & Chandel, N. S. ROS function in redoz signaling and oxidative stress. *Curr. Biol.* **24**, R453–R462 (2014).

111. Schulz, E., Gori, T. & Münzel, T. Oxidative stress and endothelial dysfunction in hypertension. *Hypertens. Res.* **34**, 665–673 (2011).

112. Alp, N. J. & Channon, K. M. Regulation of Endothelial Nitric Oxide Synthase by Tetrahydrobiopterin in Vascular Disease. *Arterioscler. Thromb. Vasc. Biol.* **24**, 413–420 (2004).

113. Belmadani, S. *et al.* A Thrombospondin-1 Antagonist of Transforming Growth Factor-β Activation Blocks Cardiomyopathy in Rats with Diabetes and Elevated Angiotensin II. *Am. J. Pathol.* **171**, 777–789 (2007).

114. Sharifi-Sanjani, M. *et al.* Cardiac CD47 drives left ventricular heart failure through Ca2+-CaMKII-regulated induction of HDAC3. *J. Am. Heart Assoc.* **3**, e000670 (2014).

115. Adams, J. C. & Lawler, J. The thrombospondins. *Cold Spring Harb. Perspect. Biol.* **3**, a009712 (2011).

116. Stenina-Adognravi, O. & Plow, E. F. Thrombospondin-4 in tissue remodeling. *Matrix Biol.* **75–76**, 300–313 (2019).

117. Chua, C. C., Hamdy, R. C. & Chua, B. H. L. Regulation of thrombospondin-1 production by angiotensin II in rat heart endothelial cells. *Biochim. Biophys. Acta* **1357**, 209–214 (1997).

118. Zhou, Y., Poczatek, M. H., Berecek, K. H. & Murphy-Ullrich, J. E. Thrombospondin 1 mediates angiotensin II induction of TGF-β activation by cardiac and renal cells under

both high and low glucose conditions. *Biochem. Biophys. Res. Commun.* **339**, 633–641 (2006).

119. Phelan, M. W., Forman, L. W., Perrine, S. R. & Faller, D. V. Hypoxia increases thrombospondin-1 transcript and protein in cultured endothelial cells. *J. Lab. Clin. Med.* **132**, 519–529 (1998).

120. Labrousse-Arias, D. *et al.* HIF-2α-mediated induction of pulmonary thrombospondin-1 contributes to hypoxia-driven vascular remodelling and vasoconstriction. *Cardiovasc. Res.* **109**, 115–130 (2016).

121. Wang, S., Skorczewski, J., Feng, X., Mei, L. & Murphy-Ullrich, J. E. Glucose up-regulates thrombospondin 1 gene transcription and transforming growth factor-β activity through antagonism of cGMP-dependent protein kinase repression via upstream stimulatory factor 2. *J. Biol. Chem.* **279**, 34311–34322 (2004).

122. Kang, J.-H. *et al.* Weakening of the repressive YY-1 site on the thrombospondin-1 promoter via c-Jun/YY-1 interaction. **36**, 300–310 (2004).

123. Frangogiannis, N. G. *et al.* Critical role of endogenous thrombospondin-1 in preventing expansion of healing myocardial infarcts. *Circulation* **111**, 2935–2942 (2005).

124. Ghoneim, C. *et al.* Activating transcription factor-1-mediated hepatocyte growth factor-induced down-regulation of thrombospondin-1 expression leads to thyroid cancer cell invasion. *J. Biol. Chem.* **282**, 15490–15497 (2007).

125. Kvansakul, M., Adams, J. C. & Hohenester, E. Structure of a thrombospondin C-terminal fragment reveals a novel calcium core in the type 3 repeats. *EMBO J.* **23**, 1223–1233 (2004).

126. Resovi, A., Pinessi, D., Chiorino, G. & Taraboletti, G. Current understanding of the thrombospondin-1 interactome. *Matrix Biol.* **37**, 83–91 (2014).

127. Kale, A., Rogers, N. M. & Ghimire, K. Thrombospondin-1 CD47 Signalling: From Mechanisms to Medicine. *Int. J. Mol. Sci.* **22**, 4062 (2021).

128. Gupta, A., Agarwal, R., Singh, A. & Bhatnagar, S. Calcium-induced conformational changes of Thrombospondin-1 signature domain: implications for vascular disease. *J. Recept. Signal Transduct.* **37**, 239–251 (2017).

129. Fenalti, G. *et al.* Structure of the human marker of self 5-transmembrane receptor CD47. *Nat. Commun.* **12**, 5218 (2021).

130. Soto-Pantoja, D. R., Kaur, S. & Roberts, D. D. CD47 signaling pathways controlling cellular differentiation and responses to stress. *Crit. Rev. Biochem. Mol. Biol.* **50**, 212–230 (2015).

131. Huang, C. Y., Ye, Z. H., Huang, M. Y. & Lu, J. J. Regulation of CD47 expression in

cancer cells. *Transl. Oncol.* **13**, 100862 (2020).

132. Chen, H. M. *et al.* Baicalein, an active component of Scutellaria baicalensis Georgi, prevents lysophosphatidylcholine-induced cardiac injury by reducing reactive oxygen species production, calcium overload and apoptosis via MAPK pathways. *BMC Complement. Altern. Med.* **14**, 233 (2014).

133. Isenberg, J. S. *et al.* Blocking thrombospondin-1/CD47 signaling alleviates deleterious effects of aging on tissue responses to ischemia. *Arterioscler. Thromb. Vasc. Biol.* **27**, 2582–2588 (2007).

134. Isenberg, J. S. *et al.* CD47 is necessary for inhibition of nitric oxide-stimulated vascular cell responses by thrombospondin-1. *J. Biol. Chem.* **281**, 26069–26080 (2006).

135. Bauer, E. M. *et al.* Thrombospondin-1 supports blood pressure by limiting eNOS activation and endothelial-dependent vasorelaxation. *Cardiovasc. Res.* **88**, 471–481 (2010).

136. Isenberg, J. S. *et al.* Thrombospondin-1 and CD47 regulate blood pressure and cardiac responses to vasoactive stress. *Matrix Biol.* **28**, 110–119 (2009).

137. Gélinas, D. S., Bernatchez, P. N., Rollin, S., Bazan, N. G. & Sirois, M. G. Immediate and delayed VEGF-mediated NO synthesis in endothelial cells: Role of PI3K, PKC and PLC pathways. *Br. J. Pharmacol.* **137**, 1021–1030 (2002).

138. Dimmeler, S., Dernbach, E. & Zeiher, A. M. Phosphorylation of the endothelial nitric oxide synthase at Ser-1177 is required for VEGF-induced endothelial cell migration. *FEBS Lett.* **477**, 258–262 (2000).

139. Duval, M., Bœuf, F. Le, Huot, J. & Gratton, J.-P. Src-mediated Phosphorylation of Hsp90 in Response to Vascular Endothelial Growth Factor (VEGF) Is Required for VEGF Receptor-2 Signaling to Endothelial NO Synthase. *Mol. Biol. Cell* **18**, 4659–4668 (2007).

140. Zhang, X. *et al.* Thrombospondin-1 modulates vascular endothelial growth factor activity at the receptor level. *FASEB J.* **23**, 3368–3376 (2009).

141. Dudzinski, D. & Michel, T. Life History of eNOS: Partners and Pathway. *Cardiovasc. Res.* **75**, 247–260 (2007).

142. Kaur, S. *et al.* Thrombospondin-1 inhibits VEGF receptor-2 signaling by disrupting its association with CD47. *J. Biol. Chem.* **285**, 38923–38932 (2010).

143. Gupta, K., Gupta, P., Wild, R., Ramakrishnan, S. & Hebbel, R. P. Binding and displacement of vascular endothelial growth factor (VEGF) by thrombospondin: effect on human microvascular endothelial cell proliferation and angiogenesis. *Angiogenesis* **3**, 147–158 (1999).

144. Isenberg, J. S., Martin-Manso, G., Maxhimer, J. B. & Roberts, D. D. Regulation of nitric oxide signaling by thrombospondin-1: implications for anti-angiogenic therapies. *Nat. Rev. Cancer* **9**, 182–194 (2009).

145. Coletta, C. *et al.* Hydrogen sulfide and nitric oxide are mutually dependent in the regulation of angiogenesis and endothelium-dependent vasorelaxation. *Proc. Natl. Acad. Sci. U.S.A.* **109**, 9161–9166 (2012).

146. Malek, M. H. & Olfert, I. M. Global deletion of thrombospondin-1 increases cardiac and skeletal muscle capillarity and exercise capacity in mice. *Exp. Physiol.* **94**, 749–760 (2009).

147. Isenberg, J. S. *et al.* Thrombospondin-1 limits ischemic tissue survival by inhibiting nitric oxide-mediated vascular smooth muscle relaxation. *Blood* **109**, 1945–1952 (2007).

148. Isenberg, J. S. *et al.* Increasing survival of ischemic tissue by targeting CD47. *Circ. Res.* **100**, 712–720 (2007).

149. Maxhimer, J. B., Shih, H. B., Isenberg, J. S., Miller, T. W. & Roberts, D. D. Thrombospondin-1/CD47 blockade following ischemia-reperfusion injury is tissue protective. *Plast. Reconstr. Surg.* **124**, 1880–1889 (2009).

150. Lopez-Dee, Z., Pidcock, K. & Gutierrez, L. S. Thrombospondin-1: Multiple paths to inflammation. *Mediators Inflamm.* **2011**, 296069 (2011).

151. Liu, Z. *et al.* Thrombospondin-1 (TSP1) contributes to the development of vascular inflammation by regulating monocytic cell motility in mouse models of abdominal aortic aneurysm. *Circ. Res.* **117**, 129–141 (2015).

152. Narizhneva, N. V. *et al.* Thrombospondin-1 up-regulates expression of cell adhesion molecules and promotes monocyte binding to endothelium. *FASEB J.* **19**, 1158–1160 (2005).

153. Gao, F. *et al.* Reduction of endothelial nitric oxide increases the adhesiveness of constitutive endothelial membrane ICAM-1 through Src-mediated phosphorylation. *Front. Physiol.* **8**, 1124 (2018).

154. Isenberg, J. S., Frazier, W. A. & Roberts, D. D. Thrombospondin-1 is a Central Regulator of Nitric Oxide Signaling in Vascular Physiology. *Cell. Mol. Life Sci.* **65**, 728–742 (2008).

155. Liu, Y. *et al.* The role of CD47 in neutrophil transmigration: Increased rate of migration correlates with increased cell surface expression of CD47. *J. Biol. Chem.* **276**, 40156–40166 (2001).

156. Doyen, V. *et al.* Thrombospondin 1 Is an Autocrine Negative Regulator of Human Dendritic Cell Activation. *J. Exp. Med.* **198**, 1277–1283 (2003).

157. Grimbert, P. *et al.* Thrombospondin/CD47 Interaction: A Pathway to Generate Regulatory T Cells from Human CD4 + CD25 − T Cells in Response to Inflammation . *J. Immunol.* **177**, 3534–3541 (2006).

158. Lamy, L. *et al.* CD47 and the 19 kDA interacting protein-3 (BNIP3) in T cell apoptosis. *J. Biol. Chem.* **278**, 23915–23921 (2003).

159. Vande Velde, C. *et al.* BNIP3 and Genetic Control of Necrosis-Like Cell Death through the Mitochondrial Permeability Transition Pore. *Mol. Cell. Biol.* **20**, 5454–5468 (2000).

160. Lamy, L. *et al.* Interactions between CD47 and Thrombospondin Reduce Inflammation. *J. Immunol.* **178**, 5930–5939 (2007).

161. Li, Y., Qi, X., Tong, X. & Wang, S. Thrombospondin 1 activates the macrophage Toll-like receptor 4 pathway. *Cell. Mol. Immunol.* **10**, 506–512 (2013).

162. Lawrence, D. W., King, S. B., Frazier, W. A. & Koenig, J. M. Decreased CD47 Expression during Spontaneous Apoptosis Targets Neutrophils for Phagocytosis by Monocyte-Derived Macrophages. *Early Hum. Dev.* **85**, 659–663 (2009).

163. Oldenborg, P. A. *et al.* Role of CD47 as a marker of self on red blood cells. *Science* **288**, 2051–2054 (2000).

164. Blazar, B. R. *et al.* CD47 (Integrin-associated Protein) engagement of dendritic cell and macrophage counterreceptors is required to prevent the clearance of donor lymphohematopoietic cells. *J. Exp. Med.* **194**, 541–549 (2001).

165. Tsai, R. K. & Discher, D. E. Inhibition of 'self' engulfment through deactivation of myosin-II at the phagocytic synapse between human cells. *J. Cell Biol.* **180**, 989–1003 (2008).

166. Gardai, S. J. *et al.* Cell-surface calreticulin initiates clearance of viable or apoptotic cells through trans-activation of LRP on the phagocyte. *Cell* **123**, 321–334 (2005).

167. Borthwick, L. A., Wynn, T. A. & Fisher, A. J. Cytokine mediated tissue fibrosis. *Biochim. Biophys. Acta* **1832**, 1049–1060 (2013).

168. Young, G. D. & Murphy-Ullrich, J. E. The tryptophan-rich motifs of the thrombospondin type 1 repeats bind VLAL motifs in the latent transforming growth factor-β complex. *J. Biol. Chem.* **279**, 47633–47642 (2004).

169. Nör, J. E. *et al.* Activation of Latent TGF-β1 by Thrombospondin-1 is a Major Component of Wound Repair. *Oral Biosci. Med.* **2**, 153–161 (2005).

170. Moodley, Y. *et al.* Macrophage recognition and phagocytosis of apoptotic fibroblasts is critically dependent on fibroblast-derived thrombospondin 1 and CD36. *Am. J. Pathol.* **162**, 771–779 (2003).

171. Smalling, R. V. *et al.* Genome-wide transcriptome analysis identifies novel gene

signatures implicated in human chronic liver disease. *Am. J. Physiol. Gastrointest. Liver Physiol.* **305**, G364–G374 (2013).

172. Min-DeBartolo, J. *et al.* Thrombospondin-I is a critical modulator in non-alcoholic steatohepatitis (NASH). *PLoS One* **14**, e0226854 (2019).

173. Csányi, G. *et al.* Thrombospondin-1 Regulates Blood Flow via CD47 Receptor-Mediated Activation of NADPH Oxidase 1. *Arterioscler. Thromb. Vasc. Biol.* **32**, 2966–2973 (2012).

174. Novelli, E. M. *et al.* Vascular TSP1-CD47 signaling promotes sickle cell-associated arterial vasculopathy and pulmonary hypertension in mice. *Am. J. Physiol. Lung Cell. Mol. Physiol.* **316**, L1150–L1164 (2019).

175. Meijles, D. N. *et al.* The matricellular protein TSP1 promotes human and mouse endothelial cell senescence through CD47 and Nox1. *Sci. Signal.* **10**, eaaj1784 (2017).

176. Yao, M. *et al.* Thrombospondin-1 activation of signal-regulatory protein-α stimulates reactive oxygen species production and promotes renal Ischemia reperfusion injury. *J. Am. Soc. Nephrol.* **25**, 1171–1186 (2014).

177. Alblas, J. *et al.* Signal Regulatory Protein α Ligation Induces Macrophage Nitric Oxide Production through JAK/STAT- and Phosphatidylinositol 3-Kinase/Rac1/NAPDH Oxidase/H2O2-Dependent Pathways. *Mol. Cell. Biol.* **25**, 7181–7192 (2005).

178. Xia, Y. *et al.* Endogenous thrombospondin 1 protects the pressure-overloaded myocardium by modulating fibroblast phenotype and matrix metabolism. *Hypertension* **58**, 902–911 (2011).

179. Sezaki, S. *et al.* Thrombospondin-1 is induced in rat myocardial infarction and its induction is accelerated by ischemia/reperfusion. *Exp. Biol. Med.* **230**, 621–630 (2005).

180. Gonzalez-Quesada, C. *et al.* Thrombospondin-1 induction in the diabetic myocardium stabilizes the cardiac matrix, while promoting vascular rarefaction through angiopoietin-2 upregulation. *Circ. Res.* **113**, 1331–1344 (2013).

181. Vila, V. *et al.* Inflammation, endothelial dysfunction and angiogenesis markers in chronic heart failure patients. *Int. J. Cardiol.* **130**, 276–277 (2008).

182. Batlle, M. *et al.* Decreased Expression of Thrombospondin-1 in Failing Hearts May Favor Ventricular Remodeling. *Transplant. Proc.* **41**, 2231–2233 (2009).

183. Mustonen, E. *et al.* Thrombospondin-4 expression is rapidly upregulated by cardiac overload. *Biochem. Biophys. Res. Commun.* **373**, 186–191 (2008).

184. Zhou, Y., Ng, D. Y. E., Richards, A. M. & Wang, P. microRNA-221 Inhibits Latent TGF-β1 Activation through Targeting Thrombospondin-1 to Attenuate Kidney Failure-

Induced Cardiac Fibrosis. *Mol. Ther. - Nucleic Acids* **22**, 803–814 (2020).

185. Zhao, X. M., Hu, Y., Miller, G. G., Mitchell, R. N. & Libby, P. Association of thrombospondin-1 and cardiac allograft vasculopathy in human cardiac allografts. *Circulation* **103**, 525–531 (2001).

186. van Almen, G. C. *et al.* MicroRNA-18 and microRNA-19 regulate CTGF and TSP-1 expression in age-related heart failure. *Aging Cell* **10**, 769–779 (2011).

187. Ritchie, R. H. & Dale Abel, E. Basic Mechanisms of Diabetic Heart Disease. *Circ. Res.* **126**, 1501–1525 (2020).

188. Kaesler, N., Babler, A., Floege, J. & Kramann, R. Cardiac remodeling in chronic kidney disease. *Toxins (Basel).* **12**, 161 (2020).

189. St. John Sutton, M. G. & Sharpe, N. Left ventricular remodeling after myocardial infarction: Pathophysiology and therapy. *Circulation* **101**, 2981–2988 (2000).

190. Selvetella, G., Hirsch, E., Notte, A., Tarone, G. & Lembo, G. Adaptive and maladaptive hypertrophic pathways: Points of convergence and divergence. *Cardiovasc. Res.* **63**, 373–380 (2004).

191. Rose, B. A., Force, T. & Wang, Y. Mitogen-Activated Protein Kinase Signaling in the Heart: Angels Versus Demons in a Heart-Breaking Tale. *Physiol. Rev.* **90**, 1507–1546 (2010).

192. Anilkumar, N., Sirker, A. & Shah, A. M. Redox sensitive signaling pathways in cardiac remodeling, hypertrophy and failure. *Front Biosci (Landmark Ed)* **14**, 3168–3187 (2009).

193. Meijles, D. N. *et al.* Redox regulation of cardiac ASK1 (Apoptosis Signal-Regulating Kinase 1) controls p38-MAPK (Mitogen-Activated Protein Kinase) and orchestrates cardiac remodeling to hypertension. *Hypertension* **1**, 1208–1218 (2020).

194. Ramos, J. W. The regulation of extracellular signal-regulated kinase (ERK) in mammalian cells. *Int. J. Biochem. Cell Biol.* **40**, 2707–2719 (2008).

195. Raman, M., Chen, W. & Cobb, M. H. Differential regulation and properties of MAPKs. *Oncogene* **26**, 3100–3112 (2007).

196. Bogoyevitch, M. A. The isoform-specific functions of the c-Jun N-terminal Kinases (JNKs): differences revealed by gene targeting. *BioEssays* **28**, 923–934 (2006).

197. Ono, K. & Han, J. The p38 signal transduction pathway: activation and function. *Cell. Signal.* **12**, 1–13 (2000).

198. Thornton, T. M. & Rincon, M. Non-classical p38 map kinase functions: cell cycle checkpoints and survival. *Int. J. Biol. Sci.* **5**, 44–52 (2009).

199. Rincón, M. & Davis, R. J. Regulation of the immune response by stress-activated

protein kinases. *Immunol. Rev.* **228**, 212–224 (2009).

200. Zarubin, T. & Han, J. Activation and signaling of the p38 MAP kinase pathway. *Cell Res. 2005 151* **15**, 11–18 (2005).

201. Cargnello, M. & Roux, P. P. Activation and Function of the MAPKs and Their Substrates, the MAPK-Activated Protein Kinases. *Microbiol. Mol. Biol. Rev.* **75**, 50–83 (2011).

202. Muslin, A. J. MAPK Signaling in Cardiovascular Health and Disease: Molecular Mechanisms and Therapeutic Targets. *Clin. Sci. (Lond).* **115**, 203–218 (2008).

203. Li, X.-M. *et al.* Downregulation of survival signalling pathways and increased apoptosis in the transition of pressure overload-induced cardiac hypertrophy to heart failure. *Clin. Exp. Pharmacol. Physiol.* **36**, 1054–1061 (2009).

204. Harris, I. S. *et al.* Raf-1 kinase is required for cardiac hypertrophy and cardiomyocyte survival in response to pressure overload. *Circulation* **110**, 718–723 (2004).

205. Yamaguchi, O. *et al.* Cardiac-specific disruption of the c-raf-1 gene induces cardiac dysfunction and apoptosis. *J. Clin. Invest.* **114**, 937–943 (2004).

206. Mutlak, M. *et al.* Extracellular signal-regulated kinase (ERK) activation preserves cardiac function in pressure overload induced hypertrophy. *Int. J. Cardiol.* **270**, 204–213 (2018).

207. Bueno, O. F. *et al.* The MEK1-ERK1/2 signaling pathway promotes compensated cardiac hypertrophy in transgenic mice. *EMBO J.* **19**, 6341–6350 (2000).

208. Purcell, N. H. *et al.* Genetic inhibition of cardiac ERK1/2 promotes stress-induced apoptosis and heart failure but has no effect on hypertrophy in vivo. *Proc. Natl. Acad. Sci. U.S.A.* **104**, 14074–14079 (2007).

209. Kehat, I. *et al.* Extracellular signal-regulated kinases 1 and 2 regulate the balance between eccentric and concentric cardiac growth. *Circ. Res.* **108**, 176–183 (2011).

210. Fisher, J. P. & Paton, J. F. R. The sympathetic nervous system and blood pressure in humans: Implications for hypertension. *J. Hum. Hypertens.* **26**, 463–475 (2012).

211. Lips, D. J. *et al.* MEK1-ERK2 Signaling Pathway Protects Myocardium from Ischemic Injury In Vivo. *Circulation* **109**, 1938–1941 (2004).

212. Liao, P. *et al.* The in vivo role of p38 MAP kinases in cardiac remodeling and restrictive cardiomyopathy. *Proc. Natl. Acad. Sci. U.S.A.* **98**, 12283–12288 (2001).

213. Braz, J. C. *et al.* Targeted inhibition of p38 MAPK promotes hypertrophic cardiomyopathy through upregulation of calcineurin-NFAT signaling. *J. Clin. Invest.* **111**, 1475–1486 (2003).

214. Nishida, K. *et al.* p38α Mitogen-Activated Protein Kinase Plays a Critical Role in

Cardiomyocyte Survival but Not in Cardiac Hypertrophic Growth in Response to Pressure Overload. *Mol. Cell. Biol.* **24**, 10611–10620 (2004).

215. Stempien-Otero, A., Kim, D.-H. & Davis, J. Molecular Networks Underlying Myofibroblast Fate and Fibrosis. *J. Mol. Cell. Cardiol.* **97**, 153–161 (2016).

216. Molkentin, J. D. *et al.* Fibroblast-Specific Genetic Manipulation of p38 Mitogen-Activated Protein Kinase in Vivo Reveals Its Central Regulatory Role in Fibrosis. *Circulation* **136**, 549–561 (2017).

217. Nadruz Jr, W., Kobarg, C. B., Kobarg, J. & Franchin, K. G. c-Jun is regulated by combination of enhanced expression and phosphorylation in acute-overloaded rat heart. *Am. J. Physiol. Heart Circ. Physiol.* **286**, H760–H767 (2004).

218. Fischer, T. A. *et al.* Activation of cardiac c-Jun NH(2)-terminal kinases and p38-mitogen-activated protein kinases with abrupt changes in hemodynamic load. *Hypertension* **37**, 1222–1228 (2001).

219. Sopontammarak, S. *et al.* Mitogen-activated protein kinases (p38 and c-Jun NH2-terminal kinase) are differentially regulated during cardiac volume and pressure overload hypertrophy. *Cell Biochem. Biophys.* **43**, 61–76 (2005).

220. Roussel, É. *et al.* Early responses of the left ventricle to pressure overload in Wistar rats. *Life Sci.* **82**, 265–272 (2008).

221. Wang, Y. *et al.* Cardiac hypertrophy induced by mitogen-activated protein kinase kinase 7, a specific activator for c-Jun NH2-terminal kinase in ventricular muscle cells. *J. Biol. Chem.* **273**, 5423–5426 (1998).

222. Choukroun, G. *et al.* Role of the stress-activated protein kinases in endothelin-induced cardiomyocyte hypertrophy. *J. Clin. Invest.* **102**, 1311–1320 (1998).

223. Petrich, B. G. *et al.* Targeted activation of c-Jun N-terminal kinase in vivo induces restrictive cardiomyopathy and conduction defects. *J. Biol. Chem.* **279**, 15330–15338 (2004).

224. Tachibana, H. *et al.* JNK1 is required to preserve cardiac function in the early response to pressure overload. *Biochem. Biophys. Res. Commun.* **343**, 1060–1066 (2006).

225. Liu, W. *et al.* Cardiac-specific deletion of mkk4 reveals its role in pathological hypertrophic remodeling but not in physiological cardiac growth. *Circ. Res.* **104**, 905–914 (2009).

226. Pajares, M. *et al.* Redox control of protein degradation. *Redox Biol.* **6**, 409–420 (2015).

227. Bortolotti, M., Polito, L., Battelli, M. G. & Bolognesi, A. Xanthine oxidoreductase: One enzyme for multiple physiological tasks. *Redox Biol.* **41**, 101882 (2021).

228. Zhao, R. Z., Jiang, S., Zhang, L. & Yu, Z. Bin. Mitochondrial electron transport chain, ROS generation and uncoupling. *Int. J. Mol. Med.* **44**, 3–15 (2019).

229. Zorov, D. B., Juhaszova, M. & Sollott, S. J. Mitochondrial Reactive Oxygen Species (ROS) and ROS-Induced ROS Release. *Physiol Rev* **94**, 909–950 (2014).

230. Zhang, M., Perino, A., Ghigo, A., Hirsch, E. & Shah, A. M. NADPH oxidases in heart failure: Poachers or gamekeepers? *Antioxidants and Redox Signaling* vol. 18 1024–1041 (2013).

231. Fulton, D. J. R. Nox5 and the regulation of cellular function. *Antioxid. Redox Signal.* **11**, 2443–52 (2009).

232. Bedard, K. & Krause, K.-H. The NOX Family of ROS-Generating NADPH Oxidases: Physiology and Pathophysiology. *Physiol. Rev.* **87**, 245–313 (2007).

233. Brown, D. I. & Griendling, K. K. Nox proteins in signal transduction. *Free Radic. Biol. Med.* **47**, 1239–53 (2009).

234. Fan, C., Katsuyama, M., Nishinaka, T. & Yabe-nishimura, C. Transactivation of the EGF receptor and a PI3 kinase – ATF-1 pathway is involved in the upregulation of NOX1 , a catalytic subunit of NADPH oxidase. **579**, 1301–1305 (2005).

235. Laurindo, F. R. M., Araujo, T. L. S. & Abrahão, T. B. Nox NADPH oxidases and the endoplasmic reticulum. *Antioxid. Redox Signal.* **20**, 2755–2775 (2014).

236. Bánfi, B., Clark, R. A., Steger, K. & Krause, K.-H. Two novel proteins activate superoxide generation by the NADPH oxidase NOX1. *J. Biol. Chem.* **278**, 3510–3513 (2003).

237. Al Ghouleh, I. *et al.* Binding of EBP50 to Nox organizing subunit p47 phox is pivotal to cellular reactive species generation and altered vascular phenotype. *Proc. Natl. Acad. Sci. U.S.A.* **113**, E5308–E5317 (2016).

238. Takac, I. *et al.* The E-loop is involved in hydrogen peroxide formation by the NADPH oxidase Nox4. *J. Biol. Chem.* **286**, 13304–13313 (2011).

239. Panday, A., Sahoo, M. K., Osorio, D. & Batra, S. NADPH oxidases: an overview from structure to innate immunity-associated pathologies. *Cell. Mol. Immunol.* **12**, 5–23 (2015).

240. Lambeth, D. J. NOX enzymes and the biology of reactive oxygen. *Nat. Rev. Immunol.* **4**, 181–189 (2004).

241. Fukai, T. & Ushio-Fukai, M. Superoxide dismutases: role in redox signaling, vascular function, and diseases. *Antioxid. Redox Signal.* **15**, 1583–606 (2011).

242. Redón, J. *et al.* Antioxidant activities and oxidative stress byproducts in human hypertension. *Hypertension* **41**, 1096–1101 (2003).

243. Rodrigo, R. *et al.* Relationship between oxidative stress and essential hypertension. *Hypertens. Res.* **30**, 1159–1167 (2007).

244. Belch, J. J. F., Bridges, A. B., Scott, N. & Chopra, M. Oxygen free radicals and congestive heart failure. *Br. Heart J.* **65**, 245–248 (1991).

245. Mallat, Z. *et al.* Elevated levels of 8-iso-prostaglandin F(2α) in pericardial fluid of patients with heart failure: A potential role for in vivo oxidant stress in ventricular dilatation and progression to heart failure. *Circulation* **97**, 1536–1539 (1998).

246. Heymes, C. *et al.* Increased myocardial NADPH oxidase activity in human heart failure. *J. Am. Coll. Cardiol.* **41**, 2164–2171 (2003).

247. Nediani, C. *et al.* NADPH oxidase-dependent redox signaling in human heart failure: Relationship between the left and right ventricle. *J. Mol. Cell. Cardiol.* **42**, 826–834 (2007).

248. Mihm, M. J., Coyle, C. M., Schanbacher, B. L., Weinstein, D. M. & Bauer, J. A. Peroxynitrite induced nitration and inactivation of myofibrillar creatine kinase in experimental heart failure. *Cardiovasc. Res.* **49**, 798–807 (2001).

249. Hill, M. F. & Singal, P. K. Antioxidant and oxidative stress changes during heart failure subsequent to myocardial infarction in rats. *Am. J. Pathol.* **148**, 291–300 (1996).

250. Griendling, K. K. & FitzGerald, G. A. Oxidative Stress and Cardiovascular Injury Part I: Basic Mechanisms and In Vivo Monitoring of ROS. *Circulation* **108**, 1912–1916 (2003).

251. Brennan, J. P. *et al.* Oxidant-induced activation of type I protein kinase A is mediated by RI subunit interprotein disulfide bond formation. *J. Biol. Chem.* **281**, 21827–21836 (2006).

252. Burgoyne, J. R. *et al.* Cysteine redox sensor in PKGIa enables oxidant-induced activation. *Science* **7**, 1393–1397 (2007).

253. Nadeau, P. J., Charette, S. J. & Landry, J. REDOX Reaction at ASK1-Cys250 Is Essential for Activation of JNK and Induction of Apoptosis. *Mol. Biol. Cell* **20**, 3628–3627 (2009).

254. Redza-Dutordoir, M. & Averill-Bates, D. A. Activation of apoptosis signalling pathways by reactive oxygen species. *Biochim. Biophys. Acta - Mol. Cell Res.* **1863**, 2977–2992 (2016).

255. Ushio-Fukai, M., Alexander, R. W., Akers, M. & Griendling, K. K. p38 mitogen-activated protein kinase is a critical component of the redox-sensitive signaling pathways activated by angiotensin II. *J. Biol. Chem.* **273**, 15022–15029 (1998).

256. Sorescu, G. P. *et al.* Bone Morphogenic Protein 4 Produced in Endothelial Cells by

Oscillatory Shear Stress Induces Monocyte Adhesion by Stimulating Reactive Oxygen Species Production From a Nox1-Based NADPH Oxidase. *Circ. Res.* **95**, 773–779 (2004).

257. Ghouleh, I. Al *et al.* Endothelial Nox1 oxidase assembly in human pulmonary arterial hypertension; driver of Gremlin1-mediated proliferation. *Clin. Sci.* **131**, 2019–2035 (2017).

258. Doughan, A. K., Harrison, D. G. & Dikalov, S. I. Molecular mechanisms of angiotensin II-mediated mitochondrial dysfunction: Linking mitochondrial oxidative damage and vascular endothelial dysfunction. *Circ. Res.* **102**, 488–496 (2008).

259. Dikalov, S. I. *et al.* Nox2-Induced production of mitochondrial Superoxide in Angiotensin ii-mediated endothelial oxidative stress and hypertension. *Antioxidants Redox Signal.* **20**, 281–294 (2014).

260. Bendall, J. K., Cave, A. C., Heymes, C., Gall, N. & Shah, A. M. Pivotal Role of a gp91phox-Containing NADPH Oxidase in Angiotensin II-Induced Cardiac Hypertrophy in Mice. *Circulation* **105**, 293–296 (2002).

261. Satoh, M. *et al.* Requirement of Rac1 in the development of cardiac hypertrophy. *Proc. Natl. Acad. Sci. U.S.A.* **103**, 7432–7437 (2006).

262. Liu, F., Fan, L. M., Geng, L. & Li, J. p47phox-Dependent Oxidant Signalling through ASK1, MKK3/6 and MAPKs in Angiotensin II-Induced Cardiac Hypertrophy and Apoptosis. *Antioxidants* **10**, 1363 (2021).

263. Grieve, D. J. *et al.* Involvement of the nicotinamide adenosine dinucleotide phosphate oxidase isoform Nox2 in cardiac contractile dysfunction occurring in response to pressure overload. *J. Am. Coll. Cardiol.* **47**, 817–826 (2006).

264. Maytin, M. *et al.* Pressure Overload-Induced Myocardial Hypertrophy in Mice Does Not Require gp91phox. *Circulation* **109**, 1168–1171 (2004).

265. Byrne, J. A. *et al.* Contrasting Roles of NADPH Oxidase Isoforms in Pressure-Overload Versus Angiotensin II-Induced Cardiac Hypertrophy. *Circ. Res.* **93**, 802–804 (2003).

266. Somanna, N. K. *et al.* The Nox1/4 dual inhibitor GKT137831 or Nox4 knockdown inhibits Angiotensin-II-induced adult mouse cardiac fibroblast proliferation and migration. AT1 physically associates with Nox4. *J. Cell. Physiol.* **231**, 1130–1141 (2016).

267. Cucoranu, I. *et al.* NAD(P)H oxidase 4 mediates transforming growth factor-β1-induced differentiation of cardiac fibroblasts into myofibroblasts. *Circ. Res.* **97**, 900–907 (2005).

268. Zhang, M. *et al.* NADPH oxidase-4 mediates protection against chronic load-induced

stress in mouse hearts by enhancing angiogenesis. *Proc. Natl. Acad. Sci. U.S.A.* **107**, 18121–18126 (2010).

269. Wang, M. *et al.* Endothelial NADPH oxidase 4 protects against angiotensin II-induced cardiac fibrosis and inflammation. *ESC Hear. Fail.* **8**, 1427–1437 (2021).

270. Pimentel, D. R. *et al.* Strain-stimulated hypertrophy in cardiac myocytes is mediated by reactive oxygen species-dependent Ras S-glutathiolation. *J. Mol. Cell. Cardiol.* **41**, 613–622 (2006).

271. Kuster, G. M. *et al.* A-Adrenergic Receptor-Stimulated Hypertrophy in Adult Rat Ventricular Myocytes Is Mediated Via Thioredoxin-1-Sensitive Oxidative Modification of Thiols on Ras. *Circulation* **111**, 1192–1198 (2005).

272. Shih, N. L. *et al.* Reactive oxygen species modulate angiotensin II-induced β-myosin heavy chain gene expression via Ras/Raf/extracellular signal-regulated kinase pathway in neonatal rat cardiomyocytes. *Biochem. Biophys. Res. Commun.* **283**, 143–148 (2001).

273. Hirotani, S. *et al.* Involvement of nuclear factor-κB and apoptosis signal-regulating kinase 1 in G-protein-coupled receptor agonist-induced cardiomyocyte hypertrophy. *Circulation* **105**, 509–515 (2002).

274. Li, J. M., Gall, N. P., Grieve, D. J., Chen, M. & Shah, A. M. Activation of NADPH oxidase during progression of cardiac hypertrophy to failure. *Hypertension* **40**, 477–484 (2002).

275. Izumiya, Y. *et al.* Apoptosis Signal-Regulating Kinase 1 Plays a Pivotal Role in Angiotensin II-Induced Cardiac Hypertrophy and Remodeling. *Circ. Res.* **93**, 874–883 (2003).

276. Heusch, P. *et al.* The contribution of reactive oxygen species and p38 mitogen-activated protein kinase to myofilament oxidation and progression of heart failure in rabbits. *Br. J. Pharmacol.* **160**, 1408–1416 (2010).

277. Widder, J. *et al.* Vascular endothelial dysfunction and superoxide anion production in heart failure are p38 MAP kinase-dependent. *Cardiovasc. Res.* **63**, 161–167 (2004).

278. Bao, W. *et al.* Effects of p38 MAPK inhibitor on angiotensin II-dependent hypertension, organ damage, and superoxide anion production. *J. Cardiovasc. Pharmacol.* **49**, 362–368 (2007).

279. Huang, C. Y. & Tan, T. H. DUSPs, to MAP kinases and beyond. *Cell Biosci.* **2**, 24 (2012).

280. Bermudez, O., Pagès, G. & Gimond, C. The dual-specificity MAP kinase phosphatases: Critical roles in development and cancer. *Am. J. Physiol. Cell Physiol.* **299**, C189–C202 (2010).

281. Junttila, M. R., Li, S. & Westermarck, J. Phosphatase-mediated crosstalk between MAPK signaling pathways in the regulation of cell survival. *FASEB J.* **22**, 954–965 (2007).

282. Kidger, A. M., Sipthorp, J. & Cook, S. J. ERK1/2 inhibitors: New weapons to inhibit the RAS-regulated RAF-MEK1/2-ERK1/2 pathway. *Pharmacol. Ther.* **187**, 45–60 (2018).

283. Gao, P. P. *et al.* The emerging roles of dual-specificity phosphatases and their specific characteristics in human cancer. *Biochim. Biophys. Acta - Rev. Cancer* **1876**, 188562 (2021).

284. Lang, R. & Raffi, F. A. M. Dual-specificity phosphatases in immunity and infection: An update. *Int. J. Mol. Sci.* **20**, 2710 (2019).

285. Liu, R. & Molkentin, J. D. Regulation of cardiac hypertrophy and remodeling through the dual-specificity MAPK phosphatases (DUSPs). *J. Mol. Cell. Cardiol.* **101**, 44–49 (2016).

286. Chang, S. C., Ren, S., Rau, C. D. & Wang, J. J. Isoproterenol-Induced Heart Failure Mouse Model Using Osmotic Pump Implantation. *Methods Mol. Biol.* **1816**, 207–220 (2018).

287. Alonso, A. & Pulido, R. The extended human PTPome: A growing tyrosine phosphatase family. *FEBS J.* **283**, 1404–1429 (2016).

288. Caunt, C. J. & Keyse, S. M. Dual-specificity MAP kinase phosphatases (MKPs): Shaping the outcome of MAP kinase signalling. *FEBS J.* **280**, 489–504 (2013).

289. Chen, H. F., Chuang, H. C. & Tan, T. H. Regulation of dual-specificity phosphatase (Dusp) ubiquitination and protein stability. *Int. J. Mol. Sci.* **20**, 2668 (2019).

290. Liu, R. *et al.* DUSP8 Regulates Cardiac Ventricular Remodeling by Altering ERK1/2 Signaling. *Circ. Res.* **119**, 249 (2016).

291. Liu, R. *et al.* Mice lacking DUSP6/8 have enhanced ERK1/2 activity and resistance to diet-induced obesity. *Biochem. Biophys. Res. Commun.* **533**, 17–22 (2020).

292. Mutlak, M. & Kehat, I. Dual specific phosphatases (DUSPs) in cardiac hypertrophy and failure. *Cell. Signal.* **84**, 110033 (2021).

293. Thul, P. J. *et al.* A subcellular map of the human proteome. *Science* **356**, 820 (2017).

294. Proteinatlas.org. DUSP16. *Human Protein Atlas* https://www.proteinatlas.org/ENSG00000111266-DUSP16/subcellular.

295. Schott, J., Reitter, S., Philipp, J., Haneke, K. & Scha, H. Translational Regulation of Specific mRNAs Controls Feedback Inhibition and Survival during Macrophage Activation. *PLOS Genet.* **10**, e1004368 (2014).

296. Jurek, A., Amagasaki, K., Gembarska, A., Heldin, C. H. & Lennartsson, J. Negative and positive regulation of MAPK phosphatase 3 controls platelet-derived growth factor-induced Erk activation. *J. Biol. Chem.* **284**, 4626–4634 (2009).

297. Kucharska, A., Rushworth, L. K., Staples, C., Morrice, N. A. & Keyse, S. M. Regulation of the inducible nuclear dual-specificity phosphatase DUSP5 by ERK MAPK. *Cell. Signal.* **21**, 1794–1805 (2009).

298. Brondello, J. M., Pouysségur, J. & McKenzie, F. R. Reduced MAP kinase phosphatase-1 degradation after p42/p44(MAPK)- dependent phosphorylation. *Science* **286**, 2514–2517 (1999).

299. Crowell, S. *et al.* Post-translational Regulation of Mitogen-activated Protein Kinase Phosphatase (MKP)-1 and MKP-2 in Macrophages Following Lipopolysaccharide Stimulation. *J. Biol. Chem.* **289**, 28753–28764 (2014).

300. Benavides-Serrato, A. *et al.* mTORC2 modulates feedback regulation of p38 MAPK activity via DUSP10/MKP5 to confer differential responses to PP242 in glioblastoma. *Genes and Cancer* **5**, 393–406 (2014).

301. Masuda, K., Shima, H., Katagiri, C. & Kikuchi, K. Activation of ERK induces phosphorylation of MAPK phosphatase-7, a JNK specific phosphatase, at Ser-446. *J. Biol. Chem.* **278**, 32448–32456 (2003).

302. Katagiri, C. *et al.* Phosphorylation of Ser-446 determines stability of MKP-7. *J. Biol. Chem.* **280**, 14716–14722 (2005).

303. Lin, Y., Chuang, S. & Yang, J. ERK1/2 Achieves Sustained Activation by Stimulating MAPK Phosphatase-1 Degradation via the Ubiquitin-Proteasome Pathway. *J. Biol. Chem.* **278**, 21534–21541 (2003).

304. Lin, Y. & Yang, J. Cooperation of ERK and SCF Skp2 for MKP-1 Destruction Provides a Positive Feedback Regulation of Proliferating Signaling. *J. Biol. Chem.* **281**, 915–926 (2006).

305. Marchetti, S. *et al.* Extracellular Signal-Regulated Kinases Phosphorylate Mitogen-Activated Protein Kinase Phosphatase 3/DUSP6 at Serines 159 and 197, Two Sites Critical for Its Proteasomal Degradation. *Mol. Cell. Biol.* **25**, 854–864 (2005).

306. Rechsteiner, M. & Rogers, S. W. PEST sequences and regulation by proteolysis. *Trends Biochem. Sci.* **21**, 267–271 (1996).

307. Kamata, H. *et al.* Reactive Oxygen Species Promote TNFalpha-Induced Death and Sustained JNK Activation by Inhibiting MAP Kinase Phosphatases. *Cell* **120**, 649–661 (2005).

308. Kim, H. S., Ullevig, S. L., Zamora, D., Lee, C. F. & Asmisa, R. Redox regulation of MAPK phosphatase 1 controls monocyte migration and macrophage recruitment.

PNAS **109**, E2803–E2812 (2012).

309. Barajas-Espinosa, A. *et al.* Redox Activation of DUSP4 by N-Acetyl Cysteine Protects Endothelial Cells from Cd2+ -Induced Apoptosis. *Free Radic Biol Med* **74**, 188–199 (2014).

310. Bai, L. *et al.* A Superoxide-Mediated Mitogen-Activated Protein Kinase Phosphatase-1 Degradation and c-Jun NH 2 -Terminal Kinase Activation Pathway for Luteolin-Induced Lung Cancer Cytotoxicity. *Mol. Pharmacol.* **81**, 549–555 (2012).

311. Choi, B. H., Hur, E. M., Lee, J. H., Jun, D. J. & Kim, K. T. Protein kinase Cδ-mediated proteasomal degradation of MAP kinase phosphatase-1 contributes to glutamate-induced neuronal cell death. *J. Cell Sci.* **119**, 1329–1340 (2006).

312. Zhou, J. *et al.* ROS-mediated Different Homeostasis of Murine Corneal Epithelial Progenitor Cell Line under Oxidative Stress. *Sci. Rep.* **6**, 36481 (2016).

313. Li, G. *et al.* SPOP promotes tumorigenesis by acting as a key regulatory hub in kidney cancer. *Cancer Cell* **25**, 455–468 (2014).

314. Mandl, M., Slack, D. N. & Keyse, S. M. Specific Inactivation and Nuclear Anchoring of Extracellular Signal-Regulated Kinase 2 by the Inducible Dual-Specificity Protein Phosphatase DUSP5. *Mol. Cell. Biol.* **25**, 1830–1845 (2005).

315. Masuda, K. *et al.* MKP-7, a JNK phosphatase, blocks ERK-dependent gene activation by anchoring phosphorylated ERK in the cytoplasm. *Biochem. Biophys. Res. Commun.* **393**, 201–206 (2010).

316. Kidger, A. M. *et al.* Dual-specificity phosphatase 5 controls the localized inhibition, propagation, and transforming potential of ERK signaling. *Proc. Natl. Acad. Sci. U.S.A.* **114**, E317–E326 (2017).

317. Cornell, T. T., Rodenhouse, P., Cai, Q., Sun, L. & Shanley, T. P. Mitogen-activated protein kinase phosphatase 2 regulates the inflammatory response in sepsis. *Infect. Immun.* **78**, 2868–2876 (2010).

318. Jeffrey, K. L. *et al.* Positive regulation of immune cell function and inflammatory responses by phosphatase PAC-1. *Nat. Immunol.* **7**, 274–283 (2006).

319. Finch, A. R., Caunt, C. J., Perrett, R. M., Tsaneva-Atanasova, K. & McArdle, C. A. Dual specificity phosphatases 10 and 16 are positive regulators of EGF-stimulated ERK activity: Indirect regulation of ERK signals by JNK/p38 selective MAPK phosphatases. *Cell. Signal.* **24**, 1002–1011 (2012).

320. Zhang, Y. *et al.* Regulation of innate and adaptive immune responses by MAP kinase phosphatase 5. *Nature* **430**, 793–797 (2004).

321. Auger-Messier, M. *et al.* Unrestrained p38 MAPK activation in Dusp1/4 double-null mice induces cardiomyopathy. *Circ. Res.* **112**, 48–56 (2013).

322. Communal, C. *et al.* Reciprocal modulation of mitogen-activated protein kinases and mitogen-activated protein kinase phosphatase 1 and 2 in failing human myocardium. *J. Card. Fail.* **8**, 86–92 (2002).

323. Zhong, C. *et al.* MAP Kinase Phosphatase-5 Deficiency Protects Against Pressure Overload-Induced Cardiac Fibrosis. *Front. Immunol.* **12**, 790511 (2021).

324. Tao, H. *et al.* Long noncoding RNA H19 controls DUSP5/ERK1/2 axis in cardiac fibroblast proliferation and fibrosis. *Cardiovasc. Pathol.* **25**, 381–389 (2016).

325. Ferguson, B. S. *et al.* Signal-dependent repression of DUSP5 by class I HDACs controls nuclear ERK activity and cardiomyocyte hypertrophy. *Proc. Natl. Acad. Sci. U.S.A.* **110**, 9806–9811 (2013).

326. Missinato, M. A. *et al.* Dusp6 attenuates Ras/MAPK signaling to limit zebrafish heart regeneration. *Dev.* **145**, dev157206 (2018).

327. Bueno, O. F. *et al.* The dual-specificity phosphatase MKP-1 limits the cardiac hypertrophic response in vitro and in vivo. *Circ. Res.* **88**, 88–96 (2001).

328. Choi, J. C. *et al.* Dual specificity phosphatase 4 mediates cardiomyopathy caused by lamin A/C (LMNA) gene mutation. *J. Biol. Chem.* **287**, 40513–40524 (2012).

329. Maillet, M. *et al.* DUSP6 (MKP3) null mice show enhanced ERK1/2 phosphorylation at baseline and increased myocyte proliferation in the heart affecting disease susceptibility. *J. Biol. Chem.* **283**, 31246–31255 (2008).

330. Glennon, P. E. *et al.* Depletion of Mitogen-Activated Protein Kinase Using an Antisense Oligodeoxynucleotide Approach Downregulates the Phenylephrine-Induced Hypertrophic Response in Rat Cardiac Myocytes. *Circ. Res.* **78**, 954–961 (1996).

331. Siddiqui, R. A., Shaikh, S. R., Kovacs, R., Stillwell, W. & Zaloga, G. Inhibition of phenylephrine-induced cardiac hypertrophy by docosahexaenoic acid. *J. Cell. Biochem.* **92**, 1141–1159 (2004).

332. Leri, A., Marcello Rota, Pasqualini, F. S., Goichberg, P. & Anversa, P. Origin of Cardiomyocytes in the Adult Heart. *Circ. Res.* **116**, 150–166 (2016).

333. Liu, J., Yin, Y., Ni, J., Zhang, P. & Liu, Z. Dual Specific Phosphatase 7 Exacerbates Dilated Cardiomyopathy , Heart Failure , and Cardiac Death by Inactivating the ERK1/2 Signaling Pathway. *J. Cardiovasc. Transl. Res.* **15**, 1219–1238 (2022).

334. Muda, M. *et al.* Molecular Cloning and Functional Characterization of a Novel Mitogen-activated Protein Kinase Phosphatase, MKP-4. *J. Biol. Chem.* **272**, 5141–5151 (1997).

335. Jiang, L. *et al.* Dual-specificity Phosphatase 9 protects against Cardiac Hypertrophy by targeting ASK1. *Int. J. Biol. Sci.* **17**, 2193–2204 (2021).

336. Christie, G. R. *et al.* The Dual-Specificity Protein Phosphatase DUSP9/MKP-4 Is Essential for Placental Function but Is Not Required for Normal Embryonic Development. *Mol. Cell. Biol.* **25**, 8323–8333 (2005).

337. Ashraf, S., Hegazy, Y. K. & Harmancey, R. Nuclear receptor subfamily 4 group A member 2 inhibits activation of ERK signaling and cell growth in response to β-adrenergic stimulation in adult rat cardiomyocytes. *Am. J. Physiol. Cell Physiol.* **317**, C513–C524 (2019).

338. Bogush, N. *et al.* DUSP5 expression in left ventricular cardiomyocytes of young hearts regulates thyroid hormone (T3)-induced proliferative ERK1/2 signaling. *Sci. Rep.* **10**, 21918 (2020).

339. Niedzielska, M. *et al.* Gene trap mice reveal an essential function of dual specificity phosphatase Dusp16/MKP-7 in perinatal survival and regulation of toll-like receptor (TLR)-induced cytokine production. *J. Biol. Chem.* **289**, 2112–2126 (2014).

340. Corre, I., Paris, F. & Huot, J. The p38 pathway, a major pleiotropic cascade that transduces stress and metastatic signals in endothelial cells. *Oncotarget* **8**, 55684–55714 (2017).

341. Erdfelder, E., FAul, F., Buchner, A. & Lang, A. G. Statistical power analyses using G*Power 3.1: Tests for correlation and regression analyses. *Behav. Res. Methods* **41**, 1149–1160 (2009).

342. Schindelin, J. *et al.* Fiji: An open-source platform for biological-image analysis. *Nat. Methods* **9**, 676–682 (2012).

343. Crowe, A. & Yue, W. Semi-quantitative Determination of Protein Expression Using Immunohistochemistry Staining and Analysis: An Integrated Protocol. *Bio-Protocol* **9**, e3465 (2019).

344. Livak, K. J. & Schmittgen, T. D. Analysis of Relative Gene Expression Data Using Real-Time Quantitative PCR and the 2−ΔΔCT Method. *Methods* **25**, 402–408 (2001).

345. Pick, E. Cell-Free NADPH Oxidase Activation Assays: A Triumph of Reductionism. in *Neutrophil: Methods and Protocols* (eds. Quinn, M. T. & DeLeo, F. R.) 660–663 (Springer Protocols, 2016).

346. O'Connell, T. D., Rodrigo, M. C. & Simpson, P. C. Isolation and Culture of Adult Mouse Cardiac Myocytes. *Cardiovasc. Proteomics* **357**, 271–296 (2007).

347. Fickling, S. A., Tooze, J. A. & Whitley, G. S. J. Characterization of human umbilical vein endothelial cell lines produced by transfection with the early region of SV40. *Exp. Cell Res.* **201**, 517–521 (1992).

348. Rogers, N. M., Zhang, Z. J., Wang, J. J., Thomson, A. W. & Isenberg, J. S. CD47 regulates renal tubular epithelial cell self-renewal and proliferation following renal

ischemia reperfusion. *Kidney Int.* **90**, 334–347 (2016).

349. Rogers, N. M., Sharifi-Sanjani, M., Csányi, G., Pagano, P. J. & Isenberg, J. S. Thrombospondin-1 and CD47 regulation of cardiac, pulmonary and vascular responses in health and disease. *Matrix Biol.* **37**, 92–101 (2014).

350. Julovi, S. M. *et al.* Blocking thrombospondin-1 signaling via CD47 mitigates renal interstitial fibrosis. *Lab. Investig.* **100**, 1184–1196 (2020).

351. Schroen, B. *et al.* Thrombospondin-2 is essential for myocardial matrix integrity: Increased expression identifies failure-prone cardiac hypertrophy. *Circ. Res.* **95**, 515–522 (2004).

352. Wang, D. *et al.* Effects of pressure overload on extracellular matrix expression in the heart of the atrial natriuretic peptide-null mouse. *Hypertension* **42**, 88–95 (2003).

353. Bauer, P. M. *et al.* Activated CD47 promotes pulmonary arterial hypertension through targeting caveolin-1. *Cardiovasc. Res.* **93**, 682–693 (2012).

354. Kojima, Y. *et al.* CD47-blocking antibodies restore phagocytosis and prevent atherosclerosis. *Nature* **536**, 86–90 (2016).

355. Zhang, S. *et al.* Acute CD47 Blockade During Ischemic Myocardial Reperfusion Enhances Phagocytosis-Associated Cardiac Repair. *JACC Basic to Transl. Sci.* **2**, 386–397 (2017).

356. Tipton, A. J., Baban, B. & Sullivan, J. C. Female SHR Have a Compensatory Increase in Renal Regulatory T Cells in Response to Elevations in Blood Pressure. *Hypertension* **64**, 557–564 (2014).

357. Simmonds, S. J., Cuijpers, I., Heymans, S. & Jones, E. A. V. Cellular and Molecular Differences between HFpEF and HFrEF: A Step Ahead in an Improved Pathological Understanding. *Cells* **9**, 242 (2020).

358. Zeng, C. *et al.* NLRP3 inflammasome-mediated pyroptosis contributes to the pathogenesis of non-ischemic dilated cardiomyopathy. *Redox Biol.* **34**, 101523 (2020).

359. Welch, W. J. *et al.* Role of extracellular superoxide dismutase in the mouse angiotensin slow pressor response. *Hypertension* **48**, 934–941 (2006).

360. Haggerty, C. M. *et al.* Telemetric blood pressure assessment in angiotensin II-Infused ApoE-/- Mice: 28 day natural history and comparison to tail-cuff measurements. *PLoS One* **10**, e0130723. (2015).

361. Westermann, D. *et al.* Selective PDE5A inhibition with sildenafil rescues left ventricular dysfunction, inflammatory immune response and cardiac remodeling in angiotensin II-induced heart failure in vivo. *Basic Res. Cardiol.* **107**, 308 (2012).

362. Regan, J. A. *et al.* A mouse model of heart failure with preserved ejection fraction due

to chronic infusion of a low subpressor dose of angiotensin II. *Am. J. Physiol. Circ. Physiol.* **309**, H771–H778 (2015).

363. Takimoto, E. & Kass, D. A. Role of oxidative stress in cardiac hypertrophy and remodeling. *Hypertension* **49**, 241–248 (2007).

364. Paik, Y. H. *et al.* The Nicotinamide Adenine Dinucleotide Phosphate Oxidase Homologues NOX1 and NOX2/gp91phox Mediate Hepatic Fibrosis in Mice. *Hepatology* **53**, 1730–1741 (2011).

365. Hecker, L. *et al.* NADPH Oxidase-4 Mediates Myofibroblast Activation and Fibrogenic Responses to Lung Injury. *Nat. Med.* **15**, 1077–1081 (2009).

366. Mittal, M., Siddiqui, M. R., Tran, K., Reddy, S. P. & Malik, A. B. Reactive oxygen species in inflammation and tissue injury. *Antioxidants Redox Signal.* **20**, 1126–1167 (2014).

367. Isenberg, J. S. *et al.* Differential interactions of thrombospondin-1, -2, and -4 with CD47 and effects on cGMP signaling and ischemic injury responses. *J. Biol. Chem.* **284**, 1116–1125 (2009).

368. Aoyama, T. *et al.* Nicotinamide adenine dinucleotide phosphate oxidase in experimental liver fibrosis: GKT137831 as a novel potential therapeutic agent. *Hepatology* **56**, 2316–2327 (2012).

369. A Trial of Setanaxib in Patients With Primary Biliary Cholangitis (PBC) and Liver Stiffness (TRANSFORM). *ClinicalTrials.gov* https://clinicaltrials.gov/ct2/show/NCT05014672 (2022).

370. GKT137831 in IPF Patients With Idiopathic Pulmonary Fibrosis (GKT137831). *ClinicalTrials.gov* https://clinicaltrials.gov/ct2/show/study/NCT03865927 (2022).

371. Ranayhossaini, D. J. *et al.* Selective recapitulation of conserved and nonconserved regions of putative NOXA1 protein activation domain confers isoform-specific inhibition of Nox1 oxidase and attenuation of endothelial cell migration. *J. Biol. Chem.* **288**, 36437–36450 (2013).

372. Meijering, E., Dzyubachyk, O. & Smal, I. Methods for cell and particle tracking. *Methods Enzymol.* **504**, 183–200 (2012).

373. James-Allan, L. B., Whitley, G. S., Leslie, K., Wallace, A. E. & Cartwright, J. E. Decidual cell regulation of trophoblast is altered in pregnancies at risk of pre-eclampsia. *J. Mol. Endocrinol.* **60**, 239–246 (2018).

374. Bowers, S. L. K., Borg, T. K. & Baudino, T. A. The dynamics of fibroblast–myocyte–capillary interactions in the heart. *Ann. N. Y. Acad. Sci.* **1188**, 143–152 (2010).

375. de Jesus, D. S. *et al.* Nox1/Ref-1-mediated activation of CREB promotes Gremlin1-driven endothelial cell proliferation and migration. *Redox Biol.* **22**, 101138 (2019).

376. Tamborindeguy, M. T. *et al.* NADPH-oxidase-derived ROS alters cell migration by modulating adhesions dynamics. *Biol. Cell* **110**, 225–236 (2018).

377. Kim, Y. M. *et al.* ROS-induced ROS release orchestrated by Nox4, Nox2, and mitochondria in VEGF signaling and angiogenesis. *Am. J. Physiol. Cell Physiol.* **312**, C749–C764 (2017).

378. Ghimire, K. *et al.* CD47 Promotes Age-Associated Deterioration in Angiogenesis, Blood Flow and Glucose Homeostasis. *Cells* **9**, 1695 (2020).

379. Wilson, K. E., Li, Z., Kara, M., Gardner, K. L. & Roberts, D. D. β1 Integrin- and Proteoglycan-Mediated Stimulation of T Lymphoma Cell Adhesion and Mitogen-Activated Protein Kinase Signaling by Thrombospondin-1 and Thrombospondin-1 Peptides. *J. Immunol.* **163**, 3621–3628 (1999).

380. Miller, T. W., Kaur, S., Ivins-O'Keefe, K. & Roberts, D. D. Thrombospondin-1 is a CD47-dependent endogenous inhibitor of hydrogen sulfide signaling in T cell activation. *Matrix Biol.* **32**, 316–324 (2013).

381. Wang, X. Q., Lindberg, F. P. & Frazier, W. A. Integrin-Associated Protein Stimulates α2β1-Dependent Chemotaxis via GI-Mediated Inhibition of Adenylate Cyclase and Extracellular-Regulated Kinases. *J. Cell Biol.* **147**, 389–400 (1999).

382. Park, G. Bin *et al.* Ligation of CD47 induces G1 arrest in EBV-transformed B cells through ROS generation, p38 MAPK/JNK activation, and Tap73 upregulation. *J. Immunother.* **37**, 309–320 (2014).

383. Li, D.-X., Chen, W., Jiang, Y.-L., Ni, J.-Q. & Lu, L. Antioxidant protein peroxiredoxin 6 suppresses the vascular inflammation, oxidative stress and endothelial dysfunction in angiotensin II-induced endotheliocyte. *Gen. Physiol. Biophys.* **39**, 545–555 (2020).

384. Zhang, X. *et al.* Angiotensin II Upregulates Endothelial Lipase Expression via the NF-Kappa B and MAPK Signaling Pathways. *PLoS One* **9**, e107634 (2014).

385. Fang, L. *et al.* Calcitonin gene-related peptide released from endothelial progenitor cells inhibits the proliferation of rat vascular smooth muscle cells induced by angiotensin II. *Mol. Cell. Biochem.* **355**, 99–108 (2011).

386. Sano, M. *et al.* ERK and p38 MAPK, but not NF-κB, Are Critically Involved in Reactive Oxygen Species–Mediated Induction of IL-6 by Angiotensin II in Cardiac Fibroblasts. *Circ. Res.* **89**, 661–669 (2001).

387. Gu, J. *et al.* Angiotensin II increases CTGF expression via MAPKs/TGF-β1/TRAF6 pathway in atrial fibroblasts. *Exp. Cell Res.* **318**, 2105–2115 (2012).

388. Li, L. *et al.* Angiotensin II increases periostin expression via Ras/p38 MAPK/CREB and ERK1/2/TGF-β1 pathways in cardiac fibroblasts. *Cardiovasc. Res.* **91**, 80–89 (2011).

389. Olson, E. R., Shamhart, P. E., Naugle, J. E. & Meszaros, J. G. Angiotensin II-induced extracellular signal-regulated kinase 1/2 activation is mediated by protein kinase Cδ and intracellular calcium in adult rat cardiac fibroblasts. *Hypertension* **51**, 704–711 (2008).

390. Shen, Y. *et al.* Prostaglandin E1 attenuates AngII-induced cardiac hypertrophy via EP3 receptor activation and Netrin-1upregulation. *J. Mol. Cell. Cardiol.* **159**, 91–104 (2021).

391. Zhang, Y. *et al.* Isorhynchophylline enhances Nrf2 and inhibits MAPK pathway in cardiac hypertrophy. *Naunyn. Schmiedebergs. Arch. Pharmacol.* **393**, 203–212 (2020).

392. Gray, M. O., Long, C. S., Kalinyak, J. E., Li, H. T. & Karliner, J. S. Angiotensin II stimulates cardiac myocyte hypertrophy via paracrine release of TGF-β1 and endothelin-1 from fibroblasts. *Cardiovasc. Res.* **40**, 352–363 (1998).

393. Touyz, R. M. & Briones, A. M. Reactive oxygen species and vascular biology: Implications in human hypertension. *Hypertens. Res.* **34**, 5–14 (2011).

394. Zhao, Q., Zhang, J. & Wang, H. PGC-1α limits angiotensin II-induced rat vascular smooth muscle cells proliferation via attenuating NOX1-mediated generation of reactive oxygen species. *Biosci. Rep.* **35**, e00252 (2015).

395. Fernandes, D. C., Manoel, A. H. O., Wosniak, J. & Laurindo, F. R. Protein disulfide isomerase overexpression in vascular smooth muscle cells induces spontaneous preemptive NADPH oxidase activation and Nox1 mRNA expression: Effects of nitrosothiol exposure. *Arch. Biochem. Biophys.* **484**, 197–204 (2009).

396. Hernanz, R. *et al.* Toll-like receptor 4 contributes to vascular remodelling and endothelial dysfunction in angiotensin II-induced hypertension. *Br. J. Pharmacol.* **172**, 3159–3176 (2015).

397. El-Benna, J., Dang, P. M. C., Gougerot-Pocidalo, M. A., Marie, J. C. & Braut-Boucher, F. p47phox, the phagocyte NADPH oxidase/NOX2 organizer: Structure, phosphorylation and implication in diseases. *Exp. Mol. Med.* **41**, 217–225 (2009).

398. Cat, A. N. D., Montezano, A. C., Burger, D. & Touyz, R. M. Angiotensin II, NADPH Oxidase, and Redox Signaling in the Vasculature. *Antioxid. Redox Signal.* **19**, 1110–1120 (2013).

399. Xie, Z. *et al.* Regulation of angiotensin II-stimulated osteopontin expression in cardiac microvascular endothelial cells: Role of p42/44 mitogen-activated protein kinase and reactive oxygen species. *J. Cell. Physiol.* **188**, 132–138 (2001).

400. Thakur, S., Du, J., Hourani, S., Ledent, C. & Li, J. M. Inactivation of adenosine A2A receptor attenuates basal and angiotensin II-induced ROS production by Nox2 in endothelial cells. *J. Biol. Chem.* **285**, 40104–40113 (2010).

401. Lother, A. *et al.* Cardiac endothelial cell transcriptome. *Arterioscler. Thromb. Vasc. Biol.* **38**, 566–574 (2018).

402. Gao, Q., Chen, K., Gao, L., Zheng, Y. & Yang, Y. G. Thrombospondin-1 signaling through CD47 inhibits cell cycle progression and induces senescence in endothelial cells. *Cell Death Dis.* **7**, e2368 (2016).

403. Kaur, S. *et al.* Thrombospondin-1 signaling through CD47 inhibits self-renewal by regulating c-Myc and other stem cell transcription factors. *Sci. Rep.* **3**, 1673 (2013).

404. Yamauchi, M., Imajoh-ohmi, S. & Shibuya, M. Novel antiangiogenic pathway of thrombospondin-1 mediated by suppression of the cell cycle. *Cancer Sci.* **98**, 1491–1497 (2007).

405. Lawler, P. R. & Lawler, J. Molecular Basis for the Regulation of Angiogenesis by Thrombospondin-1 and-2. *Cold Spring Harb. Perspect. Med.* **2**, a006627 (2012).

406. Jiménez, B. *et al.* Signals leading to apoptosis-dependent inhibition of neovascularization by thrombospondin-1. *Nat. Med.* **6**, 41–48 (2000).

407. Xing, C. *et al.* Role of oxidative stress and caspase 3 in CD47-mediated neuronal cell death. *J. Neurochem.* **108**, 430–436 (2009).

408. Xing, C. *et al.* Neurovascular Effects of CD47 Signaling: Promotion of Cell Death, Inflammation, and Suppression of Angiogenesis in Brain Endothelial Cells In Vitro. *J. Neurosci. Res.* **87**, 2571–2577 (2009).

409. Freyberg, M. A., Kaiser, D., Graf, R., Buttenbender, J. & Friedl, P. Proatherogenic flow conditions initiate endothelial apoptosis via thrombospondin-1 and the integrin-associated protein. *Biochem. Biophys. Res. Commun.* **286**, 141–149 (2001).

410. Bellamy, L. M., Johnston, A. P. W., De Lisio, M. & Parise, G. Skeletal muscle-endothelial cell cross talk through angiotensin II. *Am. J. Physiol. Cell Physiol.* **299**, 1402–1408 (2010).

411. Rossi, F., Bertone, C., Petricca, S. & Santiemma, V. Ghrelin inhibits angiotensin II-induced migration of human aortic endothelial cells. *Atherosclerosis* **192**, 291–297 (2007).

412. Lin, Q. Y., Bai, J., Liu, J. Q. & Li, H. H. Angiotensin II Stimulates the Proliferation and Migration of Lymphatic Endothelial Cells Through Angiotensin Type 1 Receptors. *Front. Physiol.* **11**, 560170 (2020).

413. Carbajo-Lozoya, J. *et al.* Angiotensin II modulates VEGF-driven angiogenesis by opposing effects of type 1 and type 2 receptor stimulation in the microvascular endothelium. *Cell. Signal.* **24**, 1261–1269 (2012).

414. Desideri, G. *et al.* Angiotensin II inhibits endothelial cell motility through an AT1-dependent oxidant-sensitive decrement of nitric oxide availability. *Arterioscler.*

Thromb. Vasc. Biol. **23**, 1218–1223 (2003).

415. Benndorf, R., Böger, R. H., Ergün, S., Steenpass, A. & Wieland, T. Angiotensin II type 2 receptor inhibits vascular endothelial growth factor-induced migration and in vitro tube formation of human endothelial cells. *Circ. Res.* **93**, 438–447 (2003).

416. Hurd, T. R., DeGennaro, M. & Lehmann, R. Redox regulation of cell migration and adhesion. *Trends Cell Biol.* **22**, 107–115 (2012).

417. Zimmerman, M. C. *et al.* Activation of NADPH Oxidase 1 Increases Intracellular Calcium and Migration of Smooth Muscle Cells. *Hypertension* **58**, 446–453 (2011).

418. Schröder, K. *et al.* Nox1 mediates basic fibroblast growth factor-induced migration of vascular smooth muscle cells. *Arterioscler. Thromb. Vasc. Biol.* **27**, 1736–1743 (2007).

419. Garrido-Urbani, S., Jemelin, S., Deffert, C., Carnesecchi, S. & Basset, O. Targeting Vascular NADPH Oxidase 1 Blocks Tumor Angiogenesis through a PPARa Mediated Mechanism. *PLoS One* **6**, e14665 (2011).

420. Li, Y. *et al.* Forestalling age-impaired angiogenesis and blood flow by targeting NOX: Interplay of NOX1, IL-6, and SASP in propagating cell senescence. *Proc. Natl. Acad. Sci. U.S.A.* **118**, e2015666118 (2021).

421. Rege, T. A. *et al.* Thrombospondin-1-induced apoptosis of brain microvascular endothelial cells can be mediated by TNF-R1. *J. Cell. Physiol.* **218**, 94–103 (2009).

422. Kobayashi, S., Nojima, Y., Shibuya, M. & Maru, Y. Nox1 regulates apoptosis and potentially stimulates branching morphogenesis in sinusoidal endothelial cells. *Exp. Cell Res.* **300**, 455–462 (2004).

423. Carnesecchi, S. *et al.* NADPH Oxidase-1 Plays a Crucial Role in Hyperoxia-induced Acute Lung Injury in Mice. *Am. J. Respir. Crit. Care Med.* **180**, 972–981 (2009).

424. Turner, N. A. & Blythe, N. M. Cardiac fibroblast p38 MAPK: A critical regulator of myocardial remodeling. *J. Cardiovasc. Dev. Dis.* **6**, 27 (2019).

425. Shvedova, M., Anfinogenova, Y., Atochina-Vasserman, E. N., Schepetkin, I. A. & Atochin, D. N. c-Jun N-terminal kinases (JNKs) in myocardial and cerebral ischemia/reperfusion injury. *Front. Pharmacol.* **9**, 715 (2018).

426. Meijles, D. N. *et al.* The anti-cancer drug dabrafenib is not cardiotoxic and inhibits cardiac remodelling and fibrosis in a murine model of hypertension. *Clin. Sci.* **135**, 1631–1647 (2021).

427. Hayashida, W. *et al.* Stage-specific Differential Activation of Mitogen-activated Protein Kinases in Hypertrophied and Failing Rat Hearts. *J Mol Cell Cardiol* **33**, 733–744 (2001).

428. Lemke, L. E. *et al.* Decreased p38 MAPK activity in end-stage failing human

myocardium: p38 MAPK α is the predominant isoform expressed in human heart. *J. Mol. Cell. Cardiol.* **33**, 1527–1540 (2001).

429. Behr, T. M. *et al.* Hypertensive end-organ damage and premature mortality are p38 mitogen-activated protein kinase-dependent in a rat model of cardiac hypertrophy and dysfunction. *Circulation* **104**, 1292–1298 (2001).

430. Esposito, G. *et al.* Induction of mitogen-activated protein kinases is proportional to the amount of pressure overload. *Hypertension* **55**, 137–143 (2010).

431. Pellieux, C., Sauthier, T., Aubert, J. F., Brunner, H. R. & Pedrazzini, T. Angiotensin II-induced cardiac hypertrophy is associated with different mitogen-activated protein kinase activation in normotensive and hypertensive mice. *J. Hypertens.* **18**, 1307–1317 (2000).

432. Kidger, A. M. & Keyse, S. M. The regulation of oncogenic Ras/ERK signalling by dual-specificity mitogen activated protein kinase phosphatases (MKPs). *Semin. Cell Dev. Biol.* **50**, 125–132 (2016).

433. Singh, G. B. *et al.* MicroRNA-200c modulates DUSP-1 expression in diabetes-induced cardiac hypertrophy. *Mol. Cell. Biochem.* **424**, 1–11 (2017).

434. Fischer, T. A., Singh, K., O'Hara, D. S., Kaye, D. M. & Kelly, R. A. Role of AT1 and AT2 receptors in regulation of MAPKS and MKP-1 by ANG II in adult cardiac myocytes. *Am. J. Physiol. Hear. Circ. Physiol.* **275**, H906-h916 (1998).

435. Echavarria, R. & Hussain, S. N. A. Regulation of Angiopoietin-1/Tie-2 Receptor Signaling in Endothelial Cells by Dual-Specificity Phosphatases 1, 4, and 5. *J. Am. Hear. Assoc. Cardiovasc. Cerebrovasc. Dis.* **2**, e000571 (2013).

436. Bellou, S. *et al.* VEGF autoregulates its proliferative and migratory ERK1/2 and p38 cascades by enhancing the expression of DUSP1 and DUSP5 phosphatases in endothelial cells. *Am. J. Physiol. Cell Physiol.* **297**, C1477–C1489 (2009).

437. Hsu, S.-F. *et al.* Dual specificity phosphatase DUSP6 promotes endothelial inflammation through inducible expression of ICAM-1. *FEBS J.* **285**, 1593–1610 (2018).

438. Yang, D., Xie, P. & Liu, Z. Ischemia/reperfusion-induced MKP-3 impairs endothelial no formation via inactivation of ERK1/2 pathway. *PLoS One* **7**, e42076 (2012).

439. Ding, T. *et al.* Antisense Oligonucleotides against miR-21 Inhibit the Growth and Metastasis of Colorectal Carcinoma via the DUSP8 Pathway. *Mol. Ther. - Nucleic Acids* **13**, 244–255 (2018).

440. Gao, L. *et al.* MicroRNA-21 deficiency attenuated atherogenesis and decreased macrophage infiltration by targeting Dusp-8. *Atherosclerosis* **291**, 78–86 (2019).

441. Nizamutdinova, I. T., Kim, Y. M., Lee, J. H., Chang, K. C. & Kim, H. J. MKP-7, a

negative regulator of JNK, regulates VCAM-1 expression through IRF-1. *Cell. Signal.* **24**, 866–872 (2012).

442. Low, H. B. *et al.* DUSP16 promotes cancer chemoresistance through regulation of mitochondria-mediated cell death. *Nat. Commun.* **12**, 2284 (2021).

443. Zhang, H. *et al.* DUSP16 ablation arrests the cell cycle and induces cellular senescence. *FEBS J.* **282**, 4580–4594 (2015).

444. Seifert, A., Taubert, H., Hombach-Klonisch, S., Fischer, B. & Santos, A. N. TCDD mediates inhibition of p53 and activation of ERα signaling in MCF-7 cells at moderate hypoxic conditions. *Int. J. Oncol.* **35**, 417–424 (2009).

445. Lin, W.-N. *et al.* Involvement of MAPKs and NF-κB in LPS-induced VCAM-1 expression in human tracheal smooth muscle cells. *Cell. Signal.* **19**, 1258–1267 (2007).

446. Pietersma, A. *et al.* P38 Mitogen Activated Protein Kinase Regulates Endothelial VCAM-1 Expression at the Post-transcriptional Level. *Biochem. Biophys. Res. Commun.* **230**, 44–48 (1997).

447. Gwag, T., Ma, E., Zhou, C. & Wang, S. Anti-CD47 antibody treatment attenuates liver inflammation and fibrosis in experimental non-alcoholic steatohepatitis models. *Liver Int.* **42**, 829–841 (2022).

448. Cui, W., Maimaitiyiming, H., Qi, X., Norman, H. & Wang, S. Thrombospondin 1 mediates renal dysfunction in a mouse model of high-fat diet-induced obesity. *Am. J. Physiol. Ren. Physiol.* **305**, 871–880 (2013).

449. Rogers, N. M. *et al.* TSP1-CD47 signaling is upregulated in clinical pulmonary hypertension and contributes to pulmonary arterial vasculopathy and dysfunction. *Cardiovasc. Res.* **113**, 15–29 (2017).

450. Xu, L. *et al.* NOX1 mediates metabolic heart disease in mice and is upregulated in monocytes of humans with diastolic dysfunction. *Cardiovasc. Res.* **118**, 2973–2984 (2022).

451. Awad, K. S., West, J. D., de Jesus Perez, V. & MacLean, M. Novel signaling pathways in pulmonary arterial hypertension (2015 Grover Conference Series). *Pulm. Circ.* **6**, 285–294 (2016).

452. Ferguson, B. S. *et al.* DUSP5-mediated inhibition of smooth muscle cell proliferation suppresses pulmonary hypertension and right ventricular hypertrophy. *Am. J. Physiol. Hear. Circ. Physiol.* **321**, 382–389 (2021).

453. Chen, L. L. *et al.* Dual-specificity phosphatase (DUSP) genetic variants predict pulmonary hypertension in patients with bronchopulmonary dysplasia. *Pediatr. Res.* **87**, 81–87 (2020).

454. Koliaki, C. *et al.* Adaptation of Hepatic Mitochondrial Function in Humans with Non-Alcoholic Fatty Liver Is Lost in Steatohepatitis. *Cell Metab.* **21**, 739–746 (2015).

455. Ferreira, D. M. S. *et al.* Apoptosis and insulin resistance in liver and peripheral tissues of morbidly obese patients is associated with different stages of non-alcoholic fatty liver disease. *Diabetologia* **54**, 1788–1798 (2011).

456. González-Terán, B. *et al.* p38γ and δ promote heart hypertrophy by targeting the mTOR-inhibitory protein DEPTOR for degradation. *Nat. Commun.* **7**, 10477 (2016).

457. Ye, P. *et al.* Dual-Specificity Phosphatase 9 Protects Against Nonalcoholic Fatty Liver Disease in Mice Through ASK1 Suppression. *Hepatology* **69**, 76–93 (2019).

458. Engelbertsen, D. *et al.* Increased lymphocyte activation and atherosclerosis in CD47-deficient mice. *Sci. Rep.* **9**, 10608 (2019).

459. Wernig, G. *et al.* Unifying mechanism for different fibrotic diseases. *Proc. Natl. Acad. Sci. U.S.A.* **114**, 4757–4762 (2017).

460. Yao, M., Sturdivant, J., Ebrahimi, A., Ganguly, S. & Elbayoumi, T. Novel Pharmaceutical Strategy for Selective Abrogation of TSP1-Induced Vascular Dysfunction by Decoy Recombinant CD47 Soluble Receptor in Prophylaxis and Treatment Models. *Biomedicines* **9**, 642 (2021).

461. Jeanne, A. *et al.* Towards the Therapeutic Use of Thrombospondin 1/CD47 Targeting TAX2 Peptide as an Antithrombotic Agent. *Arterioscler. Thromb. Vasc. Biol.* **41**, E1–E17 (2021).

462. Jiang, Z., Sun, H., Yu, J., Tian, W. & Song, Y. Targeting CD47 for cancer immunotherapy. *J. Hematol. Oncol.* **14**, 180 (2021).

463. Deng, W. *et al.* NADPH oxidase 1/4 inhibition attenuates the portal hypertensive syndrome via modulation of mesenteric angiogenesis and arterial hyporeactivity in rats. *Clin. Res. Hepatol. Gastroenterol.* **43**, 255–265 (2019).

464. Zhang, D. *et al.* NOX1 promotes myocardial fibrosis and cardiac dysfunction via activating the TLR2/NF-κB pathway in diabetic cardiomyopathy. *Front. Pharmacol.* **13**, 928762 (2022).

465. Zeng, S. Y., Yan, Q. J., Yang, L., Mei, Q. H. & Lu, H. Q. Inhibition of the ROS-EGFR Pathway Mediates the Protective Action of Nox1/4 Inhibitor GKT137831 against Hypertensive Cardiac Hypertrophy via Suppressing Cardiac Inflammation and Activation of Akt and ERK1/2. *Mediators Inflamm.* **2020**, 1078365 (2020).

466. Zeng, S. Y. *et al.* Nox1/4 dual inhibitor GKT137831 attenuates hypertensive cardiac remodelling associating with the inhibition of ADAM17-dependent proinflammatory cytokines-induced signalling pathways in the rats with abdominal artery constriction. *Biomed. Pharmacother.* **109**, 1907–1914 (2019).

467. Nosalski, R. *et al.* Nox1/4 inhibition exacerbates age dependent perivascular inflammation and fibrosis in a model of spontaneous hypertension. *Pharmacol. Res.* **161**, 105235 (2020).

468. Zhang, D. *et al.* NOX1 promotes myocardial fi brosis and cardiac dysfunction via activating the TLR2 / NF- κ B pathway in diabetic cardiomyopathy. *Front. Pharmacol.* **13**, 928762. (2022).

469. Korotchenko, V. N. *et al.* In vivo structure-activity relationship studies support allosteric targeting of a dual specificity phosphatase. *Chembiochem* **15**, 1436–1445 (2014).

470. Zandi, Z. *et al.* Dual-specificity phosphatases: therapeutic targets in cancer therapy resistance. *J. Cancer Res. Clin. Oncol.* **148**, 57–70 (2022).

471. Kaltenmeier, C. T. *et al.* A tumor cell-selective inhibitor of mitogen-activated protein kinase phosphatases sensitizes breast cancer cells to lymphokine-activated killer cell activity. *J. Pharmacol. Exp. Ther.* **361**, 39–50 (2017).

472. Neumann, T. S. *et al.* Identification of inhibitors that target dual-specificity phosphatase 5 provide new insights into the binding requirements for the two phosphate pockets. *BMC Biochem.* **16**, 19 (2015).

473. Park, H., Park, S. Y., Nam, S. W. & Ryu, S. E. Discovery of novel DUSP16 phosphatase inhibitors through virtual screening with homology modeled protein structure. *J. Biomol. Screen.* **19**, 1383–1390 (2014).

474. Suvila, K., Langén, V., Cheng, S. & Niiranen, T. J. Age of Hypertension Onset: Overview of Research and How to Apply in Practice. *Curr. Hypertens. Rep.* **22**, 68 (2020).

475. Iorga, A. *et al.* The protective role of estrogen and estrogen receptors in cardiovascular disease and the controversial use of estrogen therapy. *Biol. Sex Differ.* **8**, 33 (2017).

476. Ludwik, K. A. *et al.* RSK2 Maintains Adult Estrogen Homeostasis by Inhibiting ERK1/2-Mediated Degradation of Estrogen Receptor Alpha. *Cell Rep.* **32**, 107931 (2020).

477. Arias-Loza, P. A., Muehlfelder, M. & Pelzer, T. Estrogen and estrogen receptors in cardiovascular oxidative stress. *Pflugers Arch. Eur. J. Physiol.* **465**, 739–746 (2013).

478. Hinzey, A. *et al.* Respiratory Syncytial Virus Represses Glucocorticoid Receptor-Mediated Gene Activation. *Endocrinology* **152**, 483–494 (2011).

479. Su, X. *et al.* Interferon-γ regulates cellular metabolism and mRNA translation to potentiate macrophage activation. *Nat. Immunol.* **16**, 838–849 (2015).

480. Dougherty, J. A., Kilbane Myers, J., Khan, M., Angelos, M. G. & Chen, C. A. Dual-

Specificity Phosphatase 4 Overexpression in Cells Prevents Hypoxia/Reoxygenation-Induced Apoptosis via the Upregulation of eNOS. *Front. Cardiovasc. Med.* **4**, 22 (2017).

481. Buffet, C. *et al.* DUSP5 and DUSP6, two ERK specific phosphatases, are markers of a higher MAPK signaling activation in BRAF mutated thyroid cancers. *PLoS One* **12**, e0184861 (2017).

482. Yang, W. *et al.* Circ-ABCB10 contributes to paclitaxel resistance in breast cancer through Let-7a-5p/DUSP7 axis. *Cancer Manag. Res.* **12**, 2327–2337 (2020).

483. Buiga, P., Elson, A., Tabernero, L. & Schwartz, J. M. Regulation of dual specificity phosphatases in breast cancer during initial treatment with Herceptin: A Boolean model analysis. *BMC Syst. Biol.* **12**, 11 (2018).

484. Non, L., Duong, D. & Peehl, D. M. Chemopreventive anti-inflammatory activities of curcumin and other phytochemicals mediated by MAP kinase phosphatase-5 in prostate cells. *Carcinogenesis* **28**, 1188–1196 (2007).

485. Lee, S. *et al.* DUSP16 is an epigenetically regulated determinant of JNK signalling in Burkitt's lymphoma. *Br. J. Cancer* **103**, 265–274 (2010).

486. Hirose, J. *et al.* Bone resorption is regulated by cell-autonomous negative feedback loop of Stat5–Dusp axis in the osteoclast. *J. Exp. Med.* **211**, 153–163 (2014).

487. Hamamura, K. *et al.* Salubrinal Acts as a Dusp2 Inhibitor and Suppresses Inflammation in Anti-Collagen Antibody-Induced Arthritis. *Cell. Signal.* **27**, 828–835 (2015).

488. Ogishima, J. *et al.* The oncogene KRAS promotes cancer cell dissemination by stabilizing spheroid formation via the MEK pathway. *BMC Cancer* **18**, 1201 (2018).

489. Giraldo, A. *et al.* Feedback regulation by Atf3 in the endothelin-1-responsive transcriptome of cardiomyocytes: Egr1 is a principal Atf3 target. *Biochem. J.* **444**, 343–355 (2012).

490. Wang, H. *et al.* RNAi-Mediated Down-Regulation of CD47 Protects against Ischemia/Reperfusion-Induced Myocardial Damage via Activation of eNOS in a Rat Model. *Cell. Physiol. Biochem.* **40**, 1163–1174 (2016).

491. Cao, X., Dai, X., Parker, L. M. & Kreulen, D. L. Differential regulation of NADPH oxidase in sympathetic and sensory ganglia in deoxycorticosterone acetate-salt hypertension. *Hypertension* **50**, 663–671 (2007).

492. Fan, L. *et al.* Circular RNA expression profiling and selection of key circular rnas in the hypothalamus of heat-acclimated rats. *Front. Physiol.* **10**, 1112 (2019).

493. Ye, J. *et al.* Primer-BLAST: a tool to design target-specific primers for polymerase chain reaction. *BMC Bioinformatics* **13**, 134 (2012).

Appendix

Appendix Table 1. Demographics of NI-HF samples and controls.

Sample #	Condition	Age	Sex	Race	LVEF	Aetiology
1	NI-HF – 1	66	M	White	10-15%	NI/muscular dystrophy
2	NI-HF – 2	66	F	White	15%	NI
3	NI-HF – 3	66	M	White	10-15%	NI
4	NI-HF – 4	67	M	White	20%	DCM
5	NI-HF – 5	56	M	White	10%	DCM
6	NI-HF – 6	50	M	White	60-65%	Hypertrophic
7	NI-HF – 7	64	F	White	15-20%	NI/mixed
8	NI-HF – 8	67	M	White	10-15%	NI
9	NI-HF – 9	54	M	White	20-25%	NI
10	NI-HF – 10	57	M	Black	19%	NI
11	NI-HF – 11	55	M	White	20-25%	NI
12	NI-HF - 12	48	F	White	65-70%	Hypertrophic
13	Control – 1	56	F	White		
14	Control – 2	39	F	White		
15	Control – 3	49	F	White		
16	Control – 4	68	F	White		
17	Control – 5	36	F	White		
18	Control – 6	47	F	White		
19	Control – 7	59	M	White		
20	Control – 8	37	M	White		
21	Control – 9	28	M	White		
22	Control – 10	43	M	White		
23	Control – 11	65	M	White		
24	Control – 12	65	M	White		

Appendix Table 2. Mouse weights before and after procedure

Mouse #	Treatment	Baseline weight	Post surgery weight	Body weight at end point (24 h)	Body weight at end point (7 d)	Body weight at end point (14 d)	Heart weight at end point	Heart/body weight
1	7 d veh	23	24.6	-	25.4	-	0.1213	4.7756
2	24 h AngII	24.1	24.9	22.9	-	-	0.1236	5.3974
3	7 d AngII	21.7	25.7	-	27.3	-	0.1569	5.7473
4	14 d AngII	24.8	23.2	-	-	26	0.1505	5.7885
5	14 d veh	20.4	20.6	-	-	23.2	0.1086	4.6810
6	7 d veh	24.2	25.3	-	26	-	0.1284	4.9385
7	24 h AngII	19.7	20.7	20.1	-	-	0.1031	5.1294
8	7 d AngII	23.4	24.3	-	25.6	-	0.1401	5.4727
9	14 d AngII	21.6	23	-	-	25.3	0.1417	5.6008
10	14 d veh	23.8	24.7	-	-	26.8	0.133	4.9627
11	7 d veh	23	23.9	-	25.5	-	0.116	4.5490
12	24 h AngII	23.4	24.7	22.5	-	-	0.1439	6.3956
13	7 d AngII	21.7	23.5	-	23.2	-	0.1367	5.8922
14	14 d AngII	23.3	24.1	-	-	26.5	0.144	5.4340
15	14 d veh	24	25.1	-	-	26.4	0.1317	4.9886
16	7 d veh	22.3	23.4	-	24.3	-	0.1062	4.3704
17	24 h AngII	22.9	23.6	22	-	-	0.1247	5.6682
18	7 d AngII	22.9	24.4	-	22.2	-	0.1215	5.4730
19	14 d AngII	20	21.4	-	-	27.2	0.1484	5.4559
20	14 d veh	23.5	24.9	-	-	26.5	0.1374	5.1849
21	7 d veh	23.8	24.8	-	25.7	-	0.1236	4.8093
22	24 h AngII	21.3	22.2	19.7	-	-	0.1135	5.7614
23	7 d AngII	22.7	23.6	-	24.1	-	0.1333	5.5311
24	14 d AngII	20.3	22.1	-	-	25.3	0.1398	5.5257
25	14 d veh	22.7	23.8	-	-	26.4	0.1247	4.7235

Appendix Table 3. Human primer list

Gene	Forward primer (5'-3')	Reverse primer (5'-3')	Reference
GAPDH	GGATTTGGTCGTATTGGG	GGAAGATGGTGATGGGATT	
THBS1	AGACTCCGCATCGCAAAGG	TCACCACGTTGTTGTCAAGGG	
CD47	GATCAGCTCAGCTACTAT	ACAATGACAGTGATCACT	
NOX1	GTTTTACCGCTCCCAGCAGAA	GGATGCCATTCCAGGAGAGAG	
DUSP1	CTGCCTTGATCAACGTCTCA	ACCCTTCCTCCAGCATTCTT	478
DUSP2	TGTGGAGATCTTGCCCTACC	CTCCACCATCTGGTTGTCCT	479
DUSP4	ATTCCGCCGTCATCGTCTAC	ATAGCCACCTTTCAGCAGGC	480
DUSP5	GGAGGCCTTCGATTACATCA	AGGGCTCAGTGTCTGCAAAT	444
DUSP6	TCCCTGAGGCCATTTCTTTCATAGATG	GCAGCTGACCCATGAAGTTGAAGT	481
DUSP7	CCAAGAAGTGTGGTGTCCTG	ACAAAGTCGTAGGCGTCGTT	482
DUSP8	CTGCTACCCATGAGCCTCTC	GGGCAGCAGTTTTTCACAGT	483
DUSP9	GCATCCGCTACATCCTCAAT	ACAGTGACGGTGACAGAACG	483
DUSP10	ATCTTGCCCTTCCTGTTCCT	ATTGGTCGTTTGCCTTTGAC	484
DUSP16	GCACACCACCATTACATCATCG	AACAGTCTGAAGAGAGAGAGGC	485

Appendix Table 4. Mouse primer list

Gene	Forward primer (5'-3')	Reverse primer (5'-3')	Reference
Gapdh	TCACCACCATGGAGAAGGC	GCTAAGCAGTTGGTGGTGCA	†
Thbs1	GAGCTGTGCAGCAAACAGTC	CTTCCGAGAAGCGTGATAGG	†
Cd47	GTTCAGCTCAACTACTGT	CTCTTATTCGTATGGCTG	
Nox1	GTTTTACCGCTCCCAGCAGAA	GGATGCCACTCCAGGAAGGAA	
Dusp1	GAGCTGTGCAGCAAACAGTC	CTTCCGAGAAGCGTGATAGG	486
Dusp2	TGGAAATCTTGCCCTACCTG	CTCCTGGAACCAGGCACTTA	487
Dusp4	CTGTACCTCCCAGCACCAAT	GACGGGGATGCACTTGTACT	328
Dusp5	TGCACCACCCACCTACACTA	ATGTCAGCAGTGTGGCTGTC	488
Dusp6	TTGAATGTCACCCCCAATTT	CATCGTTCATGGACAGGTTG	328
Dusp7	TGCCAAGGACTCTACCAACC	CTAGGCAGTGCACCAAGACA	328
Dusp8	TGACCCAAAACGGAATAAGC	AGAGATGCCAGCCAGACAGT	290
Dusp9	ACCTTGAGCTGTGGCCTAGA	GGGGATCTGCTTGTAGTGGA	328
Dusp10	GCGGCAGTACTTTGAAGAGG	AGGTTCGGGGAAATAATTGG	486
Dusp16	CAGCGAGATGTCCTCAACAA	TTGGAGGCTTTTGCTTTCTC	290
†Primer design, manufacture and validation was outsourced to PrimerDesign.			

Appendix Table 5. Rat primer list

Gene	Forward primer (5'-3')	Reverse primer (5'-3')	Reference
Gapdh	CCAAGGTCATCCATGACAACTT	AGGGGCCATCCACAGTCTT	489
Thbs1	TTCAGGGGGTGCTGCAGAATG	ACGTTGGTTGAACTGGAGCA	
Cd47	AGAAGCCCGTGAAGAACGC	CACATCCCGACCACAGCAA	490
Nox1	TGAACAACAGCACTCACCAATGCC	AGTTGTTGAACCAGGCAAAGGCAC	491
Dusp1	CCTCCAAGGAGGATATGAAG	GGTGCTACAGGAGCTGCATC	†
Dusp2	TGTGCTTCTTGCGAGGTGGT	CCACCCTGGTCATAGATAGG	†
Dusp4	GGAAGCCATCGAATACATAGACGCAG	TTCATCATCAGGTAGGCCAGGCAG	†
Dusp5	CGACATTAGCTCCCACTTTCAA	AGGACCTTGCCTCCCTCTTC	489
Dusp6	AGCGACTGGAATGAGAACACA	GCAGCCCTCGTCTTTGAGT	†
Dusp7	AATCCCCATCTCTGACCACTG	TGCTAAGCAGTGCACCAAGAC	492
Dusp8	TGTCTTCTGACGACGCATACA	TCCTCTCATACTCCAGCAACTG	†
Dusp9	ACCTTGAGCTGTGGCCTAGA	GGGGATCTGCTTGTAGTGGA	328‡
Dusp10	GCCACAGACAGCAACAAGCAGAAC	ATGACAATGGTGGCAGAACGGGAC	
Dusp16	CAGCGAGATGTCCTCAACAA	TTGGAGGCTTTTGCTTTCTC	290‡

†Primer design, manufacture and validation was outsourced to PrimerDesign.
‡Mouse primer used as rat primers had not been published. Primer-BLAST[493] was used to confirm the mouse target was the #1 predicted primer target in the rat genome.

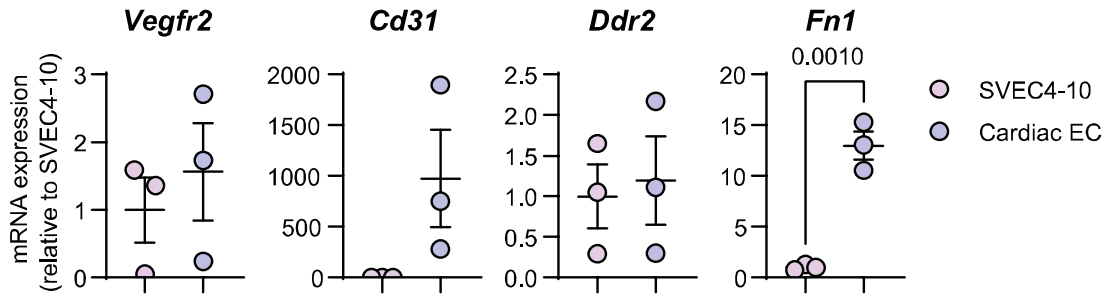

Appendix Figure 1. Confirmation of primary cardiac EC cell type
RT qPCR was performed to identify the gene expression of endothelial markers, VegfrR2 and Cd31, and the fibroblast markers, Ddr2 and Fn1, in the SVEC4-10 cell line and in primary mouse cardiac ECs grown in culture

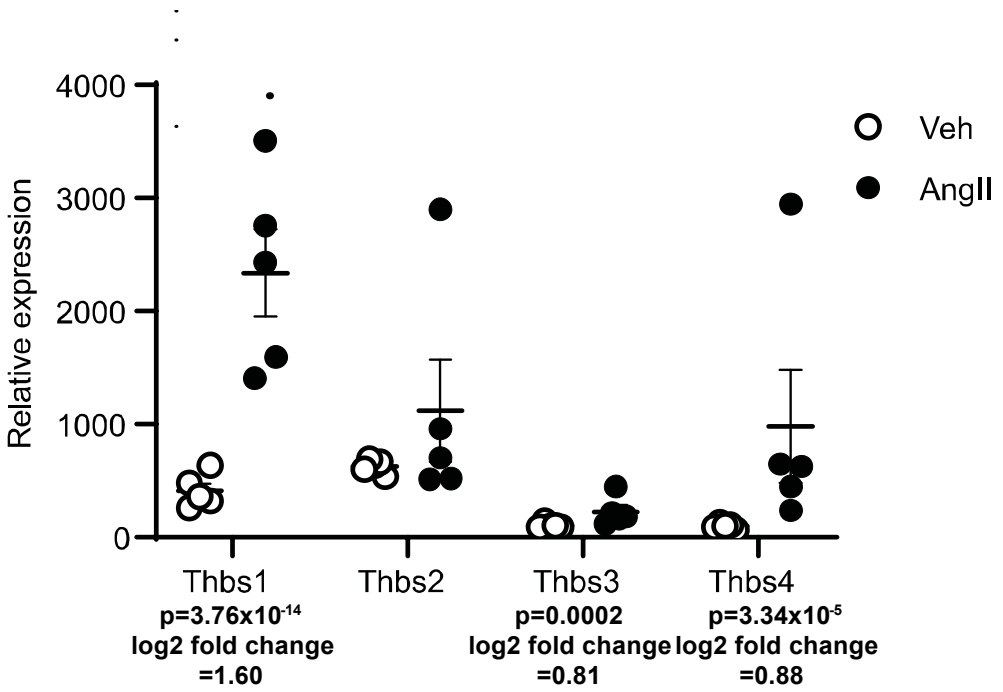

Appendix Figure 2. Thrombospondin gene expression from AngII treated mice.
Normalised plots of *Thbs* gene expression with adjusted p values and log2-fold change from RNAseq data from mice treated with AngII for 7 d. Each data point is representative an independent animal. The log2 fold change values and adjusted p-values were calculated using DESeq2. The adjusted p values and log2 fold change values are displayed for Thbs genes which were significantly upregulated.